



CSIC
CONSEJO SUPERIOR DE INVESTIGACIONES CIENTÍFICAS



UNIVERSITAS
Miguel
Hernández



INSTITUTO DE NEUROCIENCIAS

Consejo Superior de Investigaciones Científicas
Universidad Miguel Hernández de Elche
Instituto de Neurociencias

THE EFFECTS OF AGE AND INDUCED TEAR-DEFICIENCY ON CORNEAL NERVE STRUCTURE AND FUNCTION

Presented by:
Kamila Katarzyna Mizerska

For the degree of Doctor in Neuroscience from
the Miguel Hernández University

Directors:
Dr. Juana Gallar Martínez
Dr. Nicolás Cuenca Navarro

San Juan de Alicante, 2014

A QUIEN CORRESPONDA:

El Profesor **Juan Lerma Gómez**, Director del Instituto de Neurociencias de Alicante, Centro Mixto de la Universidad Miguel Hernández (UMH) y de la Agencia Estatal Consejo Superior de Investigaciones Científicas (CSIC)

INFORMA:

Que la Tesis Doctoral "*the effects of age and induced tear-deficiency on corneal nerve structure and function*" ha sido realizada por Dña. Kamila Katarzyna Mizerska, Licenciada en BIOLOGÍA, bajo la dirección de la Dra. Juana Gallar Martínez y el Dr. Nicolás Cuenca Navarro, y da su conformidad para que sea presentada a la Comisión de Doctorado de la Universidad Miguel Hernández.

Y para que así conste a los efectos oportunos, firma el presente informe en San Juan de Alicante, a 15 de diciembre de 2014


Fdo.: Juan Lerma



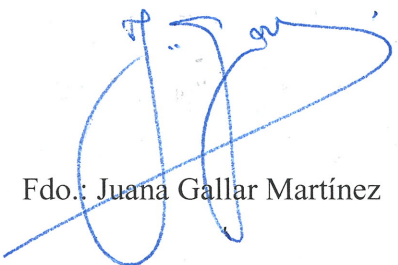
A QUIEN CORRESPONDA,

Los Dres. JUANA GALLAR MARTÍNEZ, Catedrática en el Departamento de Fisiología de la Universidad Miguel Hernández; Profesora de Investigación en el Instituto de Neurociencias de Alicante, centro mixto CSIC-UMH y NICOLÁS CUENCA NAVARRO, Profesor Titular en el Departamento de Fisiología, Genética y Microbiología de la Universidad de Alicante; Investigador de I.M.E.M. Ramon Margalef,

CERTIFICAN,

Que Doña KAMILA KATARZYNA MIZERSKA, Licenciada en BIOLOGÍA, ha realizado bajo su dirección el trabajo experimental que recoge su Tesis Doctoral "THE EFFECTS OF AGE AND INDUCED TEAR-DEFICIENCY ON CORNEAL NERVE STRUCTURE AND FUNCTION". Que han revisado los contenidos científicos y los aspectos formales del trabajo y dan su conformidad para su presentación y defensa pública.

Para que así conste, y a los efectos oportunos, firman el presente Certificado en San Juan de Alicante, a 15 de DICIEMBRE de 2014.



Fdo.: Juana Gallar Martínez



Fdo.: Nicolás Cuenca Navarro

AKNOWLEDGEMENTS

“Nunca consideres el estudio como una obligación, sino como una oportunidad para penetrar en el bello y maravilloso mundo del saber”. Albert Einstein

Un agradecimiento especial para mis directores de Tesis. A la Prof. Juana Gallar, en primer lugar por ser una persona maravillosa, por permitirme unirme a su equipo, por la paciencia y la confianza, por su ayuda en mis primeros pasos en la ciencia. Y al Dr. Nicolás Cuenca por su inigualable ayuda y sus grandes enseñanzas en morfología; gracias por su paciencia y apoyo en la resolución de todos los problemas con una sonrisa.

También muchas gracias al Prof. Carlos Belmonte por abrirme la puerta al gran mundo de la ciencia.

Mi agradecimiento más sincero a la Dra. M^a Carmen Acosta por su inestimable ayuda con cualquier tipo de trabajo y en cada etapa de la creación de esta Tesis; por dedicarme mucho tiempo, siempre paciente, simpática y comprensiva. Por sus bromas, su naturalidad y su eterna sonrisa.

Muchísimas gracias a la estupenda gente del laboratorio. A Carolina y Susana por enseñarme la parte práctica de los experimentos, por su gran ayuda en cada paso y a cada momento; por ser siempre tan buenas conmigo y apoyarme y animarme. Por cada sonrisa y grandes momentos durante estos años.

A Ángeles por hacerlo todo más fácil y más rápido; por su tranquilidad y un enfoque positivo de todo; por ser siempre tan amable y profesional.

Muchas gracias a todas las chicas de grupo de Nico: a Laura F.S., Gema, Laura C., Agustina y Violeta; por ser siempre tan buenas conmigo y por vuestra valiosa ayuda.

Dziękuję moim ukochanym Rodzicom i ukochanej Siostrze Agacie za niezastąpione wsparcie w każdym momencie, podczas wlotów i upadków, w te lepsze i gorsze dni, za nieustanną wiarę we mnie. Dziękuję całej mojej Rodzinie za bycie, mimo odległości, zawsze tak blisko mego serca.

A Efrén, por mantener el ánimo, por su apoyo y su fe en mí. Por estar siempre ahí. Por simplemente ser.

A Marie, por enseñarme que no importa donde estés, la vida es más bonita con una amiga a tu lado.

A mis colegas Ania, Edgar, Sandra, Mari, Rebeca, Carlos, Enoch; por pasar juntos unos momentos muy bonitos aquí, dentro y fuera del trabajo; por vuestra ayuda, apoyo y muchas conversaciones al estilo “never-ending story”.

Kasi i Mateuszowi za bezcenne wsparcie i za Waszą przyjaźń.

Mil gracias a todos por hacerlo posible.

INDEX

ABSTRACT

I. INTRODUCTION	1
A. Evolution and functions of the cornea: from refractive apparatus to protective organ	1
B. The cornea	2
B.1. Anatomy and structure of the cornea	2
B.1.1. Epithelium.....	4
B.1.1.1. Epithelial wound healing.....	6
B.1.2. Bowman’s membrane.....	8
B.1.3. Stroma.....	8
B.1.4. Descemet’s membrane	9
B.1.5. Endothelium	9
B.2. Innervation of the cornea.....	10
B.2.1. Autonomic innervation.....	12
B.2.2. Sensory innervation.....	12
B.2.3. Neurochemistry of corneal innervation	13
B.3. Architecture of corneal innervation	13
B.3.1. Limbal plexus	15
B.3.2. Stromal plexus	15
B.3.3. Subepithelial nerve plexus	17
B.3.4. Subbasal nerve plexus.....	18
B.3.5. Intraepithelial nerve terminals.....	21
B.4. Sensory innervation: functional nerves classification.....	24
B.4.1. Mechanoreceptors	25
B.4.2. Polymodal nociceptors	26
B.4.3. Cold thermoreceptors	27
C. Protective mechanisms of the eye surface.....	28
C.1. Blinking.....	28
C.2. Tearing.....	29
C.2.1. Tear film composition.....	29

C.2.2. Basal Tearing	31
C.2.3. Reflex tearing	32
D. Dry Eye Disease (DED)	32
III. OBJECTIVES.....	37
III. MATERIAL AND METHODS.....	39
A. Measurement of tearing rate	39
B. Surgical procedure to induce chronic tear-deficiency	40
C. Immunohistochemistry of corneal nerves.....	40
C.1. Immunofluorescence	41
C.2. Immunoperoxidase, ABC complex methods	42
D. Analysis of corneal nerve density and morphology	43
D.1. Parameters measured in the superior quadrant of the cornea	43
D.1.1. Density of epithelial nerve terminals.....	43
D.1.2. Proportion of subbasal nerve fibers	45
D.1.3. Length of subbasal nerve leashes.....	46
D.2. Parameters measured in the whole cornea.....	48
D.2.1. Corneal surface area.....	48
D.2.2. Total number of subbasal nerve leashes	51
D.2.3. Density of subbasal nerve leashes.....	52
E. Corneal epithelial wound healing.....	52
E.1. Chemical debridation of corneal epithelium	53
E.2. Data analysis	54
E.2.1. Photos analysis	54
E.2.2. Wound area	54
E.2.3. Estimated migration rate.....	54
E.2.4. Estimated time of healing.....	54
F. Electrophysiological recording of corneal sensory receptors	55
F.1. Corneal nerve terminals recording.....	55
F.2. Data analysis	57
F.3. Recording of nerve filaments from the ciliary nerves	58
G. Statistical analysis	59

IV. RESULTS	61
A. THE EFFECTS OF AGE	61
A.1. Tearing rate	61
A.2. Morphology of corneal nerves.....	61
A.2.1. Corneal surface area	62
A.2.2. Proportion of subbasal nerve fibers.....	63
A.2.3. Total number of subbasal nerve leashes.....	70
A.2.4. Density of subbasal nerve leashes.....	71
A.2.5. Length of subbasal nerve leashes.....	73
A.2.6. Density of epithelial nerve terminals in different cornea zones	78
A.3. Corneal epithelial wound healing.....	80
A.3.1. Area of the epithelial defect.....	80
A.3.2. Estimated migration rate	80
A.3.3. Estimated time of healing.....	80
A.4. Electrophysiological recording of corneal sensory receptors.....	82
A.4.1. Neural activity of corneal cold nerve terminals.....	82
A.4.2. Neural activity of mechano- and polymodal nociceptors	84
B. THE EFFECT OF INDUCED TEAR-DEFICIENCY.....	85
B.1. Tearing rate	85
B.2. Morphology of corneal nerves.....	86
B.2.1. Proportion of subbasal nerve fibers.....	86
B.2.2. Total number of subbasal nerve leashes.....	90
B.2.3. Density of subbasal nerve leashes	92
B.2.4. Length of subbasal nerve leashes	96
B.2.5. Density of epithelial nerve terminals	103
B.3. Corneal epithelial wound healing.....	108
B.3.1. One month after tear-deficiency	109
B.3.2. Six months after tear-deficiency	110
B.3.3. One versus six months after tear-deficiency	111
B.4. Electrophysiological recording of corneal sensory receptors	112
B.4.1. Neural activity of corneal cold nerve terminals.....	112
B.4.2. Neural activity of mechano- and polymodal nociceptors	117

V. DISCUSSION	121
A. Guinea pig as an animal model for studying morphology of corneal innervation, epithelial wound healing, and corneal nerve activity	121
B. Guinea pig's tearing rate	122
B.1. Methodological considerations.....	122
B.2. Tearing rate was not altered in adult animals	122
B.3. Tearing rate was altered in tear-deficient animals.....	123
C. Corneal nerve morphology	123
C.1. Methodological considerations.....	123
C.2. Animals age considerations.....	125
C.3. Morphological changes in the corneal surface area with age	126
C.4. Morphological changes in the corneal innervation with age.....	127
C.5. Morphological changes in the corneal innervation as an effect of induced tear-deficiency	131
D. Corneal epithelial wound healing	132
D.1. Methodological consideration.....	132
D.2. Corneal epithelial wound healing - the effect of age	133
D.3. Corneal epithelial wound healing - the effect of induced tear-deficiency	133
E. Electrophysiological extracellular recordings	134
E.1. The effect of age on corneal nerve activity.....	134
E.2. The effect of tear-deficiency on corneal nerve activity	135
V. CONCLUSIONS	137
VI. ABBREVIATIONS	141
VII. BIBLIOGRAPHY	143

LIST OF FIGURES

INTRODUCTION	1
Figure 1. The structure of the cornea	3
Figure 2. The central corneal epithelium structure	6
Figure 3. Schematic presentation of wound healing process	8
Figure 4. Innervation of the eye.....	11
Figure 5. Neurochemistry of the corneal innervation.....	13
Figure 6. Graphical illustration of the organizational design of the innervation pattern of the corneal epithelium	14
Figure 7. Schematic distribution of nerves in the cornea.....	15
Figure 8. Human main stromal bundles.....	16
Figure 9. Main stromal nerve bundles	16
Figure 10. Stromal free nerve endings	17
Figure 11. The arrangement of nerve bundles entering periphery of the cornea in different planes	18
Figure 12. Human stromal nerve penetrations through Bowman's membrane.....	19
Figure 13. Subbasal nerve leash in a guinea pig	19
Figure 14. Fluorescent staining of the vortex in guinea pig cornea.....	20
Figure 15. Human subbasal nerve vortices	21
Figure 16. High magnification schematic line drawing of intraepithelial nerve terminals.....	21
Figure 17. Intraepithelial nerve terminals.....	22
Figure 18. Reconstructions of superficial nerve terminals in the mouse corneal epithelium	23
Figure 19. Schematic representation of the types of sensory neurons innervating the eye	25
Figure 20. Schematic representation of the tear film.....	31
Figure 21. Schema of the major etiological causes of dry eye	34
Figure 22. Hypothetical neural mechanisms involved in the maintenance of basal tearing and production of dryness sensations by cold receptor activity.....	35
MATERIAL AND METHODS	39

Figure 23. Measurement of the tearing rate with a phenol red thread.....	39
Figure 24. Fixed and cryoprotected dissected cornea with radial cuts	41
Figure 25. Fluorescence spectrum of the fluorophore Alexa 488	42
Figure 26. Use of ImageJ software to count the number of epithelial nerve terminals.....	44
Figure 27. Quantitative analysis of the epithelial nerve endings density in different zones of the superior quadrant of cornea.....	44
Figure 28. Quantitative estimation of the tissue area occupied by subbasal nerve fibers in different zones of the superior quadrant of cornea	45
Figure 29. Use of ImageJ to calculate subbasal nerve proportion	46
Figure 30. Use of NeuroLucida to calculate the length of subbasal nerve leashes.....	47
Figure 31. Outline of the cornea showing the peripheral (A), central (B) and vortex (C) zones (red quadrilaterals)	47
Figure 32. NeuroLucida software used to measure the subbasal nerve length in the peripheral (A), middle peripheral (B) and vortex (C) zones of the cornea	48
Figure 33. Drawing of cornea contour using NeuroLucida software	49
Figure 34. Drawing of corneo-limbal border using NeuroLucida software	49
Figure 35. Definition of the central and peripheral cornea zones using NeuroLucida software	50
Figure 36. Final outline and calculation of surface areas in a sample cornea using NeuroLucida software	50
Figure 37. Outline of the cornea tissue samples the NeuroLucida software	51
Figure 38. Use of NeuroLucida software to calculate the total number of subbasal nerve leashes.....	52
Figure 39. Outline of the tissue sample showing the number of subbasal nerve leashes in the peripheral and central cornea zones.....	52
Figure 40. Scheme of corneal epithelial debridation procedure.....	53
Figure 41. Experimental setup used for the extracellular recording of single nerve terminals in the isolated cornea	57
Figure 42. Example of the change in NTI activity in a corneal cold nerve terminal evoked by thermal stimulation	58
Figure 43. Experimental setup used for the extracellular recording of single units from the ciliary nerves	59
RESULTS.....	61
Figure 44. Tearing rate in young and adult guinea pigs.....	61

Figure 45. Evolution of the corneal surface area with age.....	62
Figure 46. Changes in the proportion of tissue area occupied by subbasal nerve fibers with age	64
Figure 47. TUJ-1 positive corneal nerves in corneas of animals of different ages.....	70
Figure 48. Evolution of the number of subbasal nerve leashes with age.....	70
Figure 49. Changes in the density of subbasal nerve leashes with age.....	72
Figure 50. Fluorescence immunostaining of TUJ-1 positive subbasal nerve leashes	74
Figure 51. Changes in the length of subbasal nerve leashes with age	75
Figure 52. Tuj-1 positive subbasal nerve leashes in the peripheral and central cornea, and the vortex zone of guinea pigs of different ages	78
Figure 53. Changes in the density of corneal nerve terminals with age.....	79
Figure 54. Corneal epithelial debridation closure in young and adult animals.....	81
Figure 55. Sample recordings of the response to a cooling stimulus of two different cold thermoreceptors from the cornea of a young (left) and an adult (right) guinea pig.....	82
Figure 56. Spontaneous and stimulus-evoked activity of cold thermoreceptors in corneas of young and adult guinea pigs.....	84
Figure 57. Tearing rate in young and adult control and tear-deficient (TD) guinea pigs.....	86
Figure 58. Changes in subbasal nerve fibers proportion at different times after tear-deficiency.....	88
Figure 59. Changes in subbasal nerve fibers proportion at different times after tear-deficiency and in age-matched controls	88
Figure 60. Tuj-1 positive subbasal nerve fibers in control and tear-deficient animals.....	90
Figure 61. Evolution in the number of the subbasal nerve leashes at different times after tear-deficiency and in age-matched controls.....	91
Figure 62. Density of subbasal nerve leashes at different times after tear-deficiency and in age-matched controls	93
Figure 63. TUJ-1 positive subbasal nerve leashes in tear-deficient (TD) and age-matched control corneas of guinea pig	95
Figure 64. Changes in subbasal nerve leash length at different times after tear-deficiency	97
Figure 65. Changes in subbasal nerve leash length at different times after tear-deficiency and in age-matched animals.....	98

Figure 66. Camara lucida drawings of representative subbasal corneal nerve leashes of control and tear-deficient guinea pigs at different times after lacrimal gland removal	103
Figure 67. Changes in epithelial nerves density at different times in tear- deficient animals	104
Figure 68. Changes in epithelial nerves density at different times in tear- deficient and age-matched control animals	105
Figure 69. TUJ-1 positive epithelial nerve endings in control and tear- deficient animals	108
Figure 70. Epithelial wound healing in tear-deficient and control animals.....	110
Figure 71. Epithelial wound healing in tear-deficient and control animals.....	111
Figure 72. Epithelial wound healing at 1 and 6 months after tear-deficiency.....	112
Figure 73. Spontaneous activity of cold thermoreceptors in corneas of tear- deficient guinea pigs at 1 month after lacrimal gland removal and in young non-operated animals	114
Figure 74. Sample recordings of the response to a cooling stimulus of cold thermoreceptors recorded from two different corneas of guinea pigs subjected to lacrimal gland removal one month (left) and 8 months (right) before	116
Figure 75. Spontaneous and stimulus-evoked activity of cold thermoreceptors in corneas of tear-deficient guinea pigs at 1 and 8 months after lacrimal gland removal.....	117
DISCUSSION	121
Figure 76. Lifespan calculator of guinea pig and human.....	126
Figure 77. The increment of the corneal surface area with age is correlated with the subbasal nerves elongation	126
Figure 78. The increment of the corneal surface area and changes in the subbasal nerve number with age	127
Figure 79. The changes in subbasal nerve and epithelial nerve terminal density with age	130
Figure 80. The changes in epithelial nerve terminal and nerve fiber density with age.....	131

LIST OF TABLES

Table 1. Estimated growth rate of corneal surface area with age	63
Table 2. Change on the number of subbasal nerve leashes in the whole cornea with age.....	71
Table 3. Density of subbasal nerve leashes in the whole cornea with age	72
Table 4. Estimated rate of elongation with age of subbasal nerve leashes in different zones of the cornea.....	76
Table 5. Spontaneous and stimulus-evoked activity of cold corneal receptors in young and adult guinea pigs.....	83
Table 6. Spontaneous activity and response to natural stimuli of mechanonociceptors in young and adult guinea pig corneas	84
Table 7. Spontaneous activity and response to natural stimuli of polymodal nociceptors in young and adult guinea pig corneas	85
Table 8. Change in the number of subbasal nerve leashes at different times after tear-deficiency (TD) and in age-matched control animals	92
Table 9. Elongation of subbasal nerve leashes in tear-deficient animals at different time points after removal of the lacrimal gland and in age-matched control animals.....	99
Table 10. Estimated rate of elongation ($\mu\text{m}/\text{month}$) with of subbasal nerve leashes in different zones of the cornea of tear-deficient and control guinea pigs.....	99
Table 11. Density of nerve terminals in tear-deficient animals at different time points after removal of the lacrimal gland and in age-matched control animals.....	106
Table 12. Spontaneous and stimulus-evoked activity of cold corneal receptors recorded in age-matched control and tear-deficient (TD) guinea pigs (at 1 month after lacrimal gland removal)	113
Table 13. Spontaneous and stimulus-evoked activity of cold corneal receptors recorded in age-matched control and tear-deficient (TD) guinea pigs (at 8 months after lacrimal gland removal)	115
Table 14. Spontaneous and stimulus-evoked activity of cold corneal receptors recorded in tear-deficient (TD) guinea pigs at 1 and 8 months after lacrimal gland removal	116
Table 15. Spontaneous activity and response to natural stimuli of mechanonociceptors in age-matched control and tear-deficient (TD) guinea pig corneas.....	118
Table 16. Spontaneous activity and response to natural stimuli of polymodal nociceptors in age-matched control and tear-deficient (TD) guinea pig corneas.....	118
Table 17. Spontaneous activity and response to natural stimuli of mechanonociceptors in age-matched control and tear-deficient (TD) guinea pig corneas.....	119
Table 18. Spontaneous activity and response to natural stimuli of polymodal nociceptors in age-matched and tear-deficient (TD) guinea pig corneas	119

Table 19. Spontaneous activity and response to natural stimuli of mechano-
nociceptors in tear-deficient (TD) guinea pig corneas 120

Table 20. Spontaneous activity and response to natural stimuli of polymodal
nociceptors in tear-deficient (TD) guinea pig corneas 120



ABSTRACT

Cornea is the most anterior surface of the eye, protecting it against injury. For that, the cornea possesses the richest sensory innervation of the body, devoted to detect noxious stimuli, initiating protective reflexes and having trophic functions. Corneal nerves undergo continuous rearrangement. Although not only sensory nerves are found in the cornea, the density of corneal nerves might be considered directly proportional to corneal sensitivity, thus, any change in its density could influence its sensory and trophic functions.

The purpose of this Thesis was to examine the effect of development to adulthood and tear-deficiency on the morphology, trophism and sensory activity of corneal innervation in the guinea pig.

The morphological changes of corneal nerves were studied in different age groups (1-12 months) and 1, 3 and 8 months after the main lacrimal gland removal. Eyes were submitted to the procedure of staining with neuronal class III β -tubulin with use of immunoperoxidase and immunofluorescence techniques, analyzing the proportion of subbasal nerve fibers, the number, density and length of subbasal nerve leashes and the density of epithelial nerve terminals. The parameters were quantified either in the whole mount cornea or in different zones of the superior quadrant.

To study the trophic function corneal epithelial wounds were performed with *n*-heptanol and their evolution was regularly checked. Epithelial migration rate and estimated time of healing were calculated. To study the changes of the activity of corneal sensory nerves electrophysiological extracellular recording techniques were used, analyzing the spontaneous and evoked activity.

The corneal nerve architecture changed with age showing a reduction in the subbasal and epithelial nerve density. This might contribute to the neurotropic slowdown of epithelial wound healing. Corneal epithelial wounds recovered faster in young animals coinciding to the richer corneal innervation, which had a peak in nerve density at the age of 2 months. In spite of that, the characteristics of the spontaneous and stimulus-evoked activity of corneal nerves, and tearing rate were similar in young and adult animals.

In tear-deficient guinea pigs there were alterations of nerve morphology suggestive of nerve lesion and regeneration with time. The changes in corneal subbasal nerve architecture 1 month after lacrimal gland removal suggest that nerve damage develops shortly after induction of reduced tearing, leading to a neurotropic slowdown of epithelial wound healing. At longer times after tear-deficiency, regeneration of corneal nerves appeared to restore in part the wound healing capabilities of the corneal epithelium, as well as, to increment the lacrimation level. Whereas, among corneal receptors only cold thermoreceptors developed significant changes in their activity, being the most affected by the decrease in tear secretion.

The results of this Thesis report for the first time the evolution of corneal innervation with the development to adulthood and after the induced tear-deficiency in the guinea pig, moreover demonstrating their impact on corneal epithelial wound healing and on corneal nerve activity.

RESUMEN

La córnea es la superficie más anterior del ojo y lo protege contra posibles daños. Para ello posee la inervación sensorial más rica del cuerpo, dedicada a detectar estímulos nocivos que iniciarán reflejos protectores y que además cumple funciones tróficas; esta inervación está también sometida a un continuo reajuste. Aunque no sólo hay nervios sensoriales en la córnea, su densidad puede ser considerada directamente proporcional a la sensibilidad corneal; por eso, cualquier cambio en su densidad puede influir en sus funciones sensoriales y tróficas.

El objetivo de esta Tesis es examinar el efecto del desarrollo hasta la edad adulta y de la deficiencia lacrimal sobre la morfología, el trofismo y la actividad sensorial de la inervación corneal en la cobaya.

Las alteraciones morfológicas de los nervios corneales fueron estudiadas en distintos grupos de edad (1-12 meses) y 1, 3 y 8 meses después de la ablación de la glándula lacrimal. Los ojos se tiñeron con β -tubulina neuronal clase III, utilizando la técnica de inmunoperoxidasa e inmunofluorescencia, y luego se analizó la proporción de fibras de nervios subbasales, su número, su densidad y la longitud de los haces de nervios subbasales y la densidad de las terminaciones de los nervios epiteliales. Los parámetros fueron cuantificados en la córnea entera o en diferentes zonas del cuadrante superior de la córnea.

Para estudiar la función trófica de los nervios corneales se provocaron úlceras en el epitelio corneal, utilizando *n*-heptanol, y la evolución de su curación fue estudiada regularmente, calculando el ratio de migración epitelial y el tiempo estimado de recuperación del epitelio. Para analizar los cambios en la actividad sensorial de los nervios corneales se usaron registros electrofisiológicos extracelulares y se estudiaron tanto la actividad espontánea como la evocada.

La arquitectura de los nervios corneales cambió con la edad, mostrando una reducción en la densidad de los nervios subbasales y epiteliales con el tiempo. Ello podría contribuir a un enlentecimiento neurotrófico en la curación de las úlceras corneales. Estas úlceras se recuperaron más rápido en los animales jóvenes, posiblemente como resultado de una inervación corneal más profusa, que tiene su pico de densidad nerviosa a la edad de 2 meses. A pesar de ello, las características de la actividad espontánea y evocada por la estimulación corneal, así como el ratio de lacrimación, son similares en los animales jóvenes y en los adultos.

En las cobayas lácrimo-deficientes hubo alteraciones en la morfología de la inervación corneal, lo que sugiere una lesión de los nervios y su regeneración con el tiempo. Los cambios observados en la arquitectura de los nervios subbasales 1 mes después de quitar la glándula lacrimal sugieren que el daño de los nervios se desarrolla poco después de inducir la lacrimación reducida, provocando un enlentecimiento neurotrófico en la curación de las úlceras corneales. Con el paso del tiempo después de inducir la deficiencia lacrimal, la regeneración de los nervios corneales parece recuperar en parte la capacidad de curación de las úlceras epiteliales de la córnea, así como aumentar el nivel de lacrimación. Al mismo tiempo, de los receptores corneales sólo los receptores de frío desarrollaron cambios significativos en su actividad, demostrando una mayor afectación por la deficiencia lacrimal.

Los resultados de esta tesis muestran por primera vez la evolución de la inervación corneal con el desarrollo hasta la edad adulta y después de la inducción de una deficiencia lacrimal en cobaya, demostrando además su impacto en la curación de las úlceras epiteliales de la córnea y en la actividad de los nervios corneales.



I. INTRODUCTION

A. Evolution and functions of the cornea: from refractive apparatus to protective organ

Our bodies evolve in the rhythm of continuous changes occurring in the external environment. In this way we are adapted to contact, function and interact properly with the surrounding world. The gate to our body, that let us experience the external conditions and factors, is created by three components of somatosensory systems: nerve receptors, peripheral afferent neurons, and the central nervous system.

The somatosensory systems continuously inform us about objects through the touch, and about the position of the body and movements of its parts, through the stimulation of muscle and joints, what is called proprioception; they provide also the body temperature monitoring, and aware about the painful stimulus appearance.

Somatosensory neurons are sensitive to various stimuli, like mechanical forces, temperature changes, chemical agents, and tissue damage. These stimuli are specific for sensory receptors, which convert them to an action potential transmitted to the brain in a process called sensory transduction. This way the somatosensory system provides accurate information about the location, shape, texture, and movement of tactile stimuli (discriminative touch), the position and movement of body parts (proprioception), the temperature (thermoreception) and the application and location of painful stimuli (nociception).

Most of those sensory and somatosensory modalities are mainly informative, whereas pain is protective. Pain is defined as a range of unpleasant sensory and emotional experiences associated with actual or potential tissue damage. It is transmitted via three major pathways to the central nervous system.

Organisms are sensitive to noxious stimuli and can react to prevent or minimize tissue injury. The attribute of pain is essential to the well-being and survival of an organism.

Noxious stimuli are detected by nociceptors, which are free nerve endings located in the skin and almost all organs. One of them and actually the most sensitive and innervated tissue in the body is cornea. Since the vision plays a critical role in obtaining information from the external world it is provided with the structure ensuring the protection against injury. Thus, cornea is the most anterior surface of the eye and possesses the richest sensory innervation of

the body mostly devoted to detect noxious stimuli (Belmonte, Aracil et al. 2004). Moreover, the cornea evolved as an organ to improve the refractive power of the eye, hence, the efficiency of vision.

Vision is one of the most important animal senses. For this reason animal eyes have evolved in many designs, shapes and sizes to develop different solutions to the problem of obtaining an image (Land and Fernald 1992). Primitive eyes because of their simple built are able to provide information only about light intensity and direction. The efficiency in light collection and, hence, an image creation is possible by the presence of an additional refractive element in the front of photoreceptive layer, like lens and cornea, in the vision organ. Summarizing, over the course of time the cornea has gained many different functions, like filtration of light and focusing it on the retina, protection and nutrition of the underlying ocular tissues of the eye (Land and Fernald 1992; Jonasova and Kozmik 2008; Kubilus and Linsenmayer 2010), what undoubtedly make it the essential organ for the proper vision.

B. The cornea

The cornea is a transparent avascular connective tissue that together with sclera constitutes the outermost, fibrous part of the eye. The cornea provides the first line defense being the primary infectious and structural barrier of the eye. Together with the overlying tear film, it also provides a proper anterior refractive surface for the eye (reviewed by (Adler, Kaufman et al. 2011; DelMonte and Kim 2011)). The cornea contributes about 2/3 of the ocular power, rather more than 40 Dioptres and its refractive index is 1.376 (Saude 1993). Its transparency is the result of many factors including the structural anatomy and physiology of its cellular components. All mechanisms involved in functionality of corneal components make the corneal structure a unique and sophisticated element of the eye.

B.1. Anatomy and structure of the cornea

The cornea measures about 11 mm vertically and 12 mm horizontally in adult human; it is 540 to 700 μm thick, being thinner in the center (approx. 544 μm) and increasing its thickness in the periphery to approx. 700 μm as it reaches the limbus (Knupp, Pinali et al. 2009; Adler, Kaufman et al. 2011).

The corneal structure consists of 5 layers (Figure 1): the epithelium, Bowman's membrane, stroma, Descemet's membrane, and endothelium (Adler, Kaufman et al. 2011; Almubrad and Akhtar 2011). Among the species the cornea keeps the general structure, but differs in thickness. (Hayashi, Osawa et al. 2002; Cafaro, Ortiz et al. 2009; Henriksson, McDermott et al. 2009; Ledbetter and Scarlett 2009; Almubrad and Akhtar 2011).

One of the unique characteristics of cornea is its transparency, which makes it major refractive element of the eye (it reflects less than 1% of incident light). The cornea is transparent due to its well-arranged stromal fibrils structure (Maurice 1957; Jester 2008; Jonasova and Kozmik 2008; Knupp, Pinali et al. 2009; Hassell and Birk 2010), the lack of myelinated innervation and opaque cells, likewise because of being avascular (Ambati, Nozaki et al. 2006; Cursiefen, Chen et al. 2006; Koo and Kume 2013).

Because the corneal epithelium is relatively simple and has low metabolic demands, tissue transparency and avascularity, a number of investigators have exploited it to study the structure and function of sensory nerve terminals both in vitro and in vivo (Ivanusic, Wood et al. 2013) like doing electrophysiological recordings to characterize functional phenotypes of sensory nerves (Belmonte and Giraldez 1981; Brock, McLachlan et al. 1998), also in transgenic mice (Parra, Madrid et al. 2010).

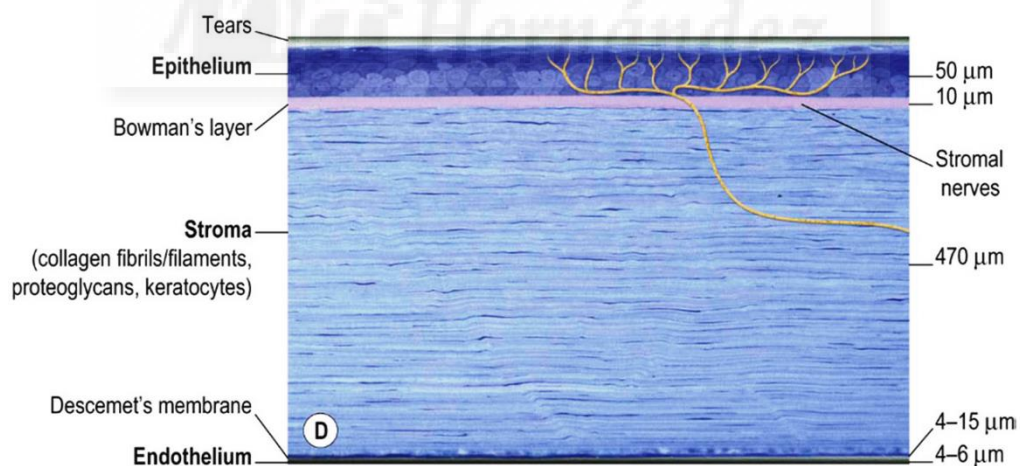


Figure 1. The structure of the cornea presented on the histologic section of the human cornea with labelled the five main layers (toluidine blue x25). Taken from Dawson *et al.*, 2011.

B.1.1. Epithelium

The corneal epithelium is a low-permeability barrier and like all the epithelia of the eye surface, is stratified, squamous, non-keratinized (Fabiani, Barabino et al. 2009; Adler, Kaufman et al. 2011). The epithelium originates from surface ectoderm during the 5th week of the embryogenesis (Saude 1993). In the human cornea the epithelium is 50 μm thick, what makes 8% of the entire cornea (Almubrad and Akhtar 2011). It is composed of four to six cell thick layers, which include the squamous cells, wing cells and basal cells held together by desmosomes (Saude 1993; Adler, Kaufman et al. 2011; DelMonte and Kim 2011)(Figure 2). In guinea pig the epithelium measures about 45 μm and it is composed of three squamous cell layers, 2-3 layers of wing cells, and 1-2 layers of basal cells, and is covered by glycocalyx (Cafaro, Ortiz et al. 2009).

Basal cells form the deepest single columnar layer attached to the underlying basal membrane by hemidesmosomes (Dohlman 1971). They are cuboidal or cylindrical cells which are the only corneal epithelial cells capable of mitosis, so they are renewed continuously. New cells are produced by mitosis and migrate to more external layers of wing cells and squamous cells (reviewed by (DelMonte and Kim 2011)). Wing cells are more flattened and about 3 layers thick. Over wings cells there is a 2 to 3 cells thick superficial layer of squamous cells that are flat and polygonal. Squamous cells are provided with extensive apical microvilli, which in turned are covered by a layer of glycocalyx (reviewed by (DelMonte and Kim 2011)), what might contribute to the stability of the tear film overlaying the epithelium (Dohlman 1971; Nichols, Dawson et al. 1983; Saude 1993). Epithelial cells are covered with a mucinous layer of the tear film, which is produced by conjunctival goblet cells (Nichols, Chiappino et al. 1985). The mucous layer seems to interact closely with glycocalyx of epithelial cells to allow spreading of the tear film while blinking. The contribution of epithelium itself to the mucinous layer was suggested by Gipson, but it was not proven (Gipson, Yankauckas et al. 1992).

The epithelium is a dynamic structure which cells are constantly lost and renewed (Nagasaki and Zhao 2003), what last form 7 to 10 days under normal conditions (Dohlman 1971), (Fabiani, Barabino et al. 2009). Epithelial homeostasis is provided by migration of corneal epithelial cells, arising from the stem cells at the limbus, to the center of cornea where they differentiate into transient amplifying cells and basal cells (reviewed by (Li, Hayashida et al. 2007)). The basal transient amplifying epithelial cells move slowly toward the center of cornea as delineated by the X, Y, Z hypothesis of Thoft and Friend, where X is the basal corneal epithelial cell proliferation, Y the limbal cell proliferation, and Z the epithelial cell loss on the

anterior surface from eyelid blinking (Thoft and Friend 1983), (Adler, Kaufman et al. 2011). Buck for the first time demonstrated the centripetal movement of epithelial cells, in the normal cornea (Buck 1985), what might cause vortex pattern of epithelial cells in the central cornea, and also could be a consequence of many cells converging in a small central area from all directions (Bron 1972). As summarized by Nagasaki and Zhao, there are five major components in the normal epithelial homeostasis: continuous generation of transient amplifying cells from the stem cells which enter into the cornea; cell division at the basal epithelium; vertical movement of basal cells and their next generations toward the surface; horizontal movement of cells toward the central cornea; loss of surface cells by exfoliation (Nagasaki and Zhao 2003).

The basal epithelial cell layer of the peripheral cornea along with the limbus and conjunctiva seem to have a subpopulation of immune cells, called Langerhans cells (Rodrigues, Rowden et al. 1981). Langerhans cells appear in the intact (He, Bazan et al. 2010), injured (Brown, Soderstrom et al. 1968) and inflamed (Hamrah, Zhang et al. 2002) tissues, what might indicate their implication in immunoinflammatory responses.

It can be said, that corneal epithelium plays the role of a protective barrier against fluid loss and pathogen penetration, and also provides a transparent medium for the vision (Fabiani, Barabino et al. 2009). The epithelial cells have the highest rates of cell division what provide the maintenance of the smooth optical surface and the complete regeneration after injury (Adler, Kaufman et al. 2011).

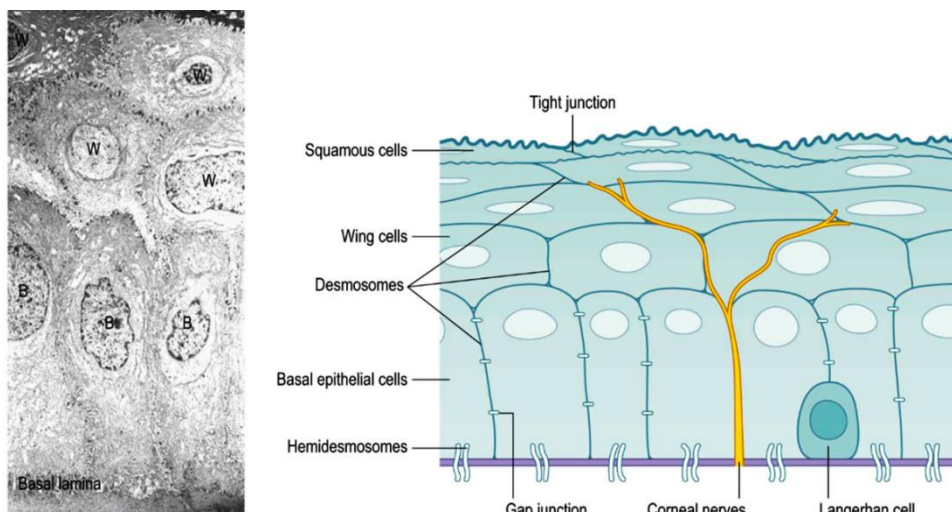


Figure 2. The central corneal epithelium structure presented on the transmission electron micrograph (x3500) on the left, and a summary diagram on the right. S = squamous cells. W = wing cells. B = basal epithelial cells. Taken from Dawson *et al.*, 2011.

B.1.1.1. Epithelial wound healing

Most wounds of the cornea involve damage to the epithelium and are caused by different factors, for example due to parasite, bacterial or viral infection, various injuries or corneal denervation in response to neurological trauma or refractive surgeries (reviewed by (Stepp, Zieske et al. 2014)).

Corneal wound healing is the end of result of a sequence of events which are controlled and regulated by many factors, like growth factors and cytokines (Imanishi, Kamiyama et al. 2000; Baldwin and Marshall 2002), lipid mediators (Kenchegowda and Bazan 2010). One of the most crucial aspects of corneal wound healing is minimalizing the scar formation; otherwise it would have serious visual consequences.

The process involved in the healing of corneal epithelial wounds is continuous, and it can be described in three separate phases. Basing on the animal studies they are called: the latent phase, cell migration and adhesion phase, and cell proliferation phase (reviewed by (Steele 1999)).

Corneal healing can be affected by many factors including the size and depth of the wound, the causative agent age, medication, preexisting diseases. Tear quality and integrity is particularly important, as any tear deficiency may compromise the wound healing process (reviewed by (Steele 1999)).

The initial latent phase involves the movement of existing basal epithelial cells at the corneal wound margin. Epithelial cells start to round and retract at the wound edge, while the basal cells proceed flattening and separation. There occurs also the reduction in hemidesmosome attachments. The final stage of the latent phase starts with the production of “filipodia” by epithelial cells, which attaching to the basal lamina provide movement of the cells (Pfister 1975).

Epithelial basal cells together with wing cells participate in the formation of leading edge, which gradually migrating from opposite directions into the center of cornea takes part in the re-epithelialization by covering the wound area with monolayer of epithelial cells (Figure 3, upper panel). During cell migration, the actin cytoskeletons (Anderson 1977) of basal cells connect with the underlying extracellular matrix to anchor the epithelium to the stroma. Here

fibronectin plays an essential role by providing a transient subepithelial matrix, where the adhesion of the migrating epithelial cells occurs. Leading epithelial cells start to migrate centripetally across stromal surface (reviewed by (Steele 1999)). After completion of epithelial monolayer that covers wound area, fibronectin disappears and the synthesis of new hemidesmosomes and other anchoring complexes is started. These second, migratory and adhesive phase lasts for between 24 and 36 hours (reviewed by (Steele 1999)).

The final phase involves proliferation of the epithelial cells until normal epithelial thickness is restored (Figure 3, lower panel). The basal epithelial cells are the main participants in this process. All the cell proliferation and differentiation is similar to that which occurs during normal homeostasis. During normal homeostasis, continuous centripetal movement of peripheral corneal epithelium toward the visual axis maintains corneal epithelial mass. In the cornea the stem cells are located near the limbus (Agrawal and Tsai 2003).

Upon division, stem cells give rise to regularly cycling transient amplifying (TA) cells located in the peripheral and central corneal epithelium. Young TA cells with multiple division capacity are preferentially located in the peripheral cornea, whereas the more mature TA cells having little proliferative reserve reside in the central cornea. Under normal circumstances not every TA cell uses its full capacity to divide. Stimulated by an injury self-renewing epithelium can expand the cell population. This results in the production of a large number of post-mitotic terminally differentiated cells (Lehrer, Sun et al. 1998).

Finally, corneal wound healing is said to be complete with the further establishment of hemidesmosomes permanently anchoring the corneal epithelium to the underlying stroma (reviewed by (Steele 1999)).

Wounding of the cornea results in extensive damage to the innervation that affects epithelial regeneration and corneal metabolism (Beuerman and Schimmelpfennig 1980) and must be repaired to restore its normal structure and function (Rozsa, Guss et al. 1983). There was shown that following experimental wounding, the intraepithelial innervation of the cornea undergoes extensive rearrangement in organization (Beuerman and Kupke 1982).

The nerve repair after experimentally induced corneal wounds was seen after application of substance P and insulin like-growth factor-1 (IGF-1) (Nakamura, Ofuji et al. 1997; Nakamura, Kawahara et al. 2003), vascular endothelial growth factor (VEGF) (Charles, Zhang et al. 2008; Pan, Fukuoka et al. 2013), opioid growth factor (OGF) (Zagon, Sassani et al. 1998; Zagon, Sassani et al. 2000).

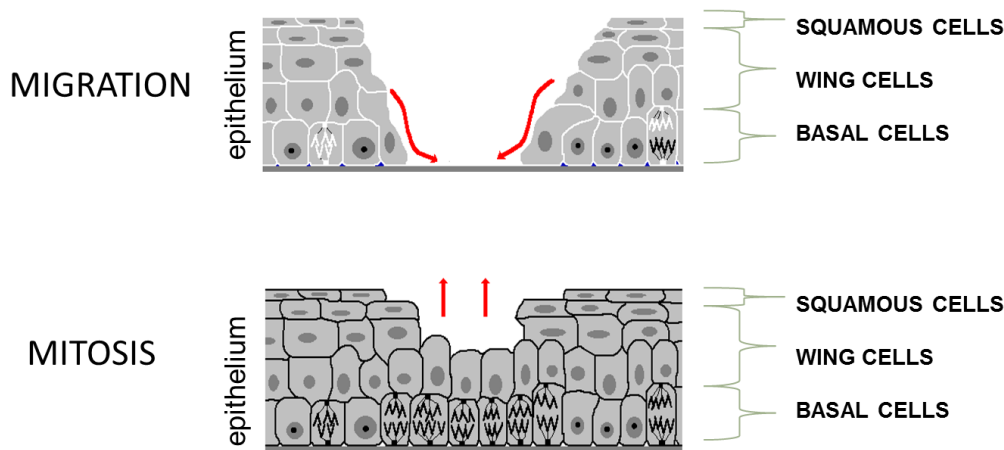


Figure 3. Schematic presentation of wound healing process. Wing cell migration and adhesion at the level of basal cells (upper panel), and the cell proliferation (lower panel).

B.1.2. Bowman's membrane

In the human cornea it is around 13-15 μm thick, what constitutes 2.34% of its thickness (Saude 1993; Almubrad and Akhtar 2011; DelMonte and Kim 2011), while in guinea pig measures about 2.2 μm (Cafaro, Ortiz et al. 2009). It is associated with the basal lamina of the epithelium and the boundary merges gradually with the stroma. It consists of dense collagen fibrils arranged randomly and more delicate than those in the stroma (Saude 1993), (Almubrad and Akhtar 2011). Bowman's layer is resistant to infections (Saude 1993) and helps the cornea maintain its shape (DelMonte and Kim 2011).

B.1.3. Stroma

Stroma provides 80-90% of the corneal thickness (reviewed by (Adler, Kaufman et al. 2011; DelMonte and Kim 2011)); and it varies depending on the species, being quite thin in different mice strains (70-90 μm), thicker in rabbits and humans (325-500 μm , respectively), and very thick in pigs and cows (1mm) (reviewed by (Adler, Kaufman et al. 2011)). In guinea pig the stroma constitutes approximately 75-80% of the total corneal thickness and measures approx. 165 μm (Cafaro, Ortiz et al. 2009).

The stroma predominantly is composed of water that is stabilized by an organized structural network of insoluble extracellular and cellular substances, collagen, keratocytes, proteoglycans, glycoproteins and salts (reviewed by (Adler, Kaufman et al. 2011)).

The corneal stroma is transparent, what is due to its uniform and well-arranged structure. It consists of extracellular matrix (ECM) with homogenously distributed collagen fibrils that are regularly packed within parallel running lamellae, between which are flattened keratocytes (Saude 1993; Jester 2008; Hassell and Birk 2010; Almubrad and Akhtar 2011). Keratocytes are the major cell type of the stroma and are involved in maintaining the ECM environment. Most of them reside in the anterior stroma and contain corneal crystallins, which are responsible for reducing backscatter of light from the keratocytes and maintaining corneal transparency (Jester, Moller-Pedersen et al. 1999; Jester 2008).

It is difficult for the stroma to regenerate. The process of stromal wound healing is slower and it can results in opacities (reviewed by (Saude 1993; Steele 1999)).

B.1.4. Descemet's membrane

Descemet's membrane is continuously secreted from the corneal endothelium along its basal surface since the 8th week of embryogenesis (DelMonte and Kim 2011). It gets thicker with age, being at birth 4 μm thick and at the end of the normal life span around 10-15 μm thick (reviewed by (Adler, Kaufman et al. 2011)). In the guinea pig the Descemet's membrane measures about 4 μm (Cafaro, Ortiz et al. 2009).

Descemet's membrane is highly extensible and it is composed of type IV and VIII collagen fibrils, the glycoproteins fibronectin, laminin and thrombospondin. It can regenerate and is resistant to infective agents (reviewed by (Adler, Kaufman et al. 2011)).

B.1.5. Endothelium

The endothelium is a high-permeability barrier (Adler, Kaufman et al. 2011), which constitutes a monolayer approximately 10 μm thick at birth (DelMonte and Kim 2011) The guinea pig's endothelium measures about 5 μm (Cafaro, Ortiz et al. 2009).

The endothelium consist of approximately 400,000 cells (reviewed by (Saude 1993)), which number continuously change throughout life (reviewed by (DelMonte and Kim 2011)).

Its primary function is maintenance of the corneal transparency by regulating corneal hydration and nutrition through uptight barrier and metabolic pump function. In healthy

corneas it prevents the bulk flow of fluids from the aqueous humor to the corneal stroma, but it still allows moderate diffusion of small nutrients, water and other metabolites to cross into the stroma through the intracellular spaces (reviewed by (Adler, Kaufman et al. 2011)).

The Endothelium doesn't have regenerative properties and its injury can lead to blindness (reviewed by (Saude 1993)). Endothelial cells have limited in vivo proliferation so they are most commonly involved in age-related or injury-related diseases (reviewed by (Adler, Kaufman et al. 2011)).

B.2. Innervation of the cornea

The trigeminal ganglion (TG) (Figure 4) communicates with the periphery through three branches: the ophthalmic, maxillary and mandibular. From them the ophthalmic division almost exclusively innervates the eyeball, hence, innervates the cornea. The cornea also receives sparse sensory innervation from the maxillary branch axons (reviewed by (Adler, Kaufman et al. 2011)). The ophthalmic branch of TG branches into the nasociliary (Figure 4), the frontal and the lachrymal nerves. The nasociliary nerve gives several branches that innervate the eye and the adjacent areas: two long ciliary nerves (Figure 4), which constitutes the major sensory output of the eye; the infratrochlear nerve innervating tissues around the eye and the lacrimal sac; the external nasal nerve; and the communicating branch to the ciliary ganglion (reviewed by (Adler, Kaufman et al. 2011)). The ciliary ganglion is parasympathetic ganglion, which sends 5-10 short ciliary nerves (Figure 4). In turn ciliary nerves carry parasympathetic fibers, sympathetic axons from the superior cervical ganglion, and the trigeminal sensory nerve fibers, which come from the communicating branch of the nasociliary nerve to the eye. This mixture of short ciliary nerves penetrates the sclera covering the eyeball around the optic nerve (reviewed by (Adler, Kaufman et al. 2011)).

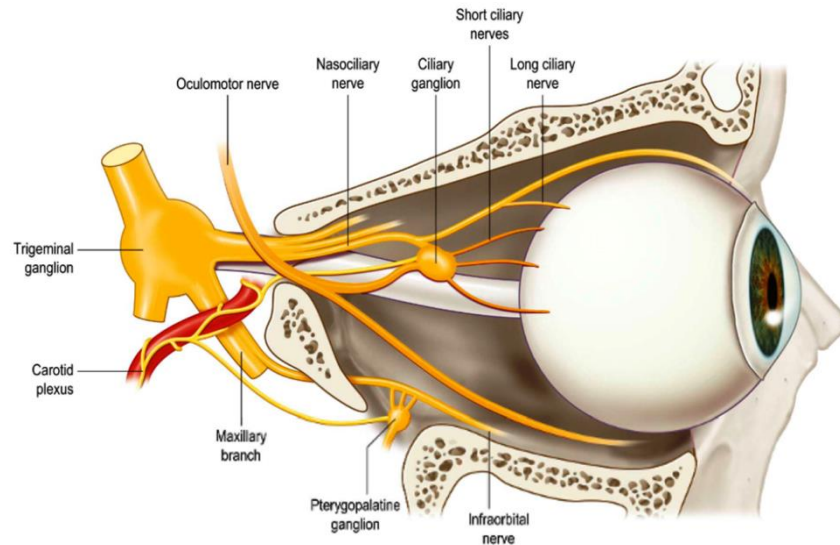


Figure 4. Innervation of the eye. Medial view of the orbit showing the sensory and autonomic nerves directed to the eye. The ophthalmic branch of the trigeminal ganglion gives the nasociliary nerve that sends long and short ciliary nerves to the eyeball, the last through the ciliary ganglion. Frontal and lacrimal nerves are not shown in this picture. The trigeminal maxillary branch gives the infraorbital nerve that innervates part of the eye and the lower lid. Sympathetic fibers from the superior cervical ganglion, traveling within the carotid plexus and parasympathetic branches of the ciliary and the pterygopalatine ganglia join short ciliary nerves. Taken from Belmonte *et al.*, 2011.

After penetrating the sclera long and short ciliary nerves containing a mixture of sensory, sympathetic and parasympathetic nerve fibers form a ring around the optic nerve. Ciliary nerves fascicles travel towards the cornea and give few collaterals providing the sparse innervation of the posterior part of the eye, and with travelling to the front part of the eye, they undergo repetitive branching innervating the ciliary body, the iris and the cornea. Finally most of the fibers form a series of ring meshwork of nerve fibers at the limbus around the cornea. A variable number of nerve trunks arising from the limbal plexus enter the corneal stroma (reviewed by (Adler, Kaufman et al. 2011)).

Cornea is supplied by sensory and autonomic innervation. Corneal nerves have many functions, like transduction of thermal, chemical or mechanical stimuli to the pain sensation, the maintenance healthy state of the cornea by avoiding of these painful stimuli and also exerting various nutritive effects on the cornea, which can be mediated by neuropeptides contained in peripheral nerve terminals (Gallar, Pozo et al. 1990). These effects provide the maintenance of epithelial cellular integrity, modulation of cell proliferation and mitosis,

stimulation of ions transport, and regulation of wound healing after corneal injuries (Marfurt 2000).

Human corneal epithelium contains approximately 5000-8000 of sensory nerve terminals per square millimeter of epithelium in rabbit (Rozsa and Beuerman 1982), and one terminal per 20 square micrometers in human (Schimmelpfennig 1982) (Marfurt 2000) what makes it the most dense and sensitive tissue in the human body.

B.2.1. Autonomic innervation

The autonomic nerve fibers consist of sympathetic fibers that derive from the superior cervical ganglion (SCG) and parasympathetic fibers that originate from the ciliary ganglion (McKenna and Lwigale 2011). Sympathetic nerves are concentrated in the anterior one-third of the stroma, however, overall sympathetic innervation density varies considerably among species (Marfurt 2000).

B.2.2. Sensory innervation

Sensory nerves are the majority of the nerves supplying cornea. They mainly derive from the ophthalmic division of the trigeminal nerve and have variety of functions, like causing the sensation of pain by mechanical, thermal and chemical stimulation of the cornea, which are essential for maintaining the corneal surface integrity (McKenna and Lwigale 2011).

Corneal trigeminal neurons constitute about 1.5% of the total number of trigeminal ganglion (TG) neurons and can be classified as myelinated (20% in the mouse) and unmyelinated (80% in the mouse) (Felipe, Gonzalez et al. 1999).

First sensory corneal nerve endings appear after the 5th gestational month. Sensory axons grow into the cornea from the surrounding nerve ring located in the limbal nerve plexus as nerve bundles. Nerve bundles are distributed uniformly and they extend radially inside the cornea, first innervating the periphery and then the entire stromal surface. Deeper stromal nerves provide the innervation of almost entire corneal surface, whereas the most superficial nerves which enter the stroma nearest to the epithelium mainly supply the periphery reviewed by (Adler, Kaufman et al. 2011).

B.2.3. Neurochemistry of corneal innervation

Neurons of trigeminal ganglion innervating the eyeball contain several neuropeptides (Figure 5), including calcitonin gene-related peptide (CGRP), which is present in about 50% of corneal neurons, the tachykinin substance P, which is present in about 20%, cholecystokinin, somatostatin, opioid peptides, pituitary adenylate cyclase activating peptide (PACAP), vasoactive intestinal peptide (VIP), galanin, neuropeptide (NPY), neuronal nitric oxide synthase (nNOS) (Tervo, Tervo et al. 1982; Felipe, Gonzalez et al. 1999; Müller, Marfurt et al. 2003), and tyrosine hydroxylase (TH) (Ivanusic, Wood et al. 2013).

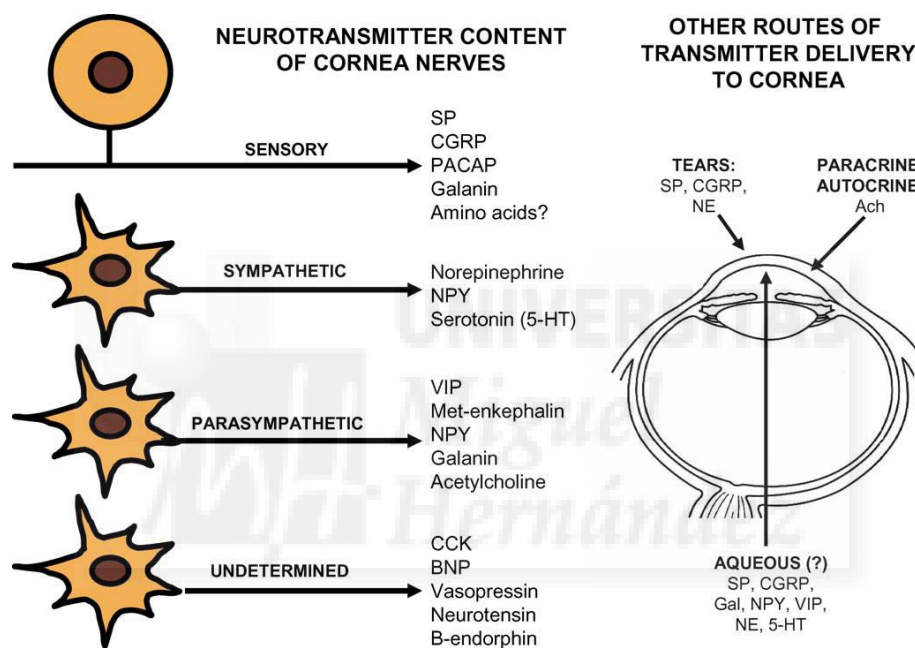


Figure 5. Neurochemistry of the corneal innervation and the pathways by which nerve transmitter substances reach the cornea. Taken from Müller *et al.*, 2003.

B.3. Architecture of corneal innervation

The corneal innervation is anatomically organized in limbal plexus and four levels of nerves (reviewed by (Adler, Kaufman et al. 2011)) (Figure 6, 7). It was described among different species of mammals, like in cat (Chan-Ling 1989; Marfurt, Kingsley et al. 1989), dog (Marfurt, Murphy et al. 2001), rat (Zander and Weddell 1951; Tervo and Tervo 1981; Marfurt, Kingsley et al. 1989; Marfurt and Echtenkamp 1995; Jones and Marfurt 1998; Dvorscak and Marfurt 2008), mouse (McKenna and Lwigale 2011; Wang, Fu et al. 2012; Ivanusic, Wood et al. 2013), rabbit (Zander and Weddell 1951; Marfurt, Kingsley et al. 1989), guinea pig (Zander

and Weddell 1951; Ivanusic, Wood et al. 2013), monkey (Zander and Weddell 1951; Marfurt, Kingsley et al. 1989), and human (Zander and Weddell 1951; Müller, Pels et al. 1996; Müller, Vrensen et al. 1997; Al-Aqaba, Fares et al. 2010; He, Bazan et al. 2010; Marfurt, Cox et al. 2010; Turuwhenua, Patel et al. 2012).

Corneal nerves are not static structures. Deep stromal nerve fiber bundles maintain a relatively constant position and configuration within the cornea while the corneal subbasal nerve plexus, and especially intraepithelial nerve terminals are subjected to a continuous elongation and terminal rearrangement throughout life (Harris and Purves 1989; Dvorscak and Marfurt 2008; Wang, Fu et al. 2012).

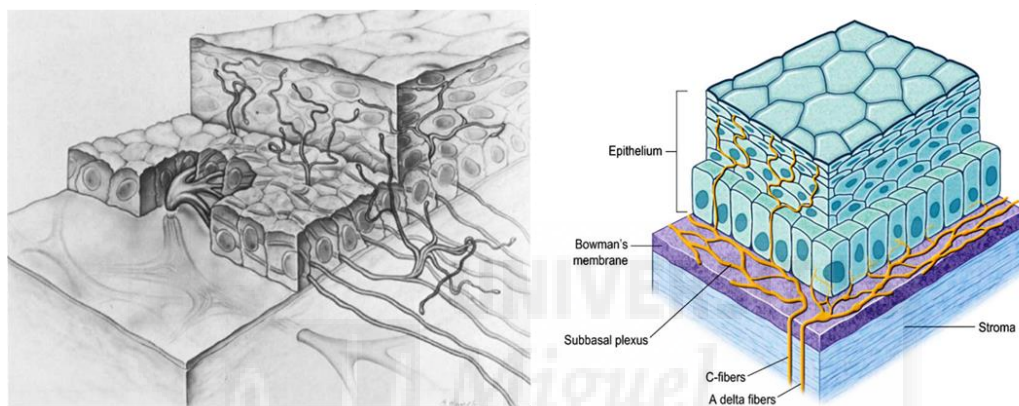


Figure 6. Graphical illustration of the organizational design of the innervation pattern of the corneal epithelium. On the left the construction of the figure, which was based on *camara lucida* drawings and photomicrographs taken at successive focal levels. The size of the axon terminals relative to the dimensions of the epithelial cell was exaggerated for the sake of clarity. Taken from Roza *et al.*, 1982. On the right the architecture of the nerve bundles in the subbasal plexus. Taken from Dawson *et al.*, 2011.

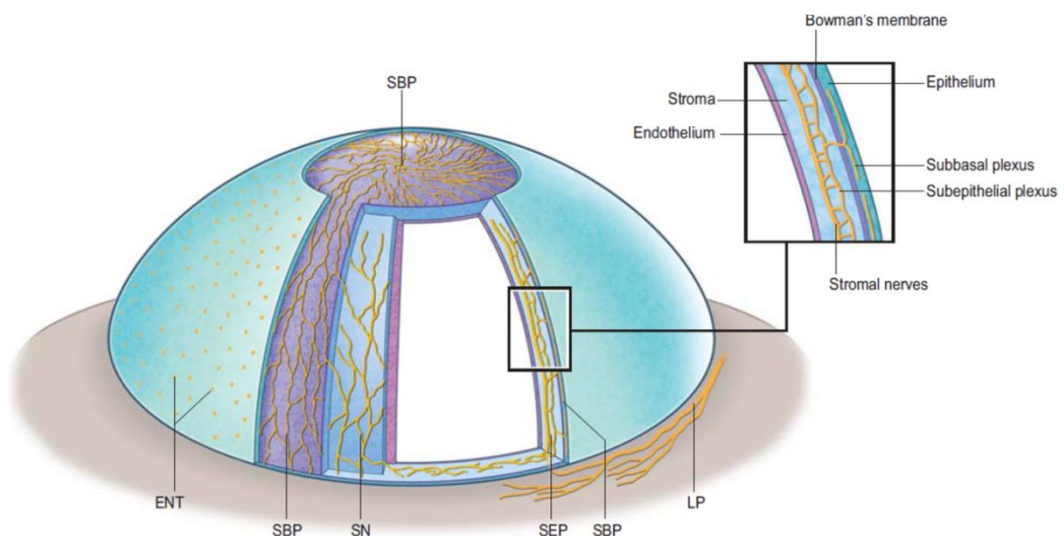


Figure 7. Schematic distribution of nerves in the cornea. From the limbal plexus (LP), stromal nerve trunks (SN) penetrate the stroma radially and divide dichotomously to form the subepithelial plexus (SEP). Branches of this plexus ascend towards the epithelium, traverse Bowman's membrane and form the subbasal plexus (SBP) between the epithelium basal layer and its basal lamina, where nerve branches run horizontally as nerve leashes, which in turn give rise to intraepithelial nerve terminals (ENT). Taken from Belmonte *et al.*, 2011.

B.3.1. Limbal plexus

The corneal innervation occurs through a precise temporal and spatial series of stages, from growth of the nerves from ophthalmic branch of trigeminal ganglion (OTG) and their attraction towards the cornea. Nerves before entering the cornea form a surrounding ring that might have role in the uniform distribution of corneal innervation (Kubilus and Linsenmayer 2010).

This ring consists of the series of nerve fibers that form pericorneal limbal plexus (LP) (Figure 7) and are the mixtures of sensory and autonomic nerves (Marfurt 2000). The sensory and autonomic nerves enter the peripheral cornea in one or several planes: most of them penetrate at about midstromal level; other, smaller nerve fascicles enter the cornea in the episcleral and conjunctival planes to innervate the perilimbal and peripheral corneal zones (Zander and Weddell 1951).

B.3.2. Stromal plexus

The anatomy of the nerve bundles radially entering the corneal stroma is quite similar among mammals varying only in their number (Zander and Weddell 1951; Marfurt, Cox et al. 2010) (Figure 8). Unlike chick, rat, and humans, where the stroma is radially innervated at regular intervals (Figure 9), mouse stromal innervation is provided by nerve bundles growing directly into the cornea from four quadrants, without forming a pericorneal nerve ring, and branching irregularly to cover the entire cornea (for details see (McKenna and Lwigale 2011)).

Soon after entering the corneal stroma, the main bundles branch immediately and run within the stroma as ribbon-like fascicles enclosed by a basal lamina and Schwann cells (Figure 8). Myelinated axons lose their myelin sheath within a millimeter after penetrating the stroma what is necessary to maintain corneal transparency (Müller, Marfurt et al. 2003).

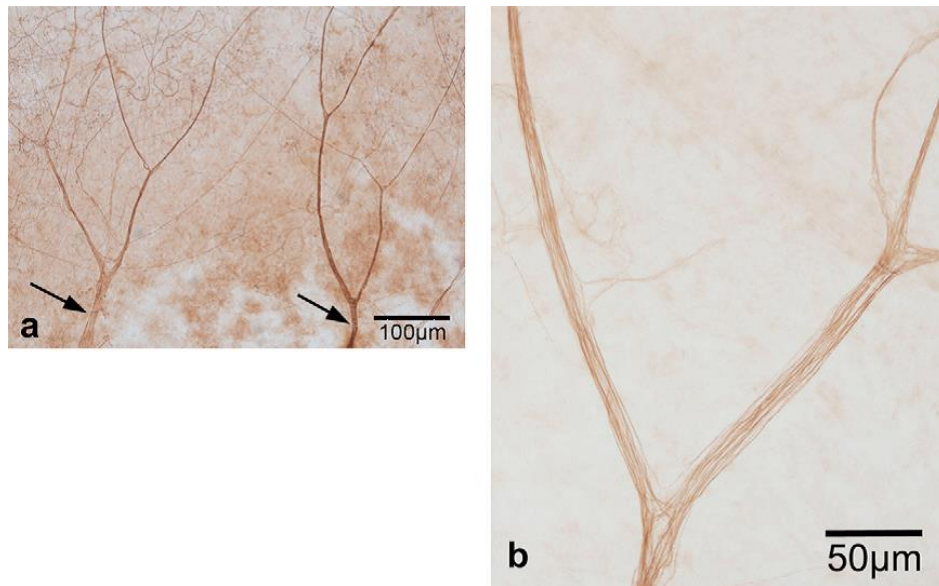


Figure 8. Human main stromal bundles (arrows) entering the peripheral cornea at the corneoscleral limbus in an anterior-cornea whole mount (a). High magnification image of a main stromal bundle in a 100 µm thick section (b). Taken from Marfurt *et al.*, 2010.

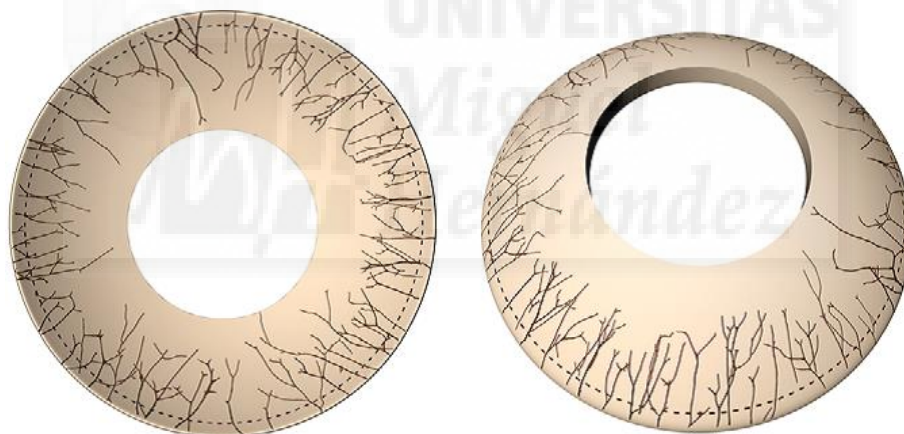


Figure 9. Main stromal nerve bundles enter the peripheral cornea uniformly from all directions in human. The dashed line indicates the approximate location of the corneoscleral limbus. Taken from Marfurt *et al.*, 2010.

Each stromal nerve bundle branches repetitively to varying numbers of progressively smaller stromal nerves that subdivide and rejoin with one another continuously concentrating in the anterior one-third of the stroma to form a dense subepithelial nerve plexus (Marfurt 2000; Marfurt, Cox et al. 2010). The subepithelial nerve plexus is most dense in the peripheral cornea and its density and anatomical complexity decrease towards the central cornea. A few nerve fibers in all areas of the cornea terminated in the stroma as free nerve endings (Zander and

Weddell 1951; Chan-Ling 1989; Marfurt, Cox et al. 2010) (Figure 10). The presence of nerve terminals in the stroma induced some speculations about their transduction functions like detection of lamellar shearing forces (Lim and Ruskell 1978) or generation of pain sensations in response to acute increment of intraocular pressure (Zuazo, Ibañez et al. 1986).

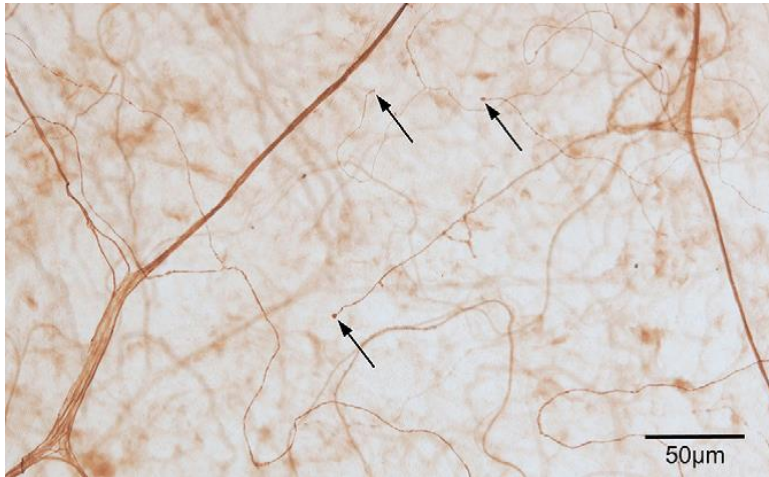


Figure 10. Stromal free nerve endings (arrows) of human cornea. Taken from Marfurt *et al.*, 2010.

B.3.3. Subepithelial nerve plexus

The corneal subepithelial nerve plexus (SEP) is a dense network of nerves that comes from the most superficial layer of the anterior stromal nerve plexus, located in a narrow band of stroma that immediately traverse Bowman's membrane (Marfurt, Cox et al. 2010) (Figure 7). The density of nerves in this plexus is higher in the peripheral than in the central cornea which receives most of its innervation from long subbasal nerves that enter the peripheral cornea directly from the limbal plexus (reviewed by (Adler, Kaufman et al. 2011)).

This nerve plexus contains two different types of nerve fibers. There is a modest population of straight or curvilinear nerves that penetrate Bowman's membrane mainly in the peripheral and intermediate cornea, shed the Schwann cell coating, bend at 90° angle and divide, each into 2-20 thinner nerve fascicles that continue to the corneal epithelium as the subbasal nerve plexus. The second is more abundant and anatomically complex population of tortuous, highly anastomotic nerves located immediately beneath Bowman's membrane without penetrating it towards the corneal epithelium (Marfurt, Cox et al. 2010).

B.3.4. Subbasal nerve plexus

Epithelial innervation is supplied by two nerve networks. Sensory nerves enter the overlying corneal epithelium either from the subepithelial plexus or directly from the conjunctiva (He, Bazan et al. 2010) (Figure 11).

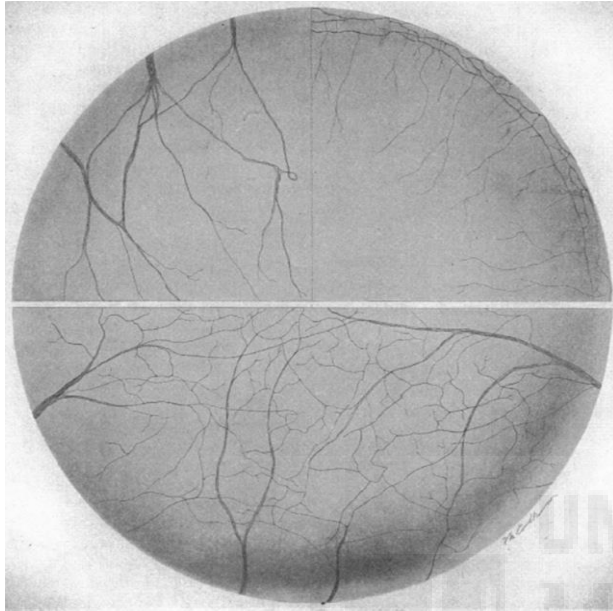


Figure 11. The arrangement of nerve bundles entering periphery of the cornea in different planes. The drawing is based on the observation of the rabbits' corneas. The nerve bundles enter the cornea from the scleral position (the upper left quadrant) and from the episcleral and subconjunctival positions (the upper right quadrant). In the lower half of the drawing is shown the manner in which the plexiform pattern of nerve fibers arises from the nerve bundles. Taken from Zander and Weddell, 1951.

Immediately after penetrating Bowman's membrane and shedding the Schwann cell (Müller, Vrensen et al. 1997), each stromal nerve branch gives several side branches, each containing 1-20 individual axons (Marfurt, Cox et al. 2010) that course parallel to the ocular surface near the interface of Bowman's membrane and the basal epithelium (Figure 12). These axons can be characterized by two types: complex basal leashes and simple, vertically oriented branch-like structures (Rozsa and Beuerman 1982).

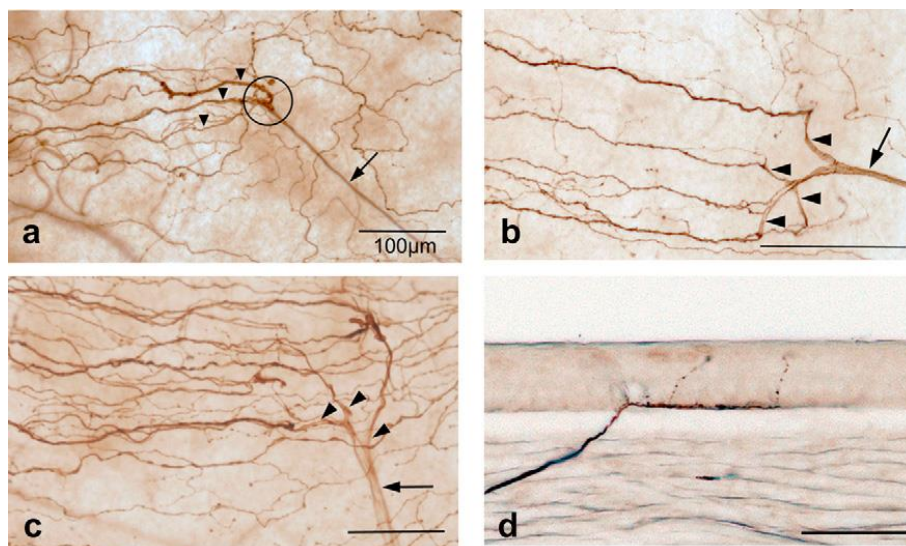


Figure 12. Human stromal nerve penetrations through Bowman's membrane in anterior-cornea whole mounts (a-c) and in a 30 mm-thick perpendicular section (d). A straight stromal nerve (arrow) penetrates Bowman's membrane (open circle) and branches into multiple subbasal nerves (arrowheads) (a). Some stromal nerves (arrows) split into multiple branches (arrowheads) immediately prior to, or while penetrating, Bowman's membrane. Each branch then gives rise to one or more subbasal nerves (b, c). A stromal nerve (arrow) penetrates Bowman's membrane and continues as a subbasal nerve (arrowheads) (d). Taken from Marfurt *et al.*, 2010.

The term “epithelial leash” is defined as a group of subbasal nerves that derives from the same parent anterior stromal nerve (Rozsa and Beuerman 1982; Schimmelpfennig 1982; Chan-Ling 1989) (Figure 13 a, b). In this thesis the group of subbasal nerves is called “subbasal nerve leash”, instead of “epithelial leash”, avoiding confusion with another group of nerves, which are located above in the epithelium. These leash formations are a unique neuroanatomical structures found only in the cornea (Marfurt 2000).

In the central cornea nerve fibers in adjacent leashes interconnect repeatedly and form a dense, homogenous subbasal nerve plexus (Schimmelpfennig 1982; Müller, Pels et al. 1996) and they are no longer recognizable as individual leashes. However, subbasal leashes in the peripheral cornea are less numerous, more widely separated (Marfurt, Cox et al. 2010). Individual subbasal nerve axons travel as far as several hundred microns in cats and rats (Chan-Ling 1989; Jones and Marfurt 1998) and up to 8 mm in humans (Marfurt, Cox et al. 2010).

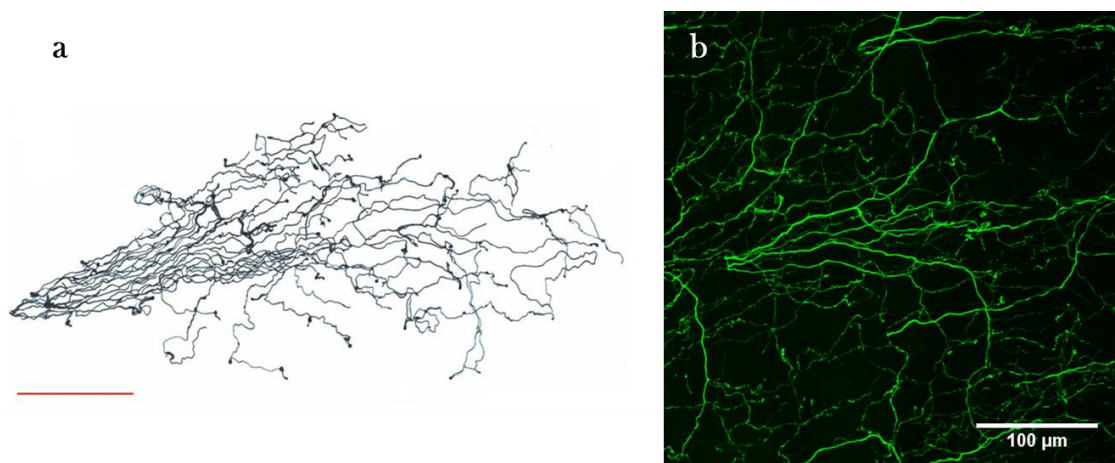
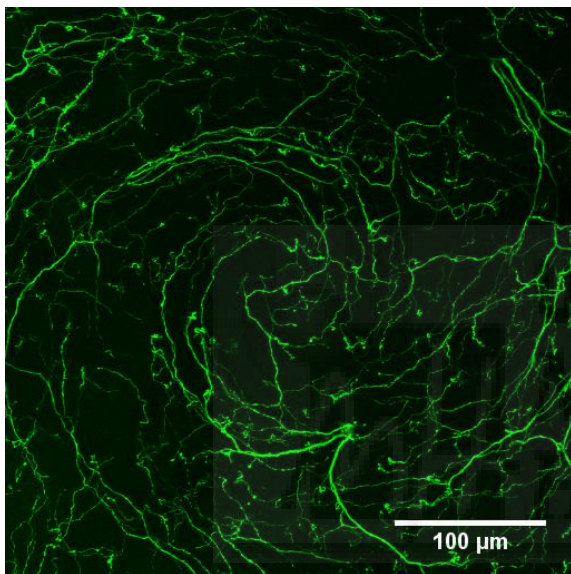


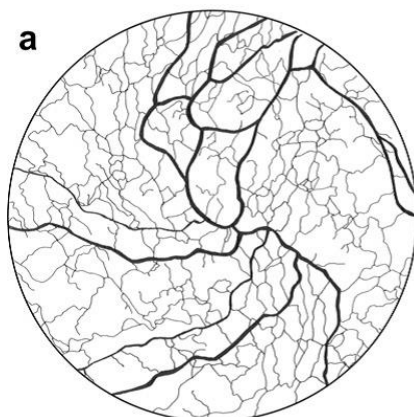
Figure 13. Subbasal nerve leash in a guinea pig. *Camara lucida* drawing (a), fluorescent staining (b). Bars=100 μm.

Subbasal nerve plexus forms a whorl-like, spiral pattern of nerve fibers, the center of which is called the vortex (Figure 14). The vortex was described in the adult mouse (McKenna and Lwigale 2011; Wang, Fu et al. 2012; Ivanusic, Wood et al. 2013), rat (Dvorscak and Marfurt 2008), and human (Marfurt, Cox et al. 2010) (Figure 15). The mechanisms that control the formation of the vortex remain unclear. It was thought to appear due to the centripetal movement of basal epithelial cells in response to a chemotropic guidance, to electromagnetic cues, and/or to population pressures (Nagasaki and Zhao 2003). However, it was shown that the centripetal projections of nerves is independent of epithelial cells migration (Leiper, Ou et al. 2009; McKenna and Lwigale 2011).



UNIVERSITAS
Miguel
León

Figure 14. Fluorescent staining of the vortex in the guinea pig cornea. Bar=100 μ m.



b



Figure 15. Human subbasal nerve vortices. Subbasal nerve fibers in some corneas rotate counterclockwise (a) while others rotate clockwise (b) about the center of the vortex. The circular region illustrated in “a” is 400 μm in diameter. In b, two thick subbasal nerves penetrate the epithelium (arrows) near the center of the vortex and arch conspicuously in a clockwise direction. Taken from Marfurt *et al.*, 2010.

B.3.5. Intraepithelial nerve terminals

The subbasal nerves run horizontally through the basal epithelium giving rise to the single fibers that split off and turn 90° vertically as thin and beaded terminal axons with a modes additional branching, which ascend between the epithelial cells to end as free nerve endings (reviewed by (Adler, Kaufman *et al.* 2011). These terminal axons are called intraepithelial nerve terminals (Marfurt, Cox *et al.* 2010) or simply nerve terminals (Dvorscak and Marfurt 2008; He, Bazan *et al.* 2010; Ivanusic, Wood *et al.* 2013) (Figure 16). The term nerve terminal refers to the entire epithelial axon, from its points of origin in subbasal nerve, and includes all of its collateral branches and terminal expansions. Intraepithelial terminals are distributed throughout all layers of the corneal epithelium, extending up to a few microns of the corneal surface, but being especially numerous in the wing and basal cell layers (Rozsa and Beuerman 1982) (Figure 17 a, b).

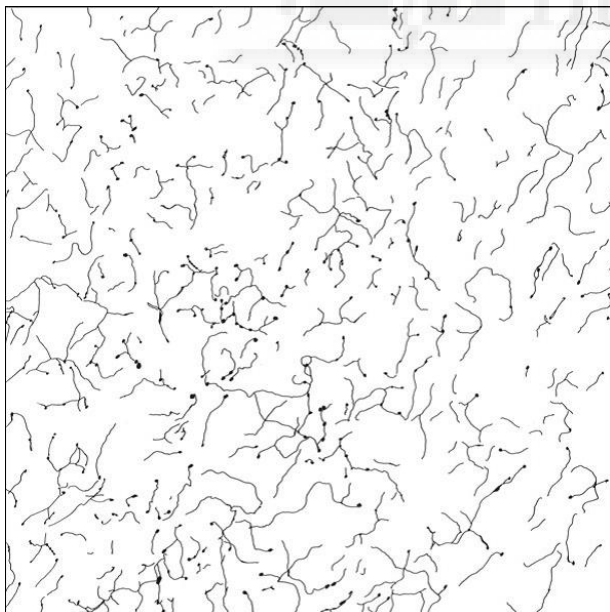


Figure 16. High magnification schematic line drawing of intraepithelial nerve terminals in the wing and squamous cell layers of a 1 mm^2 area of the human central cornea. Taken from Marfurt *et al.*, 2010.

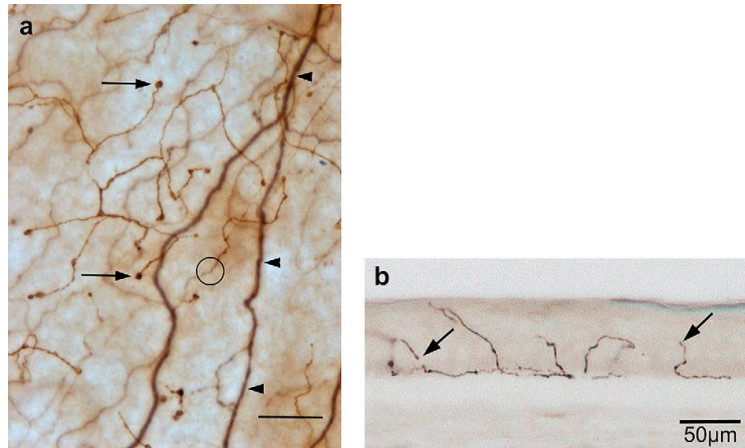


Figure 17. Intraepithelial nerve terminals (a), and nerve terminals presented in a perpendicular, 30 µm-thick section (b). Nerve terminals originate (circle) exclusively as branches of subbasal nerves (arrowheads, deeper plane of focus). Nerve terminals in the suprabasal epithelium often possess multiple collateral branches, and each branch is capped by a bulbous terminal expansion (arrows), (a). Nerve terminals end blindly as free nerve endings (arrows) in all layers of the corneal epithelium (b). Taken from Marfurt *et al.*, 2010.

Nerve terminals vary considerably in total length, predominant directional orientations and morphological complexity (Marfurt, Cox et al. 2010). According to the pattern of terminal branching, there are three different types of nerve endings in the corneal epithelium: simple, ramifying and complex (Figure. 18).

Simple terminals do not branch after leaving the subbasal nerves and end with a single, bulbar swelling in the squamous cell layer at the superficial surface of the epithelium (Figure 18 A, D, G). They are more seen in the central cornea. Immunohistochemical study showed that fibers terminated in the basal epithelium and the superficial part of epithelium, have simple endings which are CGRP and SP immunoreactive (Ivanusic, Wood et al. 2013). Since CGRP is released upon application to the cornea of heat or chemical irritants (Belmonte, Carmen Acosta et al. 2004) it can suggest that those peptidergic simple fibers are polymodal nociceptors (Ivanusic, Wood et al. 2013).

Ramifying terminals branch within the squamous cell layer of the epithelium into a number (3-4) of horizontal fibers that run parallel to the surface for up to 100 µm. Each of these branches end in a single bulbar swelling similar to those associated with simple terminals (Figure 18 B, E, H).. Ramifying terminals occur more in the peripheral cornea, where the horizontal fibers extend for longer distances than in the central cornea (Ivanusic, Wood et al. 2013).

The axons forming the complex terminals start to branch within the wing cells layer of the cornea and form a cluster of highly branched fibers that have endings in both the wing and squamous cell layers. Each of the many branches in these complex terminals has multiple bulbar endings, and many of these bulbar endings are larger than those associated with the simple and the ramifying terminals (Figure 18, C, F, I). Complex terminals are found in both the central and peripheral parts of the cornea, but their complexity and size is greatest most peripherally at the corneo-scleral limbus (Ivanusic, Wood et al. 2013).

It was found that the populations of complex nerve terminals are immunoreactive to transient receptor potential cation channel subfamily M member 8 (TRPM8) (Ivanusic, Wood et al. 2013). TRPM8 is a nonselective, calcium-permeable, cation channel, which is activated by cooling and menthol application to the cornea. It was seen that this receptor is important for cold sensation (McKemy, Neuhauser et al. 2002; Parra, Madrid et al. 2010), what supports the idea that complex endings in the corneal epithelium may be cold thermoreceptors (Ivanusic, Wood et al. 2013).

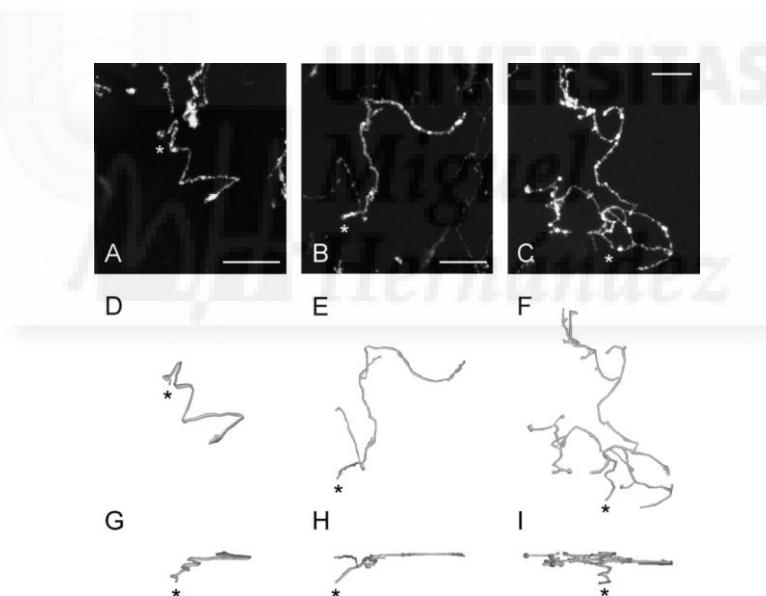


Figure 18. Reconstructions of superficial nerve terminals in the mouse corneal epithelium showing examples of simple (A, D, G), ramifying (B, E, H) and complex (C, F, I) nerve terminals. A-C, projected z-series of high power (63x objective) confocal images of corneal epithelium, labeled with antibodies directed against PGP9.5. D-F: Surface view of the 3D reconstructions of single nerve fiber terminals through an entire z-series, from the point at which they leave a subbasal nerve in the basal epithelium (asterisks), through to their endings at the surface of corneal epithelium. G-I: Side view of the same 3D reconstructions. Reconstructions are reproduced to the same scale as the confocal images. Scale bars=10 μ m. Taken from Ivanusic *et al.*, 2013.

There is close relationship between nerve terminals and epithelial cells. The epithelial cells membranes, covering the nerve terminal, show invaginations that may eventually completely surround the nerve ending. The nerve terminal branching in the corneal epithelium has punctual structures, which may be specialized nerve endings such as synapse-like structures. This relationship could suggest bidirectional exchange of diffusible substances between both structures (Müller, Pels et al. 1996), (Müller, Marfurt et al. 2003), (Kubilus and Linsenmayer 2010). This close contact also allows nerve ending to detect changes in epithelial cell shape or volume, such as those produced by ocular surface desiccation or swelling (reviewed by (Adler, Kaufman et al. 2011)).

The corneal epithelium is the most densely innervated surface tissue in the body. The number of corneal nerve endings varies among species (Rozsa and Beuerman 1982) and changes as a function of life (Dvorscak and Marfurt 2008; Wang, Fu et al. 2012) and in several ocular pathologies, but it is estimated from 3500 to 7000 nerve terminals per square millimeter dense in human (reviewed by (Adler, Kaufman et al. 2011)).

This rich innervation provides the cornea with a highly sensitive detection system, and it has been hypothesized that injury of a single epithelial cell may be sufficient to trigger pain perception (Müller, Vrensen et al. 1997).

Since nerve endings are the parts of the nerve fiber, which is responsible for the sensory stimuli transduction in to the nerve signals, the density of nerve endings is directly proportional to corneal sensitivity (Chan-Ling 1989; Belmonte, Carmen Acosta et al. 2004). Individual receptive fields of corneal sensory fibers range in size from less than 1 mm² to as much as 50 mm², and may cover up to 25% of the corneal surface (Adler, Kaufman et al. 2011).

B.4. Sensory innervation: functional nerves classification

Corneal neurons can be classified as thin myelinated A-delta type or unmyelinated C type, which axons terminate peripherally as free nerve endings called nociceptors. In the axons of A-delta neurons the conduction velocity of nerve impulses is higher than in C neurons (Belmonte and Giraldez 1981; Belmonte, Gallar et al. 1991; Gallar, Pozo et al. 1993). A-delta and C neurons also differ in some passive and active electrophysiological properties of their neuronal membrane, that in turn determine the impulse firing characteristic of the neuron (López de Armentia, Cabanes et al. 2000).

Corneal nerves are morphologically (Ivanusic, Wood et al. 2013) and functionally heterogeneous, they exhibit differences in chemical composition or electrophysiological

properties. Corneal neurons may contain several neuropeptides (Müller, Marfurt et al. 2003), in particular calcitonin gene-related peptide (CGRP, 60%) and substance P (SP, 20%) (Felipe, Gonzalez et al. 1999), and express a variable number of membrane proteins that act as receptor molecules for neurotransmitters, neuromodulators, cytokines, and growth factors, as well as ion channel proteins that regulate neuronal excitability (Belmonte, Aracil et al. 2004). The functional differences among corneal sensory fibers were confirmed in electrophysiological studies (Belmonte and Giraldez 1981; Belmonte, Gallar et al. 1991; Gallar, Pozo et al. 1993; MacIver and Tanelian 1993; Brock, McLachlan et al. 1998; Brock, Pianova et al. 2001).

Different types of corneal neurons, due to transduction properties of the peripheral terminals, can be activated by diverse modalities of stimuli, and therefore elicit varied kind of sensation (Acosta, Belmonte et al. 2001) (Figure 19).

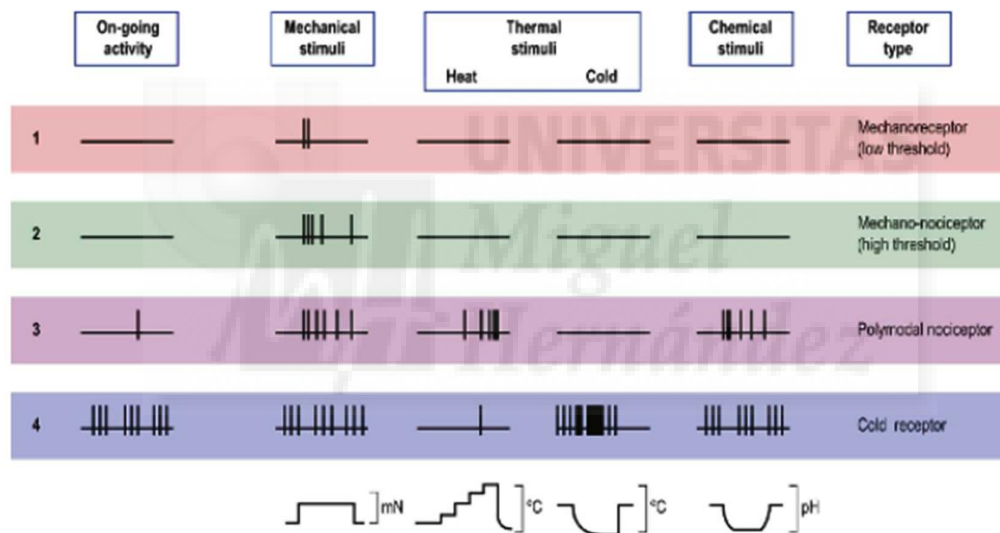


Figure 19. Schematic representation of the types of sensory neurons innervating the eye. It shows the characteristics of the impulse discharge, either spontaneous (on-going activity) or evoked by different types of stimuli, and they have been represented together with the functional classification of the peripheral terminals (receptor type). Taken from Belmonte *et al.*, 2011.

B.4.1. Mechanoreceptors

About 15-20% of thin myelinated, fast conducting A-delta corneal fibers are called mechanoreceptors. The name of this type of corneal receptors can indicate that they are

activated exclusively by mechanical forces of a magnitude close to that required to damage corneal epithelial cells (Belmonte, Aracil et al. 2004).

Mechano-nociceptors are the fast conducting, phasic and rapidly-adapting receptors, because they produce a short lasting impulse discharge in response to sustained stimuli. Therefore they inform about the presence and velocity of change of the stimulus, rather than its intensity and duration (Belmonte and Giraldez 1981; Belmonte, Gallar et al. 1991; Gallar, Pozo et al. 1993). The threshold force required to activate them is apparently low (about 0.6 mN) (reviewed by (Belmonte, Carmen Acosta et al. 2004)).

The characteristic of mechanoreceptors can point their possible contribution to the acute, sharp pain sensations produced by mechanical contact with the corneal surface (Belmonte and Giraldez 1981; Gallar, Pozo et al. 1993).

B.4.2. Polymodal nociceptors

Polymodal nociceptors constitute the majority of corneal sensory fibers (about 70%), they are thin myelinated A-delta neurons, but the most of them they are slow-conducting C type neurons (reviewed by (Belmonte, Aracil et al. 2004)).

They are activated by near-noxious mechanical energy, but their threshold is slightly lower than mechanoreceptors. Moreover they respond to heat or noxious cold, exogenous chemical irritants and endogenous chemical mediators released by damaged corneal tissue, by resistant inflammatory cells or originated from the plasma leaking from limbal vessels (Chen, Gallar et al. 1997). They also respond to increasing concentrations of CO₂, which leads to drops of pH; pH reductions often occur in inflamed tissues (reviewed by (Belmonte, Carmen Acosta et al. 2004)). During inflammation, locally released mediators stimulate polymodal nociceptors, what leads to continuous firing and produces sustained sensation of pain (Acosta, Luna et al. 2013; Acosta, Luna et al. 2014). Additionally, a fraction of the polymodal nociceptor group increases their firing rate when corneal temperature is reduced below 29°C (Belmonte and Giraldez 1981; Acosta, Belmonte et al. 2001).

Polymodal nerve endings are activated tonically by mechanical forces, but also sustained mechanical, thermal, or chemical stimuli produce a continuous, irregular repetitive discharge of nerve impulses, which persists as long as the stimulus is maintained, which is proportional to the intensity of the stimulus. Therefore, the impulse discharge signals the presence of a noxious stimulus, and moreover encodes its intensity and duration (reviewed by (Belmonte, Aracil et al. 2004)).

Polymodally nociceptors in response to the stimulus may elicit the sensation of the “fast”, immediate pain, which is provided by A-delta type neurons. The sensation of dull and long-lasting pain contributes also to A-delta type neurons, but in bigger part due to the activity of C-polymodal nociceptor fiber.

A prominent feature of polymodal nociceptors is sensitization. Sensitizing polymodal nociceptors develop an irregular low frequency impulse activity long after stimulation has disappeared. Sensitization is a decrease in threshold and an increase in the firing frequency of the nociceptors in response to the new stimulus, often accompanied by the development of ongoing activity (Bessou and Perl 1969; Belmonte and Giraldez 1981). Sensitization of the polymodal nociceptors innervating injured and/or inflamed ocular tissues is the origin of spontaneous pain and of enhanced pain in response to stimuli at the injured area (reviewed by (Belmonte, Aracil et al. 2004) .

B.4.3. Cold thermoreceptors

Cold thermoreceptors are another type of nerves, which represent 10-15% of the total population of corneal sensory fibers and they correspond to A-delta and C-fibers (Belmonte, Aracil et al. 2004).

The main feature of cold thermoreceptors is that they display rhythmic ongoing discharge of nerve impulses, often in burst at rest (Carr, Pianova et al. 2003) and increase their firing rate when the normal temperature of corneal surface, which is 33-34°C, decreases. They are able to detect small temperature variations of 0.1°C or less (Gallar, Pozo et al. 1993; Carr, Pianova et al. 2003), what allows the perception of the temperature reductions in the cornea, which evoke conscious sensations of cooling (Acosta, Belmonte et al. 2001; Murphy, Patel et al. 2001). Cold receptor fibers are also transiently silenced upon warming (Gallar, Pozo et al. 1993).

Corneal cold receptor fibers respond by increasing their frequency in response to the cooling of the corneal surface due to evaporation or application of cold solutions or cold air also (Gallar, Pozo et al. 1993; Carr, Pianova et al. 2003).

Cold thermoreceptors encode with their firing frequency the speed and magnitude of temperature reductions at the ocular surface as well as the final static temperature (Belmonte and Gallar 2011). Also the psychophysical studies performed using corneal esthesiometry in human subjects have shown the ability of discrimination corneal temperature drops of 1-2°C below basal level (Acosta, Belmonte et al. 2001; Acosta, Tan et al. 2001).

Lately it was shown, that cold thermoreceptors have also a function in signaling and maintaining ocular surface wetness through detecting small changes (the rate of $0.3^{\circ}/s$) in the corneal temperature during the interblink tear evaporation, thus, providing the basal tear secretion (Parra, Madrid et al. 2010; Belmonte and Gallar 2011).

C. Protective mechanisms of the eye surface

C.1. Blinking

Blinking plays a role in the maintenance of the humidity of the eye surface, in the drainage of tears, expression of lipids from Meibomian glands and spreading of tear lipids across the precorneal film, thus, it supports the integrity of the ocular surface. Blinking may be classified as reflex, spontaneous or voluntary (reviewed by (ACOSTA, GALLAR et al. 1999)).

Reflex blinking is a physiological protective response to specific tactile, visual or auditory stimuli. The main tactile input is from stimulation of the ophthalmic division of the trigeminal nerve, particularly the corneal surface, although any painful stimulus from any dermatome can lead to reflex blinking.

Spontaneous blinking is essentially independent of external factors and might be initiated by a decrease in the temperature of the ocular surface and under normal conditions tear evaporation, that provokes temperature decrease and hence is a stimulus for blinking (Tsubota 1998). Also spontaneous blinking may be controlled in part by a corneal reflex evoked by desiccation of the corneal surface or by reduction of corneal temperature (ACOSTA, GALLAR et al. 1999).

Human blinking is often compared to that in other animals, and averages 15 ± 20 times per min under relaxed conditions (reviewed by (Tsubota 1998)). The rate of blinking is intrinsic to the individual and the species and is influenced by the background levels of afferent signal from the ocular surface (Elder and Dart 2000).

Local ocular surface reflexes, and environmental factors that affect them, are the principal determinants of blink rate, but can be affected also by reading, other visual tasks (ACOSTA, GALLAR et al. 1999) and other cognitive functions (reviewed by (Tsubota 1998)).

Lid movements during the reflex and spontaneous blinking exhibit different latencies, velocities, durations, amplitudes and strength, suggesting that neural circuits which control them may differ in part.

C.2. Tearing

Tear film covers the ocular surface and constitutes the interface between the eye superficies and the external environment. It is essential for the health and protection of the ocular surface and for clear vision as the tear film is the first refractive surface of the eye. It maintains the humidity of the cornea, permits gas exchange between the air and epithelium and also constitutes a barrier defending from viruses and bacteria. Moreover, because of the presence of metabolites, growth factors and enzymes in the tear film, it maintains the cornea healthy and transparent (Walcott 1998).

Apart from being constantly present on the ocular surface, tear secretion may be associated with emotional upset, vomiting, coughing, and yawning. Therefore, there were recognized two types of tearing: basal and reflex. Basal tears are considered to arise from subtle stimulation of the anterior eye such as cooling and drying caused by evaporation. Reflex tearing is produced by stronger, noxious stimulation of the ocular and extraocular tissues such as the nasal mucosa (Hirata and Meng 2010). It can be assumed, that sensory nerves in cornea and conjunctiva are activated by mechanical, chemical and thermal stimuli that in turn activate the efferent parasympathetic and sympathetic nerves, which innervate the lacrimal gland and the conjunctival goblet cells, and cause mucous and fluid secretion (reviewed by (Adler, Kaufman et al. 2011)).

C.2.1. Tear film composition

The tear film is a complex mixture of secretions from multiple tissues and epithelia and consists of 4 layers: the innermost glycocalyx, the mucous layer, aqueous layer and outermost lipid layer (reviewed by(Adler, Kaufman et al. 2011)) (Figure 20).

The tear film is produced by the ocular surface epithelia and adnexa and the secretion of both must be coordinated, likewise it is balanced by drainage and evaporation. Regulation of mucous and aqueous layers, secretion is provided by neural reflexes, whereas lipid layer is regulated by release of pre-secreted meibomian gland lipids upon blinking (reviewed by (Adler, Kaufman et al. 2011)).

The innermost glycocalyx layer consists of network of polysaccharides that project from cellular surfaces microvilli of apical plasma membrane of the superficial cell layer (Nichols, Dawson et al. 1983) (Figure 20). The most important component of glycocalyx is mucins which are divided into secreted and membrane-spanning categories. Membrane-spanning mucins are

part of the glycocalyx. Secreted mucins form large gel-forming molecules that are secreted by goblet cells of conjunctiva, and small soluble mucins secreted by the lacrimal gland (Gipson and ARGÜESO 2003).

The overlying mucous layer consists mainly of the gel-forming mucin synthesized and secreted by conjunctival goblet cells (Figure 20). These mucins serve as wetting factors, which maintain the apical epithelia hydrated (Gipson and ARGÜESO 2003).

Aqueous layer, in turn, is produced by the main lacrimal gland; however other surface epithelia, like conjunctiva, accessory lacrimal glands also contribute to this layer of the tear film (Figure 20). Accessory lacrimal glands are similar to the main lacrimal gland and are placed in the conjunctiva. Aqueous tear layer is isotonic, in human and rabbit it is 300 mOsm. The electrolyte composition is similar to plasma except that it has a decreased concentration of sodium ions and increased concentration of chloride and potassium ions (Walcott 1998); small changes in osmolarity or electrolyte composition leads to aqueous deficiency dry eye, therefore it is critical to the health of the ocular surface. Aqueous layer also consists in antibacterial proteins like lysozyme, lactoferrin, secretory IgA, and lipocalin, some growth factors, lacritin, and surfactant proteins A-D (Johnson and Murphy 2004). Reflex secretion of the aqueous layers helps to wash away noxious substances and particulates into the drainage duct. Also the buffer system of the fluid helps to protect against changes in pH. Thus, the aqueous layer has many functions critical to the health and defense of the ocular surface from the environment (reviewed by (Adler, Kaufman et al. 2011).

Lipid layer is the outermost layer of the tear film (Figure 20). It is secreted by Meibomian glands, which line the upper and the lower eyelids in a single row. Meibomian gland lipids are stored in vesicles and upon a stimulus released to the duct system that opens onto the lid and later with each blink released on to the ocular surface (reviewed by (Adler, Kaufman et al. 2011). The secretory product of Meibomian glands is liquid at the lid temperature, and contains a complex mixture of non-polar lipids (wax esters, cholesterol, and cholesterol esters), polar lipids (mainly phospholipids) and proteins. The lipid tear layer forms a hydrophobic barrier to reduce evaporation of underlying aqueous layer, to prevent tear overflow onto the lids and sebum from the skin from entering the tear film (Johnson and Murphy 2004). Moreover it forms a water tight seal of the apposed lid margins during sleep, reduce tear evaporation during eyelid opening and aid in lubrication for the eyelids during blinking. Lipid enhanced the stability of the tear film and provides a smooth optical surface for the cornea. An impairment of Meibomian gland secretion leads to evaporative dry eye (Adler, Kaufman et al. 2011).

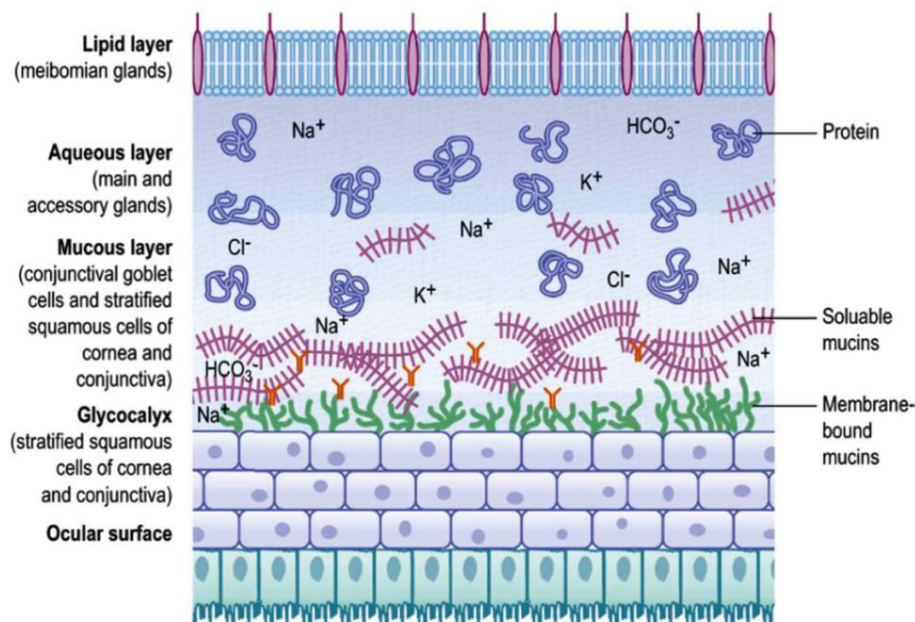


Figure 20. Schematic representation of the tear film. The tear film overlies the ocular surface. The outer lipid layer is secreted by Meibomian glands. The middle layer contains electrolytes, water, proteins and small soluble mucins produced by lacrimal glands and conjunctival epithelium. The inner mucous layer consists of gel-forming mucin, proteins, electrolytes and water secreted by conjunctival goblet cells. The glycocalyx is composed of membrane-bound mucins produced by stratified squamous cells of the corneal and conjunctival epithelial cells. Taken from Dartt, 2011.

C.2.2. Basal Tearing

The ocular surface is always covered by a tear film layer. It was thought that the lacrimal gland steadily produces tears at a certain level without any stimulation (Jordan and Baum 1980). However, it was proposed that sensory information about the degree of wetness of the ocular surface could be provided by corneal and conjunctival cold thermoreceptors (Hirata and Meng 2010; Parra, Madrid et al. 2010), which create the excitatory input to central parasympathetic neurons innervating the lacrimal gland.

Corneal nerve terminals are able to detect very small changes of the ocular surface temperature that decreases during interblinks because of tear evaporation (Belmonte and Gallar 2011). The corneal cold thermoreceptors are silenced upon warming (Parra, Madrid et al. 2010). This supports the idea, that under normal circumstances, the continuous firing from cold

thermoreceptors represents a tonic stimulus for basal tear fluid secretion (Belmonte and Gallar 2011).

Basic tearing can be measured by the Schirmer test with topical anesthesia. The Schirmer test strip is then placed in the lid margin for five more minutes. A wet portion of the strip less than 5 mm is considered abnormally low (reviewed by (Tsubota 1998)). Another method used for examining tearing rate is the phenol red thread tear test (PRT). PRT is a quantitative test for aqueous tears with minimal sensation, and the short test times which are accurate indicator for measuring residual tears in humans and several animal species including guinea pig (Trost, Skalicky et al. 2007).

C.2.3. Reflex tearing

Reflex tearing is a sudden increase in the tear flow produced by injurious or irritant ocular surface stimuli, which are mediated by polymodal nociceptors (Acosta et al., 2004). Reflex tearing is independent of the tonic influence on basal tearing exerted by cold thermoreceptors (Belmonte and Gallar 2011).

Even if basic tearing is decreased, accelerating desiccation of the ocular surface, if reflex tears are present, can provide the ocular surface epithelium with substances necessary for proper epithelial wound healing. The tears thus produced contain essential components, such as vitamin A and EGF, for the proliferation and differentiation of the corneal and conjunctival epithelium (Tsubota 1998).

D. Dry Eye Disease (DED)

Dry eye disease (DED) is a very prevalent and bothersome condition and one of the most common ophthalmological disorders, affecting approximately 20% of adults over 45 years old (reviewed by (Rosenthal and Borsook 2012)). It is more prevalent with increasing age and among women (Moss, Klein et al. 2000), and diabetic patients (Kaiserman, Kaiserman et al. 2005). Dry eye occurs in 50% of contact lens wearers (Nichols and Sinnott 2006) and it is frequent after refractive correction surgeries (Turu, Alexandrescu et al. 2012; Chao, Golebiowski et al. 2014). These surgical procedures can provoke a negative side effect resulting in abnormal sensations that occur to the ocular surface (Belmonte 2007).

From the definition dry eye is a multifactorial disease of the tears and ocular surface that results in symptoms of discomfort, visual disturbance, and tears film instability with potential damage to the ocular surface. It is accompanied by increased osmolality of the tear film and the inflammation of the ocular surface (Lemp and Foulks 2007).

Patients with dry eye typically complain of eye irritation (like foreign body sensation and burning), blurred vision, increased sensitivity to low humidity environments and to air drafts (Sade De Paiva and Pflugfelder 2004). However other authors observed that patients with dry eye exhibit corneal hypoesthesia - decreased sensitivity - after mechanical, thermal, and chemical stimulation that appears to be related to damage to the sensory innervation of the cornea (Bourcier, Acosta et al. 2005). The sensory innervation of the cornea is necessary to detect environmental stressors and, through brainstem circuits, regulate the flow of glandular secretion (Meng, 2013, the role of corneal afferent neurons). Ocular irritation in dry eye is accompanied by an unstable tear film and corneal epithelial disease called keratoconjunctivitis sicca (KCS), which is characterized by inflammation of the ocular surface and lacrimal glands (Sade De Paiva and Pflugfelder 2004; Javadi and Feizi 2011). Knowledge of the pathophysiology of dry eye can lead to the development of highly effective therapies.

For now there is no cure for dry eye syndrome, but there are treatments that help control the symptoms. The exact treatment for dry eye depends on the cause of symptoms. Therefore, etiopathogenic classification of dry eye types was proposed (Figure 21) (Workshop 2007).

Most practiced dry eye therapies are based on the use of lubricants, often called “artificial tears”, anti-inflammatory treatments, and autologous serum eye drops (reviewed by (Alves, Fonseca et al. 2013)). Cyclosporine A (CsA), which is a immunosuppressive drug used in anti-inflammatory therapy, seems to be a promising treatment against dry eye (Kymionis, Bouzoukis et al. 2008). Another natural replacement therapy could be the use of lacritrin, a tear protein selectively deficient in dry eye, which influences ocular surface health. Lacritrin applied topically promotes basal tearing (McKown, Wang et al. 2009; Karnati, Laurie et al. 2013).

The dry eye disease classification indicates two types of dry eye: aqueous deficient dry eye, caused by reduced secretion of tears, and evaporative dry eye, induced by faster tears evaporation from the ocular surface while the tearing rate is normal (Figure 21).

Aqueous tear-deficient dry eye implies that dry eye is due to a failure of lacrimal tear secretion. A unilateral aqueous deficient dry eye is uncommon but may be due to, for example, lacrimal gland inflammation, trauma to the lacrimal gland from surgery, chemical burns or irradiation. Bilateral deficiency may be due to, inter alia, keratoconjunctivitis sicca and Sjogren's

syndrome, human immunodeficiency syndrome. The most common disease in a general population is a mild aqueous deficiency due to senile degeneration of the lacrimal gland (Elder and Dart 2000). The most severe forms of aqueous tear deficiency are due to destruction or absence of the lacrimal gland and include Sjogren's syndrome, and congenital or surgical removal of the lacrimal gland (Albietz 2001). In any form of dry eye due to lacrimal gland destruction or dysfunction, dryness results from reduced lacrimal tear secretion and volume, which causes tear hyperosmolarity (Workshop 2007).

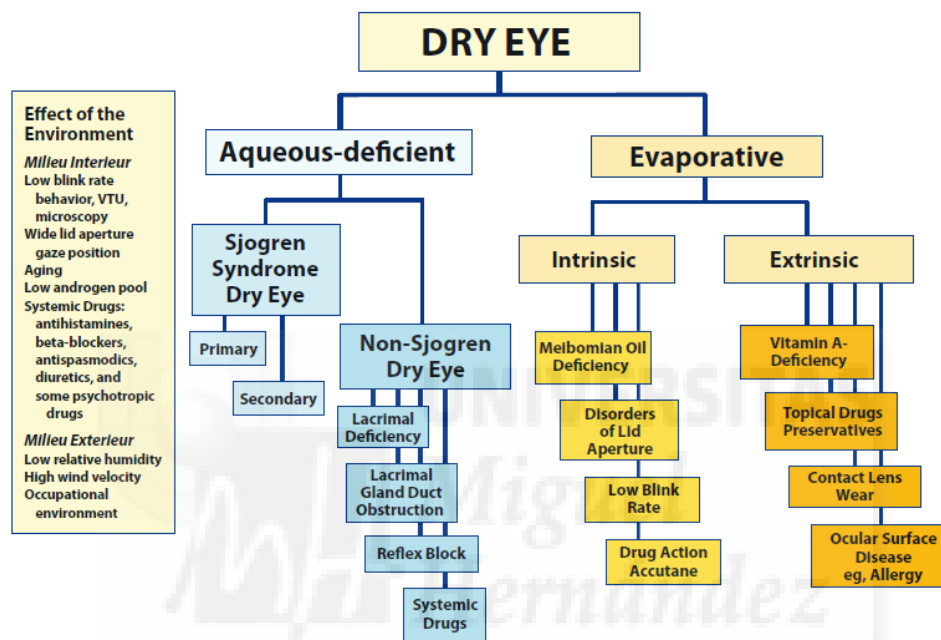


Figure 21. Scheme of the major etiological causes of dry eye. The left hand box illustrates the influence of environment on the risk of an individual to develop dry eye. The term “environment” is used broadly, to include bodily states habitually experienced by an individual, whether it reflects their “milieu interieur” or is the result of exposure to external conditions which represent the “milieu exterieur.” This background may influence the onset and type of dry eye disease in an individual, which may be aqueous-deficient or evaporative in nature. Taken from International Dry Eye Workshop, 2007.

Drying of the ocular surface, likewise tear hyperosmolarity, and/or release of inflammatory mediators to tears may produce a mechanical distortion of the epithelium layers and possibly a deformation of the intercellular spaces where nerve endings are located, leading to their mechanical stimulation. This mechanical and/or chemical excitation of polymodal nociceptors is associated with the unpleasant sensations accompanying dry eye disease (reviewed by (Belmonte and Gallar 2011)).

Increased tear osmolarity also activate corneal cold thermoreceptors (Hirata and Meng 2010), and may further contribute to the augmented firing and to the ensuing unpleasant sensations of dryness. Thus, cold thermoreceptors contribute to the conscious dryness sensations, and polymodal nociceptors could be the reason of the unpleasant feelings during ocular surface dryness (Belmonte and Gallar 2011).

When the cornea dries, peripheral fibers and their higher order neurons of the brain stem trigeminal complex gradually increase their activity (Hirata, Okamoto et al. 2004). That can suggest that nociceptor pathways also contribute to the sensory inflow that encodes the level of ocular desiccation. Unpleasant sensations of ocular dryness may also appear after traumatic or inflammatory damage to the corneal sensory nerves, even though the tear film composition or volume is not altered. Corneal sensory nerves elicit an abnormal spontaneous firing also after photorefractive surgery (Gallar, Acosta et al. 2007), and although tear secretion is normal, patients report dry eye sensations, suggesting that such abnormal activity is interpreted by the brain as ocular surface dryness (Belmonte 2007) (Figure 22).

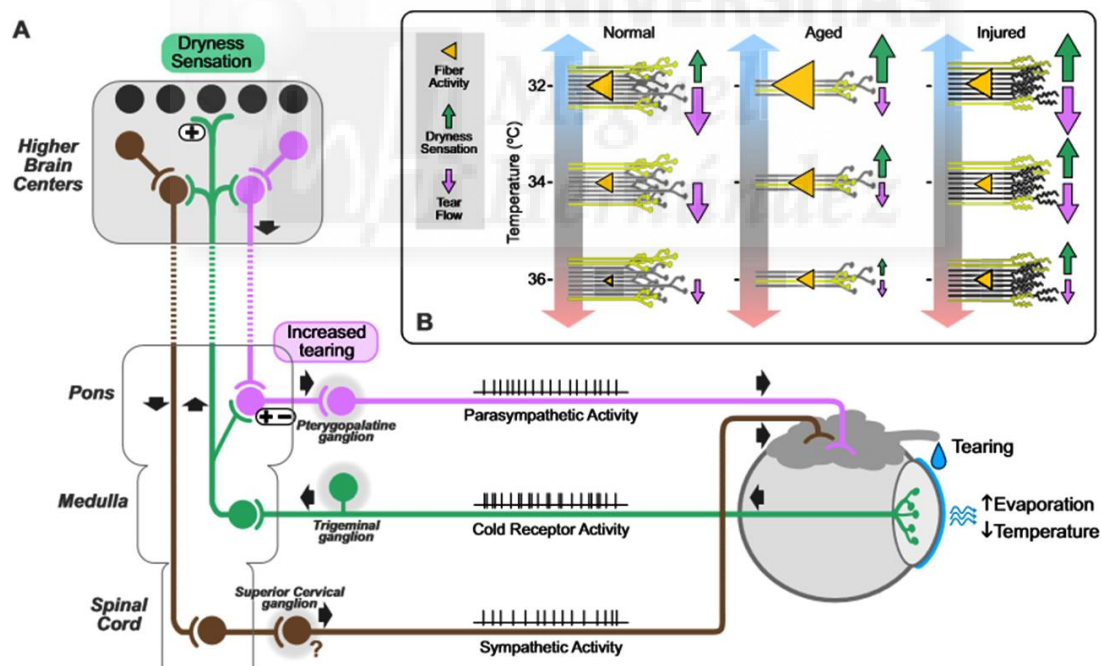


Figure 22. Hypothetical neural mechanisms involved in the maintenance of basal tearing and production of dryness sensations by cold receptor activity. At comfortable environmental temperature and humidity levels, background nerve impulse activity in cold thermoreceptors may oscillate slightly between blinks, but altogether, it does not represent a sensory input of sufficiently large temporal and spatial dimensions to evoke conscious sensations. However, such cold thermoreceptor activity still serves to maintain a tonic excitatory input to central parasympathetic neurons of the salivary nucleus, which project through the pterygopalatine

ganglion to the lacrimal glands and maintain basal tearing. Sympathetic activation may also be involved in the determination of the final composition and volume of tears. **B.** The hypothetical mechanisms governing the change in tearing rate and the apparition of conscious dryness sensations during evaporative reductions of corneal surface temperature in young and aged people and in patients with injured corneal sensory nerves consecutive to surgery or to severe eye dryness. Left: in normal individuals at comfortable environmental temperature and humidity levels, activity in corneal cold endings (10% of the total number of corneal nerve endings $100 / \text{mm}^2$; stimulates basal tear flow, but does not evoke dryness sensations. Dryness sensations appear when strong cooling elicits higher firing frequencies, although additional increases in basal tear flow are modest; conversely, reduced cooling resulting from low evaporation, decreases cold afferent activity and tearing flow. Middle: in elderly individuals, the total number of endings decreases with age to approximately 50%; this predictably reduces the total afferent sensory input to parasympathetic centers, thereby decreasing basal tear flow. The elevated evaporation that occurs with a thinner tear film, even under comfortable conditions, produces an augmented impulse activity in the surviving cold fibers that tends to counteract the reduced tearing, but also generates conscious dryness sensations. Decreases or increases in corneal temperature produced by changes in evaporation according to environmental conditions will aggravate or alleviate this state. Right: damaged nerve endings display an abnormal, augmented impulse activity that still serves to maintain relatively intact the cold receptor-dependent basal tear flow but is interpreted by the cerebral cortex as a sensory message of ocular dryness. Taken from Belmonte and Gallar, 2011.

The changes in the corneal innervation caused by dry eye disease are investigated and examined in patients with use of the in vivo confocal microscopy (IVCM) (Tuominen, Kontinen et al. 2003; Erdélyi, Kraak et al. 2007; Cruzat, Pavan-Langston et al. 2010; Labbé, Liang et al. 2013). These studies have shown that there are differences in the overall density of the subbasal plexus, what could be caused by the varying causes and stages of dry eye in different patients (Cruzat, Pavan-Langston et al. 2010). Also the subbasal nerves exhibit tortuosities and bead-like formations (Tuominen, Kontinen et al. 2003; Erdélyi, Kraak et al. 2007). IVCM have many advantages, because is rapid, noninvasive and provides excellent resolution (Cruzat, Pavan-Langston et al. 2010; Marfurt, Cox et al. 2010), however is often incapable of showing reliably images of corneal epithelial terminals and very small diameter subbasal and stromal nerves (Marfurt, Cox et al. 2010).

III. OBJECTIVES

The aim of the present PhD thesis is to determine the effects of age and chronic tear-deficiency on corneal nerve activity and morphology, and their influence on ocular trophic processes as corneal wound healing. This aim is divided in two general objectives.

- The first objective is to study the effects of age on tearing rate and corneal innervation, defining how the activity and architecture of corneal innervation changes during the first year of guinea pig's life, and the repercussion on corneal epithelial wound healing.
- The second objective is to examine in young and adult animals the effects of chronic tear-deficiency on corneal nerve morphology and activity, and on corneal epithelial wound healing.

All studies were performed in guinea pig's cornea, which is an avascular, transparent tissue innervated by sensory and autonomic nerves. Due to its morphological characteristics, the cornea is a suitable model for studying the morphology and activity of sensory nerves as well as epithelial wound healing.

For the purposes of the main objectives, first of all it was necessary to establish adequate methods to perform in the selected experimental animal the following:

- a) to perform the immunohistochemical staining of corneal nerves, and analysis of the morphology of corneal innervation,
- b) to execute the corneal epithelial debridations to analyze corneal wound healing,
- c) to measure tearing rate,
- d) to carry out the extracellular recordings of single sensory nerve units in an ex vivo preparation, and
- e) to develop a surgical technique of lacrimal gland removal to induce chronic tear-deficiency in the guinea pig.

The experiments carried out subsequently allowed to study in young and adult guinea pigs:

- a) the characteristic parameters of the corneal nerve architecture,
- b) the rate of epithelial corneal wound healing,
- c) the basal tear fluid production,
- e) the electrophysiological activity of the different types of corneal nerve fibers, and
- f) the effects of chronic tear-deficiency in young and adult animals.

All together the performed experiments provided us data to define the effects of age and chronic tear-deficiency on the function and morphology of corneal innervation, which might be a cause of the impaired epithelial wound healing, tear production and blinking rate observed in the tear-deficiency.



III. MATERIAL AND METHODS

Dunkin Hartley guinea pigs of both sexes were used in all experiments. Animals were kept at the Animal House of the University Miguel Hernández in individual cages with *ad libitum* access to water and food. The 12 h / 12 h day-night cycle and the room temperature were controlled. The study was performed in accordance with the European Union Directive (2010/63/EU) and the Spanish regulations on the protection of animals used for research, and followed a protocol approved and supervised by the Ethics Committee of the University Miguel Hernández. For each experiment animals were sacrificed with an intraperitoneal injection of 120 mg/kg sodium pentobarbitone (Dolethal, Vétocinol E.V.S.A., Madrid, Spain).

A. Measurement of tearing rate

Tearing rate was measured in 24 young and 16 adult intact animals, and in 16 young and 6 adult tear-deficient animals. For this purpose, commercial phenol red threads (Zone-Quick, Menicon, Nagoya, Japan) were used. Phenol red threads are originally yellow and change their color from yellow to red when getting wet by tears, which are slightly alkaline. The thread was placed in the nasal side of the inferior lid for 30 s and then removed (Figure 23), and the wet, red part of the thread was measured using the rule in the back of the thread package under a stereomicroscope and expressed in millimeters, with an accuracy of ± 0.5 mm (Trost, Skalicky et al. 2007; Acosta, Luna et al. 2013).

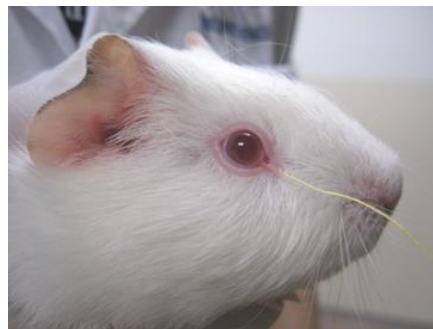


Figure 23. Measurement of the tearing rate with a phenol red thread.

B. Surgical procedure to induce chronic tear-deficiency

Chronic tear-deficiency was induced by surgical extraction of the lacrimal gland, performed in 60 guinea pigs to obtain an experimental approach of tear-deficient Dry Eye Disease (DED). Only the main lacrimal gland, located outside the orbit near the parotid gland, was removed while the intraorbital lacrimal glands remained intact (Kovacs, Quirce et al. 2010). Animals were anaesthetized with ketamine (90 mg/kg, i.p.; Imalgene® 1000, Merial Laboratorios, Barcelona, Spain) and xylazine (5 mg/kg, i.p.; Xilagesic 2%, Laboratorios Calier, Barcelona, Spain). For the unilateral exorbital lacrimal gland excision, an 8 mm skin incision on the temporal side, posterior to the lateral canthus was done. The fibrous capsule of the gland was exposed and dissected, and the lacrimal gland was carefully removed. The surgical area was checked to detect any remaining glandular tissue. Then 120 µl of the antibiotic tobramycin (3 mg/ml; Tobrex®, Alcon Cusí, Barcelona, Spain) were applied into the surgical incision and the skin was sutured with 6.0 braided silk sutures. Conjunctiva and cornea were explored regularly during the recovery time to detect signs of inflammation. The success of surgery was ascertained confirming the reduction of tearing rate at different time points after surgery.

C. Immunohistochemistry of corneal nerves

Two methods of immunohistochemical staining were carried out in 36 control corneas and 34 corneas from tear-deficient guinea pigs of different ages. The animals were sacrificed with an overdose of anesthetic and a point of suture was placed in the superior conjunctiva (at 12 h), near the limbus, to orientate the tissue after corneal excision. The eye globes were dissected and immersion-fixed in 4% paraformaldehyde (Sigma-Aldrich, St. Louis, MO, USA) in 0.1 M phosphate buffer (PB) for 45 minutes at room temperature (RT). There were performed afterwards two washes in 0.1 M PB, for 10 minutes each. Then, the eyes were cryoprotected in increasing gradients of sucrose (Panreac Química S.L.U., Barcelona, Spain). The eyes were immersed in 10% sucrose and then in 20% sucrose in 0.1 M PB at RT for 1 hour each, finalizing with overnight incubation in 30% sucrose in 0.1 M PB. The next day, the whole eye balls were put through a freeze thaw procedure by dipping them in liquid nitrogen-cooled isopentane for a few seconds. After thawing the eye balls in 30% sucrose, the corneas were dissected from the eye and four radial cuts were made with an ophthalmic knife to flatten

them (Figure 24). For orientation of the excised cornea, a short cut was also made on the limbus near the suture point used for orientation.

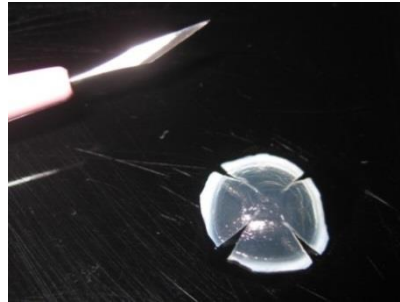


Figure 24. Fixed and cryoprotected dissected cornea with radial cuts.

Then corneas were washed in 0.1 M PB and incubated overnight in agitation at 37°C in 0.01% hyaluronidase type IV-S (Sigma-Aldrich, St. Louis, MO, USA) and 0.1% ethylenediaminetetraacetic acid (EDTA; Sigma Aldrich, St. Louis, MO, USA) diluted in 0.1 M PB pH 5.3. After washes in 0.1 M PB, the corneas were incubated in 2.28% sodium (meta) periodate (NaIO_4) (Sigma Aldrich, St. Louis, MO, USA) for 5 minutes and in 0.02% sodium borohydride (NaBH_4) (Panreac Química S.L.U., Barcelona, Spain) for 5 additional minutes at RT. After further washes with 0.1 M PB pH 7.4, the corneas were incubated in 10% normal goat serum (Jackson ImmunoResearch, West Grove, PA, USA) in 0.1 M PB for 1 hour at 4°C to block non-specific binding. Without washing, the corneas were then incubated for 2 days at 4°C under agitation in the mouse monoclonal primary antibody, neuronal class III beta-tubulin (anti-TUJ 1; Covance Research Products, Berkeley, CA, USA) diluted 1:200 plus 1% Triton™ X-100 (Sigma Aldrich, Inc., St. Louis, MO, USA) in 0.1 M PB, followed by one of the following procedures (Marfurt, Cox et al. 2010).

C.1. Immunofluorescence

After exposure to the anti-TUJ 1 antibody, the tissue was subjected to further washes in 0.1 M PB and transferred to the secondary fluorescent antibody Alexa 488 goat anti-mouse (Molecular Probes, Invitrogen, Eugene, OR, USA) (Figure 25) diluted 1:100 in 0.1 M PB plus 1% Triton™ X-100 for 1 day at 4°C. The corneas were then washed in 0.1 M PB, included in mounting media (Citifluor®, Citifluor Ltd; London, United Kingdom) and coverslipped. Then,

photomicrographs were taken with a laser scanning spectral confocal microscope (Leica TCS SL, Leica Microsystems GmbH, Mannheim, Germany) using HC PL APO CS 20x IMM/CORR NA 0.7 and HCX PL APO CS 40x OIL NA 1.25 objectives. The images (z-stacks) were acquired with the appropriate software (Leica Confocal Software, LCS). Immunohistochemical controls were performed by omission of either the primary or secondary antibodies.

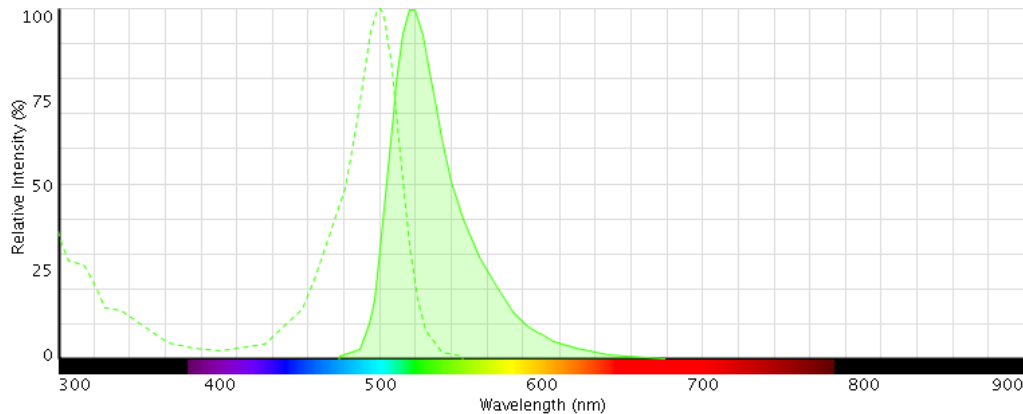


Figure 25. Fluorescence spectrum of the fluorophore Alexa 488; excitation (dotted plot) and emission (solid plot) intensities were shown.

C.2. Immunoperoxidase, ABC complex methods

After incubation in the primary antibody, the corneas were incubated for 1 day at 4°C in the secondary antibody biotinylated horse anti-mouse IgG (Jackson ImmunoResearch Labs. Inc., West Grove, PA, USA) diluted 1:100 in 0.1 M PB plus 1% Triton™ X-100. Afterwards, the corneas were rinsed again in 0.1 M PB and incubated for 1 day at 4°C in avidin-biotin-horseradish peroxidase complex (ABC reagent; Vector Laboratories, Burlingame, CA, USA). Then, the corneas were incubated under agitation in the dark for 15 minutes in 3,3'-diaminobenzidine tetrahydrochloride hydrate (DAB) (Sigma-Aldrich, St. Louis, MO, USA) at 0.05% in 0.1 M PB, and further incubated with fresh DAB solution with 0.01% H₂O₂. After obtaining the desired color of the tissue visualized under microscopy, the DAB reaction was stopped by washes in cold distilled water. Then, the corneas were mounted in the mounting media (Citifluor®) and coverslipped. The corneas were used for taking bright field photomicrographs with the Leica DM 4000 B microscope (Leica Microsystems GmbH, Mannheim, Germany) provided with 10x and 20x objectives, and for exemplary drawings made

with a drawing device (*camara lucida*) Leica MDV-DMR provided with a 40x objective (Leica Microsystems GmbH, Mannheim, Germany).

D. Analysis of corneal nerve density and morphology

The quantitative analysis of stained corneal nerves was performed with the software NeuroLucida (MBF Bioscience, Williston, VT, USA). Different parameters were used to describe corneal innervation (Marfurt, Cox et al. 2010). Some parameters were measured on the whole mount corneas by analyzing the bright field and fluorescence photomicrographs using the free software ImageJ from the National Institutes of Health. To further analyze corneal innervation, the nerves present in the peripheral and central cornea of the superior quadrant, and at the vortex zone were counted. As there have been described differences in the density and organization of corneal nerves in different topographic areas of the cornea, the same area (superior quadrant) was always studied to exclude the bias derived from analyzing different zones of the cornea in each case. In the end, the following parameters were measured:

D.1. Parameters measured in the superior quadrant of the cornea

D.1.1. Density of epithelial nerve terminals

Corneal nerves which end within the corneal epithelial cells as free nerve terminals were quantified without morphological specialization. The density of epithelial nerve terminals was calculated with ImageJ software from z-stacks series of photos of a 1 mm x 1 mm area taken in different corneal zones either with NeuroLucida microscope (using objective 20x and then composing the image with the Helicon Focus6 software) for immunoperoxidase staining or with confocal microscope Leica (using objective 40x) for immunofluorescence staining (Figure 26). The density of epithelial nerve terminals per square millimeter was measured in the peripheral, middle peripheral and vortex zones of superior quadrant of the cornea (Figure 27).

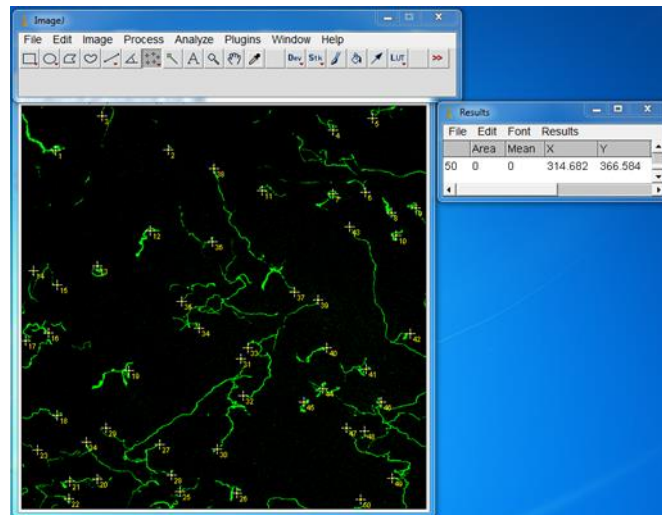


Figure 26. Use of ImageJ software to count the number of epithelial nerve terminals. Epithelial nerve terminals were marked using the multi-point tool (yellow points) of the software.

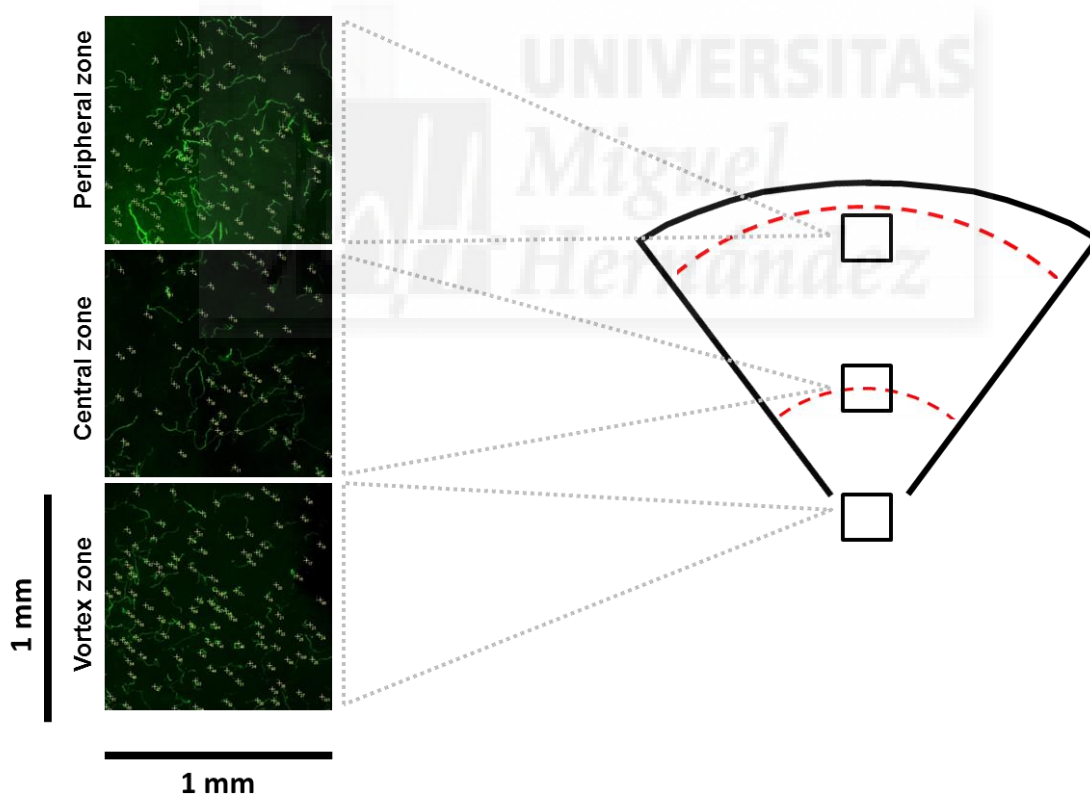


Figure 27. Quantitative analysis of the epithelial nerve endings density in different zones of the superior quadrant of cornea. Schematic representation of the areas where the quantitative analysis of the epithelial nerve endings density was performed.

D.1.2. Proportion of subbasal nerve fibers

The proportion of corneal area occupied by subbasal nerve fibers was also estimated with ImageJ software in three different areas of the superior quadrant of the corneas (Figure 28). A z-stacks series of photos of the subbasal plexus was taken in a 1 mm x 1 mm area either with NeuroLucida or florescence confocal microscope (Figure 28) and then processed with ImageJ to quantify percentage of area occupied by the subbasal nerve fibers (Figure 29).

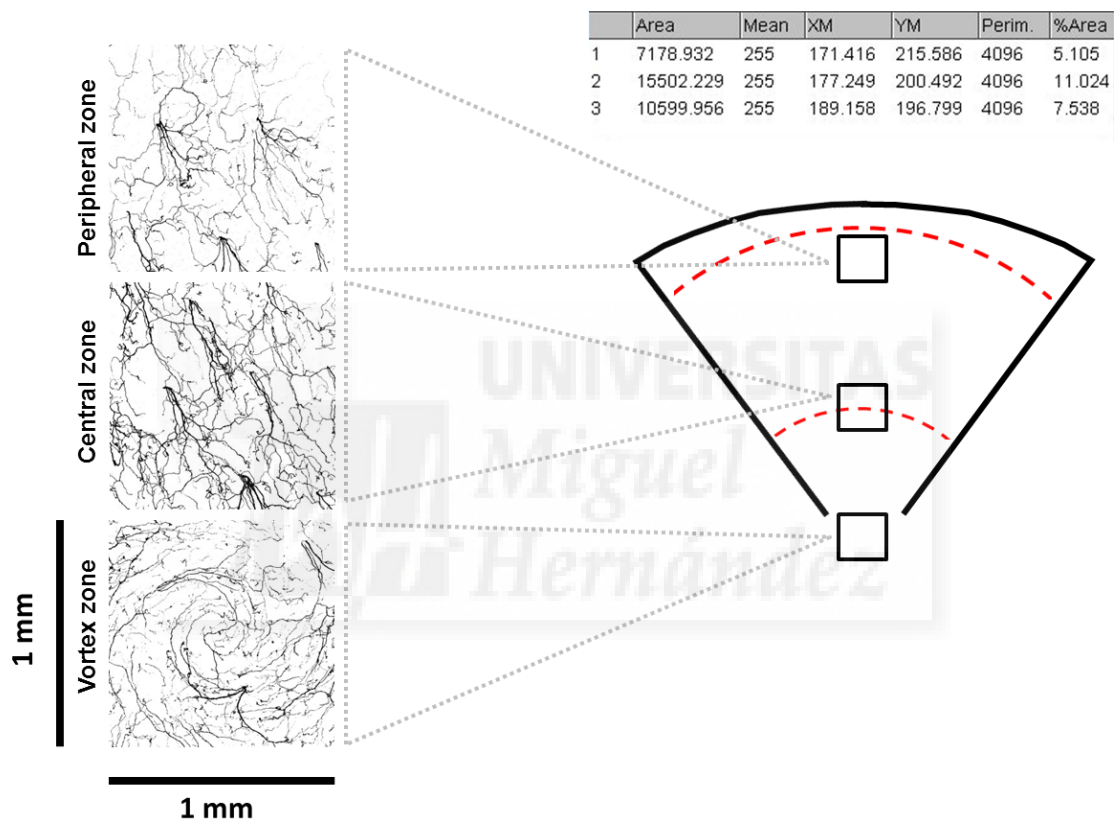


Figure 28. Quantitative estimation of the tissue area occupied by subbasal nerve fibers in different zones of the superior quadrant of cornea. Schematic representation of the areas where the quantitative estimation of subbasal nerves was performed.

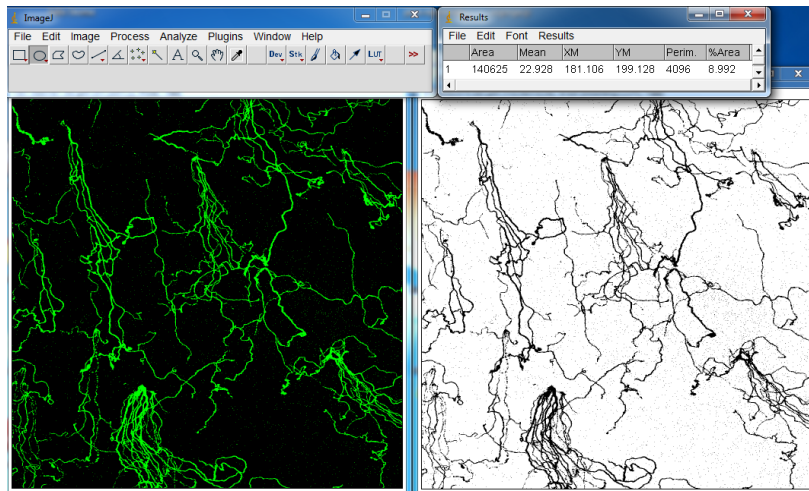


Figure 29. Use of ImageJ to calculate subbasal nerve proportion. The fluorescence z-stack photograph was converted into a binary, black and white image and the percentage of the area occupied by nerve fibers was estimated using the unstained areas as “background” (threshold) to limit to the stained nerves the fraction measurement.

D.1.3. Length of subbasal nerve leashes

Subbasal nerve fibers appears as a group of nerve bundles that derives from the same parent anterior stromal nerve, running almost in parallel along with each other at the basal epithelial cell level. Due to their morphology, they were named subbasal nerve “leashes”. The length of subbasal nerve leashes was measured in the superior quadrant of the cornea using NeuroLucida software to draw over each nerve leash a straight line beginning from the arising of the leash from the stromal nerve trunk and finishing at the longest extreme of the majority of the leash nerve bundles (Figure 30). The peripheral and central cornea zones and the vortex area were defined (Figure 31), and the length of nerve leashes in the peripheral, middle peripheral and vortex zone (Figure 32) was calculated. The estimated nerve leashes elongation with age was also calculated.

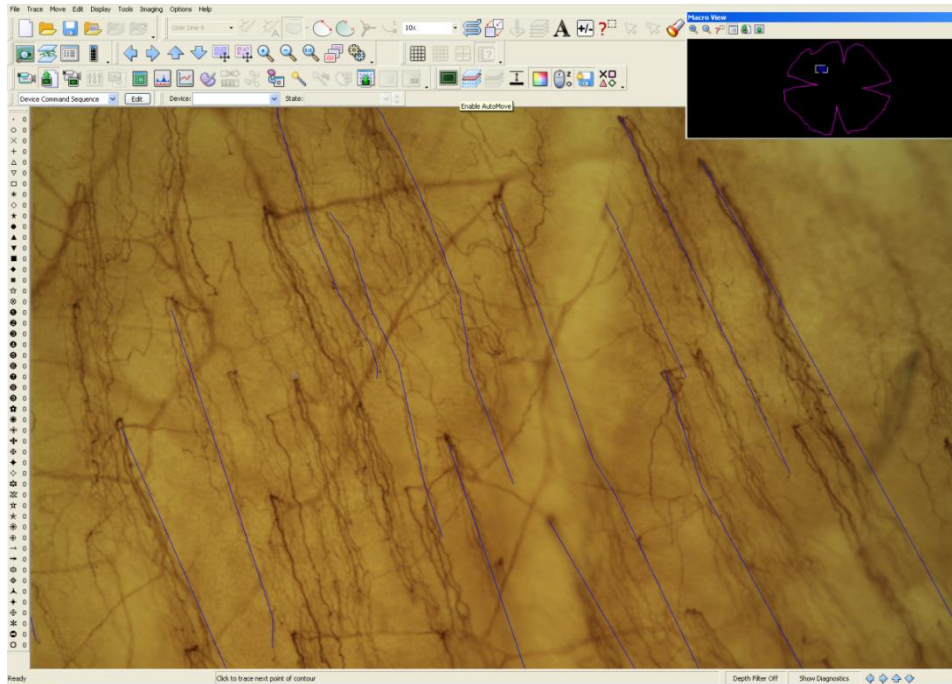


Figure 30. Use of NeuroLucida to calculate the length of subbasal nerve leashes. A blue line was drawn over each subbasal nerve leash. The actual location of the area shown in the large window is shown in the small window (white rectangle).

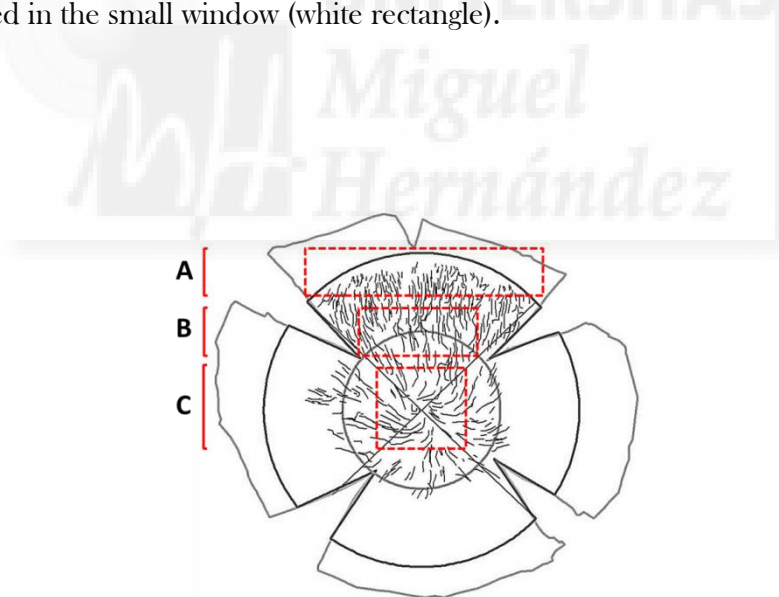


Figure 31. Outline of the cornea showing the peripheral (A), middle peripheral (B) and vortex (C) zones (red quadrilaterals). The length of subbasal nerve leashes was measured in three different zones of the superior quadrant of the cornea.

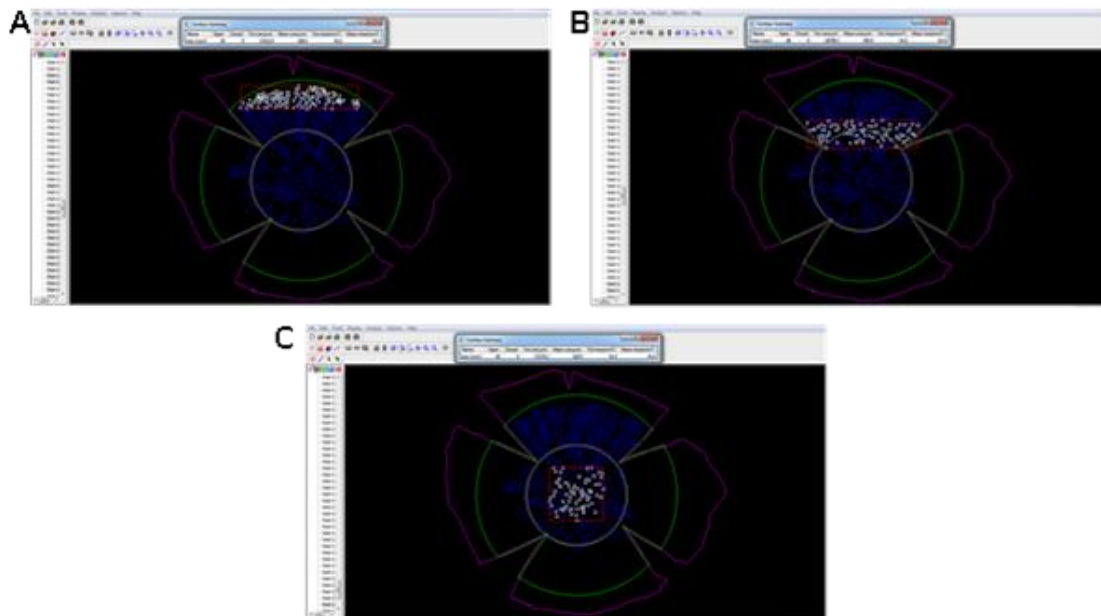


Figure 32. NeuroLucida software used to measure the subbasal nerve length in the peripheral (A), middle peripheral (B) and vortex (C) zones of the cornea. The length of the lines drawn over each subbasal nerve leash (white dots) in the peripheral (A), middle peripheral (B) and vortex (C) zones indicated by the selection tool (red quadrilaterals) was calculated by the software (data appears in the tables shown on top in A, B and C).

D.2. Parameters measured in the whole cornea

D.2.1. Corneal surface area

The contour of each cornea was outlined using the software NeuroLucida from MBF Bioscience. The line tool was employed to draw a line over the cornea contour (Figure 33). Then, a line was drawn over the corneo-limbal border (Figure 34) to obtain a circular line that delimits the cornea (Figure 35, dotted line). Then, a smaller circle inscribed in the first one (Figure 35, continuous, thin line) was drawn to separate the peripheral and central zones of the cornea. The diameter of the inner circle was half length of the outer circle diameter. The obtained draft of the cornea was used for measuring the corneal surface area (Figure 36) and the lines over the four incisions performed in the cornea allowed reflect the true shape of the tissue, and to calculate precisely the corneal surface area expressed in square millimeters (Figure 37), which was further used to calculate the nerve density. The cornea surface area was measured in animals of different ages and the estimated growth rate of the cornea was calculated as the increase of the surface area per month.

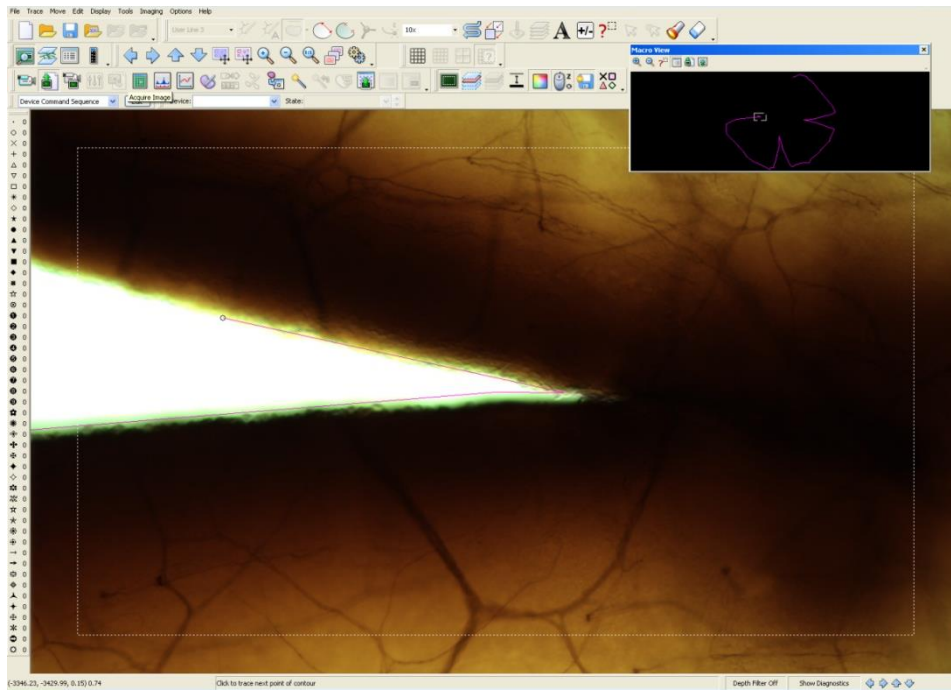


Figure 33. Drawing of cornea contour using NeuroLucida software. A pink line was drawn over the contour of the cornea. The small window shows the progress of line tracing.

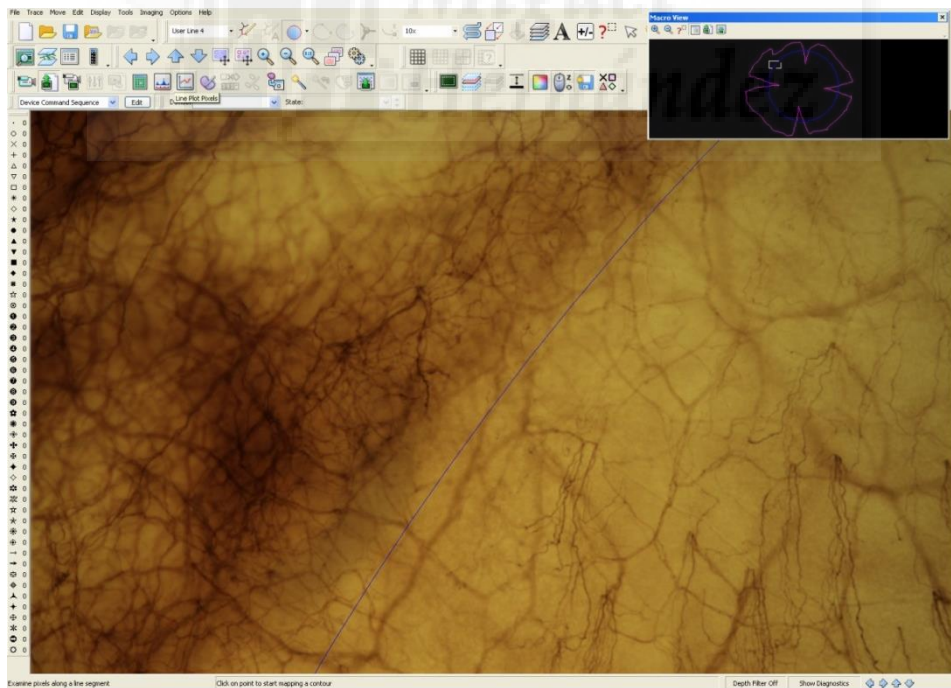


Figure 34. Drawing of corneo-limbal border using NeuroLucida software. A blue line was outlined over the corneo-limbal border (darker zone). The small window on top shows the progress of tracing.

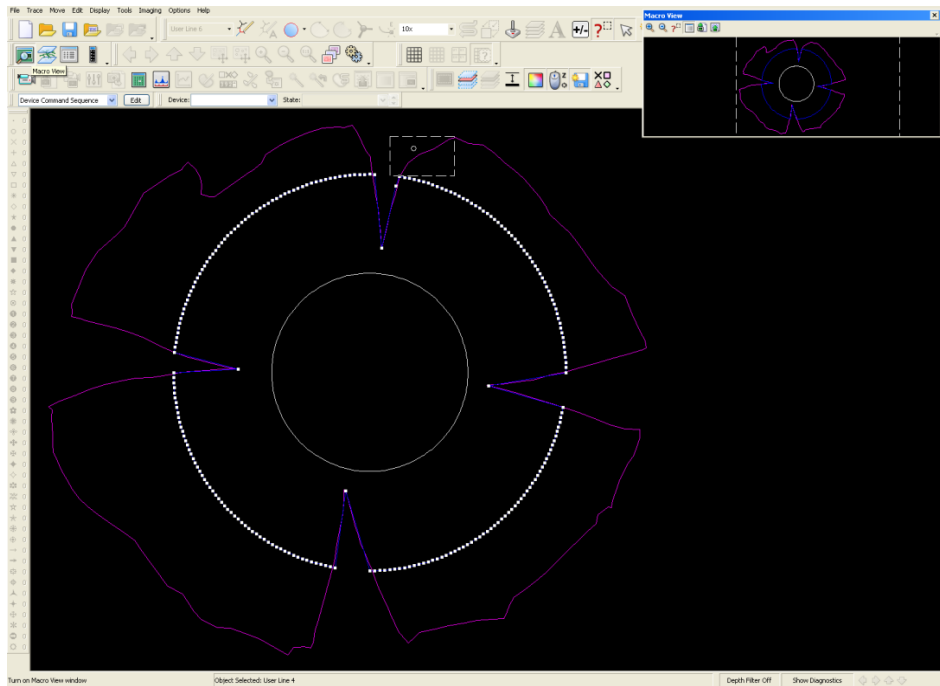


Figure 35. Definition of the central and peripheral cornea zones using NeuroLucida software. Scheme presents the final draft of a cornea sample, showing the outlines tissue border (pink line), the corneo-limbal border (dotted white line) and central cornea zone (thin continuous line).

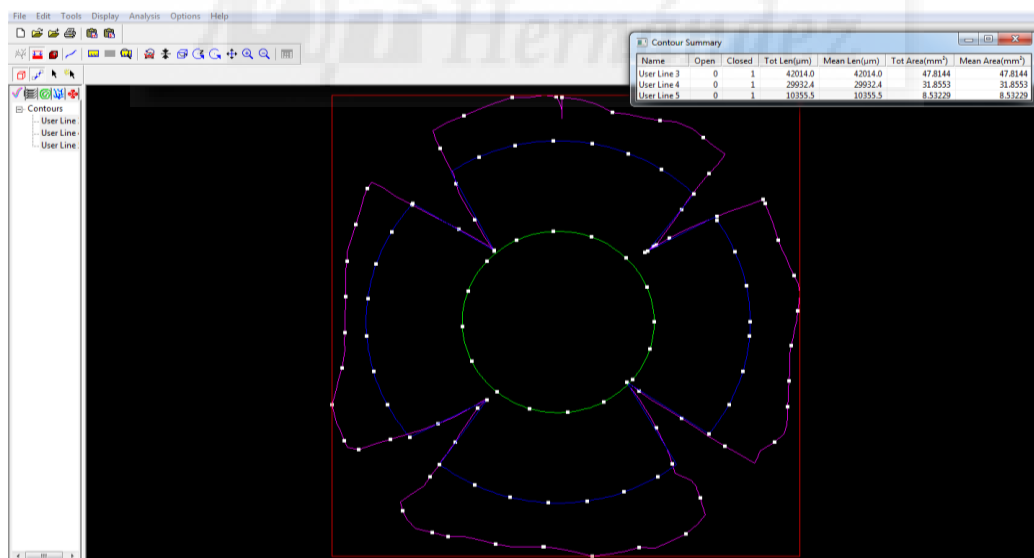


Figure 36. Final outline and calculation of surface areas in a sample cornea using NeuroLucida software. The software allowed present an scheme of the cornea sample with its contour (pink line) and corneal surface separated into peripheral (blue line) and central (green line) zones. Surface area measurements are shown in the small window.

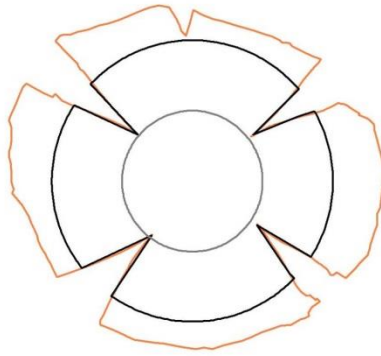


Figure 37. Outline of the cornea tissue samples the NeuroLucida software. The outlines of the shape of the tissue sample (orange line), the peripheral cornea zone (black line) and central cornea zone (grey line) are shown.

D.2.2. Total number of subbasal nerve leashes

Every subbasal nerve leash was considered as the group of subbasal nerve fibers arising at a single point from the stromal nerve trunks. Nerve leashes were marked one by one with the point marker tool of NeuroLucida software (Figure 38). The total number of subbasal nerve leashes was then counted in whole cornea, and in the peripheral and central zones. The evolution of subbasal nerve leashes with age was also calculated.

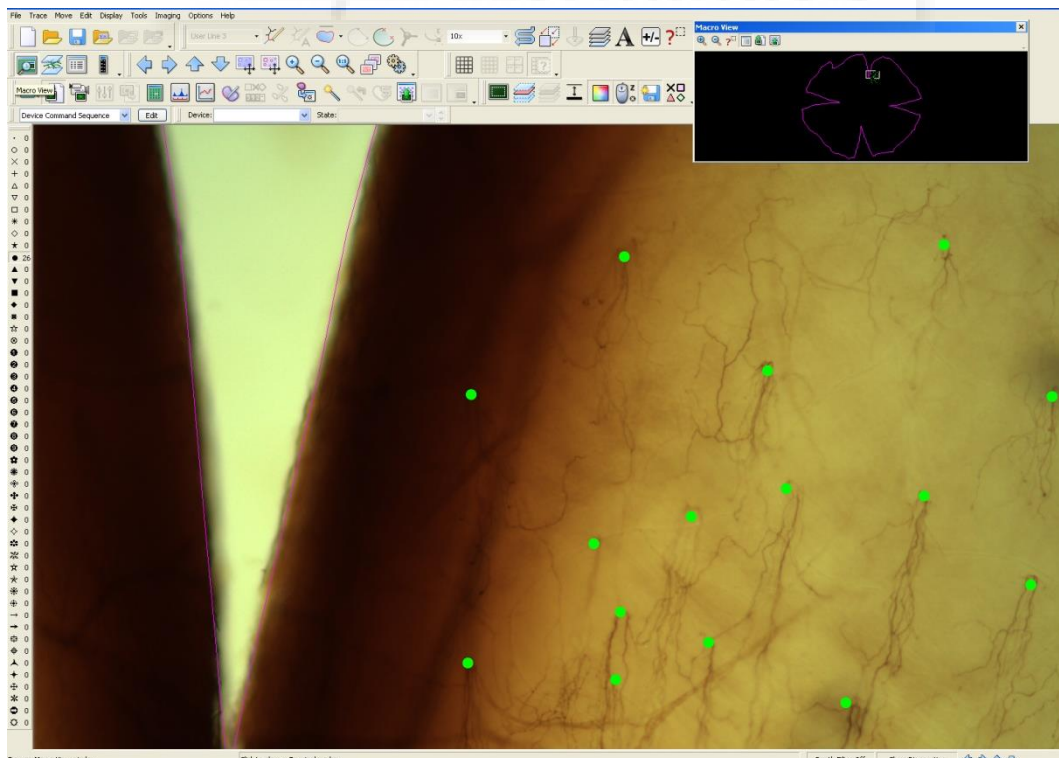


Figure 38. Use of NeuroLucida software to calculate the total number of subbasal nerve leashes. The software allows mark green points over each nerve leash arising from the stromal nerve trunks. The small window shows the contour of the tissue sample (pink line) and the actual zone shown magnified in the large window in each moment (small white rectangle).

D.2.3. Density of subbasal nerve leashes

After all subbasal nerve leashes present in a sample were marked (Figure 39, black dots), and the corneal surface was defined and separated into peripheral and central zones (Figure 39, dark and light green lines, respectively), the density of subbasal nerve leashes was quantified. The total number of subbasal nerve leashes was divided by the total surface of the cornea to obtain the corneal subbasal nerve leashes density, expressed as the number of nerves per 1 mm². The density of subbasal nerve leashes in the **peripheral** cornea and the **central** cornea was also calculated.

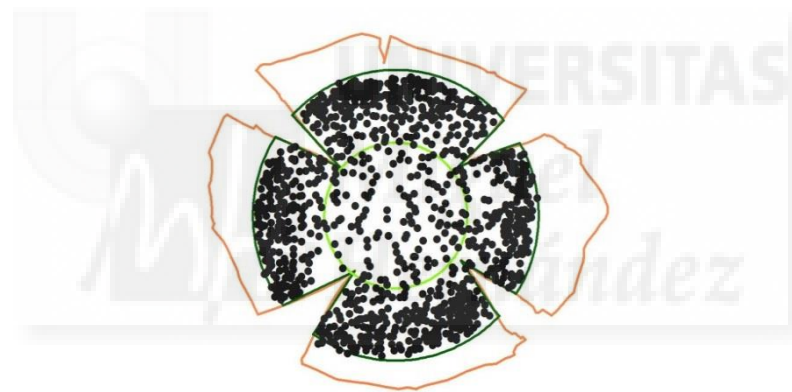


Figure 39. Outline of the tissue sample showing the number of subbasal nerve leashes in the peripheral and central cornea zones. Each subbasal nerve leash is represented as a black dot. The peripheral (dark green line) and central (light green line) zones were delimited.

E. Corneal epithelial wound healing

The wound healing study was performed to examine the rate of the repair of a corneal epithelial debridation performed as previously described (de Leeuw and Chan 1989; Gallar, Pozo et al. 1990). The experiments were performed in 5 young (2 months old) and 6 adult (7 months old) control animals, and in 5 tear-deficient young (2 months old) and 10 tear-deficient adult (7 months old) guinea pigs.

E.1. Chemical debridation of corneal epithelium

The guinea pigs were anesthetized with ketamine (90 mg/kg i.p.) and xylazine (5 mg/kg i.p.). After topical anesthesia with 10 μ l of 0.4% oxybuprocaine hydrochloride and 0.1% tetracaine hydrochloride (Anestético Doble®, Alcon Cusí, S.A., Barcelona, Spain) applied onto the eye, corneal epithelial lesions were executed in the right eye. For this purpose a 2 mm-diameter disc of Whatman No. 1 filter paper soaked in *n*-heptanol (1-heptanol, MERCK-Schuchardt, Germany) was applied to the center of the cornea for 30 seconds. The paper was then removed and the wound site was immediately rinsed with 10 ml of isotonic saline. The obtained round epithelial wounds were stained with 10 μ l of 2% fluorescein (Colircusí Fluoresceína®, Alcon Cusí, S.A., Barcelona, Spain) and then photographed regularly under cobalt blue light (MTOM-5, Takagi MFG. Co., Japan) every four hours until the complete closure of the epithelial defect (with a break between 20:00 PM and 8:00 AM). A 1 square centimeter pieced of graph paper was placed beside the eye before taken every photo (Figure 40). Afterwards the photographs were analyzed with the use of ImageJ software to calculate the change of the epithelial defect area with time.

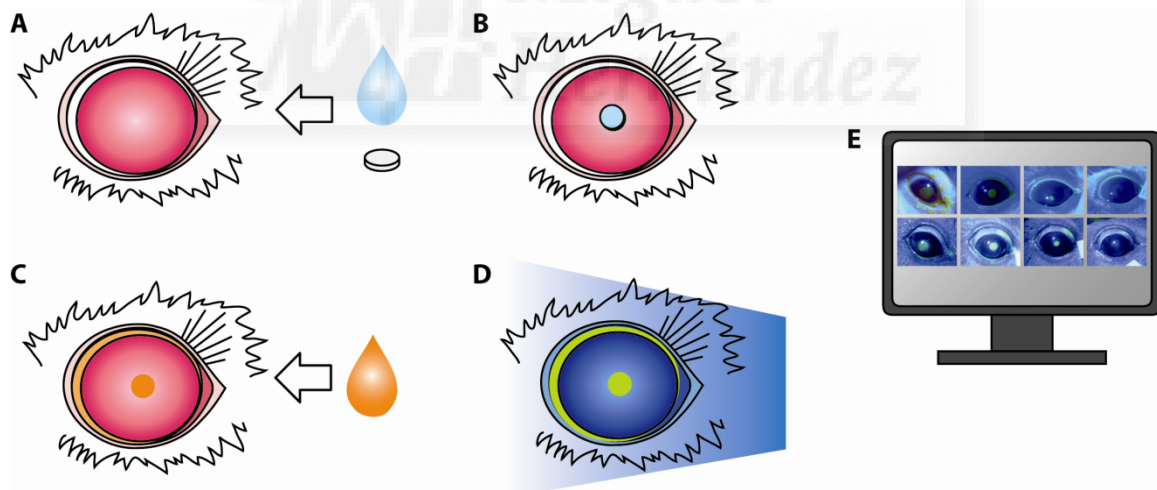


Figure 40. Scheme of corneal epithelial debridation procedure. (A) Chemical corneal epithelial wounds were performed by applying to the center of the cornea a 2 mm-diameter piece of paper soaked with *n*-heptanol. (B) After 30 seconds the paper was removed. (C) The obtained epithelial debridation was stained with fluorescein, and (D) photographed regularly until complete closure under cobalt blue illumination. (E) Photographs were collected to a PC and analyzed with ImageJ software.

E.2. Data analysis

E.2.1. Photos analysis

The photographs were analyzed one by one with the use of ImageJ software by measuring in pixels the size of every wound with the oval selection tool, and the size of the 0.25 cm² piece of paper placed next to the eye with the rectangular selection tool. Both areas were expressed in pixels and then converted to square millimeters, and the size of the lesion resulted by counting the proportion. The measured areas of wound surface at every time-point were used for evaluating three parameters: wound area, estimated migration rate (EMR) and estimated time of healing (ETH) as previously described (Gallar, Pozo et al. 1990).

E.2.2. Wound area

The area of every corneal epithelial wound, in square millimeters, was calculated at every time-point during the healing period until the complete closure of the lesion. It describes the size of initial wound and its evolution with time until complete closure of the epithelial defect.

E.2.3. Estimated migration rate

This parameter describes the velocity at which epithelial cells surrounding the defect invade the wound site to close the exposed basal membrane. It was determined for each lesioned cornea by linear regression of the wound radius decrease during the healing phase, and was given by the slope of the regression line expressed in $\mu\text{m}/\text{h}$.

E.2.4. Estimated time of healing

This parameter is the time required for the complete closure of the corneal epithelial defect. It was calculated for each lesioned cornea by extrapolation of the best fit of regression line during the healing phase until total lesion closure, and was expressed in hours.

F. Electrophysiological recording of corneal sensory receptors

The activity of cold-sensitive corneal nerve terminals and polymodal and mechanonociceptor nerve fibers was recorded to evaluate if there were any significant changes associated with age.

Extracellular recording of nerve terminal impulse (NTI) discharges with a micropipette applied onto the corneal surface favors the detection of the activity of cold receptor nerve terminals, while extracellular recording of single nerve fibers dissected out of the ciliary nerves in the back of the eye is more suitable to record from polymodal and mechano-nociceptor axons. Therefore, two preparations of the isolated cornea and of the excised whole eye with its sensory nerves were alternate to record the impulse activity of the different functional types of peripheral corneal receptors.

F.1. Corneal nerve terminals recording

Nerve terminal impulse activity was recorded from corneas of 30 young (2 months old) and 12 adult (9 months old) animals. Animals were euthanized with an overdose of anesthetic, the eyes were marked with the suture at superior conjunctiva and the corneas were dissected and incubated in physiological saline solution of the following composition (in mM): NaCl, 133.4; KCl, 4.7; CaCl₂, 2; MgCl₂, 1.2; NaHCO₃, 16.3; NaH₂PO₄, 1.3; glucose, 7.8, gassed with carbogen (95% O₂, 5% CO₂) to pH 7.4 during 30 min at room temperature. After that time the cornea was placed in the silicone-coated (Sylgard 184 ®, Dow Corning, Midland, MI, USA) recording chamber continuously perfused with physiological saline solution maintained at the temperature of around 34°C (basal temperature) with a homemade feedback-controlled Peltier device (Figure 41 A, C). Thermal stimuli were performed by changing the temperature of the perfusion solution from the basal temperature (34°C) down to 20°C for around 30 s (cooling stimulus) with the Peltier device. NTI activity was recorded using a glass-pipette electrode, with a tip diameter of around 50 µm filled with physiological saline solution, applied onto the surface of cornea (Figure 41 A, B) with a micromanipulator (Figure 41 C) and attached by slight suction. Signals were recorded with respect to a silver-silver chloride (Ag/AgCl) pellet placed in the bath (Figure 41 A, B, C). Electrical activity was amplified (1000x, AC pre-amplifier NL 103, Digitimer, Welwyn, UK), filtered (high pass 15 Hz, low pass 5 KHz, filter module NL 125; Digitimer) and collected to a PC with a CED micro-1401 acquisition system (Cambridge

Electronic Design, Cambridge, UK), and subsequently analyzed with Spike2 v7.01 (Cambridge Electronic Design, Cambridge, UK) software.

The tip of the micropipette was applied to the corneal surface the required number of times until the spontaneous activity of a single nerve terminal was found. NTI activity of a single cold sensitive nerve ending was identified by its characteristic regular ongoing discharge, usually of high frequency that changes after applying thermal stimulation: increases with cooling and decreases with warming of the physiological saline solution with the Peltier device. Spontaneous activity (SA) of cold nerve terminals at basal temperature of 34°C was recorded for at least 1 minute. Then the cooling stimulus was applied by decreasing the temperature to 20°C, followed by rewarming to the basal temperature. Recordings were stored and analyzed off-line as described before (Brock, McLachlan et al. 1998; Acosta, Luna et al. 2013; Acosta, Luna et al. 2014).

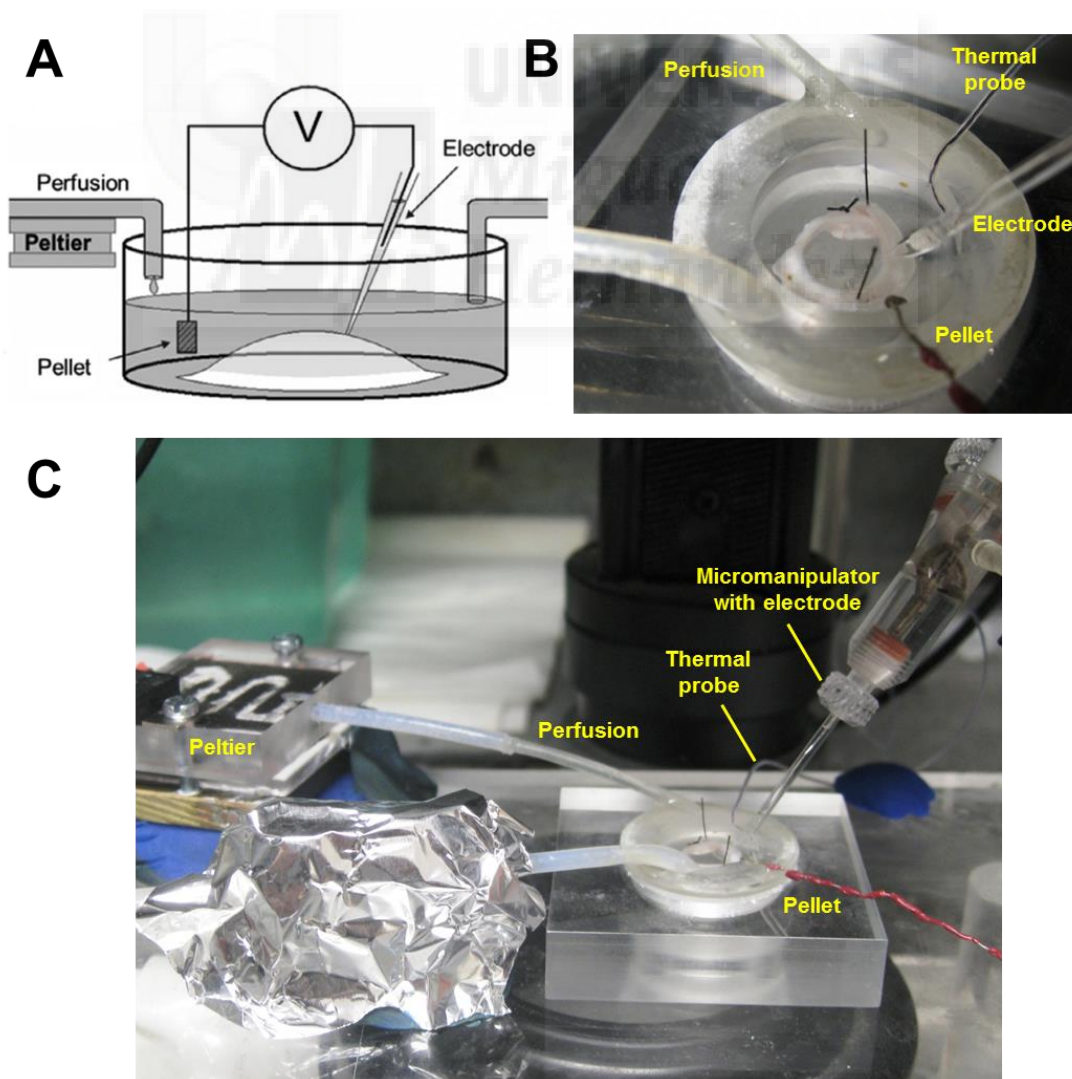


Figure 41. Experimental setup used for the extracellular recording of single nerve terminals in the isolated cornea. A. Schematic diagram of the chamber (from Acosta et al., 2013). B, C. Photographs of the original setup.

F.2. Data analysis

To quantify the response of corneal cold nerve terminals to cooling and heating stimuli, the following parameters were measured:

- a- **Mean frequency of the ongoing NTI activity**, which is the average number of impulses recorded per second measured during 1 minute at the basal temperature of 34°C, expressed in imp/s (Figure 42 a).
- b- **Cooling threshold**, which is the temperature change in °C (measured during a cooling ramp from 34°C to 20°C) at which firing frequency increases by 25% the mean NTI frequency at basal temperature of 34°C. (Figure 42 b).
- c- **Peak frequency in response to cold**, which expresses the maximal firing frequency value in imp/s attained during a cooling stimulus (Figure 42 c).
- d- **Temperature change at peak frequency**, which is the temperature change in °C required reaching the peak frequency value during the cooling stimulus (Figure 42 d).

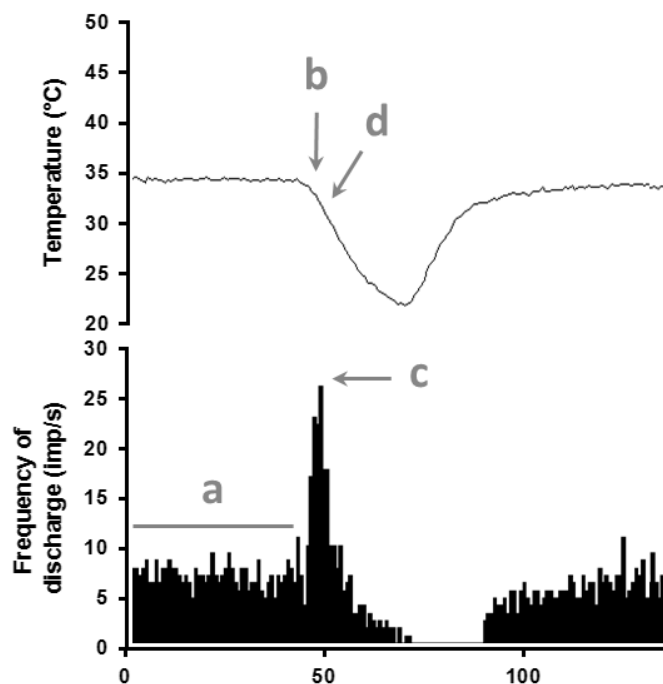


Figure 42. Example of the change in NTI activity in a corneal cold nerve terminal evoked by thermal stimulation. Upper trace: Recording of the temperature of the perfusion solution, measured with a thermal probe located near the receptive field of the nerve terminal. Lower trace: histogram of the firing frequency in impulses per second. The parameters used to quantify the cooling response were: mean frequency of the ongoing NTI activity at the basal temperature of 34°C (a); cooling threshold (b); peak firing frequency (c); temperature required to reach peak frequency during the cooling pulse (d).

F.3. Recording of nerve filaments from the ciliary nerves

Young and adult animals were euthanized with an overdose of anesthetic and connective tissue and extraocular muscles at the back of the eye were carefully removed to expose and isolate the ciliary nerves around the optic nerve. The excised eye was then placed in a chamber divided in two compartments by a Sylgard-coated plastic wall. The front of the eye was introduced into a round perforation made in the center of the dividing wall to which the bulbar conjunctiva was pinned, thereby isolating the front from the back of the eye (Figure 43 A). This prevented direct exposure of the ciliary nerves located in the back compartment to the chemical substances applied onto the corneal surface. The anterior compartment was continuously bathed with warmed (34°C) physiological saline solution of the following composition (in mM): NaCl, 133.4; KCl, 4.7; CaCl₂, 2; MgCl₂, 1.2; NaHCO₃, 16.3; NaH₂PO₄, 1.3; glucose, 7.8, gassed with 95%O₂-5%CO₂ to maintain a pH=7.4. The rear compartment was filled with warm mineral oil. Thin nerve filaments were teased apart from the ciliary nerve trunks and placed on an Ag-AgCl electrode for monopolar recording of single unit impulse activity, using conventional electrophysiological equipment (DAM50 amplifier, WPI, Sarasota, FL, USA). Electrical signals were fed into a PC through an acquisition system (CED Micro1401), and analyzed with Spike2 software. Receptive fields of afferent fibers innervating the corneoscleral surface were located using mechanical stimulation with a fine paint brush and mapped thereafter using a von Frey hair (5.88 mN). Spontaneous activity was measured during 1 min from recordings obtained before any stimulation was applied. Mechanical threshold was determined assessing the first impulse response evoked by 0.25 to 4 mN calibrated von Frey hairs of increasing diameter (Bioseb, Vitrolles, France). For chemical stimulation, a gas jet of 98.5% CO₂ was applied on the corneal receptive field during 30 s (Acosta, Luna et al. 2013; Acosta, Luna et al. 2014). Thermal stimulation was performed by heating (up to 45°C) or cooling (down to 20°C) the perfusion solution by means of a custom-made Peltier device.

Single fiber recordings of ciliary nerves were stored for off-line analysis with Spike2 software. Impulse firing of individual units discriminated accordingly to their amplitude and shape was analyzed. **The ongoing impulse activity**, expressed as the mean impulse frequency (in impulses/s) measured during 30 s at the beginning of the recording and during the interstimulus periods. Additionally, the following parameters were measured to quantify the response to CO₂ stimulation (Acosta, Luna et al. 2013):

- a- **Latency**: time delay between onset of the CO₂ pulse and the first impulse given by the unit.
- b- **Mean discharge rate**: mean number of impulses per second (imp/s) throughout the CO₂ pulse.
- c- **Postdischarge**: mean firing frequency (imp/s) during 30s immediately after the CO₂ pulse.

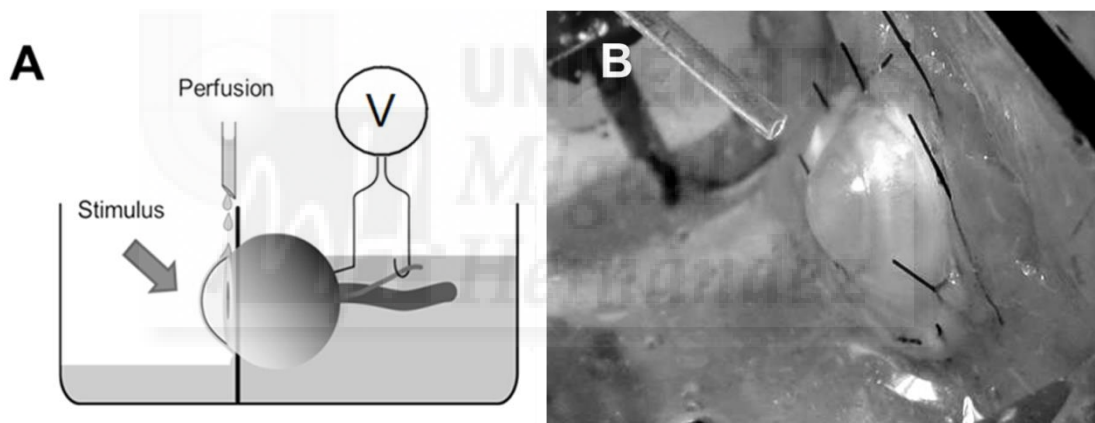


Figure 43. Experimental setup used for the extracellular recording of single units from the ciliary nerves. A. Schematic diagram of the chamber (from Acosta et al., 2013). B. Photograph of the original setup.

G. Statistical analysis

Data were collected and processed for statistical analysis (SigmaStat, v 3.5; Systat Software, Erkrath, Germany). All data were expressed as the mean \pm SEM, with n being the number of explored unit referring to presented study.

For comparing two samples an unpaired Student t-test was used. To compare three or more samples One Way ANOVA test with Bonferroni correction was used. The Linear Regression test was used to describe the distribution of data sets increasing or decreasing in linear-like fashion. Pearson Product Moment Correlation test was used to confirm the correlation between data as indicated.

In all performed tests $P < 0.05$ or below was considered significant



IV. RESULTS

A. THE EFFECTS OF AGE

A.1. Tearing rate

The tearing rate was measured in 24 young (2 months old) and 16 adult (9 months old) guinea pigs. Measurements were performed using phenol red threads and expressed as the millimeters of the thread marked by tears. Tearing rate increased slightly with age, although the difference between both age groups was no significant (Figure 44).

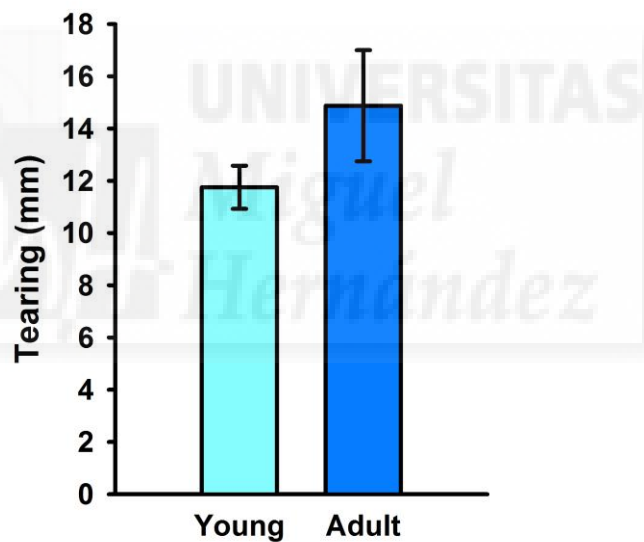


Figure 44. Tearing rate in young and adult guinea pigs. There was no significant difference in tearing rate between young (2 months old) and adult (9 months old) animals. Data are mean \pm SEM. n=24 (young), n=16 (adult). P=0.127, t-test.

A.2. Morphology of corneal nerves

The morphological study of the corneal innervation was performed in guinea pigs of different ages. The immunofluorescence and immunoperoxidase staining was carried out in the

following age groups: 1 month, 2 months, 4 months, 9 months and 12 months, to study various nerve morphology parameters either in whole mount cornea or in its superior quadrant.

A.2.1. Corneal surface area

The evolution of corneal surface area was studied by measuring the area of whole mount corneas of animals of different ages: 1 month (n=4), 2 months (n=13), 4 months (n=10), 9 months (n=14) and 12 months (n=4). As expected, corneal surface increased with age. The estimated growth rate of the cornea was calculated as the increase of the surface area (mm²) per month, being the area increments higher during the first months of the guinea pig life (Table 1; Figure 45). There was a positive correlation between corneal surface and age (Pearson correlation coefficient R=0.884, P<0.001).

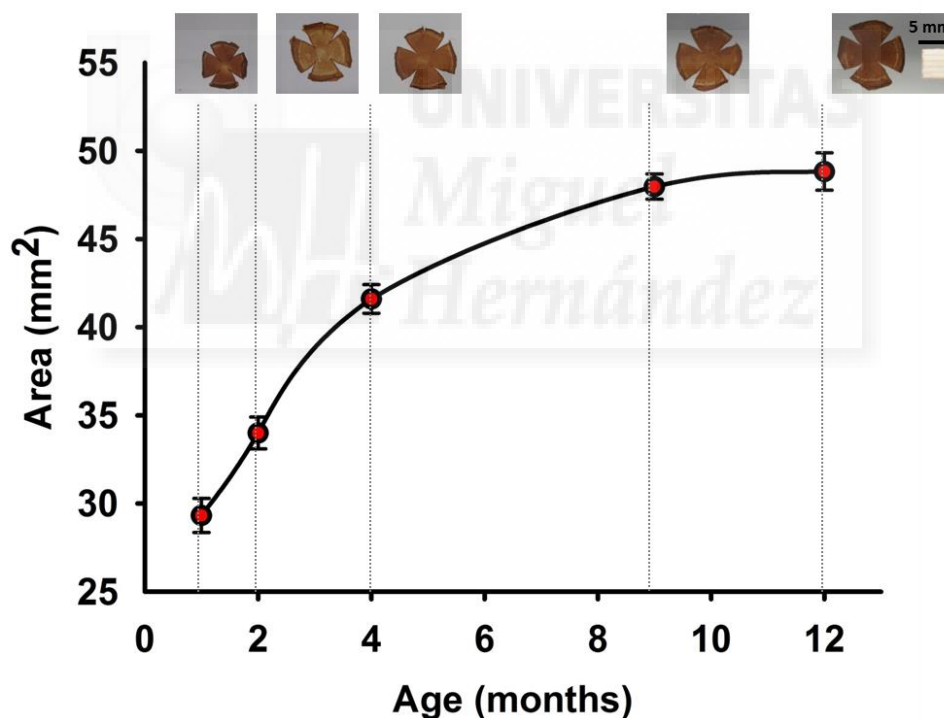


Figure 45. Evolution of the corneal surface area with age. The graph depicts the age-related change in the corneal surface area. Data are mean \pm SEM of the size of the cornea of animals of each age group; n=4-14 (see text for details); the difference between groups is significant (P<0.001, One Way ANOVA with post-hoc Bonferroni t-test). Upper panel: Representative photographs of corneas of animals of different ages stained with the diaminobenzidine technique.

Table 1. Estimated growth rate of corneal surface area with age.

Age (months)	Surface area (mm ²)	Estimated growth rate (mm ² / month)
1	29.3 ± 1	-
2	34 ± 0.9	4.7
4	41.8 ± 0.5	3.9
9	48 ± 0.7	1.24
12	48.8 ± 1.1	0.27

Data are mean ± SEM, n= 4,13,10,14 and 4 for each age group.

A.2.2. Proportion of subbasal nerve fibers

The proportion of tissue area occupied by subbasal nerve fibers was quantified with ImageJ software by calculating the percentage of one square millimeter area of tissue occupied by the subbasal nerves. The measurements were performed at three different zones of the superior quadrant of the cornea (peripheral, central, vortex) of animals of different ages: 1 month (n=4), 2 months (n=8), 4 months (n=5), 9 months (n=9), and 12 months (n=4) (Figure 47 A, B, C, D, E respectively). This method gives a rough estimate of the “density” of nerve tissue in a definite zone of the cornea, although the actual density of subbasal nerves (defined as the number of nerves per square millimeter) is presented in section A.2.4.

Figure 46 summarizes the measurements performed in peripheral (Figure 46 A), central (Figure 46 B), and vortex zones (Figure 46 C). In all cornea zones, the proportion of tissue area occupied by subbasal fibers was higher at the first month of life and decreased linearly between 1 and 4 months (Pearson correlation coefficients R=0.588, 0.558 and 0.404 for the peripheral central and vortex zones) and presented similar values afterwards in all cornea zones. The proportion of tissue surface occupied by nerve terminals in all cornea zones could be adjusted to a second order regression (Figure 46, A and C insets) and to a primer order regression (Fig. 46, B inset). The proportion of tissue area occupied by subbasal nerves was similar at all cornea zones in all age groups (Figure 46 D).

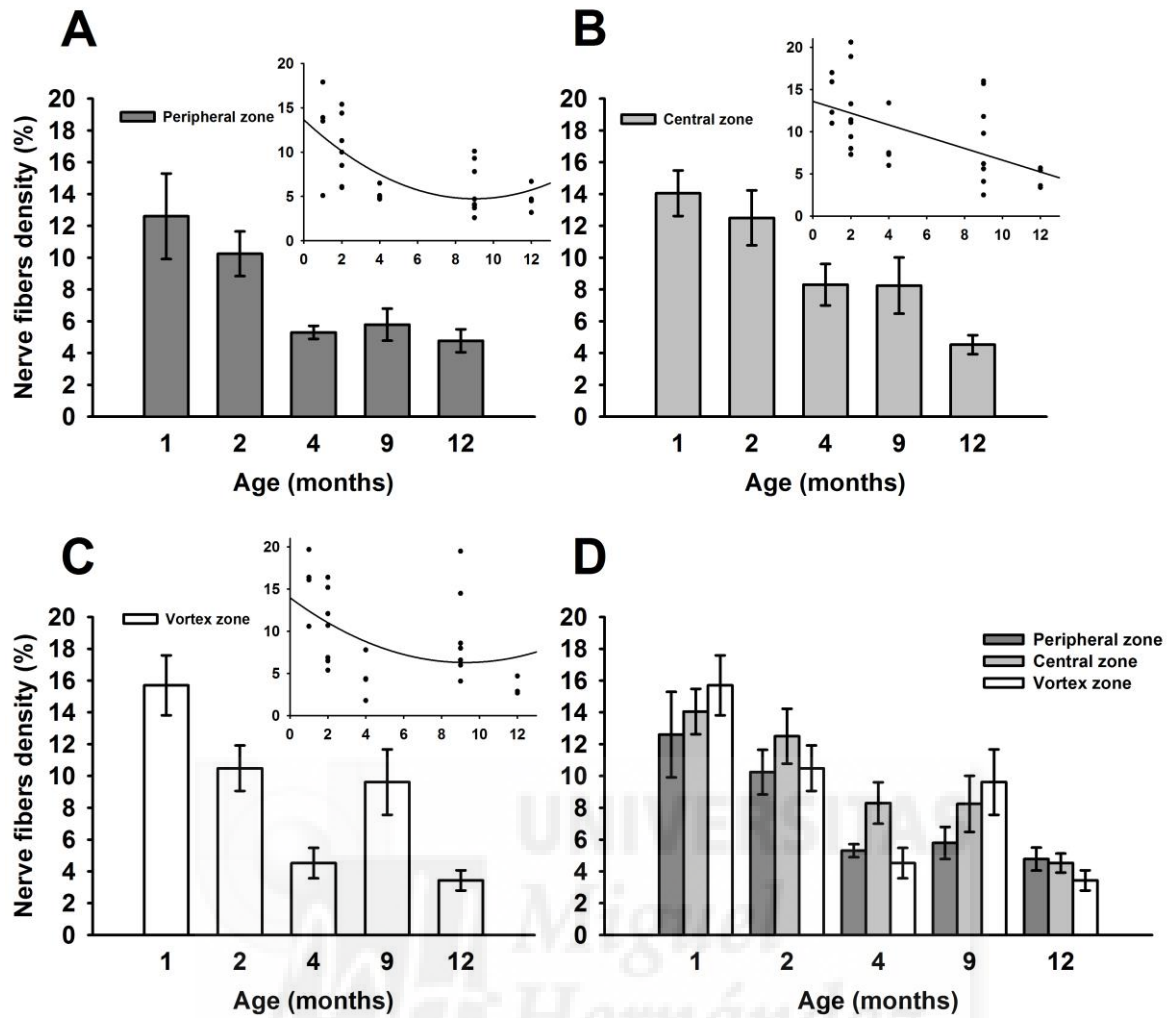
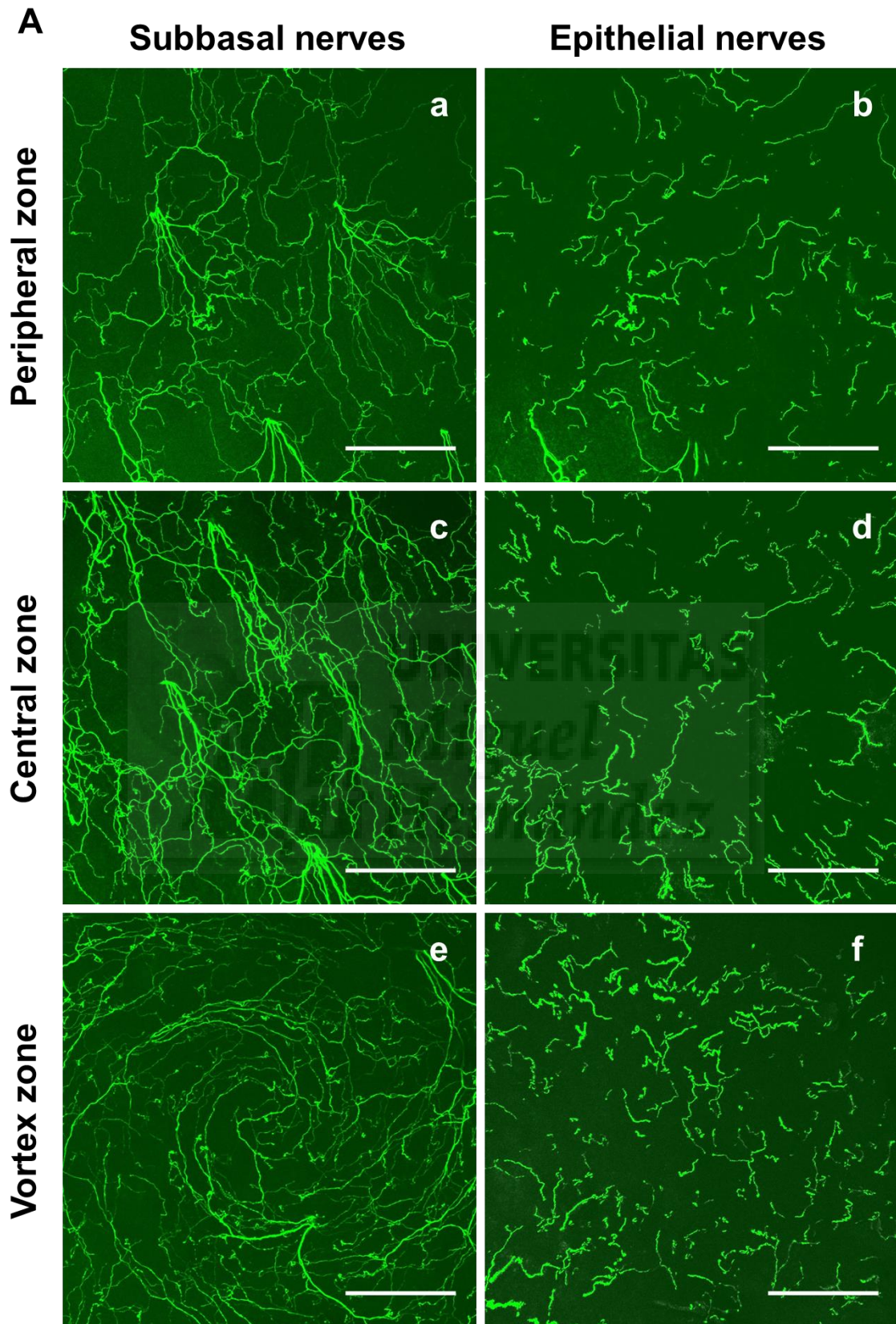
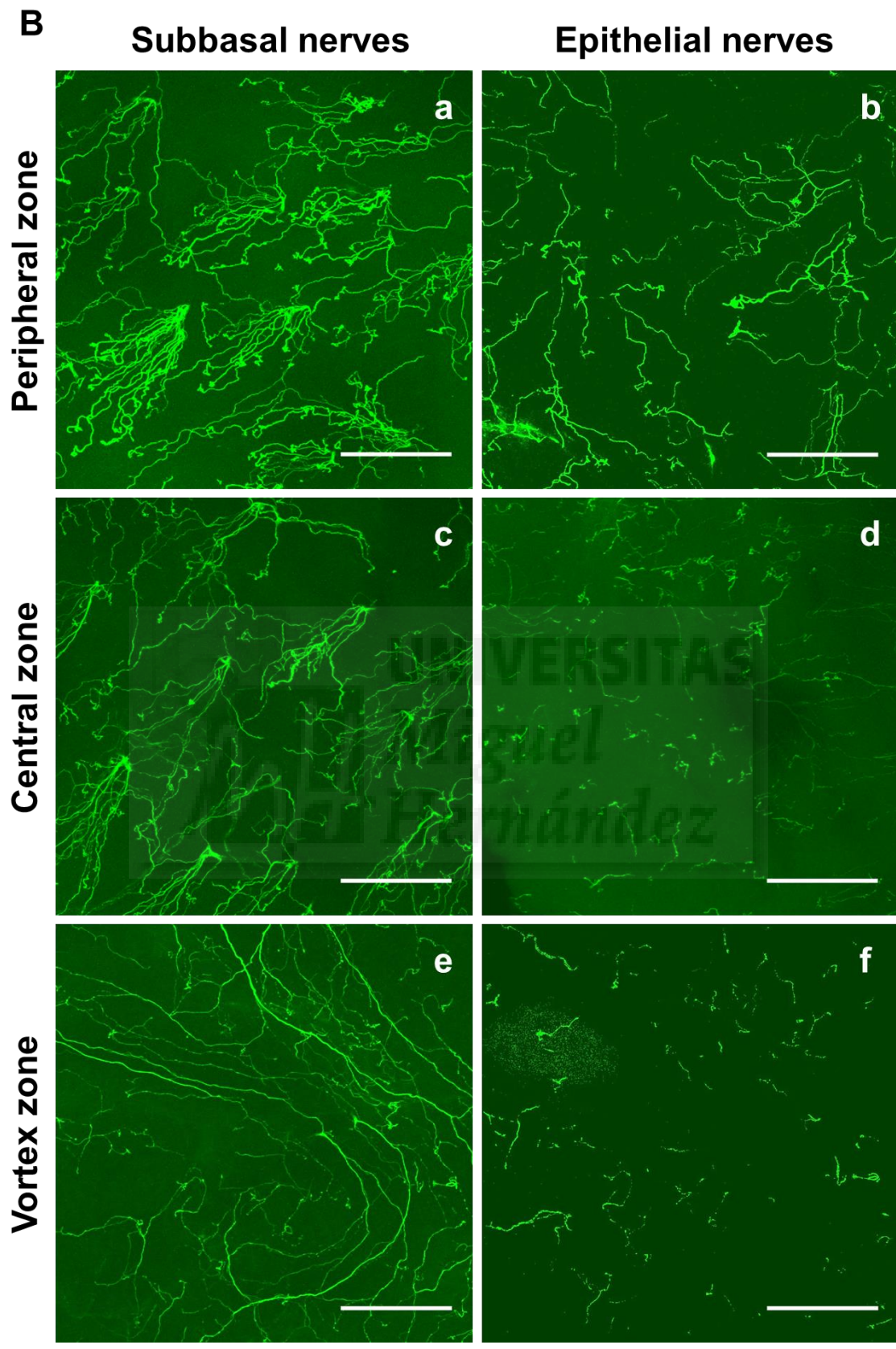
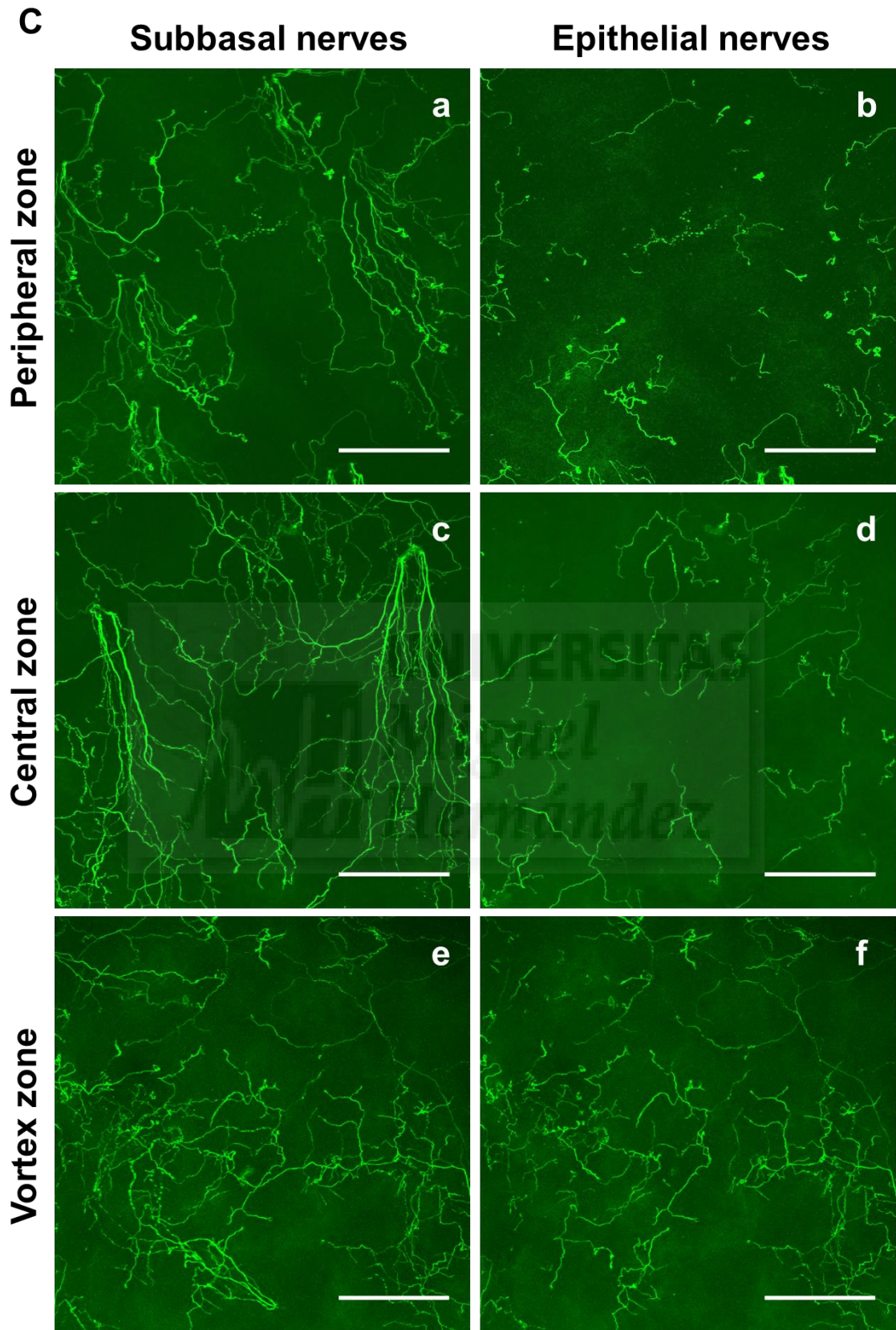
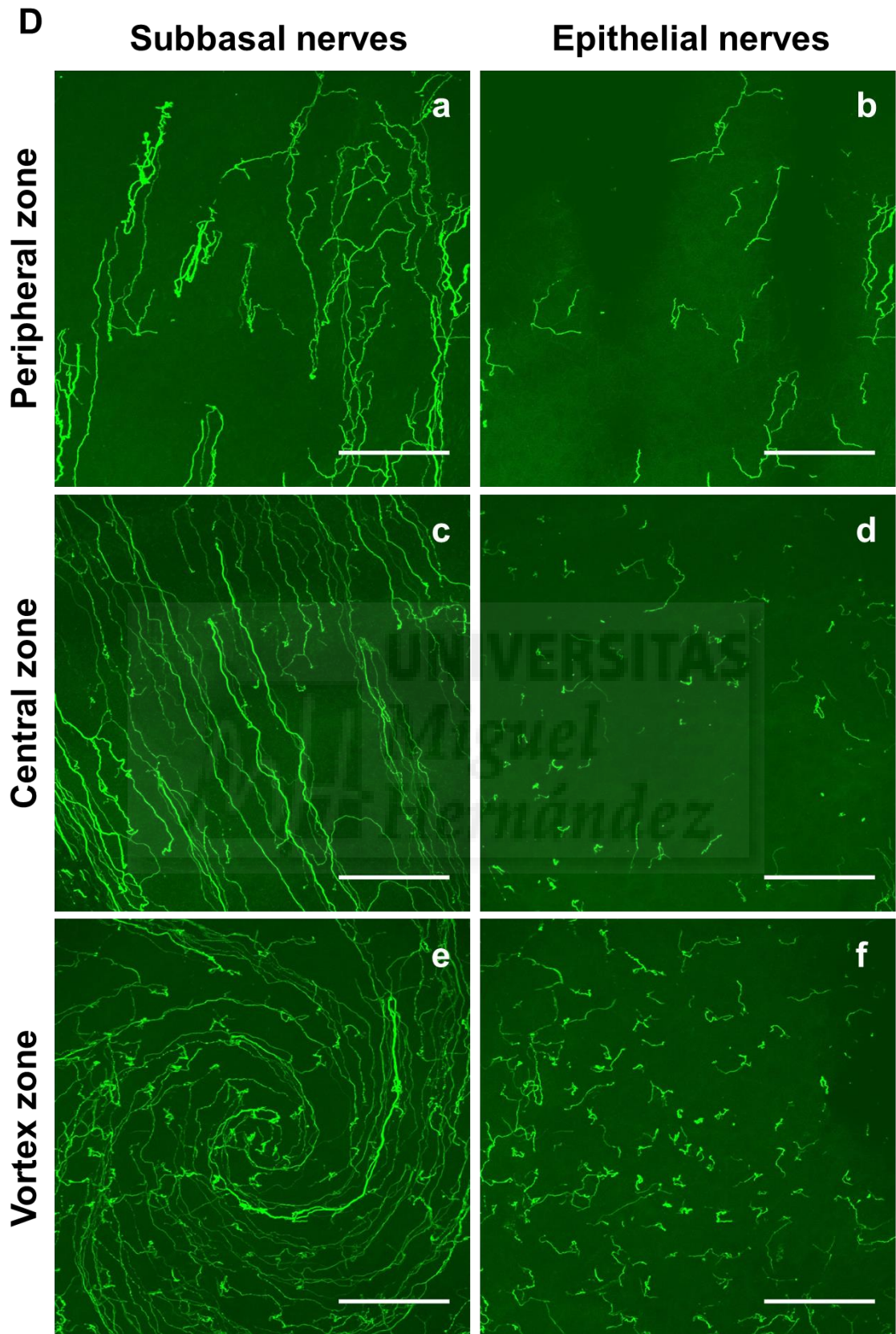


Figure 46. Changes in the proportion of tissue area occupied by subbasal nerve fibers with age. Measurements were done in a 1 mm x 1 mm area of the superior quadrant of the cornea in the (A) peripheral, (B) central, and (C) vortex zones. The insets show the adjustment to a second order linear regression: (A) $P=0.001$, $R^2=0.418$; (C) $P=0.037$, $R^2=0.190$; and to a first order linear regression: (B) $P=0.001$, $R^2=0.312$; (D) ANOVA showed no differences in nerve fiber proportion within each age group among peripheral (dark gray), central (gray), and vortex (white) zones. All data are mean \pm SEM. $n=4-9$ (see text for details).









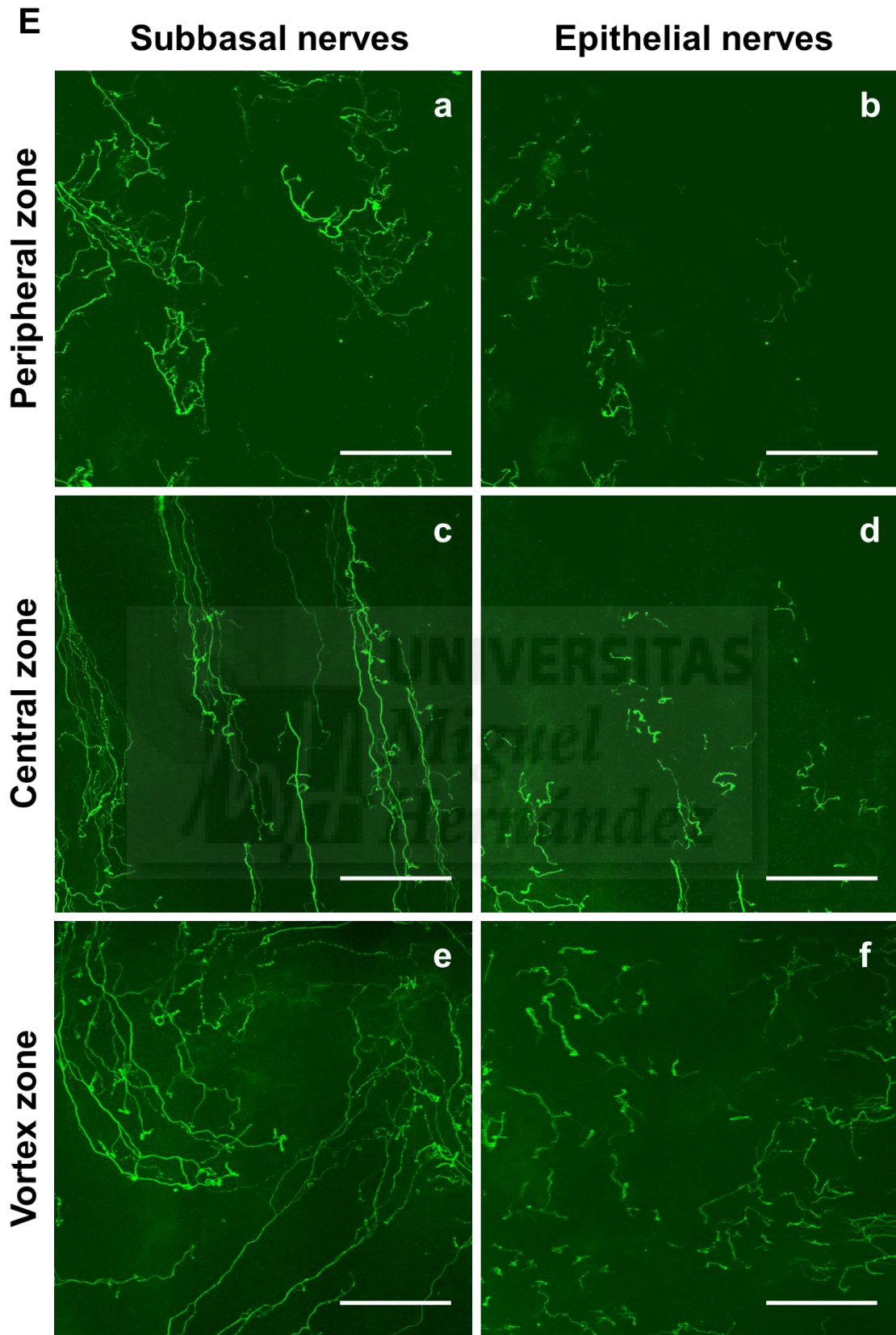


Figure 47. TUJ-1 positive corneal nerves in corneas of animals of different ages: 1 month (A), 2 months (B), 4 months (C), 9 months (D), and 12 months (E). The level of subbasal plexus (a, c, e) and the intraepithelial nerve terminals (b, d, f) present in three different zones of cornea are shown: peripheral (a, b), central (c, d) and vortex (e, f). Magnification 40x; Scale bar=100 μ m.

A.2.3. Total number of subbasal nerve leashes

The total number of subbasal nerve leashes was counted in the whole cornea of animals of different ages: 1 month (n=4), 2 months (n=7), 4 months (n=5), 9 months (n=9) and 12 months (n=4). The number of subbasal nerves in the peripheral and central zone of the cornea was also counted. The number of subbasal nerves changed significantly with age ($P < 0.001$, One Way ANOVA). An increase in the number of corneal nerve leashes was observed at 2 months compared with other age groups up to 12 months old (Table 2; Figure 48 A).

The same phenomenon of increment in total subbasal nerve leash number during second month of life and following drastic drop between third and fourth month was noticed when the number of nerve leashes was quantified separately in both, peripheral and central zones (Figure 48 B). There were significant differences in the total number of nerve leashes in the peripheral and central cornea zones between the age groups ($P < 0.001$, One Way ANOVA).

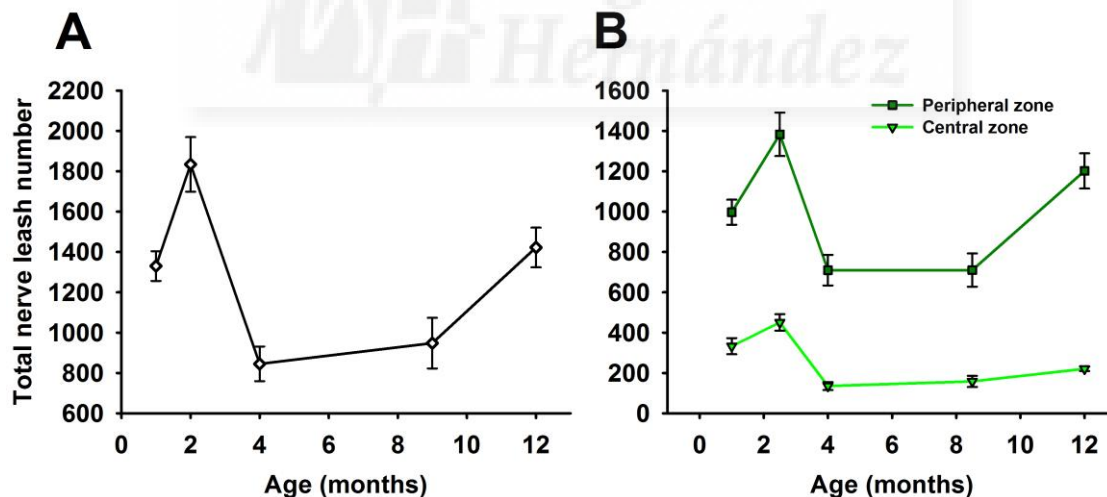


Figure 48. Evolution of the number of subbasal nerve leashes with age. Quantification was performed in whole mount immunostained corneas. (A) Average total number of nerves per cornea in animals of different ages. (B) The number of subbasal nerves in the peripheral (dark green line) and central (light green line) zones of the cornea were also counted and followed similar time courses. The total number of subbasal nerves in the peripheral area was significantly higher than in the central area ($P < 0.001$, One way ANOVA). Data are mean \pm SEM. n= 4-9 (see text for details).

Table 2. Change on the number of subbasal nerve leashes in the whole cornea with age.

Age (months)	Total nerve number	Estimated nerve leash number change per month
1	1330 ± 74	-
2	1834 ± 135	504
4	845 ± 86	-494.5
9	948 ± 126	20.6
12	1422 ± 99	158

Data are mean ± SEM, n= 4,13,10,14 and 4 for each age group.

A.2.4. Density of subbasal nerve leashes

The density of subbasal nerve leashes was estimated from the total number of nerve leashes counted and the surface area of each cornea, and expressed in number of nerves per square millimeter. The density in the whole cornea (Table 3) and in both the peripheral and central zone of the cornea was determined in animals of different ages: 1 month (n=4), 2 months (n=7), 4 months (n=5), 9 months (n=8) and 12 months (n=4) (Figure 50). There are significant differences in the density of subbasal nerve leashes in the entire cornea with age, and also in the peripheral and central cornea zones ($P < 0.001$, One Way ANOVA). The curves representing data of the total number of subbasal leashes in the entire cornea and those from the central or the peripheral zones were similar. An increase was observed at the second month of life, followed by a drop between four and nine months and an increase again at the age of twelve months, at which a value similar to that of 2 months old was attained (Figure 49). Comparing the density of nerve leashes between peripheral and central zones of the cornea in each age group, differences were found within the groups of 4 months ($P < 0.01$, t-test), 9 months ($P < 0.05$, t-test) and 12 months ($P < 0.001$, t-test) (Figure 49).

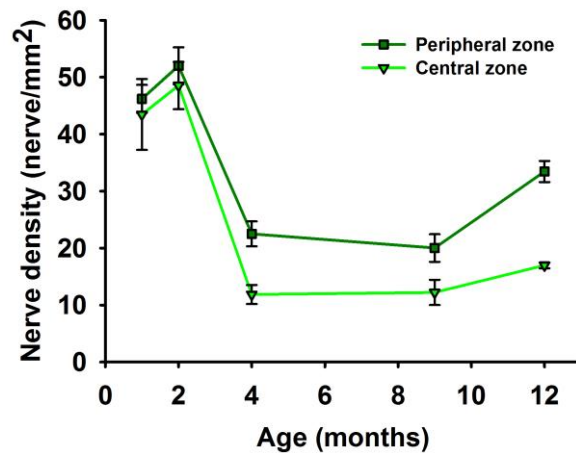
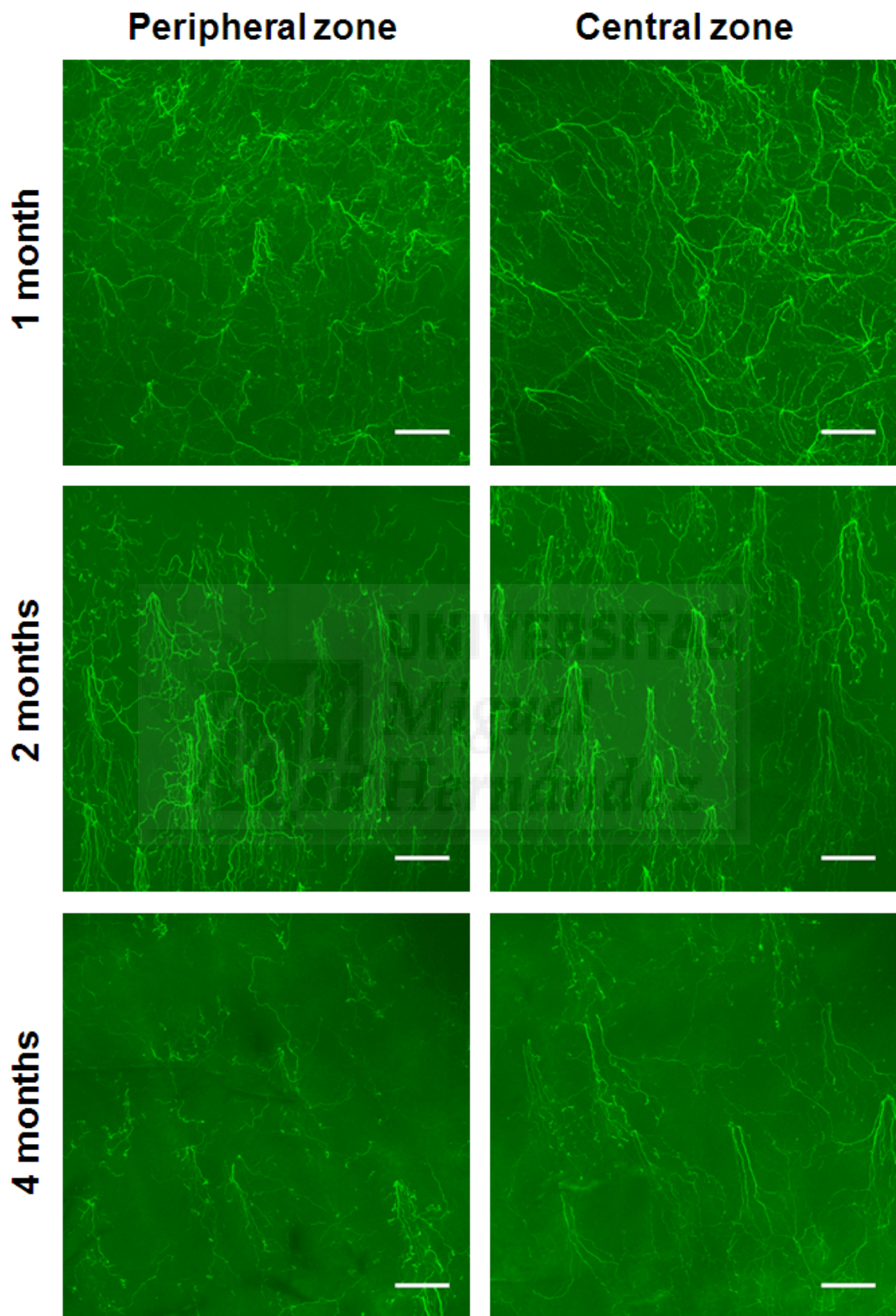


Figure 49. Changes in the density of subbasal nerve leashes with age. The number of subbasal nerves and the area were measured to estimate the nerve density in peripheral (dark green line) and central (light green line) zones. The nerve density was compared within each age group between peripheral (dark green) and central (light green) zones, being statistically significant (Student t-test, see text for details). Data are mean \pm SEM. $P < 0.001$, ANOVA, Bonferroni t-test (see text for details). $n = 4-8$ (see text for details).

Table 3. Density of subbasal nerve leashes in the whole cornea with age.

Age (months)	Nerve number/mm ²
1	45.4
2	53.9
4	20.2
9	19.8
12	29.1

Data are mean \pm SEM, $n = 4, 7, 5, 8$ and 4 for each age group.



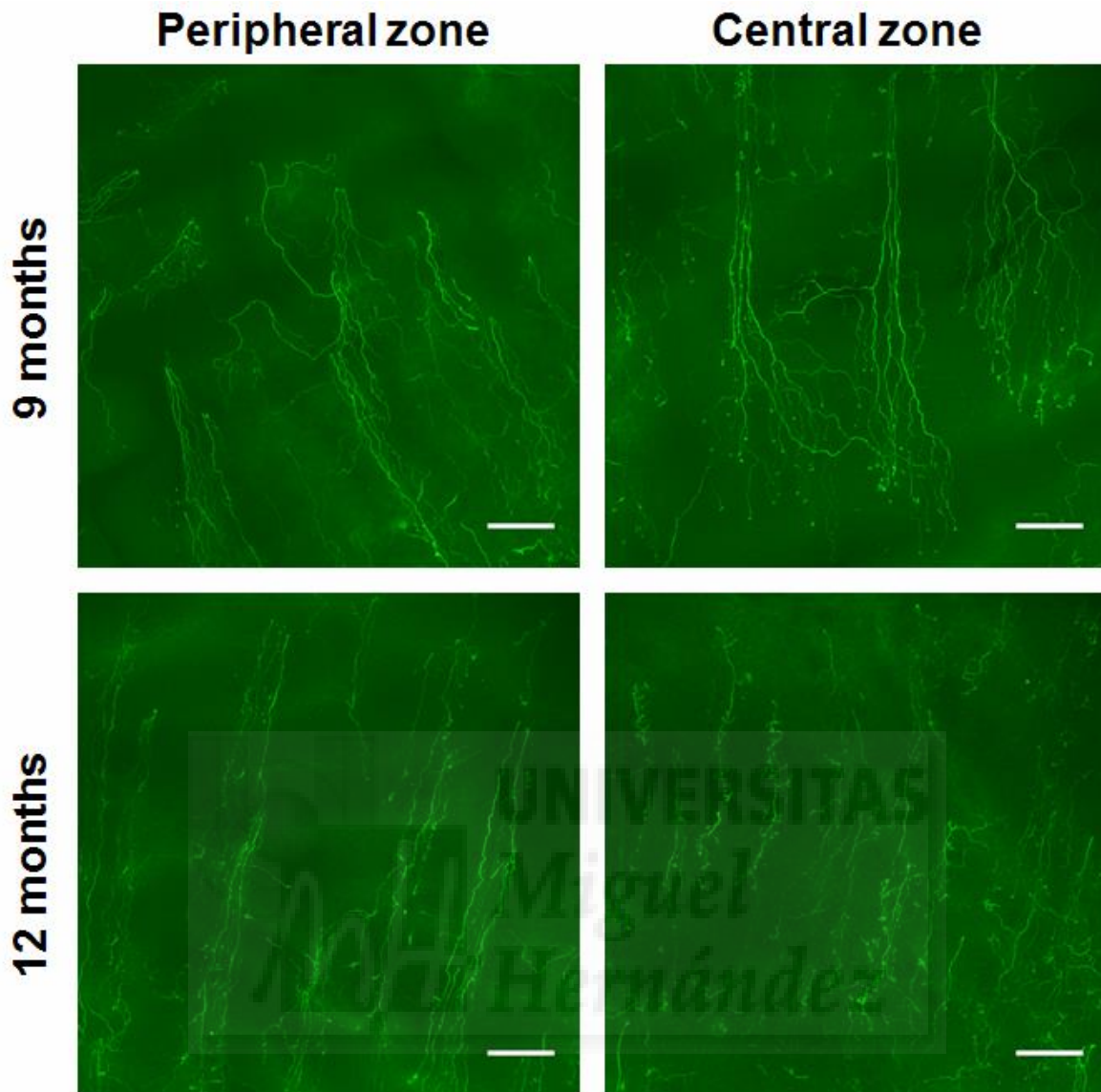


Figure 50. Fluorescence immunostaining of TUJ-1 positive subbasal nerve leashes in peripheral (left) and central (right) zones of cornea of animals of different ages: 1 month (A, B), 2 months (C, D), 4 months (E, F), 9 months (G, H), and 12 months (I, J). Magnification 10x; Bar=100 μ m.

A.2.5. Length of subbasal nerve leashes

The length of subbasal nerve leashes was measured in corneas of animals of different ages: 1 month (n=4), 2 months (n=8), 4 months (n=5), 9 months (n=9), and 12 months (n=5) (Figure 52). The measurements of the nerve length were performed in the peripheral (Figure 51 A), central (Figure 51 B) zones, and at the vortex area (Figure 51 C) of the superior quadrant of the cornea and expressed in micrometers (see methods). The increase of length of subbasal

nerves was significantly correlated with age in the peripheral and central cornea and at the vortex (Pearson correlation coefficients $R=0.809$, 0.789 and 0.783 respectively, $P<0.001$).

There were differences in the length of subbasal nerves among corneal zones within each age group. Central and vortex nerves were significantly longer than peripheral nerves in every age group of corneas (Figure 51 D).

Estimated rate of elongation with age of subbasal nerve leashes was counted for different corneal zones (Table 4).

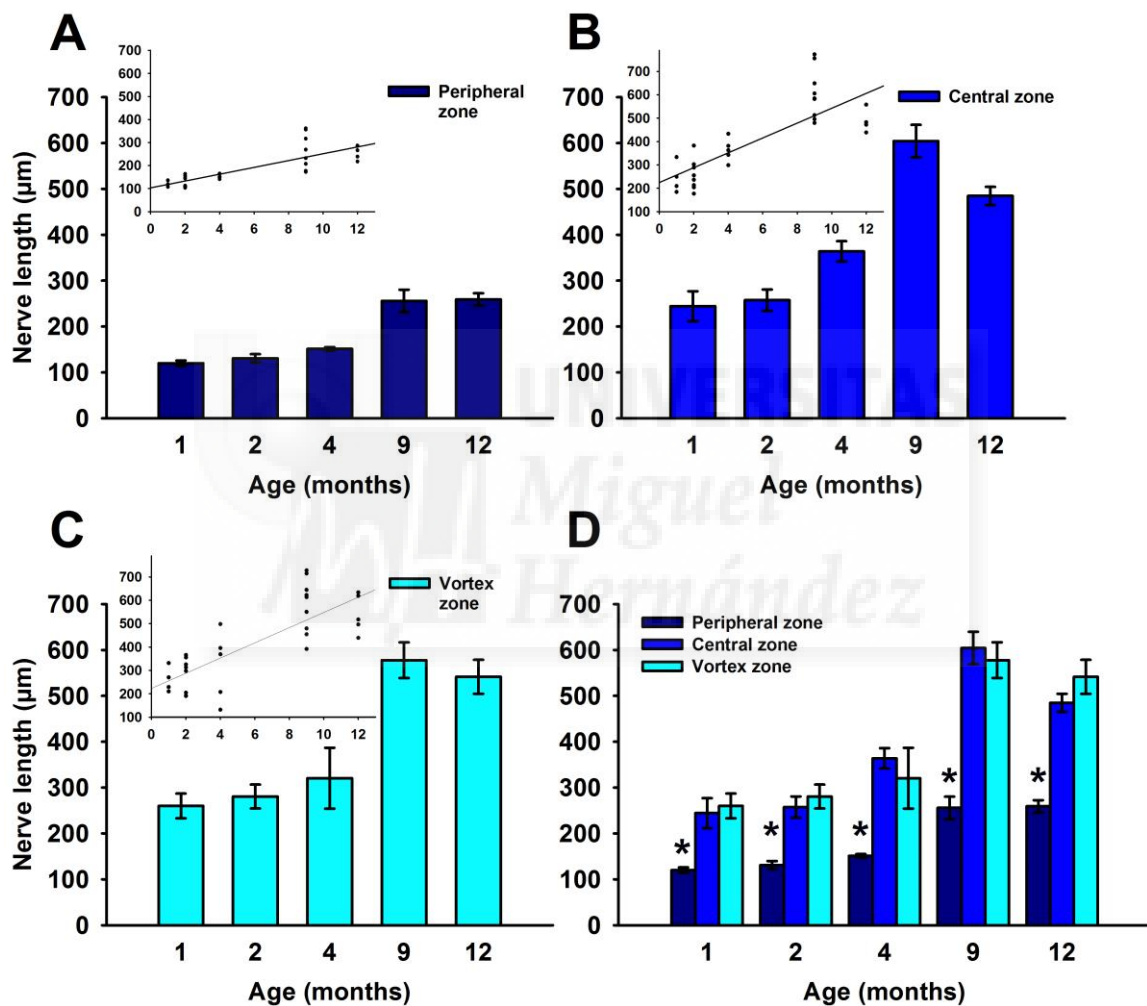
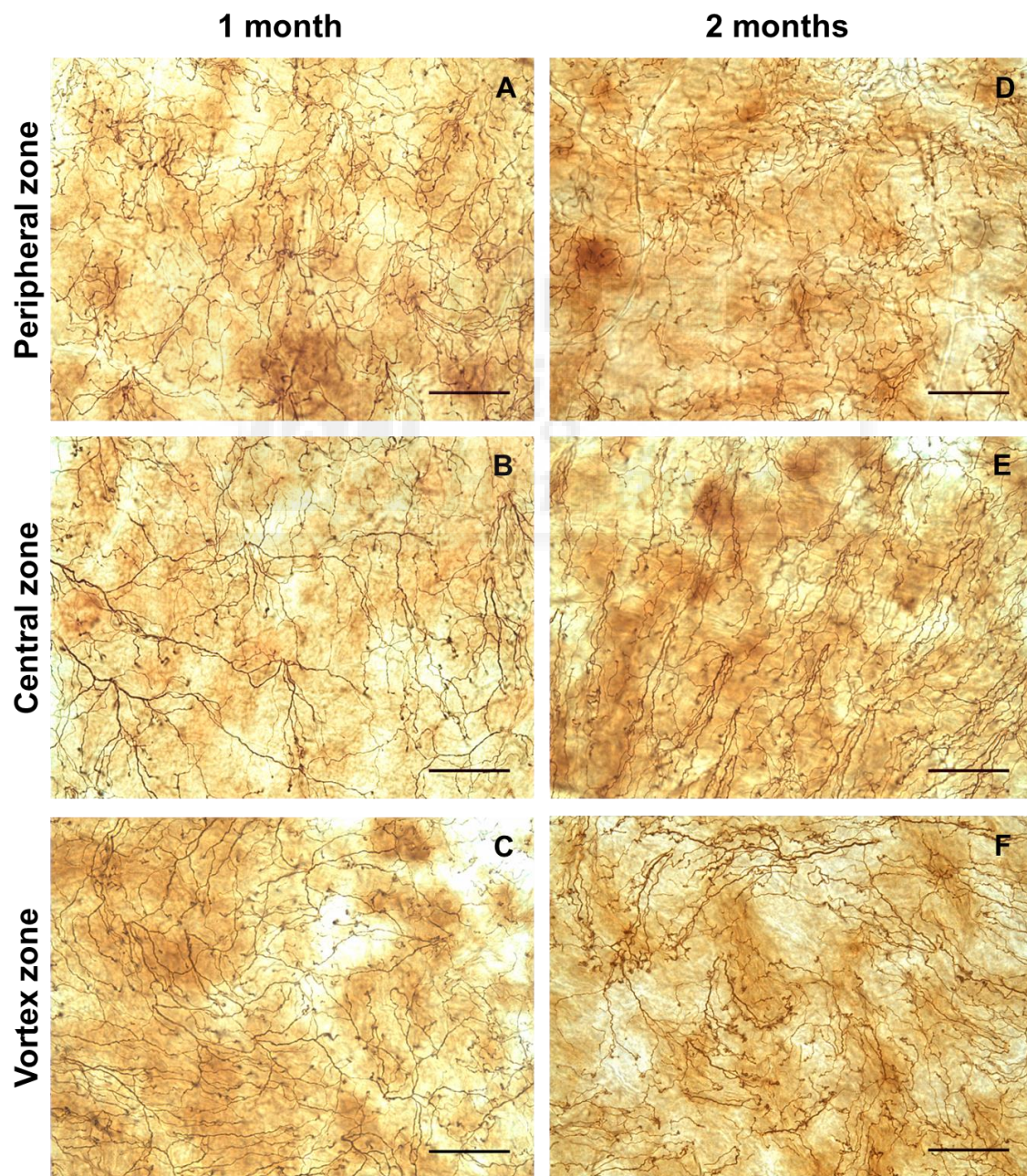


Figure 51. Changes in the length of subbasal nerve leashes with age. Measurements were done in the superior quadrant of the cornea in (A) peripheral, (B) central, and (C) vortex zones. Insets show linear regression adjustment: (A) $R^2=0.654$. (B) $R^2=0.622$. (C) $R^2=0.614$. (D) The nerve length was compared within each age group among peripheral (dark blue), central (blue), and vortex (light blue) zones, being statistically significant ($*P<0.05$, ANOVA with post-hoc Bonferroni t-test). All data are mean \pm SEM. $n=4-9$ (see text for details).

Table 4. Estimated rate of elongation with age of subbasal nerve leashes in different zones of the cornea.

Cornea zone	Length increase rate ($\mu\text{m}/\text{month}$)
Peripheral	14.8
Central	31.8
Vortex	32.5

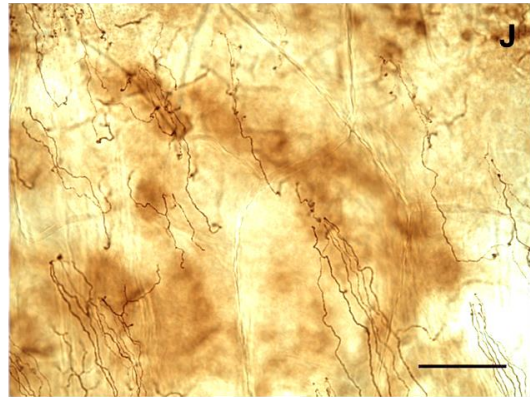
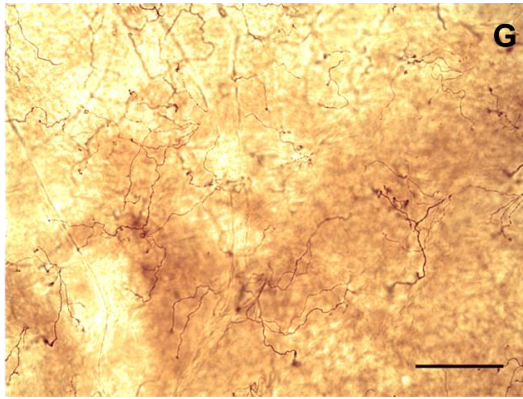
The length increment rate per month ($\mu\text{m}/\text{month}$) was estimated as the slope of the linear regression calculated with length values measured at different ages (1, 2, 4, 9 and 12 months).



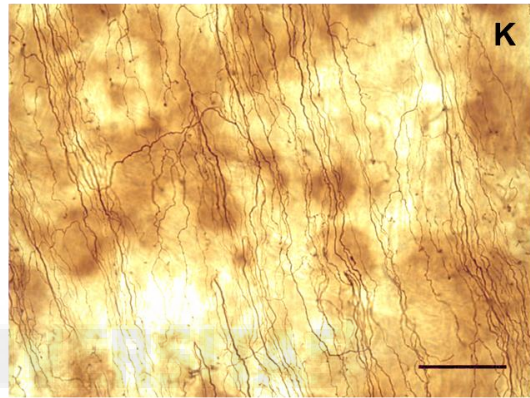
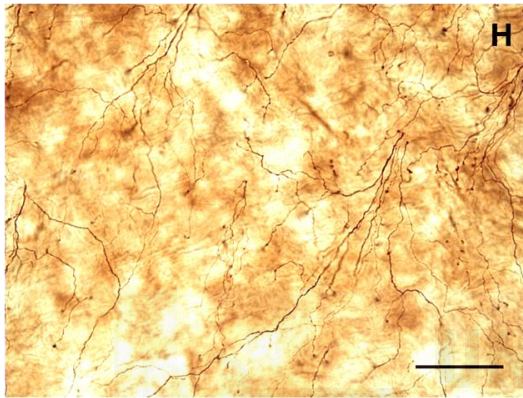
4 months

9 months

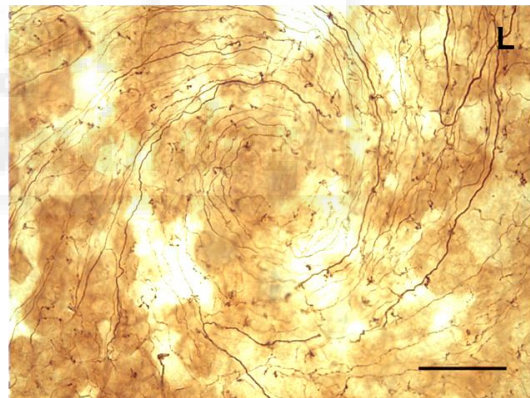
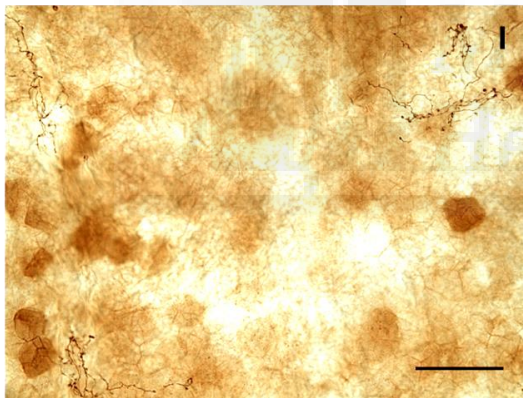
Peripheral zone



Central zone



Vortex zone



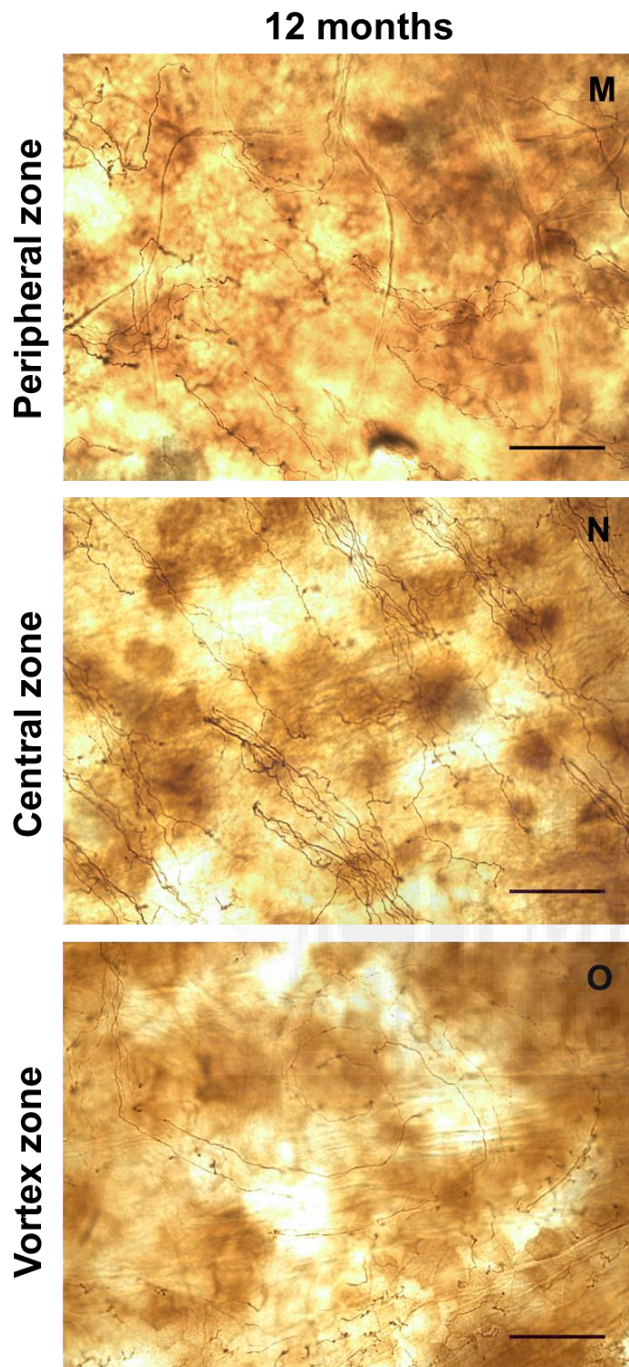


Figure 52. Tuj-1 positive subbasal nerve leashes in the peripheral and central cornea, and the vortex zone of guinea pigs of different ages. Corneas of animals of 1 month (A, B, C), 2 months (D, E, F), 4 months (G, H, I), 9 months (J, K, L), and 12 months (M, N, O) stained with the diaminobenzidine technique are shown. Magnification 20x; scale bars=100 μ m.

A.2.6. Density of epithelial nerve terminals in different cornea zones

The density of corneal nerve terminals was calculated in 1 mm x 1 mm area at three different zones of the superior quadrant of the cornea (peripheral, central, and vortex) using ImageJ software (Figure 53 A, B, C, respectively). Epithelial nerve terminals density was

calculated in corneas of 1 month (n=4), 2 months (n=8), 4 months (n=5), 9 months (n=9), and 12 months (n=4) old animals (Figure 47 A, B, C, D, E respectively).

The density of epithelial nerve terminals was higher in the age group of 1 month in all cornea zones (Figure 53). Nerve terminals density decreased linearly between 1 and 4 months (Pearson correlation coefficients $R=0.632$, 0.687 for the peripheral and central zones, $P<0.001$; and $R=0.489$ for the vortex zone, $P=0.007$) and presented similar values afterwards in all cornea zones. Overall, the density of nerve terminals in all cornea zones could be adjusted to a first order regression (Figure 53, A, B and C insets). Among all age groups vortex zone had the highest nerve terminals' density, being statistically significant at 1 and 9 months ($P<0.01$, ANOVA), (Figure 53 D).

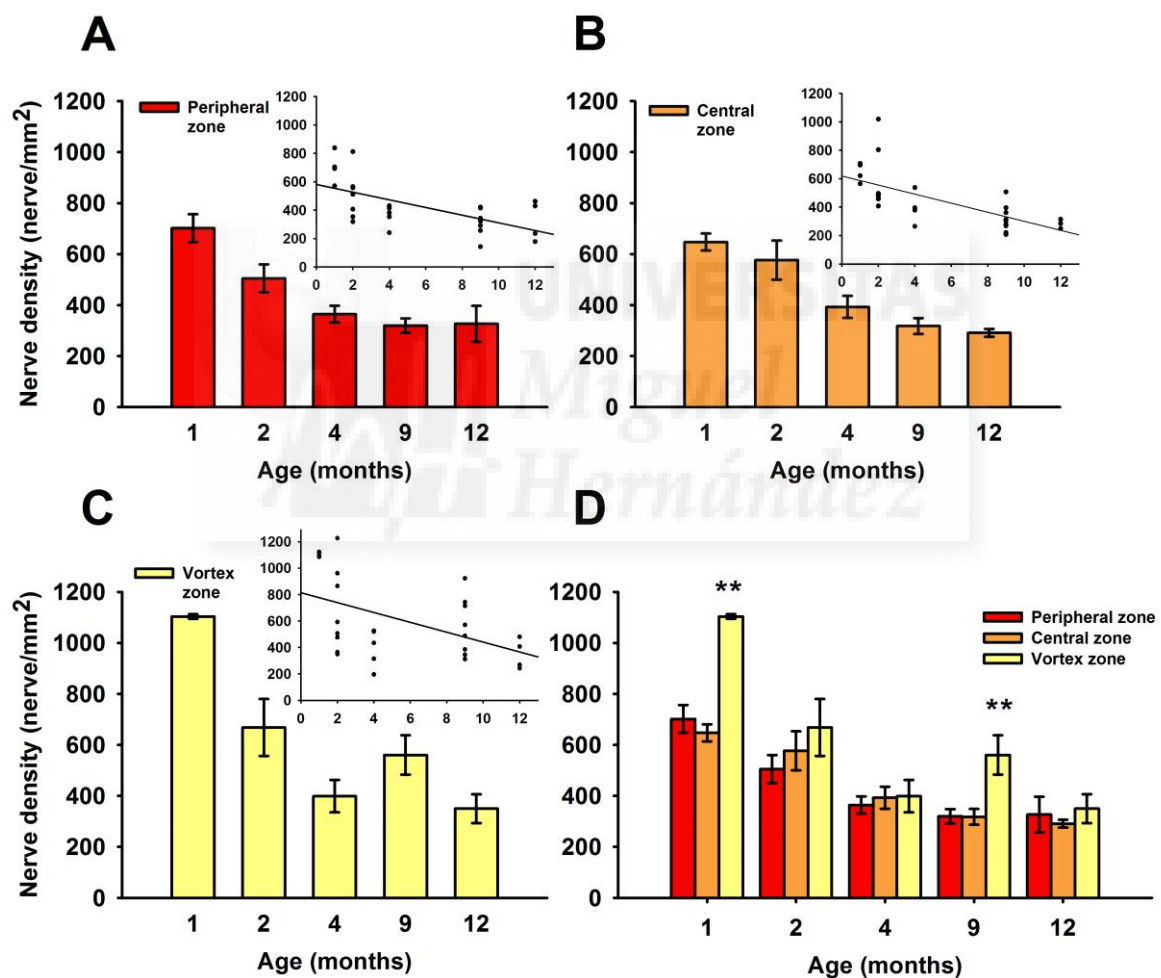


Figure 53. Changes in the density of corneal nerve terminals with age. Measurements were done in a 1 mm x 1 mm area of the superior quadrant of the cornea in the (A) peripheral, (B) central, and (C) vortex zones. The insets show the adjustment to a first order linear regression: (A) $R^2=0.399$; (B) $R^2=0.472$; (C) $R^2=0.239$. (D) The density of nerve terminals was compared within each age group among peripheral (red), central (orange), and vortex (yellow) zones (** $P<0.01$, ANOVA, Bonferroni t-test). All the data are mean \pm SEM. n=4-9 (see text for details).

A.3. Corneal epithelial wound healing

Chemical epithelial corneal debridations were performed in 5 young (2 months old) and 6 adult (7 months old) guinea pigs. Epithelial lesions were stained with fluorescein and photographed every 4 hours.

A.3.1. Area of the epithelial defect

The area of epithelial defect was measured from the photos taken at different time points using ImageJ software (see Methods for details) (Figure 54 A). In both groups of animals, the area of epithelial defect decreased linearly with time, being the epithelial wound fully closed at 20 h after corneal debridation (Figure 54 B).

A.3.2. Estimated migration rate

The migration rate of the epithelial cells surrounding the wound to cover the lesion (epithelial migration rate - EMR), and the estimated time of full wound closure (estimated time of healing - ETH) were then calculated by linear regression of the wound size area with time (Figure 54 B). The EMR was determined calculating the slope of the linear regression of the decrease in the wound radius during the epithelial defect healing phase of each animal, expressed in $\mu\text{m}/\text{h}$. There was a statistically significant difference between the mean EMR of both groups of animals (young and adult guinea pigs), being the migration rate significantly faster in young animals than in adult animals ($69 \pm 4.5 \mu\text{m}/\text{h}$ vs, $51 \pm 5.1 \mu\text{m}/\text{h}$; $P < 0.05$, Student t-test; Figure 54 C).

A.3.3. Estimated time of healing

The ETH was calculated from the linear regression analysis of each wound by extrapolating the x value (time, in hours) for a zero y value (total closure of epithelial defect). The calculated ETH was significantly shorter in young animals than in adult animals (22.3 ± 0.5 hours vs. 31.9 ± 3.1 hours; $P < 0.05$, Student t-test; Figure 54 D).

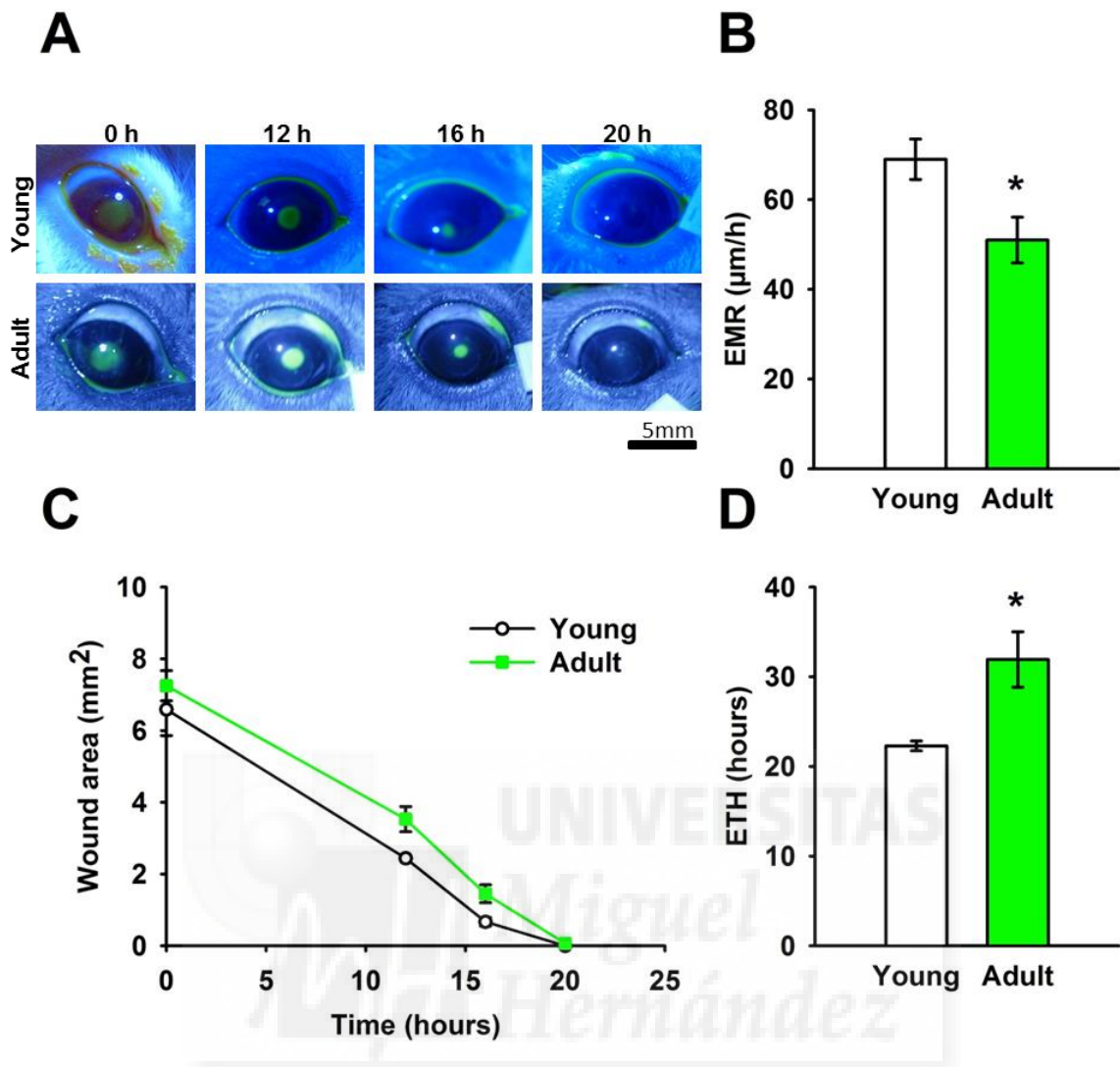


Figure 54. Corneal epithelial debridement closure in young and adult animals. (A) After chemical epithelial debridations performed in young (upper panel) and adult (lower panel) guinea pigs, the epithelial defect was stained with fluorescein and photographed at different time points during healing time; scale bar=5 mm. (B) Evolution of epithelial defect (Wound area) with time. (C) Epithelial migration rate (EMR, calculated as the slope of wound area reduction with time). (D) Estimated time of healing (ETH). Data are mean \pm SEM; * $P < 0.05$, t-test; $n=5$ (young), $n=6$ (adult).

A.4. Electrophysiological recording of corneal sensory receptors

A.4.1. Neural activity of corneal cold nerve terminals

Nerve terminal impulse (NTI) activity was recorded in 67 cold thermosensitive nerve terminals from corneas of 1.8 ± 0.2 month old animals (young group) and in 64 cold nerve terminals from corneas of 8.9 ± 0.2 month old animals (adult group), (Figure 55).

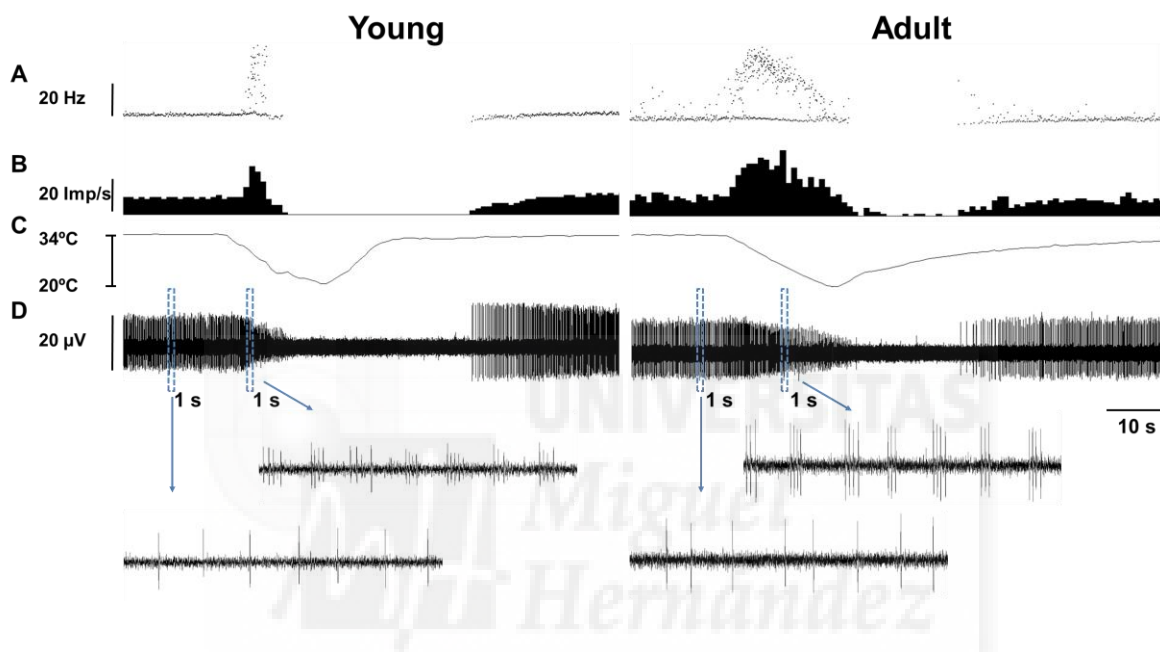


Figure 55. Sample recordings of the response to a cooling stimulus of two different cold thermoreceptors from the cornea of a young (left) and an adult (right) guinea pig. Instantaneous frequency of discharge (1 / interstimulus interval duration) in Hz (A); impulse frequency histogram of NTI activity in impulses per second (B); temperature of the bath solution (C); recording of the NTI activity (D). The insets at the lower part of the figure represent expanded views of the recording during 1 second at indicated moments of the recording (blue lines).

There were no significant differences in the firing pattern or in the ongoing firing activity of cold thermoreceptors at the basal temperature (34°C) between young and adult animals (Table 5, Figure 56 A). No changes were found between both groups of animals in the parameters used to analyze the response to a cooling pulse (from the basal temperature of 34°C to 20°C). The cooling threshold (Table 5, Figure 56 B), peak frequency during the cooling stimulus (Table 5, Figure 56 C) and the temperature change at which the peak frequency was attained (Table 5, Figure 56 D) were not different in young and adult animals (Student t-test).

Table 5. Spontaneous and stimulus-evoked activity of cold corneal receptors in young and adult guinea pigs.

Cold receptors	Young (2 months old) n=67	Adult (9 months old) n=64
Ongoing activity at 34°C (imp/s)	9.0 ± 0.5	8.1 ± 0.6
Cooling threshold (°C)	-2.7 ± 0.2	-2.5 ± 0.2
Peak frequency in response to cold (imp/s)	30.6 ± 1.3	29.0 ± 1.4
Temperature change at peak frequency (°C)	-6.1 ± 0.4	-7.1 ± 0.5

Data are the mean ± SEM. n=number of terminals.

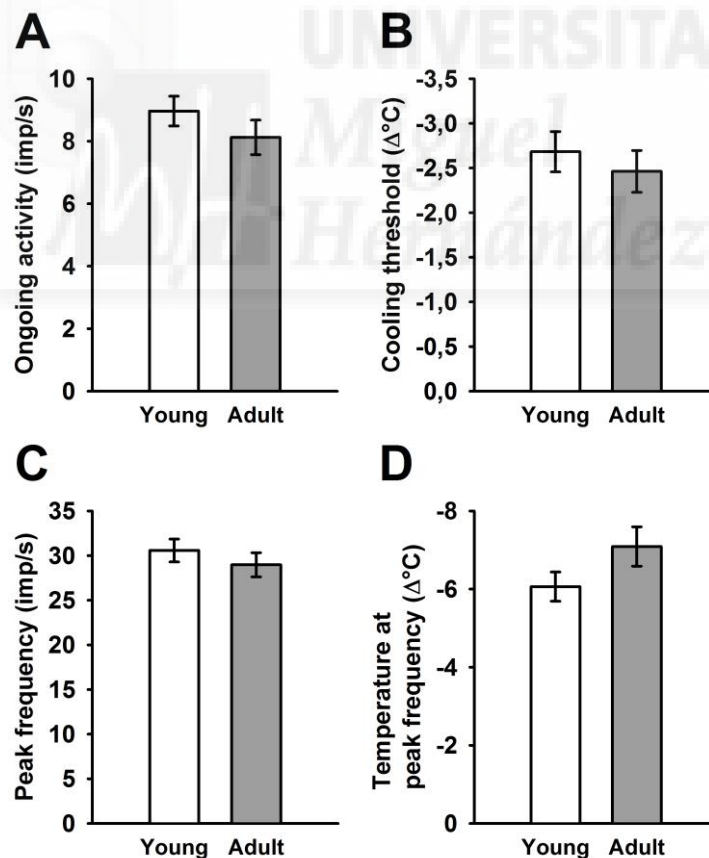


Figure 56. Spontaneous and stimulus-evoked activity of cold thermoreceptors in corneas of young and adult guinea pigs. (A) Ongoing activity at basal temperature (34°C). (B) Decrement in temperature needed to increase by 25% the basal firing frequency of discharge at 34°C (cooling threshold). (C) Peak frequency of discharge in response to a cooling stimulus from 34°C to 20°C. (D) The change of temperature at which the peak frequency was attained. Data are mean \pm SEM.

A.4.2. Neural activity of mechano- and polymodal nociceptors

Nerve activity was recorded in 108 nociceptors from corneas of 2 month old guinea pigs (young animals) and in 106 nociceptors from corneas of 9 month old (adult) guinea pigs. Mechano- and polymodal nociceptors were initially characterized based on their response to mechanical and chemical stimulation (see Methods for details). Student t-test showed no significant differences in the spontaneous activity and in the mechanical threshold of mechano- (Table 6) or polymodal nociceptors (Table 7) recorded from corneas of young and adult guinea pigs. The latency of the response to CO₂ pulses was similar in polymodal nociceptors from young and adult corneas (data not shown). The mean discharge rate in response to CO₂ pulses was slightly higher in polymodal nociceptors of adult cornea although the difference was not statistically significant (Table 7).

Table 6. Spontaneous activity and response to natural stimuli of mechano-nociceptors in young and adult guinea pig corneas.

Mechano-nociceptors	Young (2 months old) n=53	Adult (9 months old) n=52
Mechanical threshold (mN)	0.48 \pm 0.09	0.47 \pm 0.09
Spontaneous activity (imp/s)	1.3 \pm 0.7	0.9 \pm 0.4
% of fibers with SA	7.4%	7.8%

Data are the mean \pm SEM. n=number of units.

Table 7. Spontaneous activity and response to natural stimuli of polymodal nociceptors in young and adult guinea pig corneas.

Polymodal nociceptors	Young (2 months) n=55	Adult (9 months) n=54
Mechanical threshold (mN)	0.18 ± 0.02	0.34 ± 0.08
Spontaneous activity (imp/s)	1.7 ± 0.9	0.7 ± 0.2
% of fibers with SA	16.4%	14.8%
Mean discharge rate in response to CO ₂ (imp/s)	2.7 ± 0.4	3.2 ± 0.4

Data are the mean ± SEM. n=number of units.

B. THE EFFECT OF INDUCED TEAR-DEFICIENCY

B.1. Tearing rate

The tear flow was measured in guinea pigs which had been subjected to removal of the extraorbital lacrimal gland at age of 1 month. Tearing rate was measured at one month (n=16) and eight months (n=6) after lacrimal gland removal; and also in age-matched intact guinea pigs (24 young, 2 months old; and 16 adult, 9 months old guinea pigs). Tearing rate measurements were performed with phenol red threads (see Methods) and expressed as the length of wet thread in millimeters.

As indicated in section A.1, tear rate was slightly higher in adult animals but the difference with young animals was not significant (see Figure 44, 57). Tear rate was also higher in adult tear-deficient (TD) animals compared with young TD animals, being the difference statistically significant ($P < 0.05$, Student t-test), (Figure 57).

As it was expected, tearing rate was significantly reduced after removal of the extraorbital lacrimal gland, both at one month after surgery (young TD animals) and at 8 months after surgery (adult TD animals), (Figure 57).

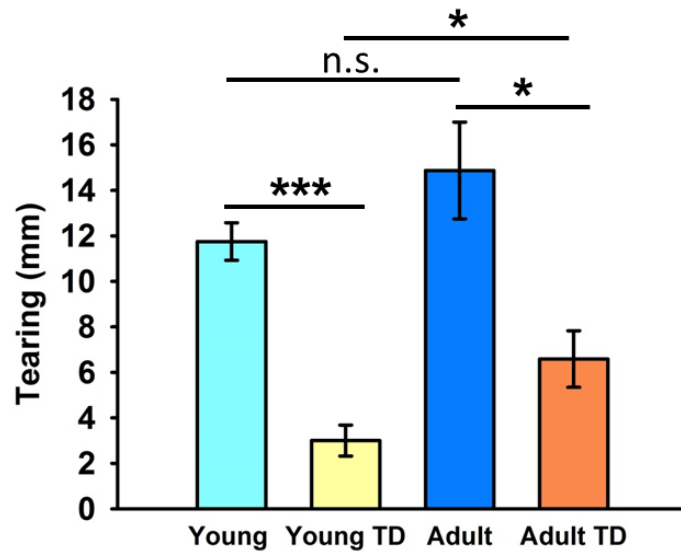


Figure 57. Tearing rate in young and adult control and tear-deficient (TD) guinea pigs. Data are mean \pm SEM. $n = 24, 16, 16$ and 6 animals for the consecutive columns. $***P < 0.001$, $*P < 0.05$, n.s.= not significant, Student t-test.

B.2. Morphology of corneal nerves

The morphological study of corneal nerves was performed in a group of tear-deficient (TD) guinea pigs whose main lacrimal gland had been removed at the age of 1 month. The architecture of corneal innervation of TD animals was examined at 1 month, 3 months and 8 months after surgery (when animals reached the age of 2, 4 and 9 months) and compared to a series of age-matched groups of control, non-operated animals (Data shown in detail in section A.2). Various parameters were measured either on the whole mount cornea or on the superior quadrant of the cornea. The estimated growth rate of the cornea in TD animals was similar to control values (data not shown).

B.2.1. Proportion of subbasal nerve fibers

To have a rough estimate of the density of nerves in TD corneas, at different time points (1 month, 3 months, 8 months) after tear-deficiency, the proportion of tissue area occupied by subbasal nerve fibers was quantified with ImageJ software. The measurements were performed by calculating the percentage of area occupied by the subbasal nerves in an area of one square millimeter of tissue at three different zones of the corneal superior quadrant (peripheral,

central, vortex) of guinea pigs whose lacrimal gland was excised 1 month (n=4), 3 months old (n=4) or 8 months (n=6) before. The data were compared with those obtained from non-operated, age-matched guinea pigs (Figure 60).

In the different corneal zones (peripheral, central and vortex), proportion of nerve fibers was significantly decreased at 1 month after lacrimal gland removal ($P < 0.05$, $P = 0.001$, $P < 0.001$, t-test), and remained reduced afterwards (Figure 58 A, B and C). The reduction of nerves observed at 1 month after TD is not attributable to age, because a statistically significant difference in the density of nerve fibers was found between TD and age-matched control corneas in peripheral ($P < 0.05$, t-test), central ($P < 0.05$, t-test), and vortex zones ($P < 0.01$, t-test) (Figure 59 A, B, C), while none significant differences were observed among corneal zones at longer times after TD (Figure 58D, 59 D).

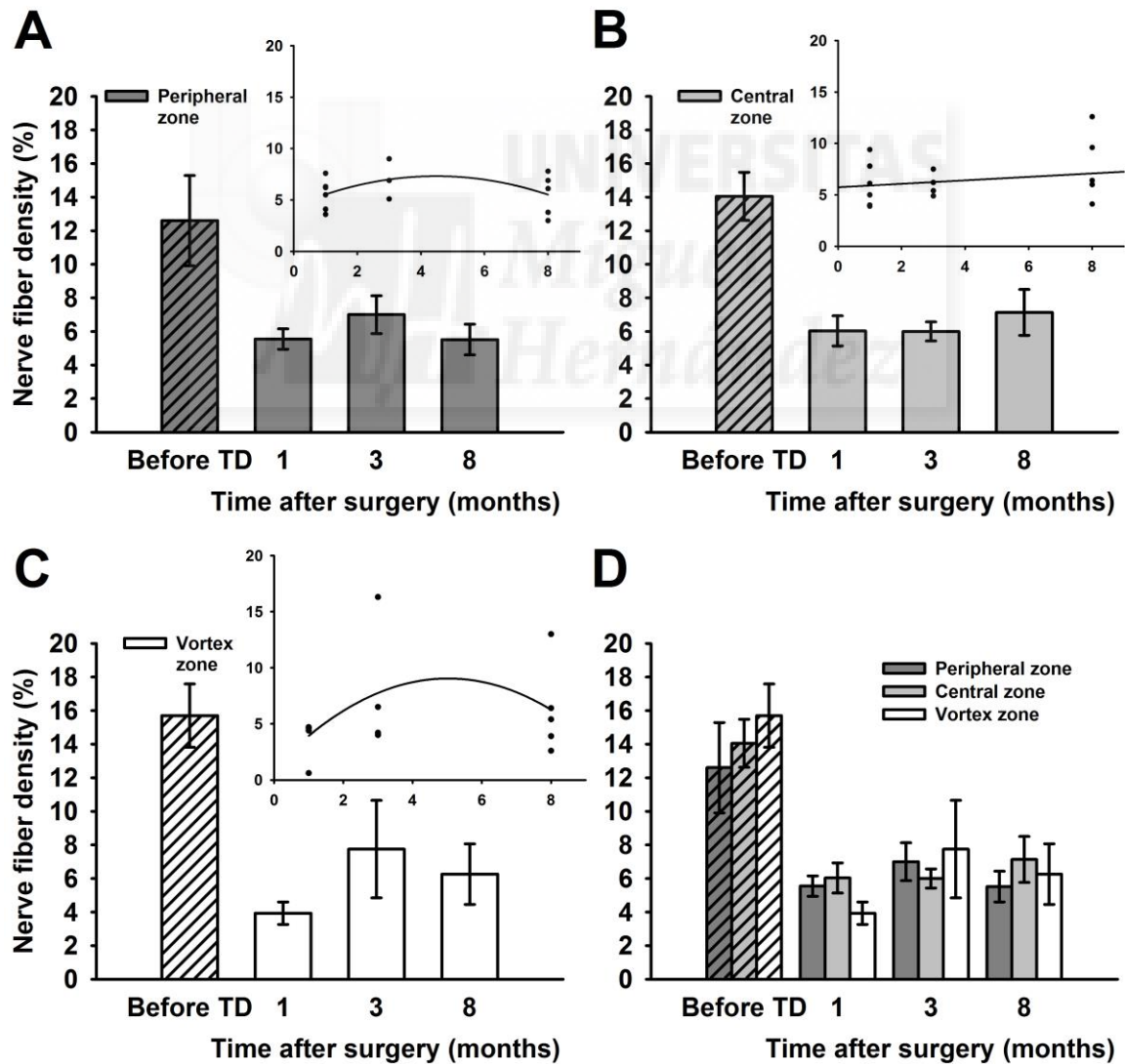


Figure 58. Changes in subbasal nerve fibers proportion at different times after tear-deficiency. Measurements were done in the superior quadrant of cornea in (A) peripheral, (B) central, and (C) vortex zones and compared with the group before induction of TD. Insets show linear regression adjustment: (A) $P=0.832$, $R^2=0.125$; (B) $P=0.413$, $R^2=0.0484$; (C) $P=0.471$, $R^2=0.171$. (D) The nerve fiber proportion was analyzed in different corneal zones: peripheral (dark gray), central (gray), and vortex (white) within TD guinea pigs groups (smooth pattern bars), at different times after removal of the exorbital lacrimal gland. Data are mean \pm SEM.

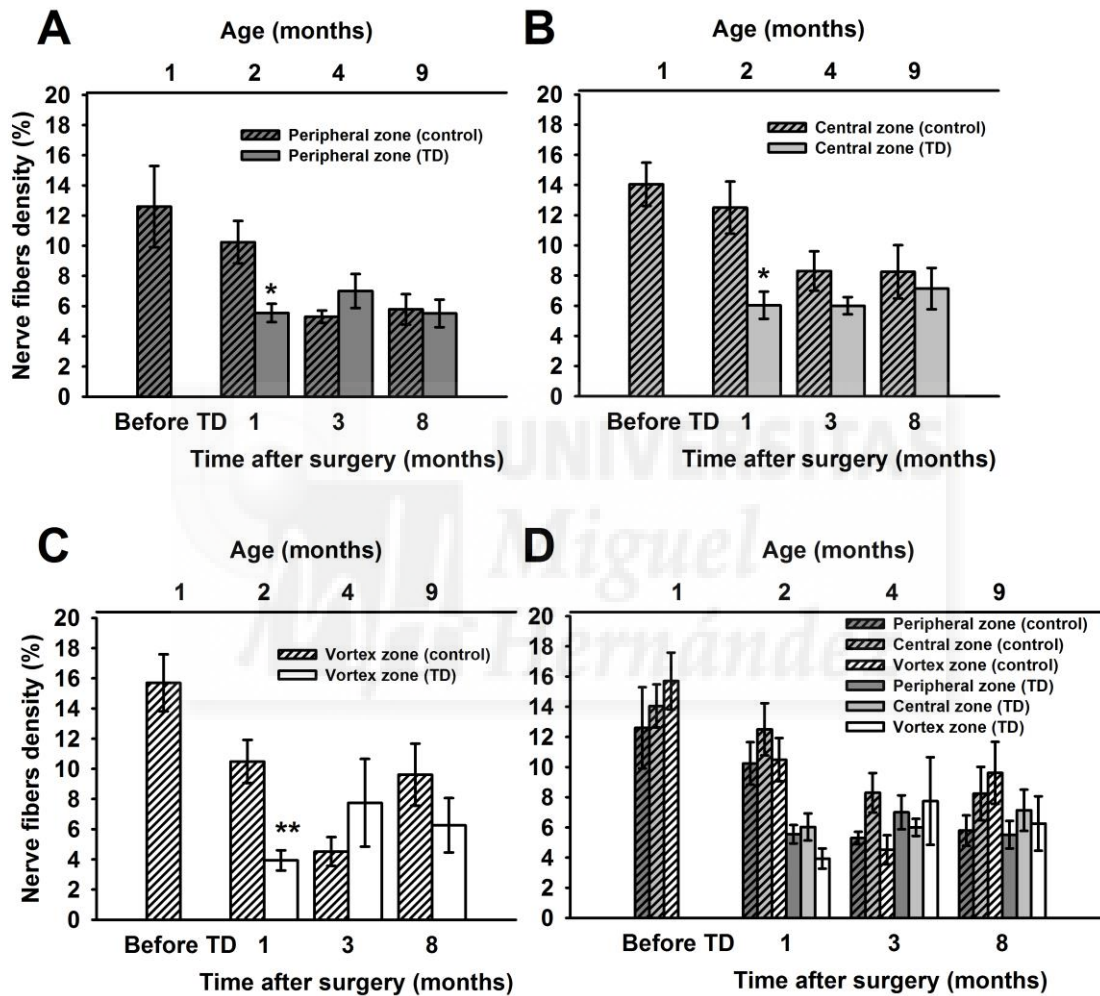
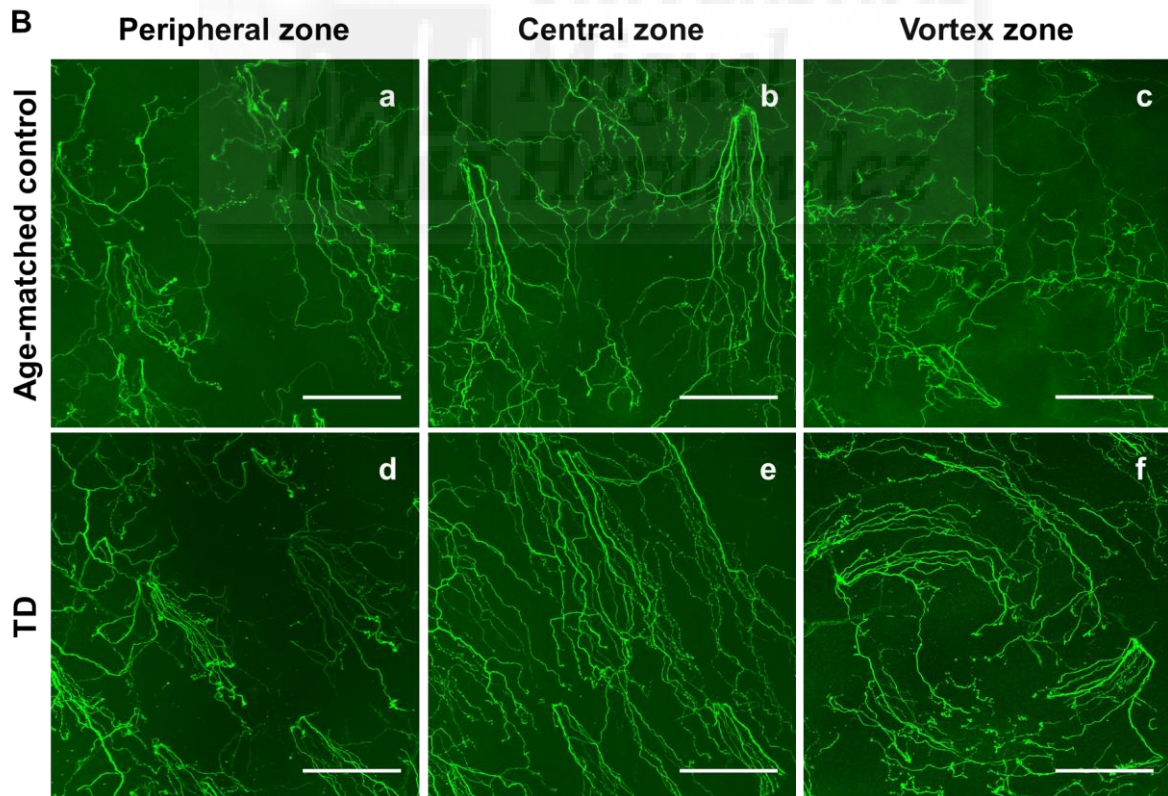
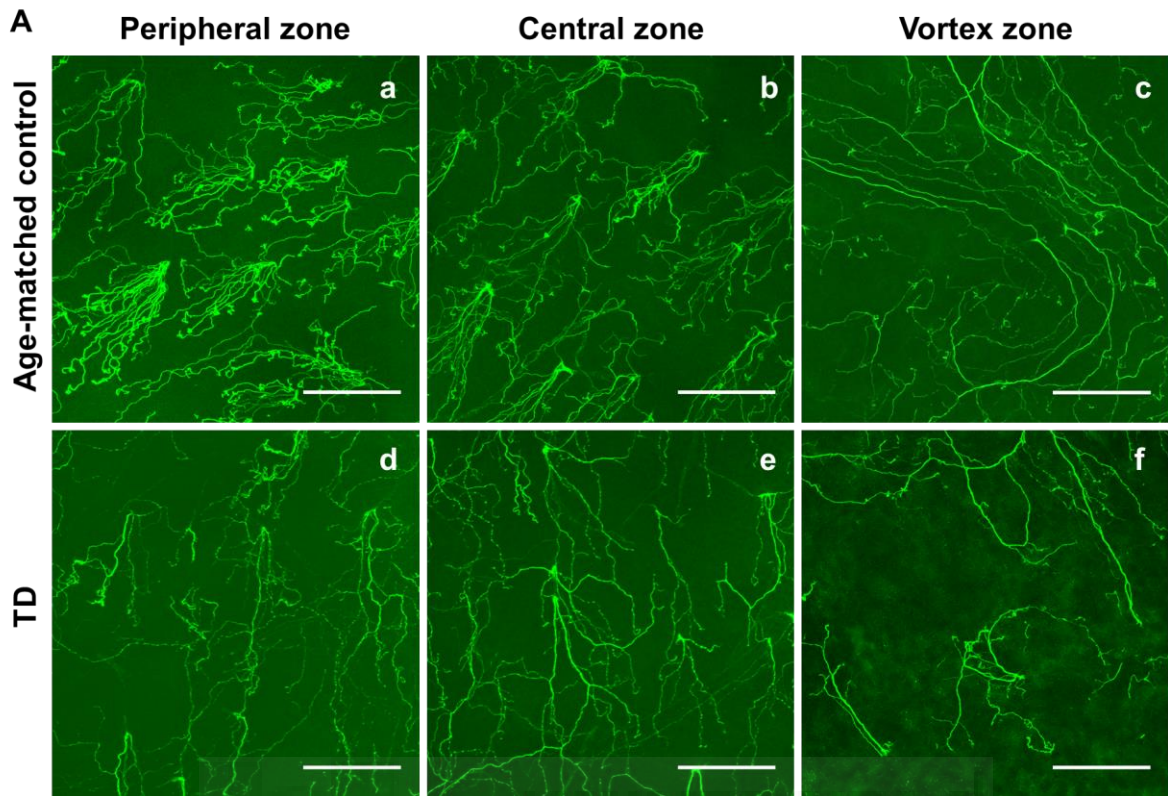


Figure 59. Changes in subbasal nerve fibers proportion at different times after tear-deficiency and in age-matched controls. Measurements were done in the superior quadrant of cornea in (A) peripheral, (B) central, and (C) vortex zones. (D) The nerve fiber proportion of TD animals was compared with the corresponding age-matched group of non-operated animals. Data are mean \pm SEM. ** $P<0.01$, * $P<0.05$, Student t-test.



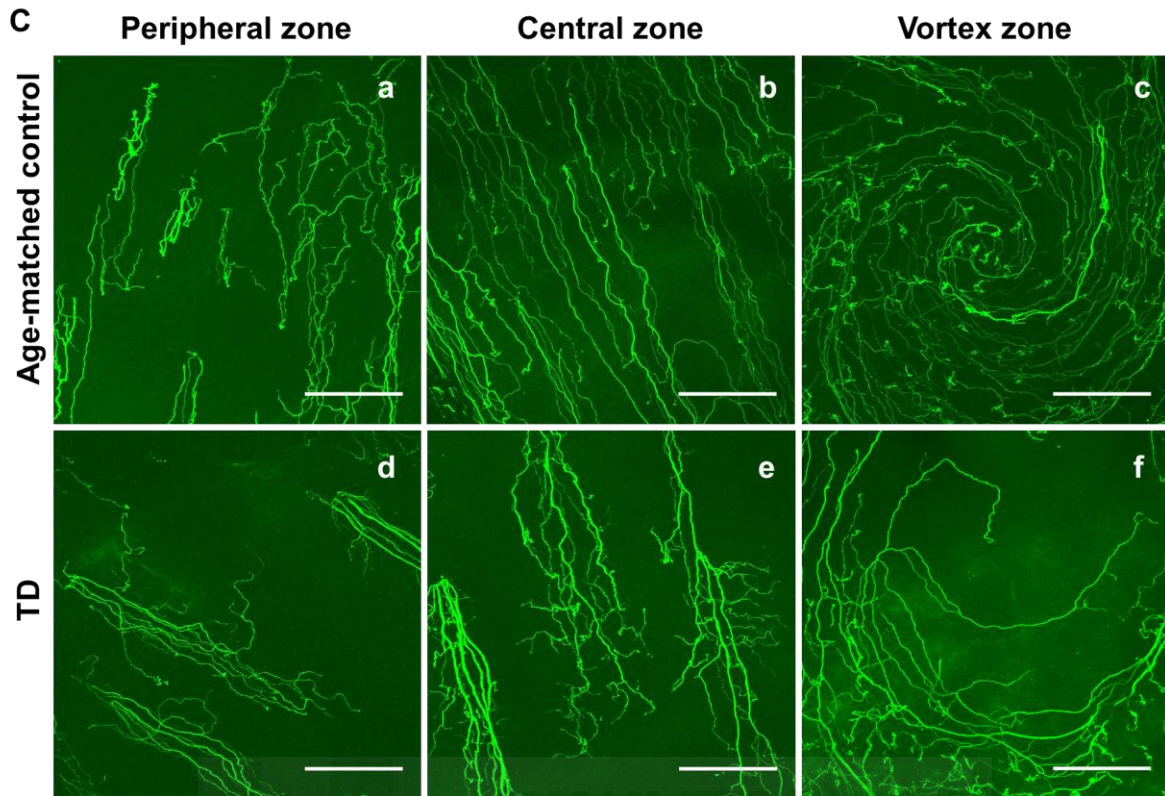


Figure 60. Tuj-1 positive subbasal nerve fibers in control and tear-deficient animals. Photographs taken in non-operated, age-matched control (a, b, c) and tear-deficient (TD) corneas (d, e, f) in 3 different zones: peripheral (a, d), central (b, e) and vortex (c, f), at different time-points after removal of the exorbital lacrimal gland: 1 month (A), 3 months (B), and 8 months (C). Magnification 40x; Scale bars=100 μ m.

B.2.2. Total number of subbasal nerve leashes

The total number of subbasal nerve leashes in the whole cornea (Figure 61 A) and in the peripheral and central zones (Figure 61 C) was counted at different times after tear-deficiency (TD), and in the corresponding age-matched control animals (Figure 61 B, D).

The number of subbasal nerve leashes decreased significantly in all cornea zones at 1 month after removal of the lacrimal gland (1330 ± 74 vs. 659 ± 78 total nerve leashes number; $P < 0.001$, t-test), (Figure 61 A). There was statistically significant difference in the number of subbasal nerve leashes 1 month after TD group (659 ± 78 nerve leashes) compared with the corresponding age-matched control animals (2 months old; 1834 ± 135 ; $P < 0.001$, t-test) (Figure 61 B). At 8 months after TD, the number of nerve leashes per cornea was similar to age-matched control corneas (Figure 61 B, D).

The estimated nerve leash number rate was counted for tear-deficient (TD) and age-matched control groups (Table 8).

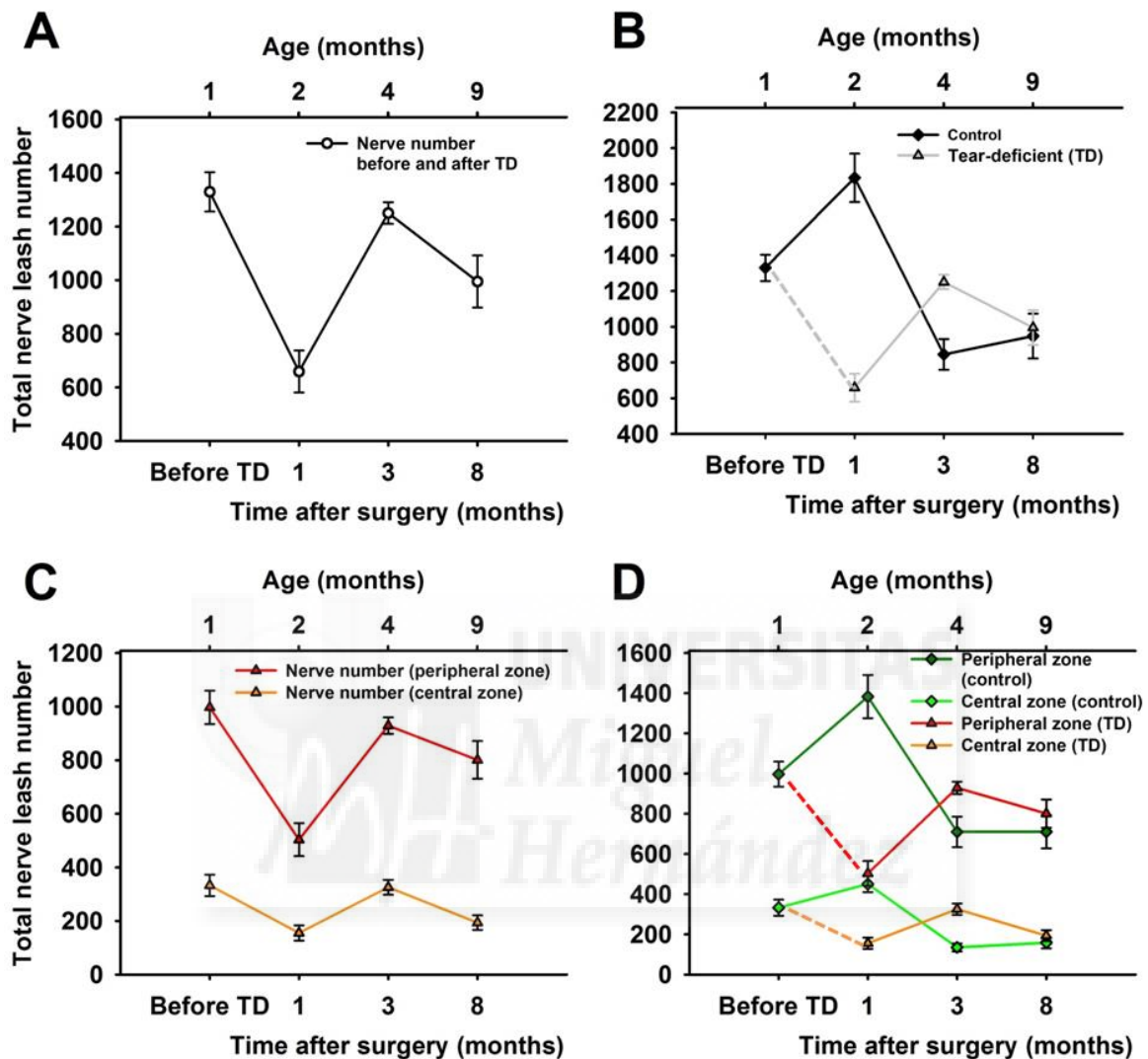


Figure 61. Evolution in the number of the subbasal nerve leashes at different times after tear-deficiency and in age-matched controls. The number of nerve leashes counted in the whole cornea (A) and in its peripheral and central zones (C) before and after TD. The number of nerve leashes counted in the whole cornea (B) and in its peripheral and central zones (D) of TD and their age-matched control corneas. Data are mean \pm SEM. ANOVA, Bonferroni t-test; student t-test (see text for details). n= 5, 3, 6 (peripheral zone), and 5, 4 and 6 (central zone) for the following TD groups in D.

Table 8. Change in the number of subbasal nerve leashes at different times after tear-deficiency (TD) and in age-matched control animals.

Time after TD	Nerve leashes number		Estimated nerve leash number rate (n/month)	
	TD	Control	TD	Control
0	1330 ± 74	1330 ± 74	-671	504
1	659 ± 78	1834 ± 135	296	-495
3	1250 ± 40	845 ± 86	-51	21
8	995 ± 97	948 ± 126	-	-

Data are mean ± SEM.

B.2.3. Density of subbasal nerve leashes

The density of subbasal nerve leashes was estimated as the number of subbasal nerve leashes per one square millimeter of peripheral or central zone at 3 different time-points (1, 3, and 8 months; n = 5, 4 and 6, respectively) after lacrimal gland removal and in the corresponding age-matched control animals (aged 1, 4 and 9 months; n = 7, 5 and 8, respectively) (Figure 63). As expected, the change in the density of subbasal nerve leashes with time of tear-deficiency at the peripheral and central zones of the cornea (Figure 62 A) followed a pattern similar to the beforehand presented evolution of the total number of subbasal nerve leashes (Figure 61 C) at different times after tear-deficiency.

The density of subbasal nerve leashes decreased significantly in both, peripheral and central zones at 1 month after removal of the lacrimal gland (46 ± 3 vs. 22 ± 3 and 44 ± 6 vs. 20 ± 4 nerve leashes/mm² in peripheral and central zones respectively; $P < 0.05$, t-test), (Figure 62 A). There were statistically significant differences in the density of subbasal nerve leashes 1 month after TD (22 ± 3 and 20 ± 4 nerve leashes/mm² in peripheral and central zone, respectively) compared with the corresponding age-matched control animals (2 months old; 52 ± 3 and 49 ± 4 ; $P < 0.001$, t-test); and 3 months after TD (32 ± 2 and 31 ± 5 nerve leashes/mm² in peripheral and central zone, respectively) compared with the corresponding age-matched control animals (4 months old; 23 ± 2 and 12 ± 2 ; $P < 0.05$, t-test) (Figure 62 B). At 8 months after TD, the number of nerve leashes per cornea was similar to age-matched control corneas (Figure 62 B).

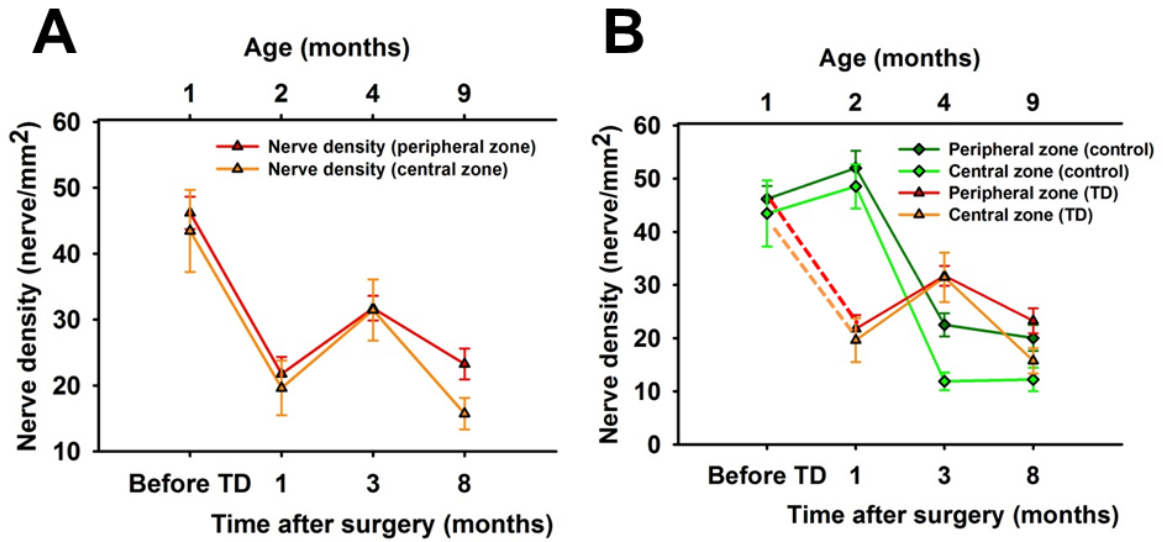
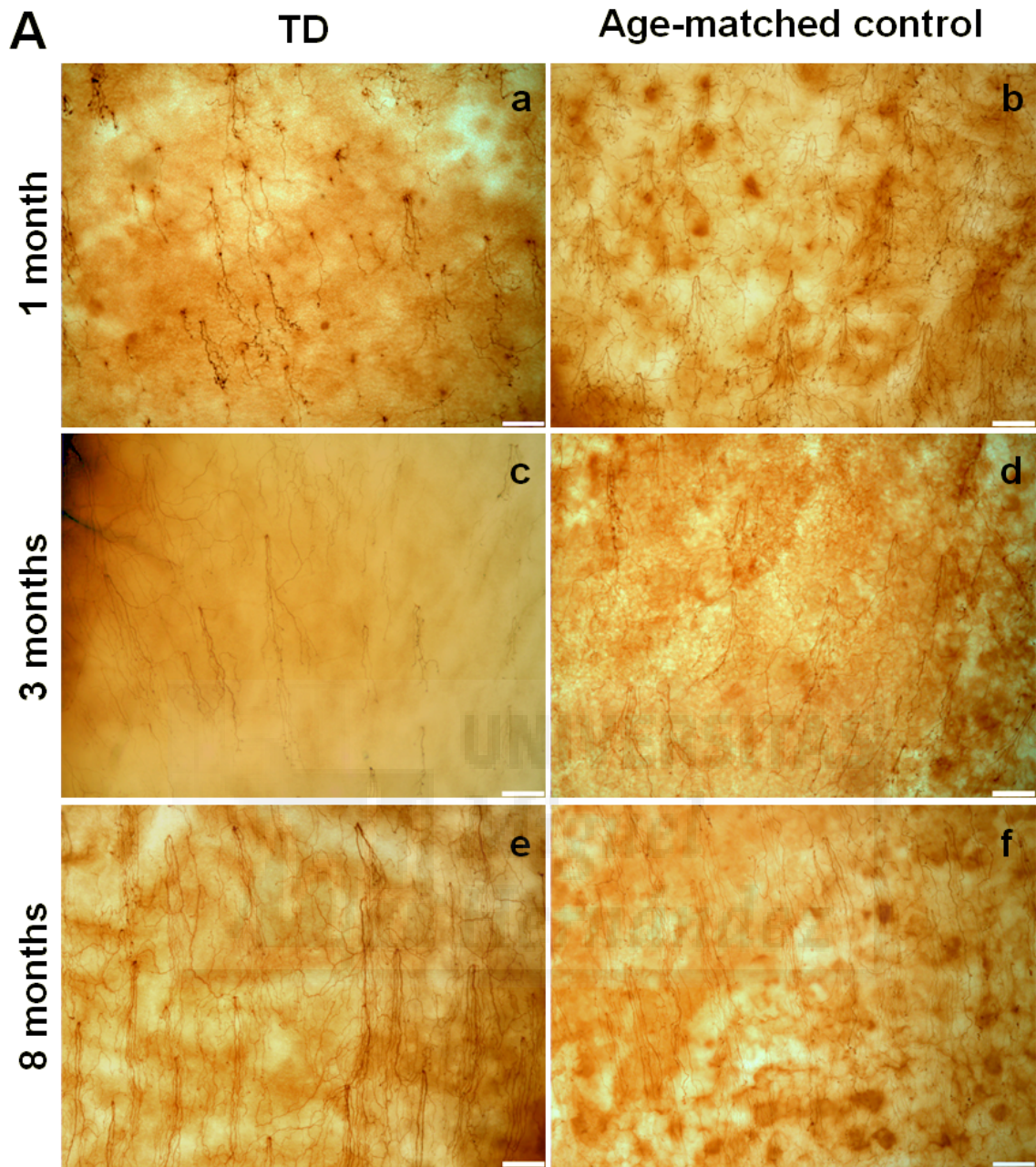


Figure 62. Density of subbasal nerve leashes at different times after tear-deficiency and in age-matched controls. The estimation was performed in the peripheral (dark green and red line) and central zones (light green and orange line) of TD and control corneas. The nerve density before and after TD (A); the nerve density 1, 3 and 8 months after TD compared with age-matched controls (B). Data are mean \pm SEM. ANOVA, Bonferroni t-test.





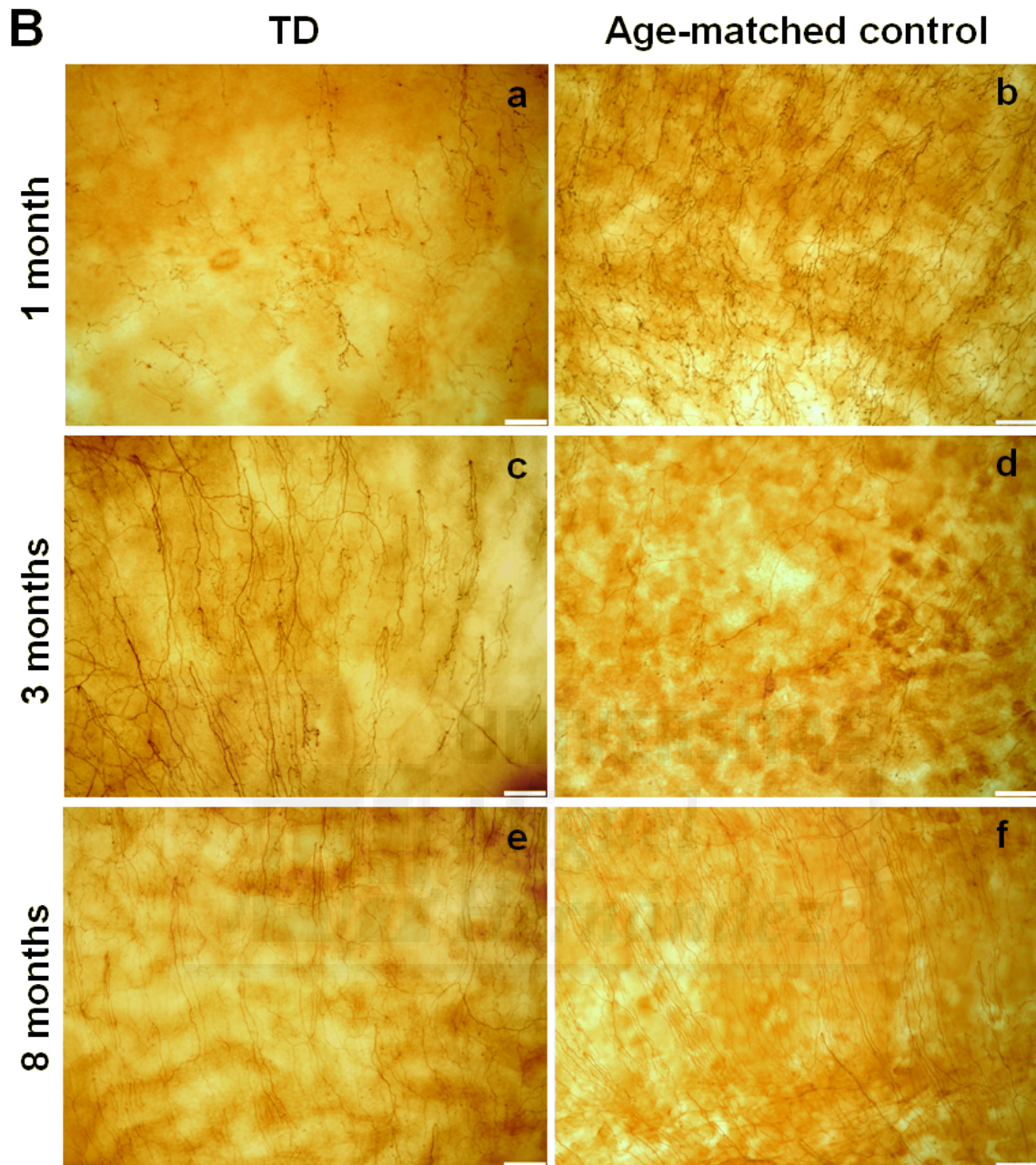


Figure 63. TUJ-1 positive subbasal nerve leashes in tear-deficient (TD) and age-matched control corneas of guinea pig. Photographs taken in peripheral (A) and central (B) zones of operated TD animals (a, c, e) at different time-points after lacrimal gland removal (1 month (a, b), 3 months (c, d), 8 months (e, f)); and of the corresponding age-matched non-operated animals (b, d, f). Magnification 10x; Scale bar=100 μ m.

B.2.4. Length of subbasal nerve leashes

The length of subbasal nerve leashes was measured in tear-deficient animals at 1 month (n=6), 3 months (n=4), and 8 months (n=6) after lacrimal gland removal, and in age-matched control animals (n = 8, 5 and 9, respectively) (Figure 66 A, B, C, respectively). The length of nerve leashes was measured in peripheral (Figure 64 A), central (Figure 64 B), and vortex zones (Figure 64 C) and expressed in micrometers (Table 9). Linear regression analysis was performed and the slope was considered the rate of nerve length in $\mu\text{m}/\text{month}$ (Table 10).

Despite the slightly lower length increase rate observed in TD corneas (Table 10), there were no significant differences in any of corneal zones (peripheral, central and vortex) while comparing the subbasal nerve length between tear-deficient and control corneas at every time-point (Figure 65 A, B, C).

There were regional differences in nerve length between peripheral, central and vortex zones in both tear-deficient and control corneas, being shorter the nerves of the peripheral zone (Figure 65 D).



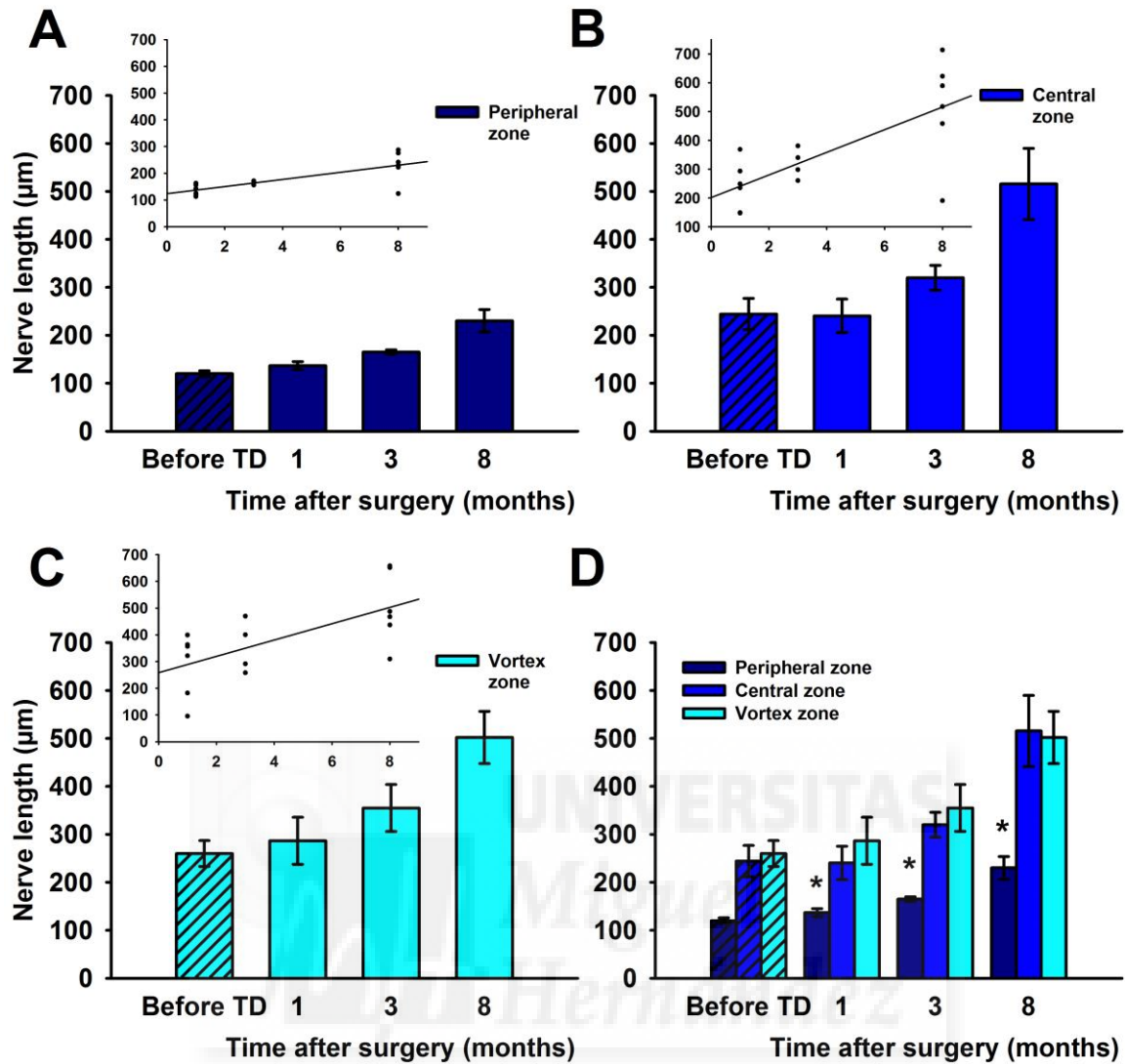


Figure 64. Changes in subbasal nerve leash length at different times after tear-deficiency. Measurements were done in the superior quadrant of cornea separated to (A) peripheral, (B) central, and (C) vortex zones. Insets: Linear regression adjustments (see text and table 10 for details). (D) The nerve length was compared within each age group among peripheral (dark blue), central (blue), and vortex (light blue) zones in tear-deficient (smooth pattern bars). Data from the peripheral (dark blue), central (blue), and vortex (light blue) zones in animals before TD induction (line pattern bars) are shown. Data are mean \pm SEM. * $P < 0.05$, ANOVA, Bonferroni t-test. $n = 6, 3, 6, 6, 4, 6, 6, 4$ and 6 for the consecutive TD columns in D.

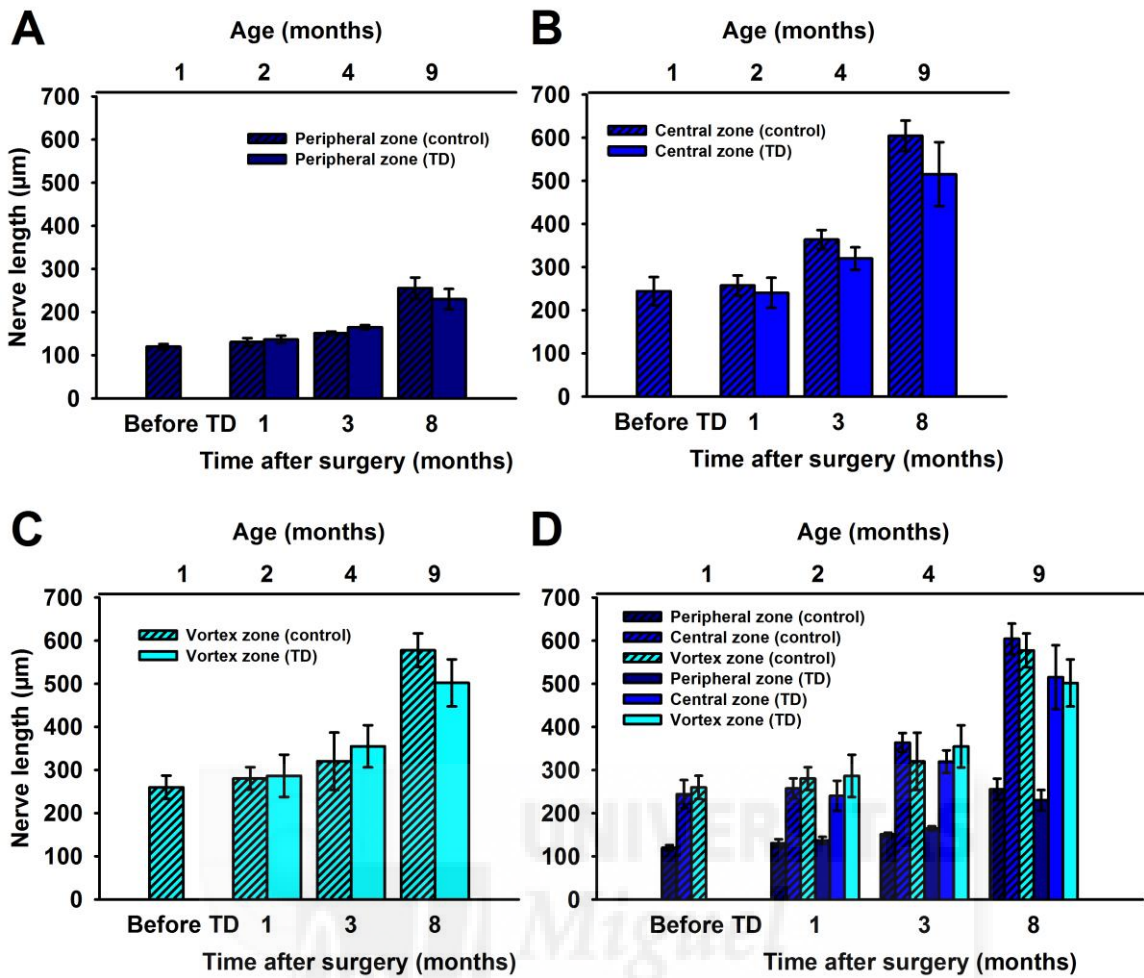


Figure 65. Changes in subbasal nerve lash length at different times after tear-deficiency and in age-matched animals. Measurements were done in the superior quadrant of cornea separated to (A) peripheral, (B) central, and (C) vortex zones. The nerve length was analyzed 1, 3 and 8 months after lacrimal gland removal and compared with age-matched controls. Data are mean \pm SEM. Student t-test did not show any differences between different TD groups and their age-matched controls.

Table 9. Elongation of subbasal nerve leashes in tear-deficient animals at different time points after removal of the lacrimal gland and in age-matched control animals. The length of nerve leashes in peripheral, central, and vortex zones are shown.

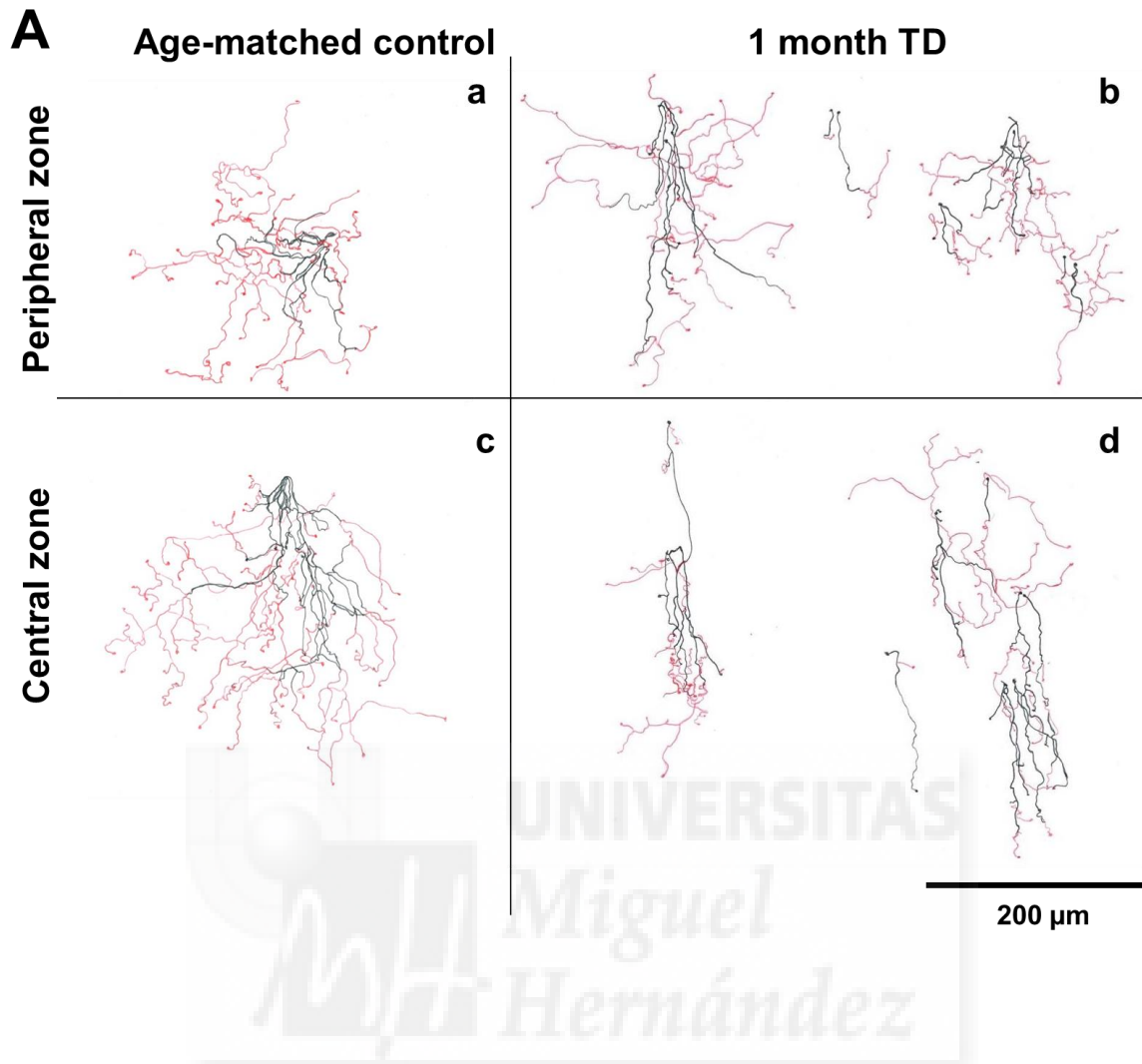
Time after TD (months)	Nerve leash length (μm)	
	TD	Age matched control
Peripheral cornea		
0	120.1 \pm 5.9	120.1 \pm 5.9
1	136.7 \pm 8.4	130.8 \pm 9
3	165.2 \pm 4.7	151.2 \pm 3.9
8	230.1 \pm 23.6	255.7 \pm 24.6
Central cornea		
0	244.2 \pm 32.6	244.2 \pm 32.6
1	240.4 \pm 34.8	257.5 \pm 23.3
3	319.9 \pm 26	363.9 \pm 22.2
8	515.5 \pm 74.2	604.3 \pm 35.4
Vortex		
0	260 \pm 26.9	260 \pm 26.9
1	286.6 \pm 50	280.5 \pm 26
3	355 \pm 48.9	320.4 \pm 66.4
8	501.9 \pm 54.6	577.7 \pm 39

Data are mean \pm SEM

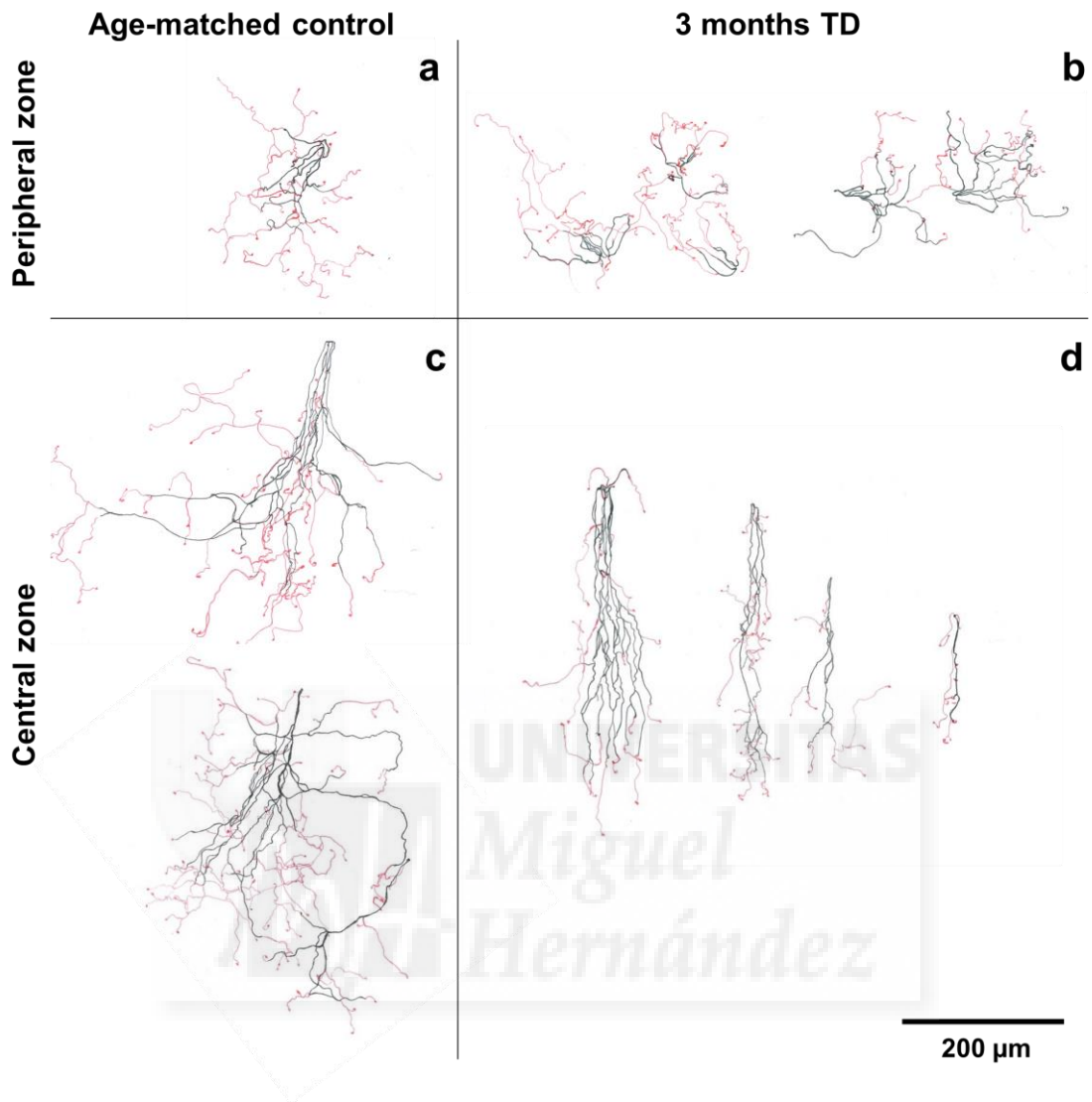
Table 10. Estimated rate of elongation ($\mu\text{m}/\text{month}$) with of subbasal nerve leashes in different zones of the cornea of tear-deficient and control guinea pigs.

Cornea zone	Tear-deficient	Control
Peripheral	13.3	18.3
Central	39.3	49.3
Vortex	30.6	43.8

The length increment rate per month ($\mu\text{m}/\text{month}$) was estimated as the slope of the linear regression calculated with length values measured in tear-deficient and age-matched control corneas. TD: $R^2 = 0.587, 0.848$ and 0.430 , $P < 0.001, < 0.001$ and 0.006 . Control: $R^2 = 0.598, 0.803$ and 0.634 , $P < 0.001$, respectively.



B



C

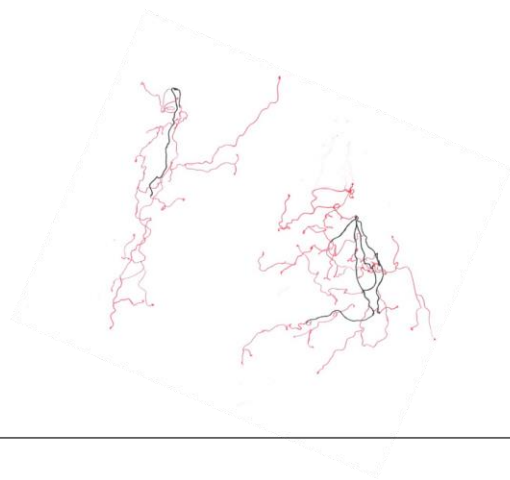
Age-matched control

8 months TD

Peripheral zone



a

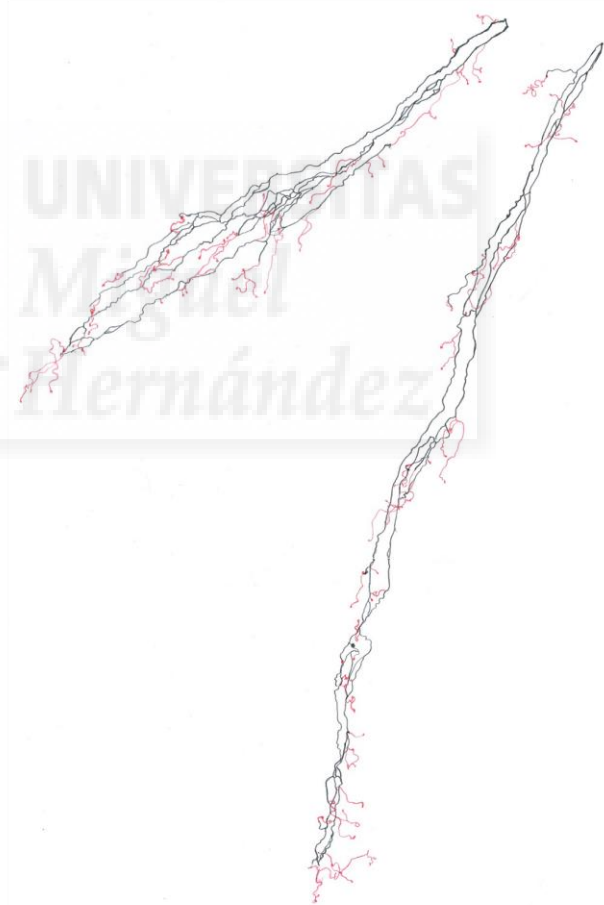


b

Central zone



c



d

200 μ m

Figure 66. Camara lucida drawings of representative subbasal corneal nerve leashes of control and tear-deficient guinea pigs at different times after lacrimal gland removal. Nerves were drawn at level of subbasal plexus (black) and of intraepithelial nerve terminals (red) in control (a, c) and TD (b, d) corneas in peripheral (a, b) and central (c, d) zones at different time points after surgery (A: 1 month; B: 3 months; C: 8 months) and the corresponding age-matched animals. Magnification 40x. Scale bars= 200 μ m.

B.2.5. Density of epithelial nerve terminals

Density of epithelial nerve terminals was quantified in tear-deficient animals at age of 1 month (n=5), 3 months (n=4), and 8 months (n=6) after lacrimal gland removal, and also in the corresponding age-matched control groups (aged 2 months, n=8; 4 months, n=5, and 9 months, n=9). The measurements were performed in 1 mm x 1 mm area of the peripheral, central, and vortex zones (Figure 69 A, B, C), and expressed as nerves per square millimeter.

In the peripheral cornea, epithelial nerve terminals density decreased linearly with time after tear-deficiency (Figure 67 A). In the peripheral and central zones and the vortex, nerve terminals density decreased significantly at 1 month after surgery and maintained reduced density afterwards (Table 11, Figure 67 A, B, C).

There were no significant differences in the density of nerve terminals among peripheral, central and vortex zone within each age-group after induced tear-deficiency (One Way ANOVA), (Figure 67 D).

Taking into account the age-matched groups, epithelial nerve terminals density in tear-deficient and controls corneas in the different corneal zones did not show any significant differences (One Way ANOVA), (Figure 68 A, B, C and D).

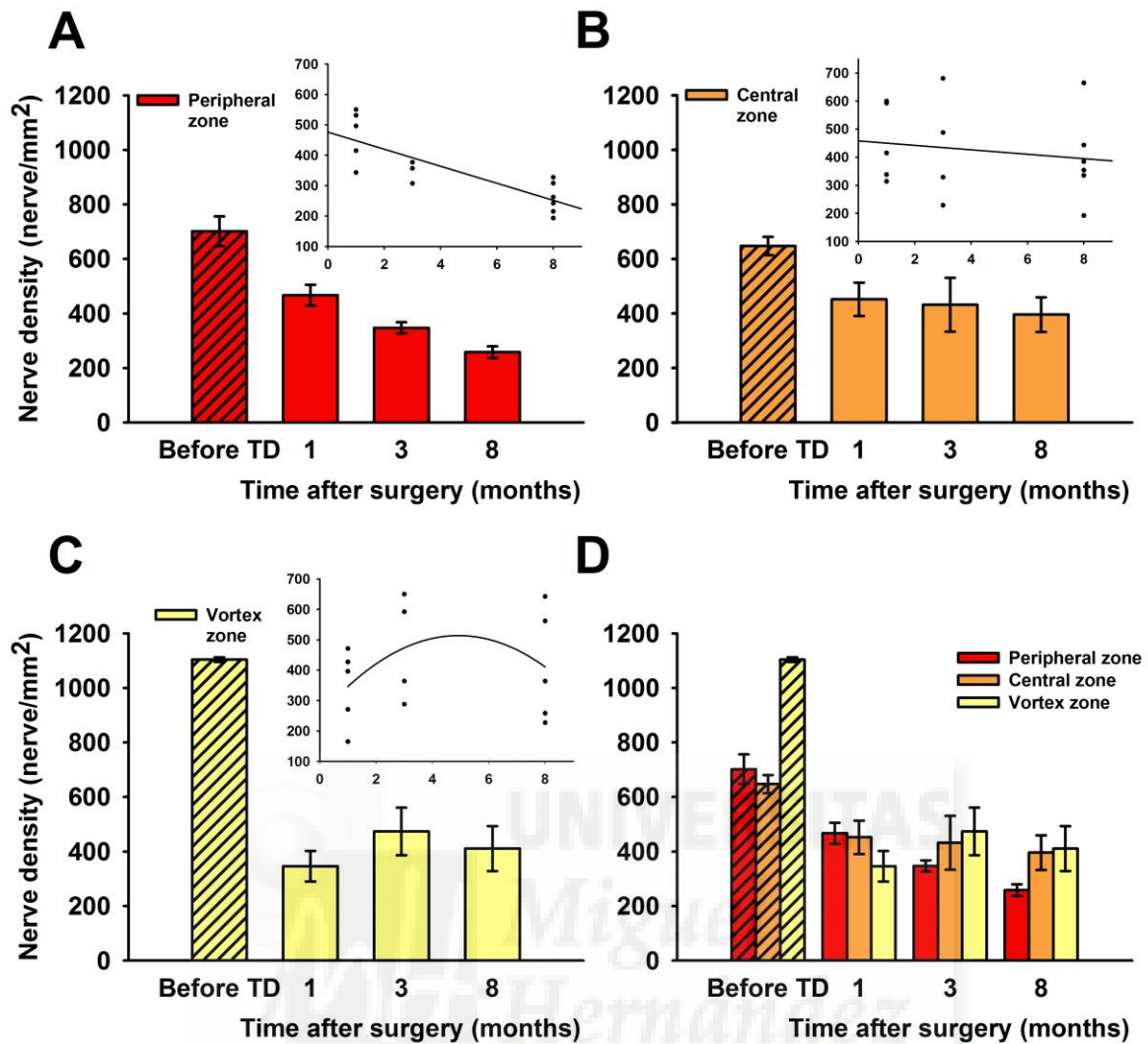


Figure 67. Changes in epithelial nerves density at different times in tear-deficient animals. Measurements were done in the (A) peripheral, (B) central, and (C) vortex zones of the superior quadrant of the cornea. Insets show linear regression adjustment: (A) $P < 0.001$, $R^2 = 0.673$; (B) $P = 0.554$, $R^2 = 0.0277$; (C) $P = 0.705$, $R^2 = 0.111$. (D) The density of epithelial nerve terminals in tear-deficient animals was compared between peripheral (red), central (orange) and vortex (yellow) zones within each TD group (smooth pattern bars) of guinea pigs. Data from the peripheral (red), central (orange), and vortex (yellow) zones in animals before TD induction (line pattern bars) are shown. Data are mean \pm SEM. $n = 5, 5, 5, 3, 4, 4, 6, 6$ and 5 for the consecutive TD columns in D.

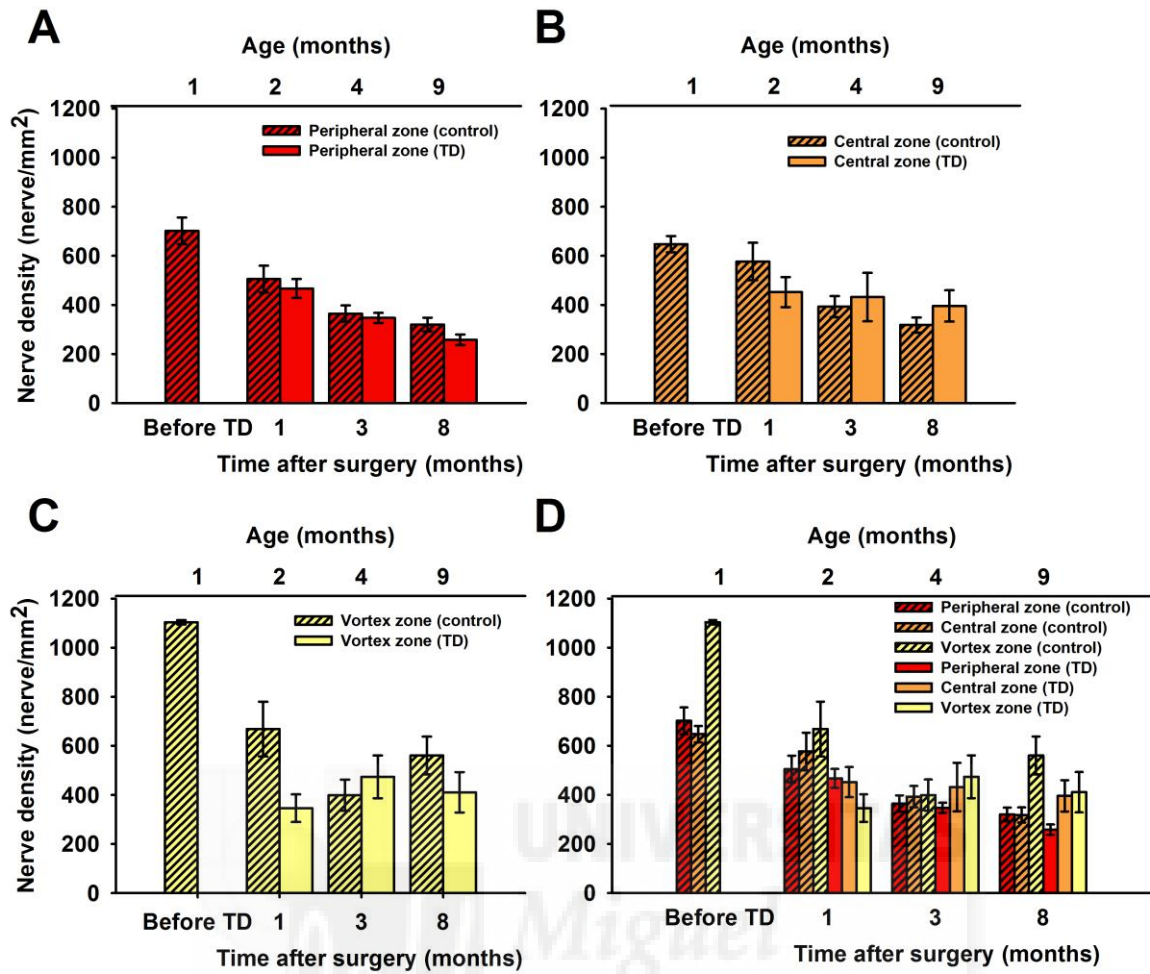
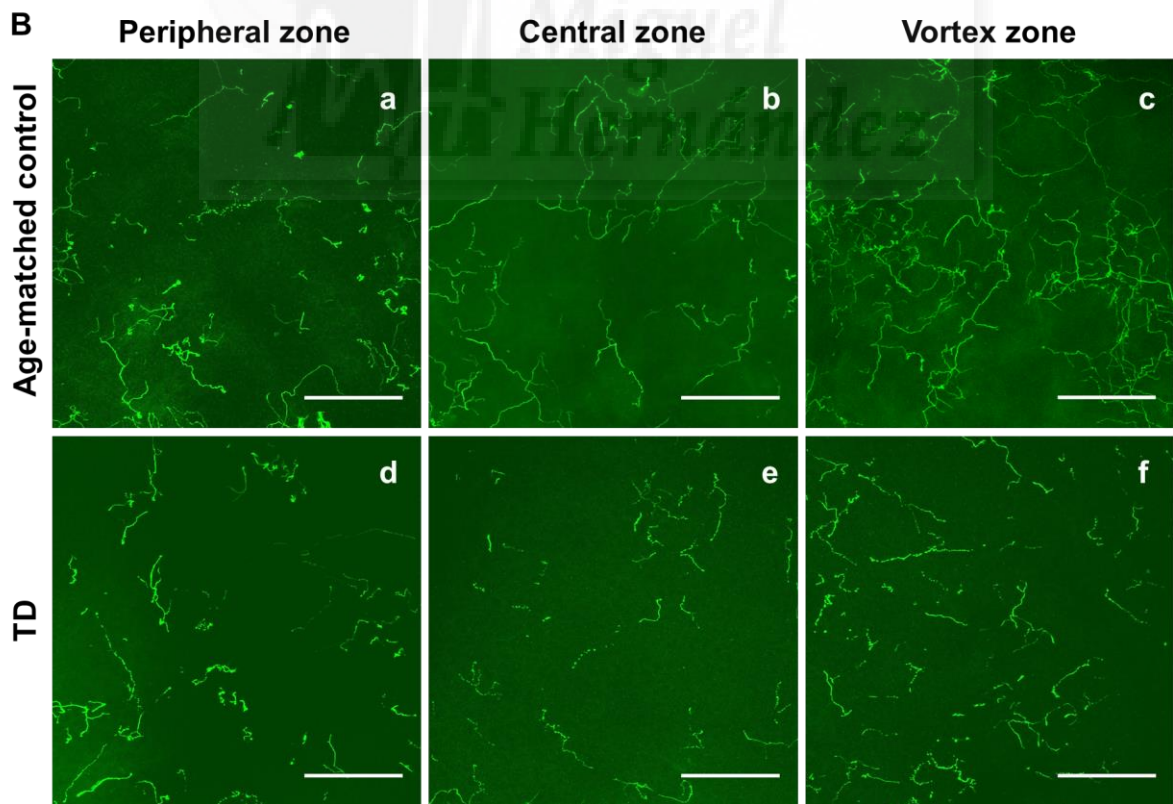
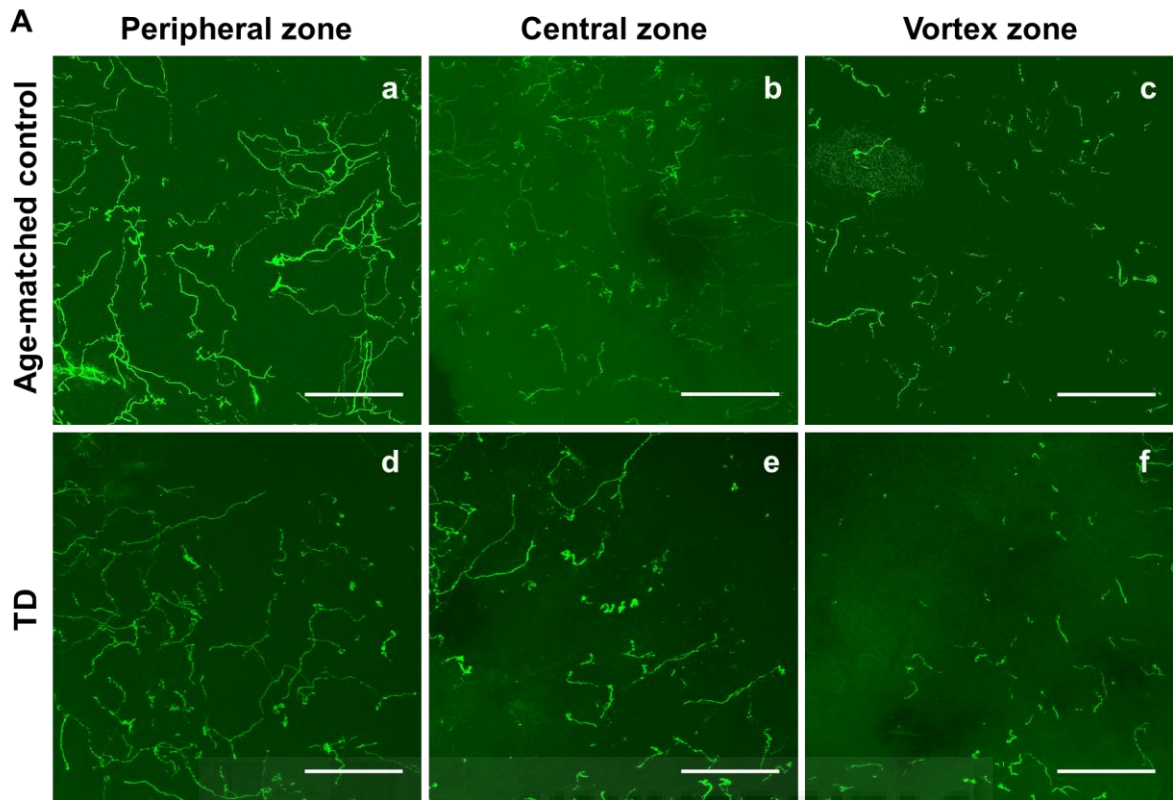


Figure 68. Changes in epithelial nerves density at different times in tear-deficient and age-matched control animals. Measurements were done in the (A) peripheral, (B) central, and (C) vortex zones of the superior quadrant of the cornea. (D) The density of epithelial nerve terminals in tear-deficient animals (smooth pattern bars) was compared with age-matched (line pattern bars) guinea pigs. Data from the peripheral (red), central (orange), and vortex (yellow) zones of are shown. Data are mean \pm SEM. Student t-test.

Table 11. Density of nerve terminals in tear-deficient animals at different time points after removal of the lacrimal gland and in age-matched control animals. The density of nerve terminals in peripheral, central, and vortex zones are shown.

Time after TD (months)	Nerve terminal density (nerve/mm ²)	
	TD	Age matched control
Peripheral cornea		
0	702 ± 55	702 ± 55
1	467 ± 39**	505 ± 55
3	347 ± 21	364 ± 33
8	258 ± 21	320 ± 28
Central cornea		
0	647 ± 33	647 ± 33
1	452 ± 61*	577 ± 76
3	432 ± 99	393 ± 43
8	396 ± 64	318 ± 31
Vortex		
0	1104 ± 9	1104 ± 9
1	346 ± 56***	668 ± 112
3	474 ± 87	399 ± 64
8	411 ± 82	561 ± 77

Data are mean ± SEM. ***P<0.001, **P<0.01, *P<0.05, student t-test.



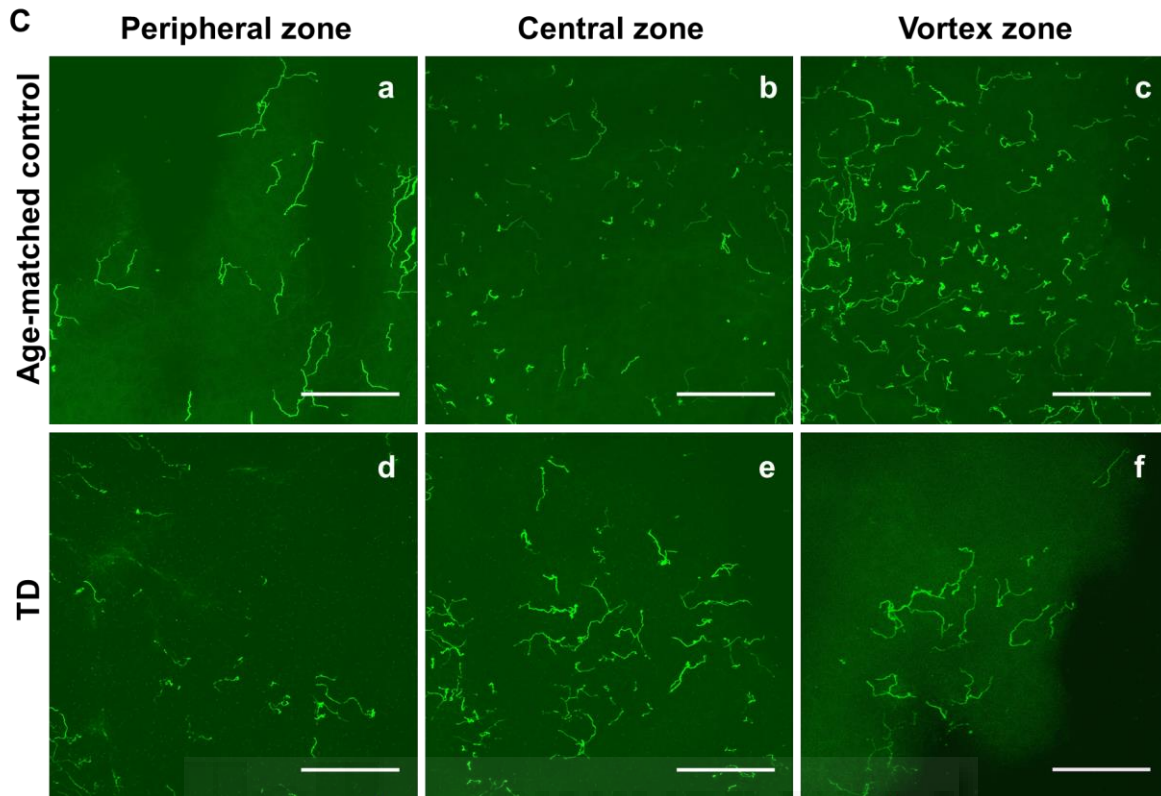


Figure 69. TUJ-1 positive epithelial nerve endings in control and tear-deficient animals. Photographs taken in control (a, b, c) and in TD corneas (d, e, f) in 3 different zones of the cornea (peripheral (a, d); central (b, e); vortex (c, f)), at different time-points after lacrimal gland removal (1 month (A); 3 months (B); 8 months (C)) and in age-matched corneas are shown. Magnification 40x; Scale bars=100 μ m.

B.3. Corneal epithelial wound healing

Chemical epithelial corneal wounds were performed in guinea pigs at 1 month (n=7) and 6 (n=10) months after surgical removal of the lacrimal gland, and in age-matched non-operated guinea pigs (n= 5 and 6, respectively). The epithelial defects were stained with fluorescein and photographed at defined time points until full closure (Figure 70 A), and the photographs were stored and used for further analysis of epithelial defect area (Figure 70 B), migration rate of epithelial cells surrounding wound (Figure 70 C) and estimated time of wound closure (Figure 70 D).

B.3.1. One month after tear-deficiency

Area of the epithelial defect. In one month TD and control animals, the area of epithelial defect decreased linearly with time. Epithelial wound fully closed at 20 h after corneal debridement in control animals, while epithelial defect persisted up to 40 h in guinea pigs subjected to lacrimal gland removal one month before (Figure 70 B). The initial size of the wound was larger in the tear-deficient group ($9.0 \pm 1.4 \text{ mm}^2$) comparing to control ($6.6 \pm 0.7 \text{ mm}^2$), although the difference was not significant ($P=0.207$, t-test) (Figure 70 B).

Epithelial migration rate and estimated time of healing. At one month after tear-deficiency, epithelial migration rate (EMR) was slower ($43 \pm 2 \text{ } \mu\text{m/h}$) than in age matched animals ($69 \pm 4.5 \text{ } \mu\text{m/h}$, $P<0.001$, t-test) (Figure 70 C). In the same way, at 1 month after TD guinea pigs needed more time for the complete closure of the wound (ETH: 45.8 ± 3.2 hours) than control animals (22.3 ± 0.5 hours, $P<0.001$, t-test) (Figure 70 D).

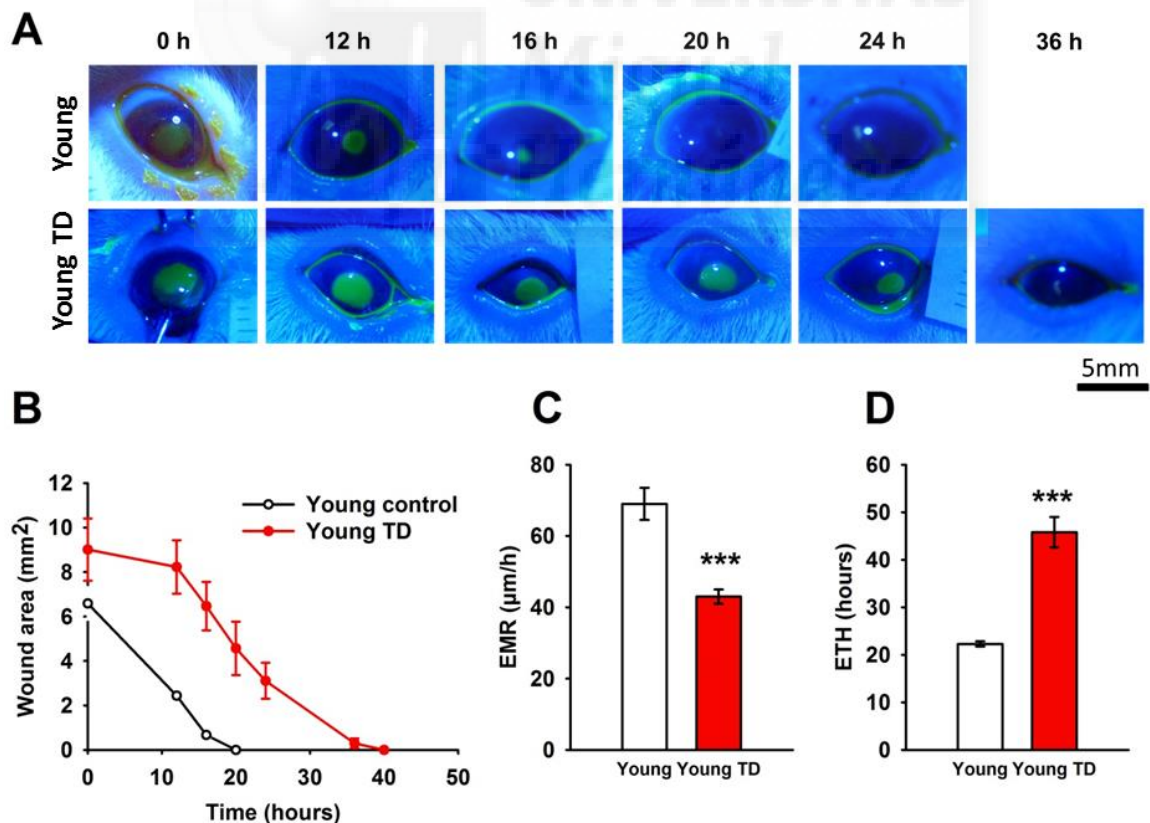


Figure 70. Epithelial wound healing in tear-deficient and control animals. (A) Photographs of epithelial debridations stained with fluorescein taken every 4 hours during healing time in TD (lower panel) guinea pigs subjected to lacrimal gland removal one month before, and in age-matched control (upper panel) guinea pigs. Scale bar=5 mm. (B) Wound area (in mm²) measured from the photos using ImageJ software. (C) Epithelial migration rate (EMR) and (D) Estimated time of healing (ETH) were calculated by regression analysis of the wound area with time. Data are mean \pm SEM; n = 7 (control) and 5 (TD); P<0.001, t-test.

B.3.2. Six months after tear-deficiency

Area of the epithelial defect. At 6 months after tear-deficiency and in age-matched guinea pigs, the initial size of wound was similar in TD group (7.3 ± 0.7 mm²) and control group (7.3 ± 0.4 mm²). The area of epithelial defect decreased also linearly with time. The lesion was fully close at 20 after debridation in control animals. The defect persisted at 24 h after the lesion in TD guinea pigs (Figure 71 A, B) but it was not statistically different from control.

Epithelial migration rate and estimated time of healing. It was not found any difference in the epithelial migration rate calculated in TD animals at 6 months after lacrimal gland removal (58 ± 5.1 μ m/h) comparing to age-matched control animals (51 ± 5.1 μ m/h; P=0.379, t-test) (Figure 71 C). The estimated time of healing in TD group (30.5 ± 2.9 hours) was also similar to the value of age-matched animals (31.9 ± 3.1 hours; P=0.750, t-test) (Figure 71 D).

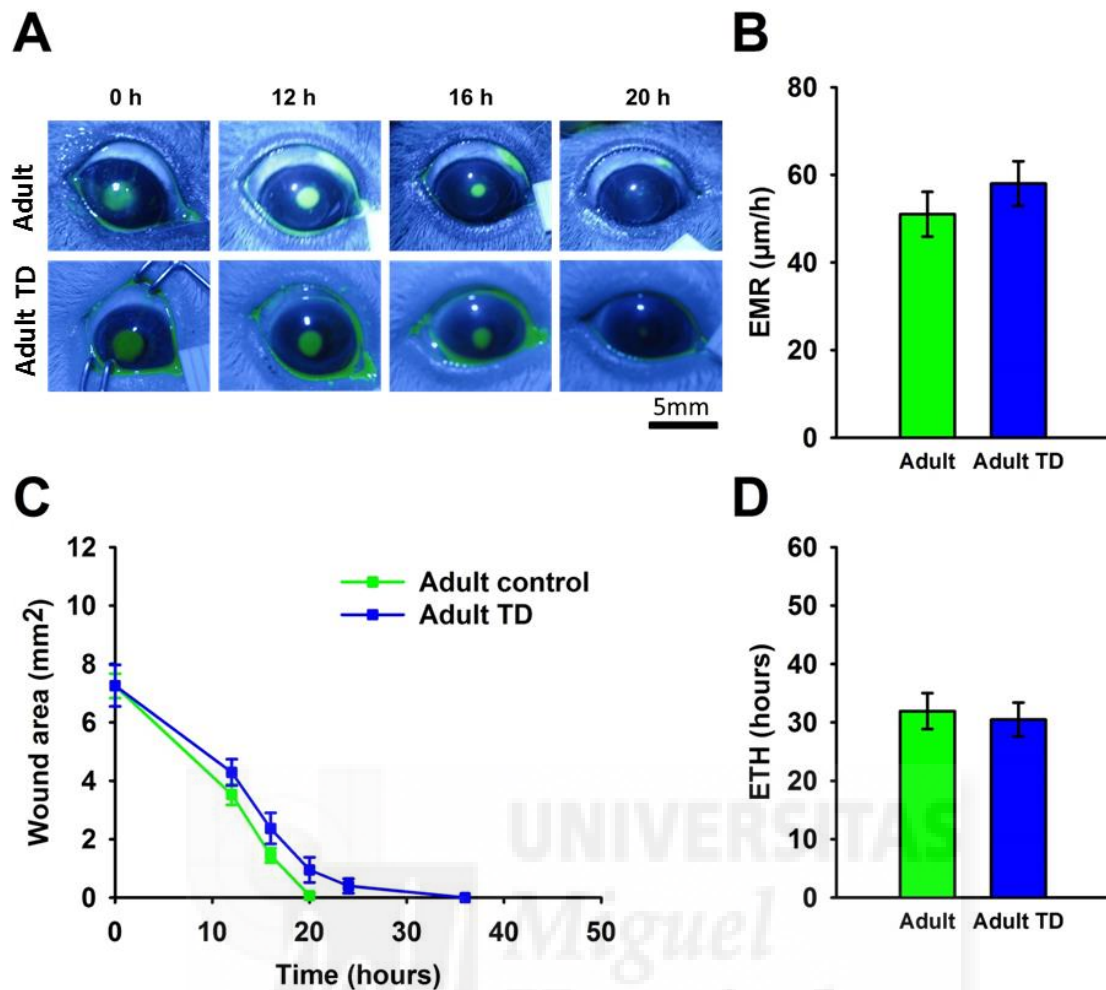


Figure 71. Epithelial wound healing in tear-deficient and control animals. (A) Photographs of epithelial debridations stained with fluorescein taken every 4 hours during healing time in TD (lower panel) guinea pigs subjected to lacrimal gland removal six months before, and in age-matched control (upper panel) guinea pigs. Scale bar=5 mm. (B) Wound area (in mm²) measured from the photos using ImageJ software. (C) Epithelial migration rate (EMR) and (D) Estimated time of healing (ETH) were calculated by regression analysis of the wound area with time. Data are mean ± SEM; n = 6 (control) and 10 (TD); P<0.001, t-test.

B.3.3. One versus six months after tear-deficiency

Wound healing was significantly impaired at 1 month after TD compared with 6 months after TD (Figure 72 A, B). Epithelial migration rate was significantly slower at one month after TD ($43 \pm 2 \mu\text{m/h}$) compared to 6 months ($58 \pm 5.1 \mu\text{m/h}$; $P=0.05$, t-test) (Figure 72 C), and the estimated time of healing was longer at 1 month (45.8 ± 3.2 hours) in comparison with 6 months after TD (30.5 ± 2.9 hours; $P=0.01$, t-test) (Figure 72 D). The initial size of lesion was slightly larger at 1 month TD ($9 \pm 1.4 \text{ mm}^2$) compared to 6 months TD ($7.3 \pm 0.7 \text{ mm}^2$).

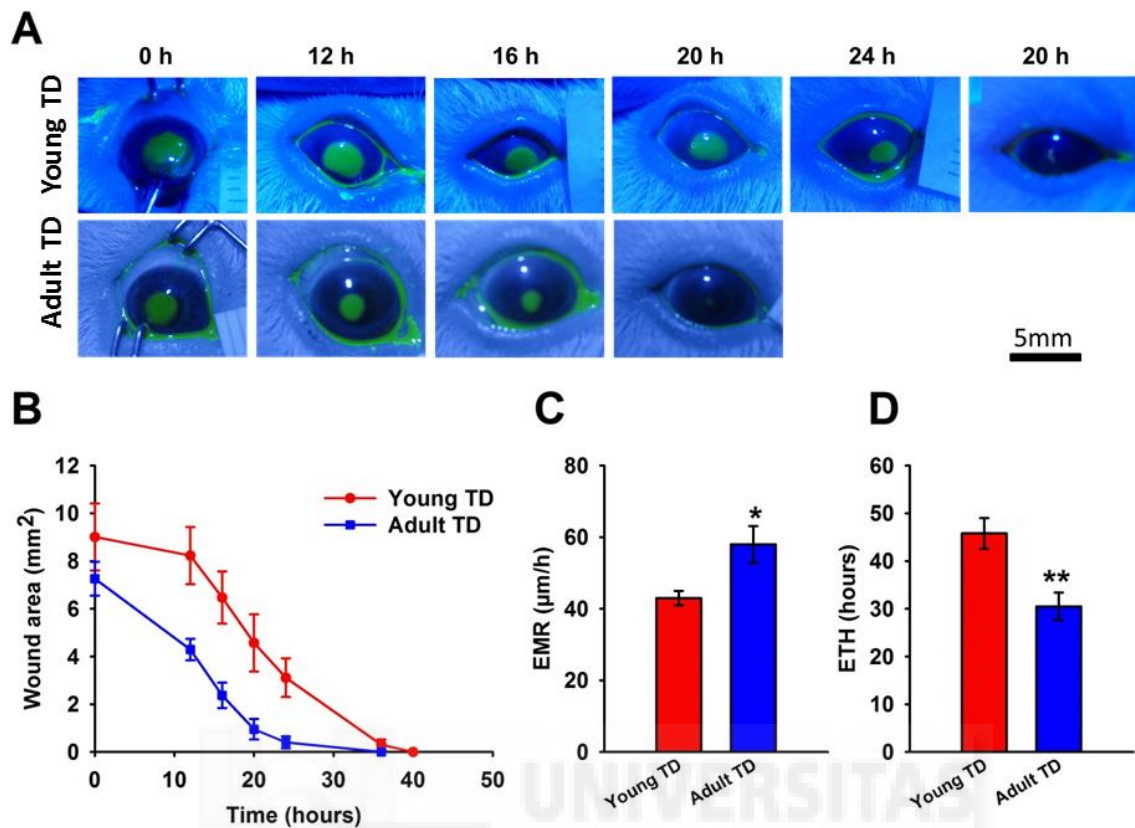


Figure 72. Epithelial wound healing at 1 and 6 months after tear-deficiency. (A) Photographs of epithelial debridations stained with fluorescein taken every 4 hours during healing time in TD guinea pigs at one month (lower panel) and six months (upper panel) after surgery. Scale bar=5 mm. (B) Wound area (in mm²) measured from the photos using ImageJ software. (C) Epithelial migration rate (EMR) and (D) Estimated time of healing (ETH) were calculated by regression analysis of the wound area with time. Data are mean \pm SEM; n = 7 (1 month TD) and 10 (6 months TD); **P<0.01, *P<0.05, t-test.

B.4. Electrophysiological recording of corneal sensory receptors

B.4.1. Neural activity of corneal cold nerve terminals

Nerve terminal impulse (NTI) activity was recorded in 57 cold thermosensitive nerve terminals from corneas of animals 1 month after lacrimal gland removal (1 month TD) and in 57 from corneas of animals 8 months after induced tear-deficiency (8 months TD). The activity was compared with results obtained from age-matched control groups.

Comparing young age-matched control to 1 month TD guinea pigs, the ongoing activity of cold thermoreceptors, the cooling threshold and the temperature change at peak frequency were significantly increased, (Figure 73 A, B, C, D, Table 12). No significant changes were observed when comparing 8 months TD guinea pigs with age matched animals (Table 13).

Table 12. Spontaneous and stimulus-evoked activity of cold corneal receptors recorded in age-matched control and tear-deficient (TD) guinea pigs (at 1 month after lacrimal gland removal).

Cold receptors	Young control n=67	1 month TD n=57
Ongoing activity at 34°C (imp/s)	9.0 ± 0.5	13.2 ± 1.0***
Cooling threshold (°C)	-2.7 ± 0.2	-1.1 ± 0.1***
Peak frequency in response to cold (imp/s)	30.6 ± 1.3	31.1 ± 1.8
Temperature change at peak frequency (°C)	-6.1 ± 0.4	-4.8 ± 0.3*

Data are the mean ± SEM. n=number of terminals. *P<0.05, ***P<0.001, t-test.

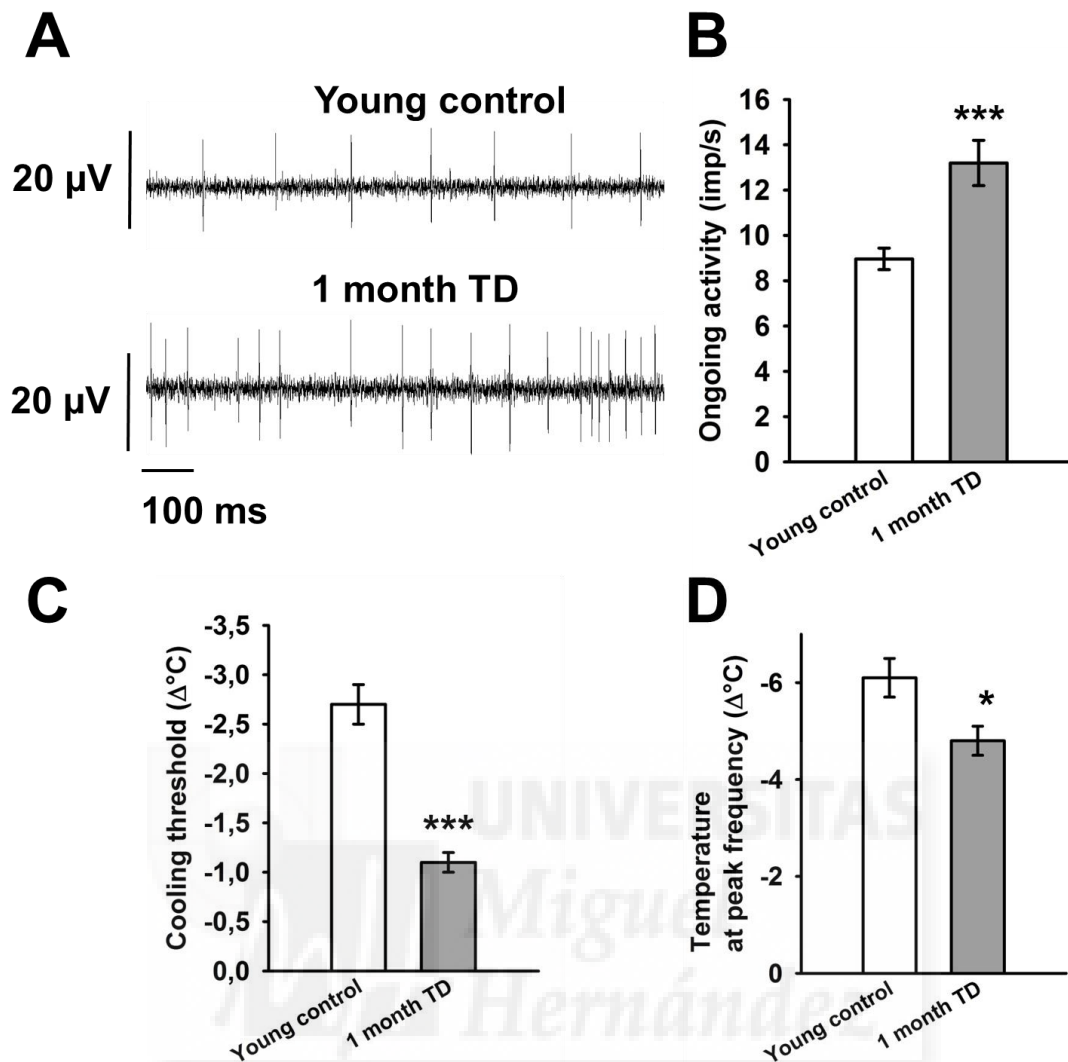


Figure 73. Spontaneous activity of cold thermoreceptors in corneas of tear-deficient guinea pigs at 1 month after lacrimal gland removal and in young non-operated animals. (A) Ongoing activity at basal temperature (34°C) at a time interval of 1 second in young control (upper panel) and 1 month TD (lower panel) animals. (B) Ongoing activity at basal temperature (34°C). (C) Decrement in temperature needed to increase by 25% the basal firing frequency of discharge at 34°C (cooling threshold). (D) The change of temperature at which the peak frequency was attained. Data are mean \pm SEM. *** $P < 0.001$, * $P < 0.05$, t-test.

Table 13. Spontaneous and stimulus-evoked activity of cold corneal receptors recorded in age-matched control and tear-deficient (TD) guinea pigs (at 8 months after lacrimal gland removal).

Cold receptors	Adult control n=64	8 months TD n=57
Ongoing activity at 34°C (imp/s)	8.1 ± 0.6	10.1 ± 1.5
Cooling threshold (°C)	-2.5 ± 0.2	-2.7 ± 0.7
Peak frequency in response to cold (imp/s)	29.0 ± 1.4	26.1 ± 2.5
Temperature change at peak frequency (°C)	-7.1 ± 0.5	-5.7 ± 0.7

Data are the mean ± SEM. n=number of terminals. n.s., t-test.

No changes were found between 1 month TD and 8 months TD animals in the parameters used to analyze the response to a cooling pulse (from the basal temperature of 34°C to 20°C) (Figure 74) except for the cooling threshold ($P < 0.05$, t-test), (Table 14, Figure 75 B).

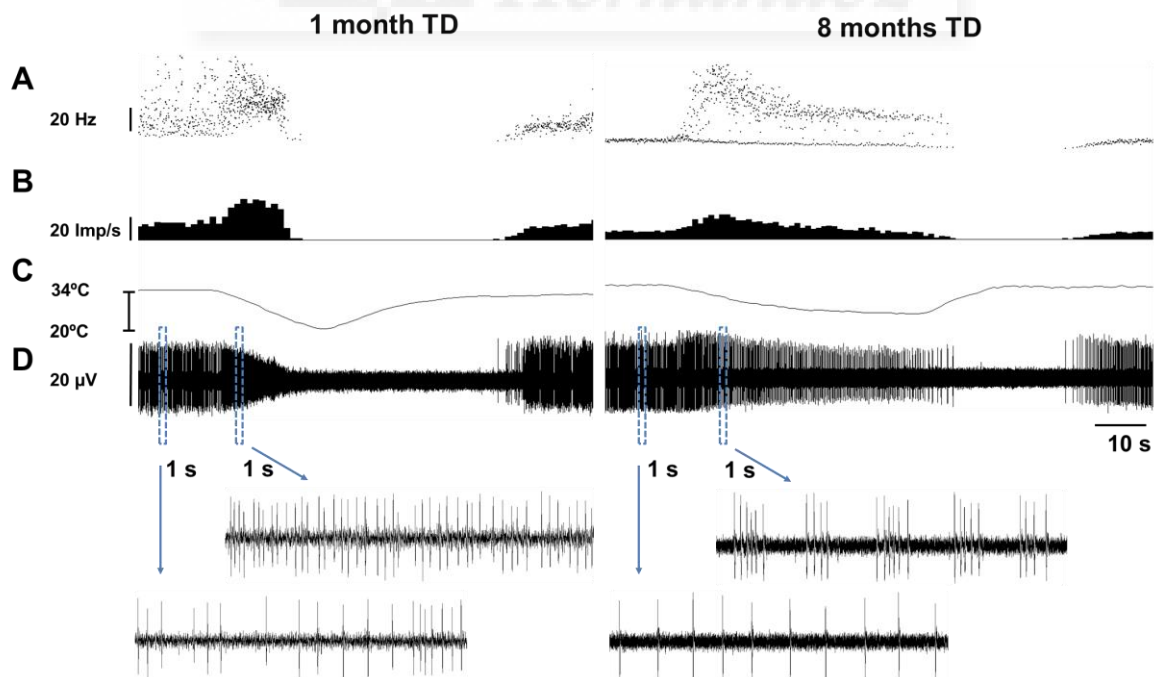


Figure 74. Sample recordings of the response to a cooling stimulus of cold thermoreceptors recorded from two different corneas of guinea pigs subjected to lacrimal gland removal one month (left) and 8 months (right) before. Instantaneous frequency of discharge (1 / interstimulus interval duration) in Hz (A); impulse frequency histogram of NTI activity in impulses per second (B); temperature of the bath solution (C); recording of the NTI activity (D). The insets at the lower part of the figure represent expanded views of the recording during 1 second at indicated moments of the recording (blue lines).

Table 14. Spontaneous and stimulus-evoked activity of cold corneal receptors recorded in tear-deficient (TD) guinea pigs at 1 and 8 months after lacrimal gland removal.

Cold receptors	1 month TD n=57	8 months TD n=57
Ongoing activity at 34°C (imp/s)	13.2 ± 1.0	10.1 ± 1.5
Cooling threshold (°C)	-1.1 ± 0.1	-2.7 ± 0.7*
Peak frequency in response to cold (imp/s)	31.1 ± 1.8	26.1 ± 2.5
Temperature change at peak frequency (°C)	-4.8 ± 0.3	-5.7 ± 0.7

Data are the mean ± SEM. n=number of terminals. *P<0.05, t-test.

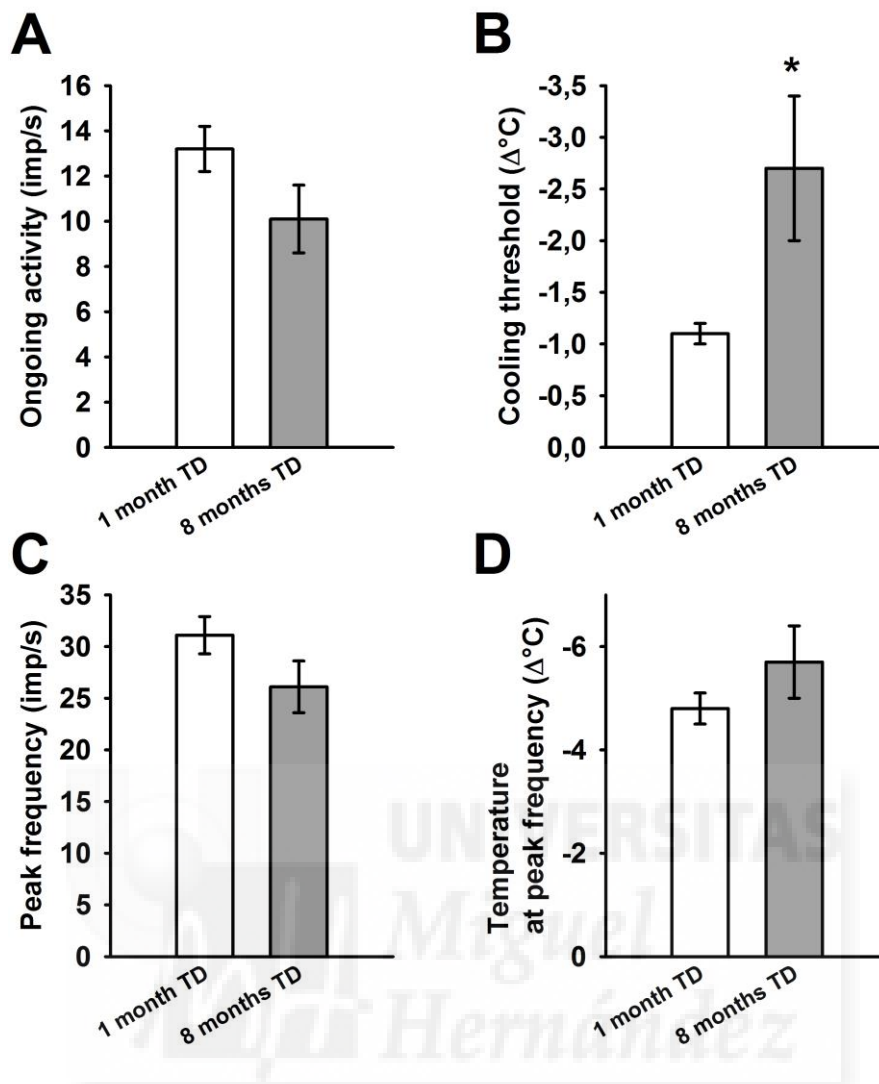


Figure 75. Spontaneous and stimulus-evoked activity of cold thermoreceptors in corneas of tear-deficient guinea pigs at 1 and 8 months after lacrimal gland removal. (A) Ongoing activity at basal temperature (34°C). (B) Decrement in temperature needed to increase by 25% the basal firing frequency of discharge at 34°C (cooling threshold). (C) Peak frequency of discharge in response to a cooling stimulus from 34°C to 20°C. (D) The change of temperature at which the peak frequency was attained. Data are mean ± SEM. *P<0.05, t-test.

B.4.2. Neural activity of mechano- and polymodal nociceptors

Nerve activity was recorded in 48 nociceptors from corneas of 1 month TD guinea pigs and in 18 nociceptors from corneas of 8 months TD guinea pigs. Mechano- and polymodal nociceptors were initially characterized based on their response to mechanical and chemical stimulation (see Methods for details).

Comparing 1 month TD animals to their age-matched control group there were no significant differences in the spontaneous activity and in the mechanical threshold of mechano- (Table 15) or polymodal nociceptors (Table 16), likewise, the latency of the response to CO₂ pulses was similar in polymodal nociceptors comparing both groups (data not shown).

Table 15. Spontaneous activity and response to natural stimuli of mechano-nociceptors in age-matched control and tear-deficient (TD) guinea pig corneas.

Mechano-nociceptors	Young control n=53	1 month TD n=27
Mechanical threshold (mN)	0.48 ± 0.09	0.55 ± 0.1
Spontaneous activity (imp/s)	1.3 ± 0.7	0.29
% of fibers with SA	7.4%	3.7%

Data are the mean ± SEM. n=number of units.

Table 16. Spontaneous activity and response to natural stimuli of polymodal nociceptors in age-matched control and tear-deficient (TD) guinea pig corneas.

Polymodal nociceptors	Young control n=55	1 month TD n=21
Mechanical threshold (mN)	0.18 ± 0.02	0.19 ± 0.04
Spontaneous activity (imp/s)	1.7 ± 0.9	0.55 ± 0.35
% of fibers with SA	16.4%	15%
Mean discharge rate in response to CO ₂ (imp/s)	2.7 ± 0.4	2.1 ± 0.4

Data are the mean ± SEM. n=number of units.

While comparing 8 months TD guinea pigs to their age-matched controls there were no significant differences in the parameters measured for mechano- (Table 17) and polymodal nociceptors (Table 18). The latency of the response to CO₂ pulses in polymodal nociceptors was not significantly different comparing both groups (data not shown).

Table 17. Spontaneous activity and response to natural stimuli of mechano-nociceptors in age-matched control and tear-deficient (TD) guinea pig corneas.

Mechano-nociceptors	Adult control n=52	8 months TD n=10
Mechanical threshold (mN)	0.47 ± 0.09	0.27 ± 0.06
Spontaneous activity (imp/s)	0.9 ± 0.4	0
% of fibers with SA	7.8%	0%

Data are the mean ± SEM. n=number of units.

Table 18. Spontaneous activity and response to natural stimuli of polymodal nociceptors in age-matched and tear-deficient (TD) guinea pig corneas.

Polymodal nociceptors	1 month TD n=21	8 months TD n=8
Mechanical threshold (mN)	0.19 ± 0.04	0.41 ± 0.17
Spontaneous activity (imp/s)	0.55 ± 0.35	1.06 ± 0.55
% of fibers with SA	15%	23%
Mean discharge rate in response to CO ₂ (imp/s)	2.1 ± 0.4	3.3 ± 0.8

Data are the mean ± SEM. n=number of units.

Student t-test showed no significant differences in the spontaneous activity and in the mechanical threshold of mechano- (Table 19) or polymodal nociceptors (Table 20) recorded from corneas of 1 month TD and 8 months TD guinea pigs. The latency of the response to CO₂ pulses was similar in polymodal nociceptors from 1 month TD and 8 months TD corneas (data not shown).

Table 19. Spontaneous activity and response to natural stimuli of mechano-nociceptors in tear-deficient (TD) guinea pig corneas.

Mechano-nociceptors	1 month TD n=27	8 months TD n=10
Mechanical threshold (mN)	0.55 ± 0.1	0.27 ± 0.06
Spontaneous activity (imp/s)	0.29	0
% of fibers with SA	3.7%	0%

Data are the mean ± SEM. n=number of units.

Table 20. Spontaneous activity and response to natural stimuli of polymodal nociceptors in tear-deficient (TD) guinea pig corneas.

Polymodal nociceptors	Adult control n=54	8 months TD n=8
Mechanical threshold (mN)	0.34 ± 0.08	0.41 ± 0.17
Spontaneous activity (imp/s)	0.7 ± 0.2	1.06 ± 0.55
% of fibers with SA	14.8%	23%
Mean discharge rate in response to CO ₂ (imp/s)	3.2 ± 0.4	3.3 ± 0.8

Data are the mean ± SEM. n=number of units.

V. DISCUSSION

The results of this work brought us closer to understanding the dynamics of the innervation of corneal epithelium while growing from youth to adulthood and in chronic tear-deficiency as it is present in dry eye disease. The corneal nerves are known for their trophic function and important role in the maintenance of corneal surface integrity. In the present studies we have investigated the changes in morphology and neural activity of corneal nerves, and we have also investigated the influence of the alterations in corneal nerve density, which is known to occur with aging and in dry eye disease, on corneal epithelial wound healing.

A. Guinea pig as an animal model for studying morphology of corneal innervation, epithelial wound healing, and corneal nerve activity

In our studies we used Dunkin Hartley guinea pigs of both sexes and different ages between 1 and 12 months. The use of guinea pig as an experimental model for ophthalmological diseases has been already documented (see the review by (Cafaro, Ortiz et al. 2009). Even though the corneal sensitivity in the guinea pig is lower comparing to other animals (Troost, Skalicky et al. 2007; Wieser, Tichy et al. 2013), there are experimental evidences showing that this species represents a very good animal model for electrophysiological characterization of the activity of corneal cold thermoreceptors and nociceptors (Brock, McLachlan et al. 1998; Acosta, Tan et al. 2001; Brock, Pianova et al. 2001; Acosta, Luna et al. 2013; Acosta, Luna et al. 2014). Since guinea pig is an experimental model used preferentially in our laboratory, it is advisable to know more about the possible changes in the corneal innervation which occur with age and during disease.

Dry Eye Disease (DED) is a very prevalent and bothersome condition affecting millions of people, being more prevalent with increasing age. There are many animal models of DED, which imitate the different pathogenic mechanisms of this disorder (Barabino and Dana 2004). One of them is the reduction of lacrimal secretion that involves the removal of the main lacrimal gland (Barabino and Dana 2004). The main lacrimal gland removal has been also performed in other species as the squirrel monkeys to study the effects on tear production (Maitchouk, Beuerman et al. 2000), or the rat to explore the effect of dry eye on corneal neurons activity (Kurose and Meng 2013).

The experimental model of tear-deficiency in guinea pig has not been yet explored in terms of possible changes in corneal innervation. This part of the present study was then aimed to explain the influence of tearing reduction on the morphology and functional activity of the different subclasses of corneal nerves, and therefore, to discuss the impact of the impaired corneal innervation on the abnormal sensations evoked from the eye and the altered trophic status of corneal epithelium that occur in Dry Eye Disease.

B. Guinea pig's tearing rate

B.1. Methodological considerations

One of the most commonly performed methods of measuring tear production is Schirmer tear test without anesthesia. It measures the tear flow produced within a given time frame and shows a great variety between species (Wieser, Tichy et al. 2013). Since guinea pig is known to have very low tear flow, the commercial paper strips used the Schirmer tear test failed as a technique for measuring lacrimation rate in these animals (Trost, Skalicky et al. 2007). Then, in the present study tearing rate was measured with use of the phenol red thread tear test (PRT), which is a quantitative test for aqueous tears with minimal sensation, and the short test times which are accurate indicator for measuring residual tears in humans and several animal species including guinea pig (Trost, Skalicky et al. 2007).

The tear production was measured during 30 seconds in the different experimental groups of young and adult intact animals, and in age-matched groups of young and adult animals with enow removed lacrimal glands, allowing evaluate the possible effect of age and dry eye condition on the lacrimation rate.

B.2. Tearing rate was not altered in adult animals

Tearing rate was slightly but not significantly higher in adult guinea pig (14.9 ± 2.1 mm) than in young animals (11.8 ± 0.8 mm). The tear flow production measured by other authors using also PRT in one year-old guinea pigs gave values of 6 ± 4.7 mm, even though the tear rate was measured during shorter time period of 15 seconds (Trost, Skalicky et al. 2007). All together, the data suggest that the lacrimation rate is maintained and even increases during first year of the guinea pig's life.

B.3. Tearing rate was altered in tear-deficient animals

Tear-deficient animals showed a reduced tear flow rate at one month after lacrimal gland removal (3 ± 0.7 mm) compared with age-matched intact animals (11.8 ± 0.8 mm). The reduction in lacrimation was maintained also at eight months after lacrimal gland removal (6.6 ± 1.2 mm) compared to age-matched, adult animals (14.9 ± 2.1 mm). In the study performed on squirrel monkeys, it was found that the tear production was changed drastically 1 week after lacrimal gland ablation, whereas 20 weeks later the tearing rate increased significantly reaching values closer to the normal. In this case, the authors suggested that the recovery of tear production was due to an increase of the accessory lacrimal glands tear production (Maitchouk, Beuerman et al. 2000). The differences between the results obtained in this study and in the present work could be due to the use of disparate animal species, to differences in the study protocol, or to the small number of animals and not specified age in the study of Maitchouk et al.

We observed the slight changes in tear rate between young tear-deficient (3 ± 0.7 mm) and adult tear-deficient (6.6 ± 1.2 mm) animals, which could be the result of an increased contribution of the accessory lacrimal glands to tear production, as suggested by (Maitchouk, Beuerman et al. 2000), and also could also reflect the recovery of corneal nerve density found in adult guinea pigs subjected to tear-deficiency at one month of age (see below).

C. Corneal nerve morphology

C.1. Methodological considerations

The morphology of corneal innervation has been already described in many mammal species (Zander and Weddell 1951; Tervo and Tervo 1981; Chan-Ling 1989; Marfurt, Kingsley et al. 1989; Marfurt and Echtenkamp 1995; Jones and Marfurt 1998; Marfurt, Murphy et al. 2001; Dvorscak and Marfurt 2008; McKenna and Lwigale 2011; Wang, Fu et al. 2012; Ivanusic, Wood et al. 2013), including human (Zander and Weddell 1951; Müller, Pels et al. 1996; Müller, Vrensen et al. 1997; Al-Aqaba, Fares et al. 2010; He, Bazan et al. 2010; Marfurt, Cox et al. 2010; Turuwhenua, Patel et al. 2012).

Microscopic observation of the corneal nerve architecture and morphology is based on different methods of tissue staining like the use of gold chloride, acetylcholinesterase-, and other immunohistological techniques (Zander and Weddell 1951; Rozsa and Beuerman 1982;

Schimmelpfennig 1982; Marfurt, Murphy et al. 2001). Moreover, corneal ultrastructure has been studied in electron microscopy studies (Zander and Weddell 1951; Lim and Ruskell 1978; Rozsa and Beuerman 1982; Schimmelpfennig 1982; Müller, Pels et al. 1996; Müller, Vrensen et al. 1997; Marfurt, Murphy et al. 2001). More recently in vivo confocal microscopy (IVCM) is successfully used in preclinical animal research (Esquenazi, He et al. 2007), likewise for clinical diagnosis of pathology of the cornea and as a monitoring tool (Patel and McGhee 2005).

However, the above-mentioned methods have some limitations that hinder the detailed description of corneal nerves. The conventional histology is unable to show detailed innervation of corneal layers and requires fresh corneas (He, Bazan et al. 2010), because of the rapid over time postmortem nerve degeneration (Müller, Vrensen et al. 1997). The transmission electron microscopy images are in turn limited to very small areas of the corneal surface, while IVCM images of the animal and human corneas are recorded preferentially from the corneal apex. Moreover, nerve branches and terminals of less than 0.5 μm in diameter cannot be imaged with IVCM, tandem scanning confocal microscopes, or scanning slit confocal microscopes (He, Bazan et al. 2010).

For the purpose of present morphological studies we used the beta III-tubulin immunohistochemical and immunofluorescence staining techniques, which provide optimal demonstration of guinea pig corneal nerve structures. Beta-III tubulin is a pan-neuronal marker that stains all nerve fibers in the cornea. The immunohistochemical technique with diaminobenzidine (DAB) used also in this study has the advantage that the chromogen is permanent and does not fade under prolonged illumination, what is very useful for long process of nerve quantification and for making corneal drafts with the *camera lucida* attached to a light microscope.

The use of whole mount cornea preparations made possible to visualize in three dimensions the entire epithelial nerve network, from the subbasal nerves origins to superficial terminals. By changing the plane of focus, it allowed also to observe any alterations in subbasal nerve fibers and nerve terminal density caused during development from youth to adulthood, or induced by short or long-term tear-deficiency. Whole mount cornea preparations were used to quantify subbasal nerve leashes and epithelial nerve terminals. It also permitted acquisition of nerve density data and their estimation for 1-mm² areas in three different corneal zones (peripheral, central and vortex), always in the same location in each cornea (the superior quadrant). Moreover the whole mount preparations permitted the comparison of changes in the nerve density and morphology between peripheral and central corneal zones. The separation of

the cornea to 3 different zones using dedicated software gives also the possibility of estimating the density of subbasal nerve terminals and, then, the comparison of the different parameters measured in the different corneal zones. This method allowed analyzing the density of corneal nerve fibers and terminals from the corneal apex to corneal periphery. Nevertheless, there are some sources of possible errors that have to be taken into account because they might influence the final results, as the errors in manual quantification of nerve structures caused by inappropriate microphotographs resolution, deficient staining or failure of the investigator during the identification of the structures. Apart from it worth mentioning that some nerve structures might be degenerated after animal death (Müller, Vrensen et al. 1997).

C.2. Animals age considerations

In the studies on the effects of age on corneal innervation, the selected animal age groups were compared with their equivalent human stage of age. This way, it is possible to compare groups of animals equal to newborn, child, teenager, adult, middle-age, and quinquagenarian (Wang, Fu et al. 2012). The lifespan of experimental rodents like mouse and rat is shorter than the life of guinea pig, wherefore the studies on the influence of age are easier and faster to perform in rodents. There are very few scientific works mentioning about the guinea pig lifetime. The most reliable reports of the lifespan of the guinea pig come from private internet webpages (Figure 76), informing about average maximum age up to 8 years; or from few works (Terril, Clemons et al. 1998; Tonge, Bardsley et al. 2013), where the average maximum age is from 4 up to 7 years. Despite the discrepancies in the data, we selected five different time-points for measuring morphological parameters: 1 month, 2 months, 4 months, 9 months, and 12 months, where the last ones is supposed to be equivalent of 20 years old human (Figure 76), hence it can be called adult group. Guinea pigs of from 1 to 4 months old were considered as young group, while from 7-12 months as adult group.

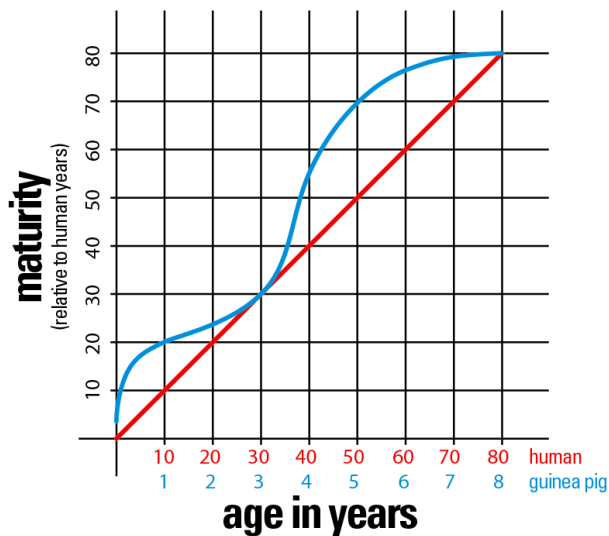


Figure 76. Lifespan calculator of guinea pig and human. Taken from www.guineapigtoday.com.

C.3. Morphological changes in the corneal surface area with age

The human corneal surface reaches adult size around 2 years of age and measures around 138 mm² (reviewed by (Adler, Kaufman et al. 2011)). The studies performed in mice showed that the corneal surface area increased linearly from birth until postnatal month 2 and then remained fairly constant without significant differences observed between the age groups (Wang, Fu et al. 2012). In the present study we measured the corneal surface area in 1, 2, 4, 9, and 12 months old guinea pigs. We observed that the fastest growth of the cornea occurs between the third and fourth months of age (6 mm²/month); and that the corneal surface area increases slowly afterwards until 1 year of guinea pig's life, reaching an area of around 50 mm². The continuous corneal growth may explain the proportional nerve elongation (Figure 77), as well as some changes in nerve number (Figure 78), density and structure.

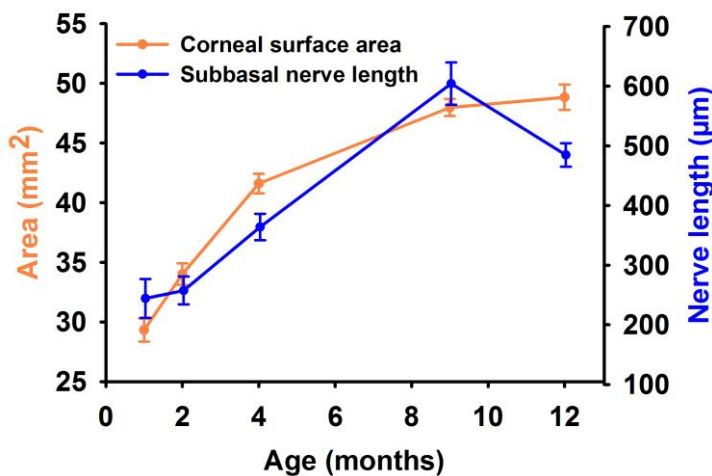


Figure 77. The increment of the corneal surface area with age is correlated with the subbasal nerves elongation. The graph depicts the age-related changes in the corneal surface area (left axis), and in the subbasal nerve length from the central corneal zone (right axis). Data are mean ± SEM. n=4-14 (see results for details).

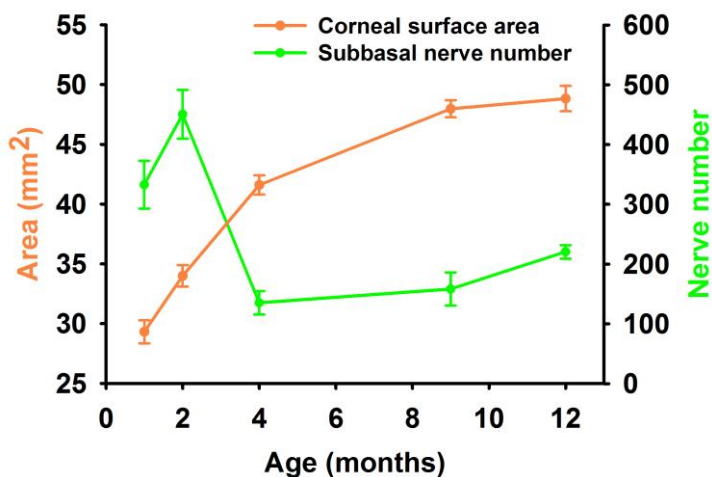


Figure 78. The increment of the corneal surface area and changes in the subbasal nerve number with age. The graph depicts the age-related changes in the corneal surface area (left axis), and in the subbasal nerve number (right axis). Data are mean \pm SEM. n=4-14 (see results for details).

C.4. Morphological changes in the corneal innervation with age

Many studies on age-related changes in the epithelial innervation of the cornea have been performed in mouse (McKenna and Lwigale 2011; Wang, Fu et al. 2012), rat (Dvorscak and Marfurt 2008), and human (Erie, McLaren et al. 2005; He, Bazan et al. 2010). It is important to note that the changes in the subbasal nerve fiber and nerve terminals density, which are associated with age, must be interpreted with caution, because of the inherent resolution limitations of used techniques and instruments.

In our study we analyzed only some parameters describing the characteristic of the typical “nerve units” present at the subbasal nerve plexus, the so called **subbasal nerve leashes**. The term “leash” describes a group of subbasal nerve fibers deriving from the same parent anterior stromal nerve, and is named “epithelial leash” (Rozsa and Beuerman 1982; Schimmelpfennig 1982; Chan-Ling 1989; Wang, Fu et al. 2012), or subbasal nerve bundle in other works (Erie, McLaren et al. 2005). The methodological approach used in the present study allows us to demonstrate, for the first time, the subbasal nerve leashes number and density calculated manually in whole mount corneas, as well as their distribution into peripheral and central cornea zones. We found that the number, as well as, the density of subbasal nerve leashes increased from month 1 to month 2 of age, reaching the peak in the number and density and then decreasing drastically at month 4, followed by a gradual increase until month 12 of age. The same phenomenon was observed when analyzing the innervation of the whole cornea or separated into the peripheral and central zones. The lowest number and density of subbasal nerve leashes was observed at month 4, and at the next measured time-point (which

was month 9) it was not much higher. The highest number and density was found at 2 months of age. We observed that, independently on the time-point, the number and density of subbasal leashes was higher in the peripheral zone than in central zone of cornea, what is contrary with the studies performed in mice (Wang, Fu et al. 2012) and in human (Marfurt, Cox et al. 2010). The changes of the number and density of subbasal nerve leashes is not often quantified. There is a report describing no changes in the density of subbasal nerve leashes with age in human subjects (Erie, McLaren et al. 2005). The reason we took this parameter in our consideration was that subbasal nerve leash is a very characteristic and unique morphological unit present only in the cornea. Furthermore subbasal nerve leashes are well distinguishable and easy for quantifying in the cornea of guinea pig. Finally, their number, density, length and shape are readily noticeable, which in turn permits to detect changes of corneal nerve morphology occurring due to their natural rearrangement during development or associated with other factors.

For the first time, our study documented the presence of corneal subbasal nerve vortices in the guinea pig cornea. The whorl-like patterns described in other animal species, including human, were identified in the central zone of cornea in every age group. The finding that the morphological appearance of subbasal nerve vortex did not change with age was already described in rat (Dvorscak and Marfurt 2008). The presence of vortex has been already described in mouse (Charles and Rosenblatt 2007; McKenna and Lwigale 2011; Wang, Fu et al. 2012; Ivanusic, Wood et al. 2013), rat (Dvorscak and Marfurt 2008), and human (Patel and McGhee 2005; Marfurt, Cox et al. 2010).

Marfurt et al showed that the subbasal nerve length varied widely in human cornea, being the shortest near to the center of the vortex and close to the limbus, and the longest in the superior corneal quadrant (Marfurt, Cox et al. 2010). We also observed large diversity in the subbasal nerve length and for that reason we decided to analyze only one quadrant (the superior quadrant) of guinea pig cornea, with distinction between 3 different zones. This led us avoid incorrect averaging the length of subbasal nerve leashes, which highly varies between corneal quadrants. In the present study, we have showed that there is a significant correlation between subbasal nerves morphology and age in the guinea pig (Wang, Fu et al. 2012). We have observed that the length of subbasal nerve leashes increases linearly until the month 9 and then slightly but not significantly decreases at month 12 of age. The subbasal nerve leashes length significantly varies between peripheral, central and vortex zones being the shortest in the peripheral and relatively of the similar longitude in the central and vortex zones. It was shown that the subbasal nerves do not run for long distances in the guinea pig cornea (Ivanusic, Wood

et al. 2013). We have shown for the first time that the length of subbasal nerve leashes in the guinea pig changes with age reaching approximately 600 μm long in the central cornea of 9 month-old animals (Figure 77).

The nerve terminals presented a gradual decrease in density from month 1 until month 12, demonstrating some variations between the different corneal zones. In the peripheral and central zones, terminal density decreased almost linearly with age, whereas in the vortex zone there was a large decrease at month 4 and then an increase at 9 and 12 months of age. The significant diminishing in corneal nerve terminal density that occurred at month 4 might be correlated with the great decrease in the number and density of subbasal nerve leashes that appeared at the same age (Figure. 79). The observed decrease of nerve terminal density with age observed in the guinea pig has been also described in the mouse (Wang, Fu et al. 2012), where both the corneal nerve terminal density and number decreased in a nearly linear fashion after postnatal month 2 until month 15 of age. Another study showing the anatomic evidence of a significant decrease in corneal nerve terminal density as a function of age was performed in rat (Dvorscak and Marfurt 2008). We found in almost every age group that the highest nerve terminal density was measured in the vortex zone; this phenomenon has been already described in human, where the terminals number was higher in the central zone of cornea (He, Bazan et al. 2010). The nerve terminal density presented similar values in all corneal zones in 4 months-old animals, which might be due to the asynchronous growth of the corneal surface area that was faster rate at this time-point of the lifespan. We have shown in our study that the age-related loss of corneal nerve terminal density begins early in life, what was also seen in the rat (Dvorscak and Marfurt 2008) and mouse (Wang, Fu et al. 2012). This has been also suggested by experiments performed on human subjects using a noncontact corneal esthesiometer to measure corneal sensitivity, which declined in a linear fashion from 20 to 70 years of age (Murphy, Patel et al. 2004; Acosta, Alfaro et al. 2006). These findings suggest that the decrement in the corneal terminal density is not a phenomenon restricted to advanced age. Even though our studies cannot reflect the changes in corneal nerve terminals density that occurs in older animals, the studies performed on mice (Wang, Fu et al. 2012), and rat (Dvorscak and Marfurt 2008), confirm this phenomenon. Considering the nerve terminals as the parts of the nerve fiber responsible for transducing sensory stimuli into neural signals, corneal nerve terminal density could be directly proportional to corneal sensitivity (Rozsa and Beuerman 1982). It has been already shown that corneal sensitivity decreases with increasing age in humans (Millodot 1977; Bourcier, Acosta et al. 2005). The age-related loss of the nerve terminals might be a reason of altered corneal sensitivity in elderly subjects; however, other

factors, like impaired synaptic processing of corneal sensory information in the central nervous system (Erie, McLaren et al. 2005), age-related decreases in level of patient alertness (Murphy, Patel et al. 2004), and decreased nerve responsiveness resulting from altered tear film composition (Bourcier, Acosta et al. 2005), may also contribute to this phenomenon.

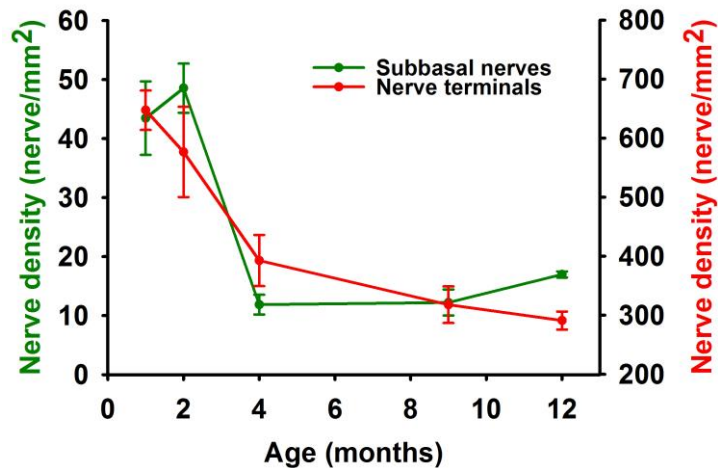


Figure 79. The changes in subbasal nerve and epithelial nerve terminal density with age. The graph presents the age-related changes in the density of subbasal nerves (left axis), and in the density of nerve terminals (right axis) measured in central corneal zone. Data are mean \pm SEM. n=4-9 (see results for details).

The subbasal nerve fiber density showed similar pattern of nerves distribution with age as seen in the case of nerve terminal density (Figure80). The density of nerve fibers reached its peak at month 1 and then decreased significantly in month 4 of guinea pig life. In month 9 it was maintained at approximately the same level to decrease again in month 12. However, the nerve fiber density in the corneal vortex zone showed a significant increment in month 9 that was followed by significant decrement in month 12. The study in mice demonstrated that the subbasal nerve fiber density decreased significantly from 2 to 15 months of age (Wang, Fu et al. 2012). The progressive reduction in the nerve fiber density with increasing age was observed also in human (He, Bazan et al. 2010). Nonetheless the studies in rat demonstrated that subbasal nerve density increases significantly between 6 and 24 months of age (Dvorscak and Marfurt 2008). In turn another clinical study shows no correlation between patient age and subbasal nerve fiber density (Erie, McLaren et al. 2005). We found that the density of subbasal nerve fibers was higher in the central and vortex zones of cornea than in the peripheral zone. Similar findings were described in human (He, Bazan et al. 2010). However, we have observed that in month 12 the nerve fiber density seemed to be approximately at the same level in all corneal zones. The reason for the disparities in the findings between species may include differences in animal models, instrument resolution, light intensity settings, location and size of the corneal surface areas examined, and the methods used to calculate nerve fiber density.

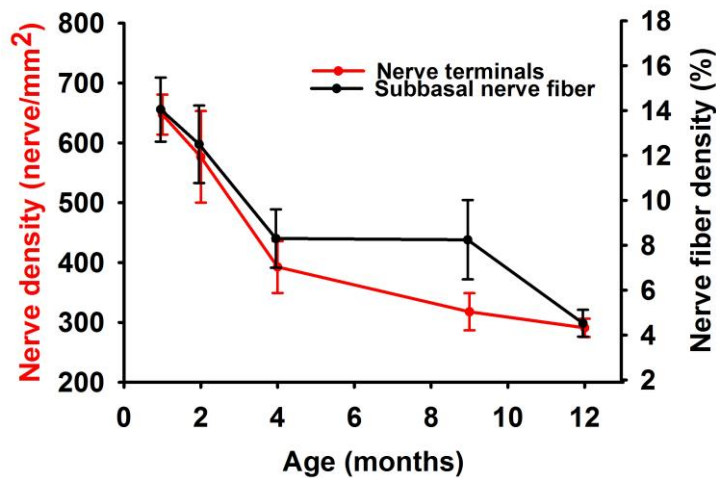


Figure 80. The changes in epithelial nerve terminal and nerve fiber density with age. The graph presents the age-related changes in the density of nerve terminals (left axis), and in the density of nerve fibers (right axis) measured in central corneal zone. Data are mean \pm SEM. n=4-9 (see results for details).

C.5. Morphological changes in the corneal innervation as an effect of induced tear-deficiency

The experimental model of induced tear-deficiency in guinea pig used in our studies was obtained by the main lacrimal gland ablation. The lacrimal gland was removed in 1 month animals and the effect of induced tear loss was examined 1 month, 3 months and 8 months after its removal. The differences in measured parameters inside the same animal age group might be caused by the incomplete main lacrimal gland removal; differences in the accessory lacrimal glands tear secretion; individual adaptation among different animal subjects.

Most of morphological studies investigating the dry eye disease are based on the *in vivo* confocal microscopy (IVCM) (Hoşal, Örneke et al. 2004; Benítez-del-Castillo, Acosta et al. 2007; Labbé, Alalwani et al. 2012; Labbé, Liang et al. 2013). As already mentioned, the use of confocal microscopy is noninvasive technique *in vivo* and makes dynamic study possible in real time, but on the other hand it has a potential limitation, because the measurements are made only in the center of the cornea and nerve branches and terminals of less than 0.5 μm in diameter cannot be imaged.

Present study describes for the first time changes in the corneal innervation caused by induced tear-deficiency (TD) in the guinea pig. Three different age-groups of TD were compared with their age-matched controls with regard to various parameters.

The corneas showed the biggest changes in the nerve morphology one month after lacrimal gland removal. The subbasal nerve leashes number and density decreased significantly in the whole mount corneas, as well as, in the corneas separated into peripheral and central

zones. We have not seen any changes in the length of subbasal nerve lashes in this age group. However the nerves seemed to be more tortuous as it was seen in other studies on dry eye (Tuominen, Konttinen et al. 2003). The nerve terminal density 1 month after lacrimal gland removal has not been significantly different; however terminal density in the corneal vortex zone was much decreased. The density of subbasal nerve fibers exhibited significant decrease in all corneal zones in the 1 month TD guinea pigs. The group of 1 month TD demonstrated the changes in the corneal innervation, which are comparable with the results in human subjects with Dry Eye Disease examined with IVCN, where the subbasal nerve fiber density was much decreased (Benítez-del-Castillo, Acosta et al. 2007; Labbé, Alalwani et al. 2012; Labbé, Liang et al. 2013). The changed density of subbasal nerves could be the reason of the decreased corneal sensitivity, what is called corneal hypoesthesia in the patients with dry eye (Bourcier, Acosta et al. 2005; Benítez-del-Castillo, Acosta et al. 2007).

We have observed an unexpected increment in the number and density of subbasal nerve lashes in the corneas 3 months after lacrimal gland removal. The reasons of this augmentation is unknown, but it might be due to a high metabolic activity, possibly directed to repair the alterations at epithelial level, and also due to the extremely rapid growth of the corneal surface area observed at that time-point and thus the higher level of growth factors and neuropeptides. The length, as well as, the nerve terminal density did not exhibit any significant changes 3 months after lacrimal gland ablation. There were not any significant alternation in the subbasal nerve lash number and density, subbasal nerve length, nerve terminal density and subbasal nerve fiber density in the animal group 8 months after lacrimal gland removal. The animal groups 3 and 8 months after induced TD seemed to have the corneal innervation similar to control groups. This phenomenon could be due to recovered tearing level through accessory lacrimal glands secretion.

D. Corneal epithelial wound healing

D.1. Methodological consideration

There are different types of wounds and animal models used to study corneal wound healing. The corneal wound healing includes chemical and mechanical wound models (reviewed by (Stepp, Zieske et al. 2014)). Some models are better for studying corneal scarring and others for recurrent erosions and basement membrane defect. In our study we performed a

corneal epithelial debridation with use of *n*-heptanol following procedure described before (Cintron, Hassinger et al. 1979; Perez, Lopez-Briones et al. 1987; de Leeuw and Chan 1989; Gallar, Pozo et al. 1990). *N*-heptanol removes the corneal epithelial layers down to Bowman's membrane, but does not damage the epithelium basal lamina (Cintron, Hassinger et al. 1979). This experimental nerve wounding model of the cornea involves acute damage to corneal nerves and is restricted to intraepithelial axon terminals (de Leeuw and Chan 1989). The aim of our studies was to investigate **the effect of age** and **the effect of induced tear-deficiency** on corneal epithelial wound healing in guinea pig. To evaluate the influence of examined factors we analyzed decrease in the wound area during epithelial healing by measuring estimated migration rate (EMR) of epithelial cells surrounding the wound, and estimated time for wound closure (ETH), as calculated before (Gallar, Pozo et al. 1990).

D.2. Corneal epithelial wound healing - the effect of age

The effect of age on corneal epithelial lesion repair was checked by comparing the group of young (2 months of age) and adult (7 months of age) guinea pigs. We found in our study that epithelial wound healing is significantly decreased in adult animals. This effect is expected, since from the morphological study of corneal innervation we know that around month 8 of guinea pig life corneal nerves demonstrate lower density of subbasal nerve leashes, nerve fibers and also nerve terminals. These results together with the studies in experimental animals which suggest that damage to corneal innervation affects epithelial regeneration and corneal metabolism (Beuerman and Schimmelpfennig 1980; Vannas, Holden et al. 1987) could explain the slower epithelial wound repair in adult animals. This can confirm that superficial corneal wounds can readily damage the subbasal nerves, thereby reducing important sensory functions, and trophic effects of these nerves that maintain integrity of the corneal epithelium.

D.3. Corneal epithelial wound healing - the effect of induced tear-deficiency

The effect of induced tear-deficiency was examined in guinea pig 1 month and 6 months after lacrimal gland removal. In the group of young animals, as expected, the corneal wound healing was significantly slower in the tear-deficient guinea pig comparing to its control. We observed also that initial size of the wound area was bigger in TD corneas, what might suggest their poor trophic condition.

We have not observed any significant difference in the epithelial wound healing in the group of animals 6 months after lacrimal gland removal. Since the corneal nerves have trophic properties, which are necessary to maintain a healthy ocular surface, this result could be due to the recovered corneal innervation at this time-point.

In the model of corneal epithelial debridation with *n*-heptanol performed in rabbits, regenerated epithelial cells covered the entire wound area three days later (de Leeuw and Chan 1989). The studies performed in mice suggest that events within the first 14 hours are important for nerve regeneration and epithelial restoration, and 24 hours is the time when epithelial cells migrated as a monolayer to cover the wound and sufficiently to exclude fluorescein applied to the ocular surface (Li, Burns et al. 2011). The various time of healing might be due to species differences, for example in the corneal nerve pattern, and also due to the initial size of the induced wound. The authors observed that after the wound performance the deep stromal nerves were unaffected; and between 3 and 10 weeks after wounding, no further qualitative changes were detectable in the regeneration pattern of corneal nerves (de Leeuw and Chan 1989).

Additionally, while compared young TD animals (2 months of age) with adult TD (7 months of age), we found as expected that the epithelial lesion closure was slower in the young TD group. As we assumed before, since adult tear-deficient animals have recovered the corneal innervation, the trophic condition of their corneas is better. Also it could be due to recovered lacrimation through the factors present in the tears that favor nerve regeneration. It was shown that some factors, like T cells, IL-17, neutrophils, platelets, and VEGF are necessary for efficient corneal nerve regeneration following epithelial abrasion (Li, Burns et al. 2011; Pan, Fukuoka et al. 2013).

E. Electrophysiological extracellular recordings

E.1. The effect of age on corneal nerves activity

In our studies we have shown that the decrease in nerve terminal density begins early in life. Confirmation of this finding could be morphological studies of age-related changes in the corneal innervation performed in rat (Dvorscak and Marfurt 2008), and in mouse (Wang, Fu et al. 2012). Since it is assumed that corneal nerve density is directly proportional to corneal sensitivity (Rozsa and Beuerman 1982), the results showing that corneal sensitivity declines in a

linear fashion beginning at approximately age 20 and decreases by almost half between 20 and 50 years of age (Murphy, Patel et al. 2004), could support that it is due to decrease in corneal nerve density. Based on these results we can deduce that similar age-related changes may occur in human corneas. Clinical studies reported that incidence of dry eye increases significantly with age (Workshop 2007). We have demonstrated no significant differences in the activity of single cold-sensitive corneal nerve terminals between young and adult guinea pigs. Our findings together with the morphological evidence might suggest that the changes in corneal nerve sensitivity (Murphy, Patel et al. 2004) are due to quantitative, not qualitative impairment in corneal innervation that occurs with early aging.

E.2. The effect of tear-deficiency on corneal nerve activity

Comparing the recordings from corneas of animals with the main lacrimal gland removed 1 and 8 months before we have found that the cooling threshold was significantly higher in the animals 8 months after induced tear-deficiency, being similar to the cooling threshold recorded from age-matched control animals. It could be affiliated with the partly recovered innervation of the corneal epithelium observed 8 months after lacrimal gland removal. The lower cooling threshold in the 1 month TD animals could indicate that the cornea is more sensitive to the temperature changes shortly after tear-deficiency, what might be due to the alterations in the corneal nerves morphology seen in this animal group.

There were no significant differences seen in the spontaneous and evoked activity of mechano- and polymodal nociceptors comparing 1 month TD and 8 months TD animals. This finding might emphasize, that after induced tear-deficiency mainly the activity of cold thermoreceptors seems to be altered, therefore, any abnormal sensation appearing in the examined patients with dry eye might be due to changed activity of those corneal receptors.

Shortly after lacrimal gland removal (1 month TD) cold thermoreceptors showed significantly increased ongoing activity and significantly lower cooling threshold in comparison with age-matched control animals.

It is assumed that the age-related decrease in corneal innervation disrupts the reflex circuits that drive blinking and lacrimation, and also diminishes the essential corneal nerve-supplied trophic factors, leading to decreased corneal sensitivity, dry eye and impaired wound healing (Belmonte 2007; He, Bazan et al. 2010; Belmonte and Gallar 2011).

The results of this PhD Thesis provided new data on the morphology of the corneal epithelial innervation in the guinea pig, describing for the first time the changes occurring in those nerves associated with age during maturation from youth to adulthood. This work also provides new data on the short and long-term effects of experimentally induced dry eye on corneal nerve morphology. The continuous rearrangement and modifications of corneal nerves with time, and in particular the alterations consecutive to the nerve reduction provoked by tearing loss have a negative influence on the trophic status of the cornea, with a slowdown of the corneal wound healing rate, as showed in our results. Despite the quantitative changes in corneal nerve density, corneal cold thermoreceptor and nociceptor units display similar activity in young and adult animals.

To complete the presented studies it would be interesting to see what happens with corneal innervation in terms of nerve density and corneal nerve activity in older animals. It would be also interesting to analyze the effect on corneal innervation of inducing dry eye not in young but in adult or old animals, imitating the appearance of DED in humans, in which the disease usually develops during the adulthood. These data would complement the results obtained in the present work, aimed to describe the morphological and functional changes of corneal nerves that could be on the basis of reduced tearing and ocular dryness sensations developed with age and in dry eye disease.

V. CONCLUSIONS

1. The corneal nerve architecture changes with age in the guinea pig, exhibiting a reduction in the subbasal and epithelial nerve density in adult animals. This reduction in nerve density is thought to be due to a small but significant delay in epithelial wound healing in adult animals compared to young guinea pigs.
2. The corneal surface area increases linearly with age until 9 months then continues to grow, however, at a slower rate. The length of corneal subbasal nerves increases in parallel with corneal growth. The subbasal vortex whirl is present in the central zone of the cornea of the guinea pig at all studied ages.
3. Despite the changes in corneal nerve density and morphology occurring with age, the characteristics of the spontaneous and stimulus-evoked activity of the different types of corneal nerve fibers are similar in young and adult guinea pigs. This suggests that there are no functional changes in corneal nerves between young and adult guinea pigs.
4. Tear production is comparable in young and adult animals, although the tearing rate tends to increase in adult guinea pigs.
5. The surgical excision of the exorbital lacrimal gland causes a long lasting reduction of tear production in guinea pigs. Tear-deficient animals have an altered nerve morphology suggesting a lesion followed by regeneration. The changes in corneal subbasal nerve architecture following the removal of the lacrimal gland one month prior, indicates that nerve damage develops shortly after the induction of reduced tearing. The regeneration process that follows causes the density of subbasal and epithelial nerves to be comparable in tear-deficient animals 8 months post-surgery and their age-matched controls. Despite the recovery of nerve density 8 months after lacrimal gland removal, the regenerated corneal nerves present an abnormal distribution and architecture.

6. Neural activity of the corneal sensory nerve fibers is found to be altered in animals one month after surgical removal of the lacrimal gland. There is a significant increase in the spontaneous activity and cooling-evoked response of cold thermoreceptors one month post-surgery. Also, the spontaneous activity and CO₂-evoked response of polymodal nociceptor fibers are slightly elevated in these tear-deficient animals. This points towards a sensitization of corneal nerve fibers. These alterations in corneal nerve activity decrease, or even disappear 8 months after surgery.

7. The morphological and functional changes of corneal nerves seen one month after tear-deficiency induction may lead to a significant neurotrophic slowdown of epithelial wound healing as observed in this group. The regeneration of corneal nerves with time seems to restore the wound healing capabilities of the corneal epithelium, as found at longer times after lacrimal gland excision. These findings further support the role of corneal nerves in providing trophic supply to maintain the integrity of the corneal surface.

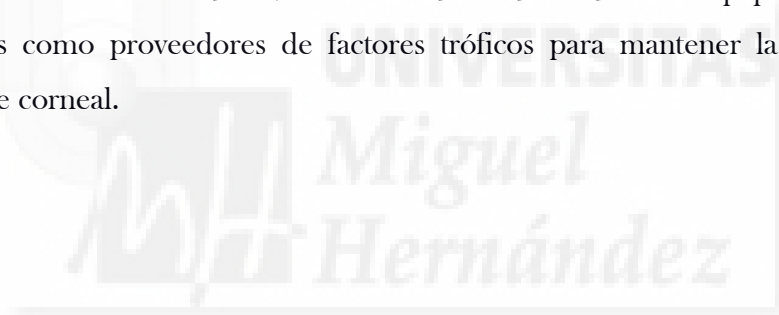


CONCLUSIONES

1. La arquitectura de la inervación corneal cambia durante el crecimiento en el cobaya, reduciéndose la densidad de los nervios sub-basales y epiteliales en animales adultos; esta disminución podría ser el origen del pequeño, aunque significativo, retraso en la curación de las úlceras corneales experimentales observado en los animales adultos cuando se compara con los jóvenes.
2. El área de la superficie corneal aumenta de forma lineal con la edad hasta los nueve meses de edad, creciendo después a menor ritmo. La longitud de los nervios sub-basales de la córnea aumenta en paralelo al crecimiento corneal. El remolino formado por los nervios sub-basales está presente en la zona central de la córnea del cobaya en todas las edades estudiadas.
3. A pesar de los cambios en la densidad y la morfología de los nervios corneales que ocurren con el crecimiento, las características de la actividad espontánea y la evocada de los diferentes tipos de fibras nerviosas corneales son similares en cobayas adultos y jóvenes, lo que sugiere que la maduración desde la juventud a la adultez no provoca cambios funcionales en los nervios corneales en el cobaya.
4. La tasa de producción lagrimal es similar en animales jóvenes y adultos, aunque muestra una tendencia al aumento en estos últimos.
5. La escisión quirúrgica de la glándula lagrimal principal provocó una reducción a largo plazo de la producción lagrimal en el cobaya. En los animales con deficiencia de lágrima hay alteraciones en la morfología de los nervios que sugieren daño nervioso y posterior regeneración. Los cambios en la arquitectura de los nervios sub-basales observados un mes después de la ablación de la glándula lagrimal sugieren que el daño de los nervios se produce poco tiempo después del inicio de la reducción lagrimal; el subsiguiente proceso de regeneración hace que, a los ocho meses tras la cirugía, la densidad de los nervios sub-basales y epiteliales sea comparable a la de animales intactos de la misma edad. A pesar de la recuperación de la densidad nerviosa, los nervios corneales regenerados muestran una distribución y arquitectura anormales ocho meses después de la cirugía.

6. La actividad neural de las fibras nerviosas sensoriales corneales está alterada un mes después de la ablación de la glándula lacrimal. Tanto la actividad espontánea como la respuesta al enfriamiento de los receptores de frío aumenta significativamente. Asimismo, la actividad espontánea y la respuesta de los nociceptores polimodales a un pulso de CO₂ está ligeramente alterada un mes después de la inducción de la deficiencia lacrimal. Estos cambios sugieren una sensibilización de las fibras nerviosas corneales a ese tiempo tras la cirugía, que tiende a disminuir o desaparecer tras ocho meses de evolución.

7. Tanto los cambios morfológicos como funcionales de los nervios corneales observados un mes después de la extirpación de la glándula lagrimal pueden provocar alteraciones neurotróficas, observándose un retraso significativo de la curación de úlceras corneales experimentales. La regeneración de los nervios corneales observada a largo plazo después de la deficiencia lacrimal parece recuperar la capacidad de reparación del epitelio corneal. Estos descubrimientos defienden además el papel de los nervios corneales como proveedores de factores tróficos para mantener la integridad de la superficie corneal.



VI. ABBREVIATIONS

CaCl ₂ -	calcium chloride
CGRP -	calcitonin gene-related peptide
CO ₂ -	carbon dioxide
CsA -	cyclosporine A
DAB -	3,3'-diaminobenzidine tetrahydrochloride hydrate
DED -	dry eye disease
ECM -	extracellular matrix
EDTA -	ethylenediaminetetraacetic acid
EGF -	epidermal growth factor
EMR -	estimated migration rate
ENT -	intraepithelial nerve terminals
ETH -	estimated time of healing
H ₂ O ₂ -	hydrogen peroxide
IgA -	immunoglobulin A
IGF-1 -	insulin like-growth factor-1
IgG -	immunoglobulin G
IVCM -	in vivo confocal microscopy
KCl -	potassium chloride
KCS -	keratoconjunctivitis sicca
LCS -	Leica Confocal Software
LD -	tear-deficient
LP -	limbal plexus
MgCl ₂ -	magnesium chloride
NaBH ₄ -	sodium borohydride
NaCl -	sodium chloride
NaH ₂ PO ₄ -	monosodium phosphate
NaHCO ₃ -	sodium bicarbonate
NaIO ₄ -	sodium (meta)periodate
nNOS -	neuronal nitric oxide synthase
NPY -	neuropeptide

NTI -	nerve terminal impulse
O ₂ -	oxygen
OGF -	opioid growth factor
OTG -	ophthalmic branch of trigeminal ganglion
PACAP -	pituitary adenylate cyclase activating peptide
PB -	phosphate saline
PRT -	phenol red thread tear test
RT -	room temperature
SA -	spontaneous activity
SBP -	subbasal plexus
SCG -	superior cervical ganglion
SEP -	subepithelial plexus
SN -	stromal nerve trunks
SP -	Substance P
TA -	transient amplifying cells
TG -	trigeminal ganglion
TH -	tyrosine hydroxylase
TRPM8 -	transient receptor potential cation channel subfamily M member 8
VEGF -	vascular endothelial growth factor
VIP -	vasoactive intestinal peptide

VII. BIBLIOGRAPHY

- Acosta, M. C., M. L. Alfaro, et al. (2006). "Influence of age, gender and iris color on mechanical and chemical sensitivity of the cornea and conjunctiva." Experimental eye research **83**(4): 932-938.
- Acosta, M. C., C. Belmonte, et al. (2001). "Sensory experiences in humans and single-unit activity in cats evoked by polymodal stimulation of the cornea." The Journal of physiology **534**(2): 511-525.
- ACOSTA, M. C., J. GALLAR, et al. (1999). "The influence of eye solutions on blinking and ocular comfort at rest and during work at video display terminals." Experimental eye research **68**(6): 663-669.
- Acosta, M. C., C. Luna, et al. (2013). "Changes in sensory activity of ocular surface sensory nerves during allergic keratoconjunctivitis." PAIN® **154**(11): 2353-2362.
- Acosta, M. C., C. Luna, et al. (2014). "Corneal Sensory Nerve Activity in an Experimental Model of UV Keratitis." Investigative ophthalmology & visual science **55**(6): 3403-3412.
- Acosta, M. C., M. E. Tan, et al. (2001). "Sensations evoked by selective mechanical, chemical, and thermal stimulation of the conjunctiva and cornea." Investigative ophthalmology & visual science **42**(9): 2063-2067.
- Adler, F. H., P. L. Kaufman, et al. (2011). Adler's Physiology of the Eye, Elsevier Health Sciences.
- Agrawal, V. B. and R. Tsai (2003). "Corneal epithelial wound healing." Indian journal of ophthalmology **51**(1): 5.
- Al-Aqaba, M. A., U. Fares, et al. (2010). "Architecture and distribution of human corneal nerves." British Journal of Ophthalmology **94**(6): 784-789.
- Albietz, J. M. (2001). "Dry eye: an update on clinical diagnosis, management and promising new treatments." Clinical and experimental optometry **84**(1): 4-18.
- Almubrad, T. and S. Akhtar (2011). "Structure of corneal layers, collagen fibrils, and proteoglycans of tree shrew cornea." Molecular vision **17**: 2283.
- Alves, M., E. C. Fonseca, et al. (2013). "Dry eye disease treatment: a systematic review of published trials and a critical appraisal of therapeutic strategies." The ocular surface **11**(3): 181-192.
- Ambati, B. K., M. Nozaki, et al. (2006). "Corneal avascularity is due to soluble VEGF receptor-1." Nature **443**(7114): 993-997.

- Anderson, R. (1977). "Actin filaments in normal and migrating corneal epithelial cells." Investigative ophthalmology & visual science **16**(2): 161-166.
- Baldwin, H. C. and J. Marshall (2002). "Growth factors in corneal wound healing following refractive surgery: a review." Acta ophthalmologica Scandinavica **80**(3): 238-247.
- Barabino, S. and M. R. Dana (2004). "Animal models of dry eye: a critical assessment of opportunities and limitations." Investigative ophthalmology & visual science **45**(6): 1641-1646.
- Belmonte, C. (2007). "Eye dryness sensations after refractive surgery: impaired tear secretion or "phantom" cornea?" Journal of refractive surgery (Thorofare, NJ: 1995) **23**(6): 598-602.
- Belmonte, C., A. Aracil, et al. (2004). "Nerves and sensations from the eye surface." The ocular surface **2**(4): 248-253.
- Belmonte, C., M. Carmen Acosta, et al. (2004). "Neural basis of sensation in intact and injured corneas." Experimental eye research **78**(3): 513-525.
- Belmonte, C. and J. Gallar (2011). "Cold thermoreceptors, unexpected players in tear production and ocular dryness sensations." Investigative ophthalmology & visual science **52**(6): 3888-3892.
- Belmonte, C., J. Gallar, et al. (1991). "Excitation by irritant chemical substances of sensory afferent units in the cat's cornea." The Journal of physiology **437**(1): 709-725.
- Belmonte, C. and F. Giraldez (1981). "Responses of cat corneal sensory receptors to mechanical and thermal stimulation." The Journal of physiology **321**(1): 355-368.
- Benítez-del-Castillo, J. M., M. C. Acosta, et al. (2007). "Relation between corneal innervation with confocal microscopy and corneal sensitivity with noncontact esthesiometry in patients with dry eye." Investigative ophthalmology & visual science **48**(1): 173-181.
- Bessou, P. and E. Perl (1969). "Response of cutaneous sensory units with unmyelinated fibers to noxious stimuli." J Neurophysiol **32**(6): 1025-1043.
- Beuerman, R. and K. Kupke (1982). "Neural regeneration following experimental wounds of the cornea in the rabbit." The Structure of the Eye: 319-330.
- Beuerman, R. and B. Schimmelpfennig (1980). "Sensory denervation of the rabbit cornea affects epithelial properties." Experimental neurology **69**(1): 196-201.
- Bourcier, T., M. C. Acosta, et al. (2005). "Decreased corneal sensitivity in patients with dry eye." Investigative ophthalmology & visual science **46**(7): 2341-2345.
- Brock, J. A., E. M. McLachlan, et al. (1998). "Tetrodotoxin-resistant impulses in single nociceptor nerve terminals in guinea-pig cornea." The Journal of physiology **512**(1): 211-217.

- Brock, J. A., S. Pianova, et al. (2001). "Differences between nerve terminal impulses of polymodal nociceptors and cold sensory receptors of the guinea-pig cornea." The Journal of physiology **533**(2): 493-501.
- Bron, A. (1972). "Vortex patterns of the corneal epithelium." Transactions of the ophthalmological societies of the United Kingdom **93**: 455-472.
- Brown, J., C. W. Soderstrom, et al. (1968). "Langerhans' cells in guinea pig cornea: response to chemical injury." Investigative ophthalmology & visual science **7**(6): 668-671.
- Buck, R. C. (1985). "Measurement of centripetal migration of normal corneal epithelial cells in the mouse." Investigative ophthalmology & visual science **26**(9): 1296-1299.
- Cafaro, T. A., S. G. Ortiz, et al. (2009). "The cornea of Guinea pig: structural and functional studies." Veterinary ophthalmology **12**(4): 234-241.
- Carr, R. W., S. Pianova, et al. (2003). "Effects of heating and cooling on nerve terminal impulses recorded from cold-sensitive receptors in the guinea-pig cornea." The Journal of general physiology **121**(5): 427-439.
- Chan-Ling, T. (1989). "Sensitivity and neural organization of the cat cornea." Investigative ophthalmology & visual science **30**(6): 1075-1082.
- Chao, C., B. Golebiowski, et al. (2014). "The role of corneal innervation in LASIK-induced neuropathic dry eye." The ocular surface **12**(1): 32-45.
- Charles, Q. Y. and M. I. Rosenblatt (2007). "Transgenic corneal neurofluorescence in mice: a new model for in vivo investigation of nerve structure and regeneration." Investigative ophthalmology & visual science **48**(4): 1535-1542.
- Charles, Q. Y., M. Zhang, et al. (2008). "Vascular endothelial growth factor mediates corneal nerve repair." Investigative ophthalmology & visual science **49**(9): 3870-3878.
- Chen, X., J. Gallar, et al. (1997). "Reduction by antiinflammatory drugs of the response of corneal sensory nerve fibers to chemical irritation." Investigative ophthalmology & visual science **38**(10): 1944-1953.
- Cintron, C., L. Hassinger, et al. (1979). "A simple method for the removal of rabbit corneal epithelium utilizing n-heptanol." Ophthalmic Research **11**(2): 90-96.
- Cruzat, A., D. Pavan-Langston, et al. (2010). In vivo confocal microscopy of corneal nerves: analysis and clinical correlation. Seminars in ophthalmology, Informa Healthcare New York.
- Cursiefen, C., L. Chen, et al. (2006). "Nonvascular VEGF receptor 3 expression by corneal epithelium maintains avascularity and vision." Proceedings of the National Academy of Sciences **103**(30): 11405-11410.
- de Leeuw, A. M. and K. Y. Chan (1989). "Corneal nerve regeneration. Correlation between morphology and restoration of sensitivity." Investigative ophthalmology & visual science **30**(9): 1980-1990.

DelMonte, D. W. and T. Kim (2011). "Anatomy and physiology of the cornea." Journal of Cataract & Refractive Surgery **37**(3): 588-598.

Dohlman, C. H. (1971). "The Function of the Corneal Epithelium in Health and Disease The Jonas S. Friedenwald Memorial Lecture." Investigative ophthalmology & visual science **10**(6): 383-407.

Dvorscak, L. and C. F. Marfurt (2008). "Age-related changes in rat corneal epithelial nerve density." Investigative ophthalmology & visual science **49**(3): 910-916.

Elder, M. J. and J. K. Dart (2000). "9 Tears and the Dry Eye." Nervous Control of the Eye: 257.

Erdélyi, B., R. Kraak, et al. (2007). "In vivo confocal laser scanning microscopy of the cornea in dry eye." Graefe's archive for clinical and experimental ophthalmology **245**(1): 39-44.

Erie, J. C., J. W. McLaren, et al. (2005). "The effect of age on the corneal subbasal nerve plexus." Cornea **24**(6): 705-709.

Esquenazi, S., J. He, et al. (2007). "Comparative in vivo high-resolution confocal microscopy of corneal epithelium, sub-basal nerves and stromal cells in mice with and without dry eye after photorefractive keratectomy." Clinical & experimental ophthalmology **35**(6): 545-549.

Fabiani, C., S. Barabino, et al. (2009). "Corneal epithelial proliferation and thickness in a mouse model of dry eye." Experimental eye research **89**(2): 166-171.

Felipe, C. D., G. G. Gonzalez, et al. (1999). "Quantification and immunocytochemical characteristics of trigeminal ganglion neurons projecting to the cornea: effect of corneal wounding." European Journal of Pain **3**(1): 31-39.

Gallar, J., M. C. Acosta, et al. (2007). "Impulse activity in corneal sensory nerve fibers after photorefractive keratectomy." Investigative ophthalmology & visual science **48**(9): 4033-4037.

Gallar, J., M. Pozo, et al. (1993). "Response of sensory units with unmyelinated fibres to mechanical, thermal and chemical stimulation of the cat's cornea." The Journal of physiology **468**(1): 609-622.

Gallar, J., M. A. Pozo, et al. (1990). "Effects of capsaicin on corneal wound healing." Investigative ophthalmology & visual science **31**(10): 1968-1974.

Gipson, I., M. Yankauckas, et al. (1992). "Characteristics of a glycoprotein in the ocular surface glycocalyx." Investigative ophthalmology & visual science **33**(1): 218-227.

Gipson, I. K. and P. ARGüESO (2003). "Role of mucins in the function of the corneal and conjunctival epithelia." International review of cytology **231**: 1-49.

- Hamrah, P., Q. Zhang, et al. (2002). "Novel characterization of MHC class II–negative population of resident corneal Langerhans cell–type dendritic cells." Investigative ophthalmology & visual science **43**(3): 639-646.
- Harris, L. W. and D. Purves (1989). "Rapid remodeling of sensory endings in the corneas of living mice." The Journal of Neuroscience **9**(6): 2210-2214.
- Hassell, J. R. and D. E. Birk (2010). "The molecular basis of corneal transparency." Experimental eye research **91**(3): 326-335.
- Hayashi, S., T. Osawa, et al. (2002). "Comparative observations on corneas, with special reference to Bowman's layer and Descemet's membrane in mammals and amphibians." Journal of morphology **254**(3): 247-258.
- He, J., N. G. Bazan, et al. (2010). "Mapping the entire human corneal nerve architecture." Experimental eye research **91**(4): 513-523.
- Henriksson, J. T., A. M. McDermott, et al. (2009). "Dimensions and morphology of the cornea in three strains of mice." Investigative ophthalmology & visual science **50**(8): 3648-3654.
- Hirata, H. and I. D. Meng (2010). "Cold-sensitive corneal afferents respond to a variety of ocular stimuli central to tear production: implications for dry eye disease." Investigative ophthalmology & visual science **51**(8): 3969-3976.
- Hirata, H., K. Okamoto, et al. (2004). "A novel class of neurons at the trigeminal subnucleus interpolaris/caudalis transition region monitors ocular surface fluid status and modulates tear production." The Journal of Neuroscience **24**(17): 4224-4232.
- Hoşal, B., N. Örnek, et al. (2004). "Morphology of corneal nerves and corneal sensation in dry eye: a preliminary study." Eye **19**(12): 1276-1279.
- Imanishi, J., K. Kamiyama, et al. (2000). "Growth factors: importance in wound healing and maintenance of transparency of the cornea." Progress in retinal and eye research **19**(1): 113-129.
- Ivanusic, J. J., R. J. Wood, et al. (2013). "Sensory and sympathetic innervation of the mouse and guinea pig corneal epithelium." Journal of Comparative Neurology **521**(4): 877-893.
- Javadi, M.-A. and S. Feizi (2011). "Dry eye syndrome." Journal of ophthalmic & vision research **6**(3): 192.
- Jester, J. V. (2008). Corneal crystallins and the development of cellular transparency. Seminars in cell & developmental biology, Elsevier.
- Jester, J. V., T. Moller-Pedersen, et al. (1999). "The cellular basis of corneal transparency: evidence for 'corneal crystallins'." Journal of cell science **112**(5): 613-622.
- Johnson, M. E. and P. J. Murphy (2004). "Changes in the tear film and ocular surface from dry eye syndrome." Progress in retinal and eye research **23**(4): 449-474.

Jonasova, K. and Z. Kozmik (2008). Eye evolution: lens and cornea as an upgrade of animal visual system. Seminars in cell & developmental biology, Elsevier.

Jones, M. and C. Marfurt (1998). "Peptidergic innervation of the rat cornea." Experimental eye research **66**(4): 421-435.

Jordan, A. and J. Baum (1980). "Basic tear flow. Does it exist?" Ophthalmology **87**(9): 920-930.

Kaiserman, I., N. Kaiserman, et al. (2005). "Dry eye in diabetic patients." American journal of ophthalmology **139**(3): 498-503.

Karnati, R., D. E. Laurie, et al. (2013). "Lacritin and the tear proteome as natural replacement therapy for dry eye." Experimental eye research **117**: 39-52.

Kenchegowda, S. and H. E. Bazan (2010). "Significance of lipid mediators in corneal injury and repair." Journal of lipid research **51**(5): 879-891.

Knupp, C., C. Pinali, et al. (2009). "The architecture of the cornea and structural basis of its transparency." Advances in protein chemistry and structural biology **78**: 25-49.

Koo, H.-Y. and T. Kume (2013). "FoxC1-Dependent Regulation of Vascular Endothelial Growth Factor Signaling in Corneal Avascularity." Trends in cardiovascular medicine **23**(1): 1-4.

Kovacs, I., S. Quirce, et al. (2010). "Increased Responsiveness of Corneal Cold Receptors in an Experimental Model of Dry Eye." ARVO Meeting Abstracts **51**(5): 3403.

Kubilus, J. K. and T. F. Linsenmayer (2010). "Developmental corneal innervation: interactions between nerves and specialized apical corneal epithelial cells." Investigative ophthalmology & visual science **51**(2): 782-789.

Kubilus, J. K. and T. F. Linsenmayer (2010). "Developmental guidance of embryonic corneal innervation: roles of Semaphorin3A and Slit2." Developmental biology **344**(1): 172-184.

Kurose, M. and I. D. Meng (2013). "Dry eye modifies the thermal and menthol responses in rat corneal primary afferent cool cells." Journal of neurophysiology **110**(2): 495-504.

Kymionis, G. D., D. I. Bouzoukis, et al. (2008). "Treatment of chronic dry eye: focus on cyclosporine." Clinical ophthalmology (Auckland, NZ) **2**(4): 829.

Labbé, A., H. Alalwani, et al. (2012). "The relationship between subbasal nerve morphology and corneal sensation in ocular surface disease." Investigative ophthalmology & visual science **53**(8): 4926-4931.

Labbé, A., Q. Liang, et al. (2013). "Corneal nerve structure and function in patients with non-Sjögren dry eye: clinical correlations." Investigative ophthalmology & visual science **54**(8): 5144-5150.

- Land, M. F. and R. D. Fernald (1992). "The evolution of eyes." Annual review of neuroscience **15**(1): 1-29.
- Ledbetter, E. C. and J. M. Scarlett (2009). "In vivo confocal microscopy of the normal equine cornea and limbus." Veterinary ophthalmology **12**(s1): 57-64.
- Lehrer, M. S., T.-T. Sun, et al. (1998). "Strategies of epithelial repair: modulation of stem cell and transit amplifying cell proliferation." Journal of cell science **111**(19): 2867-2875.
- Leiper, L. J., J. Ou, et al. (2009). "Control of patterns of corneal innervation by Pax6." Investigative ophthalmology & visual science **50**(3): 1122-1128.
- Lemp, M. A. and G. N. Foulks (2007). "The definition and classification of dry eye disease." The ocular surface **5**(2): 75-92.
- Li, W., Y. Hayashida, et al. (2007). "Niche regulation of corneal epithelial stem cells at the limbus." Cell research **17**(1): 26-36.
- Li, Z., A. R. Burns, et al. (2011). "IL-17 and VEGF are necessary for efficient corneal nerve regeneration." The American journal of pathology **178**(3): 1106-1116.
- Lim, C. and G. Ruskell (1978). Corneal nerve access in monkeys. Current Research in Ophthalmic Electron Microscopy, Springer: 15-23.
- López de Armentia, M., C. Cabanes, et al. (2000). "Electrophysiological properties of identified trigeminal ganglion neurons innervating the cornea of the mouse." Neuroscience **101**(4): 1109-1115.
- MacIver, M. and D. L. Tanelian (1993). "Structural and functional specialization of A delta and C fiber free nerve endings innervating rabbit corneal epithelium." The Journal of Neuroscience **13**(10): 4511-4524.
- Maitchouk, D. Y., R. W. Beuerman, et al. (2000). "Tear production after unilateral removal of the main lacrimal gland in squirrel monkeys." Archives of ophthalmology **118**(2): 246-252.
- Marfurt, C., R. Kingsley, et al. (1989). "Sensory and sympathetic innervation of the mammalian cornea. A retrograde tracing study." Investigative ophthalmology & visual science **30**(3): 461-472.
- Marfurt, C. F. (2000). "Nervous control of the cornea." Nervous Control of the Eye. Amsterdam, Harwood Academic Publishers: 41.
- Marfurt, C. F., J. Cox, et al. (2010). "Anatomy of the human corneal innervation." Experimental eye research **90**(4): 478-492.
- Marfurt, C. F. and S. F. Echtenkamp (1995). "The effect of diabetes on neuropeptide content in the rat cornea and iris." Investigative ophthalmology & visual science **36**(6): 1100-1106.
- Marfurt, C. F., C. J. Murphy, et al. (2001). "Morphology and neurochemistry of canine corneal innervation." Investigative ophthalmology & visual science **42**(10): 2242-2251.

- Maurice, D. M. (1957). "The structure and transparency of the cornea." The Journal of physiology **136**(2): 263.
- McKemy, D. D., W. M. Neuhauser, et al. (2002). "Identification of a cold receptor reveals a general role for TRP channels in thermosensation." Nature **416**(6876): 52-58.
- McKenna, C. C. and P. Y. Lwigale (2011). "Innervation of the mouse cornea during development." Investigative ophthalmology & visual science **52**(1): 30-35.
- McKown, R. L., N. Wang, et al. (2009). "Lacritin and other new proteins of the lacrimal functional unit." Experimental eye research **88**(5): 848-858.
- Millodot, M. (1977). "The influence of age on the sensitivity of the cornea." Investigative ophthalmology & visual science **16**(3): 240-242.
- Moss, S. E., R. Klein, et al. (2000). "Prevalence of and risk factors for dry eye syndrome." Archives of ophthalmology **118**(9): 1264-1268.
- Müller, L., L. Pels, et al. (1996). "Ultrastructural organization of human corneal nerves." Investigative ophthalmology & visual science **37**(4): 476-488.
- Müller, L., G. Vrensen, et al. (1997). "Architecture of human corneal nerves." Investigative ophthalmology & visual science **38**(5): 985-994.
- Müller, L. J., C. F. Marfurt, et al. (2003). "Corneal nerves: structure, contents and function." Experimental eye research **76**(5): 521-542.
- Murphy, P. J., S. Patel, et al. (2004). "Noninvasive assessment of corneal sensitivity in young and elderly diabetic and nondiabetic subjects." Investigative ophthalmology & visual science **45**(6): 1737-1742.
- Murphy, P. J., S. Patel, et al. (2001). "The minimum stimulus energy required to produce a cooling sensation in the human cornea." Ophthalmic and Physiological Optics **21**(5): 407-410.
- Nagasaki, T. and J. Zhao (2003). "Centripetal movement of corneal epithelial cells in the normal adult mouse." Investigative ophthalmology & visual science **44**(2): 558-566.
- Nakamura, M., M. Kawahara, et al. (2003). "Restoration of corneal epithelial barrier function and wound healing by substance P and IGF-1 in rats with capsaicin-induced neurotrophic keratopathy." Investigative ophthalmology & visual science **44**(7): 2937-2940.
- Nakamura, M., K. Ofuji, et al. (1997). "The NK1 receptor and its participation in the synergistic enhancement of corneal epithelial migration by substance P and insulin-like growth factor-1." British journal of pharmacology **120**(4): 547-552.
- Nichols, B., M. Chiappino, et al. (1985). "Demonstration of the mucous layer of the tear film by electron microscopy." Investigative ophthalmology & visual science **26**(4): 464-473.

- Nichols, B., C. Dawson, et al. (1983). "Surface features of the conjunctiva and cornea." Investigative ophthalmology & visual science **24**(5): 570-576.
- Nichols, J. J. and L. T. Sinnott (2006). "Tear film, contact lens, and patient-related factors associated with contact lens-related dry eye." Investigative ophthalmology & visual science **47**(4): 1319-1328.
- Pan, Z., S. Fukuoka, et al. (2013). "Vascular endothelial growth factor promotes anatomical and functional recovery of injured peripheral nerves in the avascular cornea." The FASEB Journal **27**(7): 2756-2767.
- Parra, A., R. Madrid, et al. (2010). "Ocular surface wetness is regulated by TRPM8-dependent cold thermoreceptors of the cornea." Nature medicine **16**(12): 1396-1399.
- Patel, D. V. and C. N. McGhee (2005). "Mapping of the normal human corneal sub-basal nerve plexus by in vivo laser scanning confocal microscopy." Investigative ophthalmology & visual science **46**(12): 4485-4488.
- Perez, E., L. Lopez-Briones, et al. (1987). "Effects of chronic sympathetic stimulation on corneal wound healing." Investigative ophthalmology & visual science **28**(2): 221-224.
- Pfister, R. R. (1975). "The healing of corneal epithelial abrasions in the rabbit: a scanning electron microscope study." Investigative ophthalmology & visual science **14**(9): 648-661.
- Rodrigues, M., G. Rowden, et al. (1981). "Langerhans cells in the normal conjunctiva and peripheral cornea of selected species." Investigative ophthalmology & visual science **21**(5): 759-765.
- Rosenthal, P. and D. Borsook (2012). "The corneal pain system. Part I: the missing piece of the dry eye puzzle." The ocular surface **10**(1): 2-14.
- Rozsa, A. J. and R. W. Beuerman (1982). "Density and organization of free nerve endings in the corneal epithelium of the rabbit." Pain **14**(2): 105-120.
- Rozsa, A. J., R. B. Guss, et al. (1983). "Neural remodeling following experimental surgery of the rabbit cornea." Investigative ophthalmology & visual science **24**(8): 1033-1051.
- Sade De Paiva, C. and S. C. Pflugfelder (2004). "Corneal epitheliopathy of dry eye induces hyperesthesia to mechanical air jet stimulation." American journal of ophthalmology **137**(1): 109-115.
- Saude, T. (1993). Ocular anatomy and physiology, Blackwell Scientific Publications.
- Schimmelpfennig, B. (1982). "Nerve structures in human central corneal epithelium." Graefe's archive for clinical and experimental ophthalmology **218**(1): 14-20.
- Steele, C. (1999). "Corneal wound healing: a review." Optometry Today **24**: 28-32.
- Stepp, M. A., J. D. Zieske, et al. (2014). "Wounding the cornea to learn how it heals." Experimental eye research **121**: 178-193.

- Terril, L. A., D. J. Clemons, et al. (1998). The laboratory guinea pig, CRC Press.
- Tervo, K. and T. Tervo (1981). "The ultrastructure of rat corneal nerves during development." Experimental eye research **33**(4): 393-402.
- Tervo, T., K. Tervo, et al. (1982). "Ocular neuropeptides." Medical biology **60**(2): 53-60.
- Thoft, R. A. and J. Friend (1983). "The X, Y, Z hypothesis of corneal epithelial maintenance." Investigative ophthalmology & visual science **24**(10): 1442-1443.
- Tonge, D. P., R. G. Bardsley, et al. (2013). "Evidence of changes to skeletal muscle contractile properties during the initiation of disease in the ageing guinea pig model of osteoarthritis." Longevity & Healthspan **2**(1): 15.
- Trost, K., M. Skalicky, et al. (2007). "Schirmer tear test, phenol red thread tear test, eye blink frequency and corneal sensitivity in the guinea pig." Veterinary ophthalmology **10**(3): 143-146.
- Tsubota, K. (1998). "Tear dynamics and dry eye." Progress in retinal and eye research **17**(4): 565-596.
- Tuominen, I. S., Y. T. Kontinen, et al. (2003). "Corneal innervation and morphology in primary Sjögren's syndrome." Investigative ophthalmology & visual science **44**(6): 2545-2549.
- Țuru, L., C. Alexandrescu, et al. (2012). "Dry eye disease after LASIK." Journal of medicine and life **5**(1): 82.
- Turuwhenua, J. T., D. V. Patel, et al. (2012). "Fully automated montaging of laser scanning in vivo confocal microscopy images of the human corneal subbasal nerve plexus." Investigative ophthalmology & visual science **53**(4): 2235-2242.
- Vannas, A., B. Holden, et al. (1987). "Epithelial metabolism of the corneal graft is abnormal." British Journal of Ophthalmology **71**(8): 593-597.
- Walcott, B. (1998). "The lacrimal gland and its veil of tears." Physiology **13**(2): 97-103.
- Wang, C., T. Fu, et al. (2012). "Changes in mouse corneal epithelial innervation with age." Investigative ophthalmology & visual science **53**(8): 5077-5084.
- Wieser, B., A. Tichy, et al. (2013). "Correlation between corneal sensitivity and quantity of reflex tearing in cows, horses, goats, sheep, dogs, cats, rabbits, and guinea pigs." Veterinary ophthalmology **16**(4): 251-262.
- Workshop, I. D. E. (2007). "Methodologies to diagnose and monitor dry eye disease. In: 2007 Report of the International Dry Eye Workshop (DEWS)." Ocul Surf **5**: 108-152.
- Zagon, I. S., J. W. Sassani, et al. (1998). "Re-epithelialization of the rabbit cornea is regulated by opioid growth factor." Brain research **803**(1): 61-68.

Zagon, I. S., J. W. Sassani, et al. (2000). "Reepithelialization of the human cornea is regulated by endogenous opioids." Investigative ophthalmology & visual science **41**(1): 73-81.

Zander, E. and G. Weddell (1951). "Observations on the innervation of the cornea." Journal of anatomy **85**(Pt 1): 68.

Zuazo, A., J. Ibañez, et al. (1986). "Sensory nerve responses elicited by experimental ocular hypertension." Experimental eye research **43**(5): 759-769.

